

See discussions, stats, and author profiles for this publication at: <https://www.researchgate.net/publication/5752808>

# ChemInform Abstract: Chirality-Sensing Supramolecular Systems

ARTICLE *in* CHEMICAL REVIEWS · FEBRUARY 2008

Impact Factor: 46.57 · DOI: 10.1021/cr050005k · Source: PubMed

---

CITATIONS

441

---

READS

133

3 AUTHORS, INCLUDING:



Victor Borovkov

Tallinn University of Technology

107 PUBLICATIONS 1,960 CITATIONS

SEE PROFILE



Yoshihisa Inoue

Osaka University

577 PUBLICATIONS 14,441 CITATIONS

SEE PROFILE

## Chirality-Sensing Supramolecular Systems

Guy A. Hembury, Victor V. Borovkov,\* and Yoshihisa Inoue\*

Japan Science and Technology Agency and Department of Applied Chemistry, Osaka University, 2-1 Yamada-oka, Suita 565-0871, Japan

Received March 16, 2007

### Contents

1. Introduction	1	6.2. Chiral Conformation Sensing	48
2. Basic Principles	2	6.3. Macroevironmental Chirality Sensing	52
2.1. Types of Chirality	2	7. Supramolecular Systems with Chiral Memories	53
2.1.1. Configurational Chirality	3	8. Direct Chirality Observation on Surfaces	57
2.1.2. Conformational Chirality	3	9. Chirality in Supramolecular Polymeric Assemblies	61
2.2. Chirality Induction, Recognition, and Discrimination	3	10. Chirality Sensing and Control in Polymeric Assemblies	66
2.2.1. Chirality Induction	3	11. Conclusions	69
2.2.2. Chiral Recognition and Discrimination	4	12. Note Added after ASAP Publication	69
2.3. Observing and Quantifying Chirality	4	13. References	69
3. Chirality Sensing and Induction in Convergent Host–Guest Assemblies	7		
3.1. Target-Specific Sensors	7		
3.2. Induction via Cavity Encapsulation	12		
4. Enantiodiscriminating Host–Guest Systems	16		
4.1. Insights into Controlling Parameters in Enantiodiscriminating Systems	16		
4.2. Enantiodiscrimination Detection by Fluorescence	21		
5. External and Internal Controlling Factors	26		
5.1. Solvent as an Active Component in Supramolecular Chirality	26		
5.1.1. Solvent Influence on Chirality Magnitude	27		
5.1.2. Solvent-Mediated Chirality Inversion	31		
5.2. Influence of Temperature on Supramolecular Chirality	36		
5.2.1. Temperature-Induced Monodisperse-to-Supramolecular Transitions	36		
5.2.2. Temperature-Induced Structural Changes in Supramolecular Assemblies	37		
5.2.3. Temperature-Induced Changes in Enthalpy and Entropy Contributions	39		
5.3. Influence of Phase Transitions on Supramolecular Chirality	40		
6. Porphyrin-Based Systems	42		
6.1. Point-Chirality Sensing	43		

### 1. Introduction

Chirality that is induced, monitored, controlled, or applied via the principles of a supramolecular approach is a modern interdisciplinary field of research that deals with asymmetry information transfer within multimolecular systems via noncovalent interactions. Since a chiral supramolecular sensing event may profoundly affect the nature of one part, or several parts, or even the whole of a multicomponent assembly, its implications are enormous for a broad range of molecular sciences. This intriguing phenomenon is widely seen in many natural (such as the DNA double helix and the secondary  $\alpha$ -helix structure of proteins)<sup>1</sup> and various artificial and biomimetic systems, making it of prime importance not only for fundamental science but also for a number of practical applications in such areas as catalysis,<sup>2</sup> nonlinear optics,<sup>3</sup> polymer and materials science,<sup>4</sup> molecular and chiral recognition,<sup>5</sup> molecular devices,<sup>6</sup> and absolute configuration assignment.<sup>7</sup>

Therefore, a detailed understanding of the underpinning mechanisms and various influencing factors is of particular significance for smart control and further useful application of chiral supramolecular science. Considering the vast body of literature on the subject of supramolecular chirality generation (or chirogenesis), it is clear that the modes of chiral molecular communication are largely noncovalent in nature; primarily, these include attractive or repulsive electrostatic interactions, hydrogen bonding,<sup>8,4c</sup> van der Waals contacts,  $\pi$ – $\pi$ <sup>9</sup> interactions, and repulsive steric interactions,<sup>10</sup> with these acting either independently or cooperatively to produce the observed chiral structures. Thus, it is with this in mind that we must approach the analyses of such dynamic

\* To whom correspondence should be addressed. E-mails: victrb@chem.eng.osaka-u.ac.jp, inoue@chem.eng.osaka-u.ac.jp.



Guy Hembury was born in Leicester, U.K., in 1974. He received his doctorate in 1999 from the University of Sheffield, U.K., working within the group of Prof. Chris Hunter. Subsequently, he joined the Inoue Photochirogenesis Project in Osaka, Japan, working until 2002. He then spent 2 years at the Entropy Control Project, Japan. In 2005, he returned to the U.K., taking up a position within the Molecular Materials Centre at the University of Manchester. His current interests include the development of synchrotron-based experiments for probing the structural pathways of solution-phase chemical reactions and self-assembly phenomena; the application of experimental and machine-learning methods to identify the molecular-level parameters controlling crystal polymorphism; and the development of evolutionary-inspired high-throughput microfluidic instrumentation for automated reaction control and formulation.

supramolecular chiral systems, with recent years showing a great increase in the sophistication with which research groups have been able to rationalize and apply supramolecular principles to a large range of complex chiral assemblies.

Indeed, from the above-mentioned perception of supramolecular chirality phenomena in natural systems and the increasingly successful application to smart artificial systems, clearly this subject is approaching a greater scientific maturity where it may become a broader, more commonly used “tool” for academic research and industry alike. However, as with other emergent new molecular- and nanotechnologies, there must be a solid base of chiral supramolecular science before we can confidently realize successful chiral supramolecular technologies.

Thus, in this review, we intended to present an overview of key areas and representative examples considered for successfully understanding and applying supramolecular systems for chirality-sensing purposes. First, we provide an introduction to the different manifestations of (supra)-molecular chirality, in conjunction with commonly used analytical methods for observing and understanding these systems, along with consideration of associated theories with which data should be considered. Second, an overview of recent works that deal with the most widely considered areas of chiral supramolecular science, particularly asymmetry induction and control in various host–guest assemblies, followed by consideration of the phenomena of enantiodiscrimination in host–guest systems, will be presented. Third, an overview of work that considers how the various external (temperature, phase transition, solvent polarity, pH, viscosity, light, etc.) and internal (bonding strength, steric and electronic effects, stoichiometry, etc.) modulating stimuli can be appreciated and understood in a chirality context will be shown. Fourth, a consideration of recent work in different branches of chirogenesis such as chiral memory, surfaces, polymers, and nanostructures that well-illustrate the rational design of sophisticated supramolecular systems with potential for functional application will be done. Finally, a



Victor Borovkov was born in Moscow, Russia, in 1961. He received a Ph.D. degree from Moscow Institute of Fine Chemical Technology in 1988. Following a postdoctoral period at Osaka University, he worked at different research organizations in Japan and joined Japan Science and Technology Agency in 1997. His current research interests include porphyrin chemistry, chirality, and supramolecular chemistry.



Yoshihisa Inoue, born in Nara, Japan, in 1949, is a professor at Osaka University and the project director of the former ICORP Entropy Control Project. He received his Ph.D. from Osaka University in 1977. After a short stay at the Institute of Scientific and Industrial Research as JSPS fellow, he joined the faculty of Department of Applied Chemistry, Himeji Institute of Technology, in 1977. While on leave, he spent 1 year (1978–1979) as research associate at Columbia University, working with Nicholas Turro. In 1985, he moved to the Basic Research Laboratory and then to Department of Material Science, Himeji Institute of Technology, in 1990. In 1994, he returned to Osaka University as a full professor. He is now interested in supramolecular chemistry in the ground and excited states.

perspective of current limitations and possible approaches to overcoming these problems will be described, along with future opportunities for the wider advancement of supramolecular chirality.

## 2. Basic Principles

### 2.1. Types of Chirality

The term chirality originates from the Greek *hkeir*, which means *hand* and describes objects that exist as a pair of non-superimposable mirror images, which are called enantiomers. Molecules and molecular systems can be chiral by asymmetrically arranging atoms in space around a center, axis, or plane, which are called point, axial, and planar chirality, respectively. Not only covalently bonded molecules with defined configuration and conformation but also noncovalently interacting supramolecular assemblies with conformational flexibilities and even transient molecular conformations can form chiral structures or architectures. Hence,

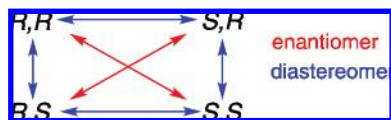


**Figure 1.** Four possible chiral combinations of stereoisomers in the case of two chiral centers.

some introduction to molecular and supramolecular chirality will be given first.

### 2.1.1. Configurational Chirality

This is where the chirality arises directly from the arrangement of the covalent structure of the molecule. Point chirality is often considered as the most fundamental form of chirality. In this, the chirality originates from the different substituents bonded three-dimensionally to a central atom that results in  $C_1$  symmetry for the whole molecule (with the classic case being four different substituents around an  $sp^3$  carbon atom; however, it should be noted that, in some particular cases, a molecule possessing a  $C_2$  or  $C_3$  symmetry axis can also be chiral). The relative spatial arrangement of these substituents (according to the Cahn–Ingold–Prelog priority rule system for absolute configuration assignment) results in either a clockwise spatial order or an anticlockwise spatial order corresponding to the *R* and *S* enantiomer, respectively (possessing non-superimposable mirror images). Whether an enantiomer has a (+) or (−) specific rotation is nontrivial, although some theoretical work utilizing time-dependent density functional theory (TDDFT) with simple and rigid molecules has shown increasing success.<sup>11</sup> However, this is currently of limited applicability, especially for supramolecular systems because of their, typically, larger sizes and dynamic nature, although future developments in theory and computing power will undoubtedly address this subject as well. When there are two chiral centers in a single molecule, there are four possible chiral combinations; see Figure 1. The interrelationships between these reveal that there are two pairs of enantiomers (possessing indistinguishable physical and chemical properties in the absence of external chiral effects such as circularly polarized light, chiral environment, chiral reagents, etc.) and two pairs of diastereomers (having different physical, chemical, and optical properties), with one different chiral center in each pair. In the case of  $n$  chiral centers in a molecule, the total number of different stereoisomers is  $2^n$  with  $2^{n-1}$  enantiomeric pairs.

Besides, configurational chirality does not need to possess point-chiral centers but may arise from the inherently chiral nature of the covalent structure, as can be seen in the “picotubes” synthesized by Okamoto and co-workers.<sup>12</sup>

### 2.1.2. Conformational Chirality

The clear distinction must be realized between conformational and configurational chirality, when discussing chirality in a (supra)molecular context. This form of chirality arises from the (re)arrangement of part or all of a molecule or assembly under a chiral influence that removes any elements of symmetry from it (N.B. = no bonds are broken in the process). This chirality may occur via (1) supramolecular interactions with a chirality inductor, which is then lost on removal of the controlling interactions (excepting special cases of the chirality memory phenomena (see section 7)) or (2) an intramolecular chiral conformation that is maintained by steric hindrance (to a change of internal conformation) and/or other factors, such as hydrogen bonding, for example, that preclude racemization.

**2.1.2.1. Helical Chirality.** This form of chirality, a special kind of facial chirality, is widely cited in the literature, and its usefulness is more often appreciated. Examples of helical chirality can be abundantly found in natural systems (DNA,  $\alpha$ -helix of proteins, and polysaccharides) as well as in artificial ones (polymers and oligomers<sup>13</sup> and nonplanar single molecules such as helices, dipyrins, and tetrapyrroles<sup>14</sup>). Here, the chirality arises from the unidirectional nature of the twist propagation along the long axis of the molecule or assembly, though this need not be of an oligomeric or polymeric nature. Here also, there is no prerequisite for point-chiral centers, and cases where the extended (nonhelical) molecule is achiral are not uncommon.<sup>15</sup> However, in this case (lacking point-chirality centers), the corresponding racemization equilibrium should be shifted toward one particular enantiomer upon spontaneous resolution and/or external chiral influences. Thus, the convention is that, on looking from either end downward along the helical axis, it is termed *P* helicity if the rotation is clockwise and termed *M* helicity if the rotation is anticlockwise. Consequently, in natural systems, B- and A-forms of DNA possess *P* helicity, with the less common Z-form having *M* helicity.

Atropisomers are conformational enantiomers that are generated by the formation of two or more stable (non-interconverting) rotational isomers. This can be either inherent, in which steric constraints of the covalent structure of the molecule prevent rotation (and, thus, racemization) around the atropisomeric bond (this type of conformational isomers can be seen in the case of *N*-heterocyclic octahedral ruthenium complexes<sup>16</sup>), or induced, where rotation is precluded by conformational restriction brought on by, for example, a guest’s confinement in a host’s cavity.<sup>17</sup> Because of the fact that a source of point chirality is not needed to generate chirality, the enantiomers of atropisomers can also be expressed in terms of *P* and *M* helicity, as described previously. Furthermore, in supramolecular systems, cooperative effects may increase the energy barrier between chiral conformational isomers to the level that allows the separation between diastereomorphic and enantiomorphic structures.

## 2.2. Chirality Induction, Recognition, and Discrimination

These are often confused and should be considered in terms of the host’s and guest’s chirality and their effects on the physical, chemical, and chiroptical properties of the system as a whole.

### 2.2.1. Chirality Induction

Induced chirality is of particular interest when considering supramolecular systems. Here, chirality is generated in an achiral guest molecule as a result of an asymmetry information transfer and retaining process from a chiral host or vice versa. This asymmetry transfer process normally results in a form of conformational chirality (see above) that is held by some steric forces and/or hydrogen bonding in the 3D optically active form, even though the free non-interacting covalent structure is itself still achiral. The influencing factors in chirality induction are typically of steric or electronic chiral field nature, with this 3D optically active form held by these chirally constricting environments. An additional, and often overlooked factor in induced 3D optically active systems is that of the reverse chirality modulation effect, in which the chirality of the inductor is itself affected by its interaction with the now optically active guest (or corresponding host) molecule, resulting in changes to its electronic and conformational chiral characteristics.<sup>18</sup>



The conformational changes arising from chirality induction, and the determination of the underlying mechanisms, rely on being able to obtain suitable data. This information may be obtained from a change in the system's physical or chemical properties induced by the influence of the chiral steric and electronic fields. Typical "outputs" are as follows: spectroscopic differences, changes in thermodynamic quantities such as the binding constant, differing colors, chiral macroscale structures (for example, in polymer shape and in surface chemistry, etc.). In the case when both (or more) components of a supramolecular system are optically active, the effect of chiral recognition is often observed, as discussed below.

### 2.2.2. Chiral Recognition and Discrimination

In this category, both the host and guest molecules are chiral and we are concerned with the phenomena of the ability of a chiral host to discriminate between two enantiomeric guests. In the previous case of the achiral host and the chiral guest (and vice versa), the resulting complexes are enantiomeric, thus possessing identical physical–chemical properties that are nonchirality sensitive, such as UV–vis and fluorescence spectra, binding constants, enthalpy and entropy values, NMR shifts, and others, but that exhibit equal but opposite values of chirally sensitive properties, such as absorption and fluorescence circular dichroism (CD) characteristics, and specific optical rotations. However, in the case where a chiral host compound interacts with a pair of enantiomeric guests, the intermolecular chiral interactions that the host experiences for each enantiomer are different (arising from the different relative orientations of the interacting groups), with the result being two diastereomeric complexes. As a result, all the physical and chemical properties mentioned above are now different and can be easily monitored by conventional spectroscopic methods.

### 2.3. Observing and Quantifying Chirality

The phenomenon of chirality is burdened with an unhelpfully large and overlapping lexicon, although attempts have been made to address this.<sup>19</sup> This also extends to the terminology used for the labeling of differing types of chirality, for example (+) and (−), *l* and *d*, *L* and *D*, *R* and *S*, *P* and *M*, etc., and to the units used in quantitative measurements. Accordingly, next we give a brief explanation of the commonly used units and their interrelationships.

The most commonly used technique for examining chiral systems is analysis of its circular dichroism. The phenomenon of circular dichroism is essentially the wavelength-dependent preference with which a sample will preferentially absorb left- or right-handed circularly polarized light (CPL) (circularly polarized light is a beam of light that describes either a left- or right-handed helix along its axis of propagation), with the degree of this preferential absorption being a measure of its magnitude of chirality. There are a number of different types of CD techniques currently used, which relate to the wavelengths associated with a particular molecular absorption or emission (and will be discussed in more detail below). For instance, electronic circular dichroism (ECD), which is the most widely applied technique, is concerned with absorptions in the UV–vis region associated with electronic transitions between different molecular orbitals ( $\lambda = \text{ca. } 190\text{--}900 \text{ nm}$ ).

When subjected to ECD analysis, the resulting spectrum will give a signal(s) (positive or negative magnitude), termed a Cotton effect, that is a measure of the sample's ellipticity

( $\theta$ ), which is measured in millidegrees (mdeg), against the wavelength. This value will clearly depend on such factors as the sample's concentration (*c*) and path length (*l*) (which determine the number of chiral chromophores that the CPL is incident upon), as well as the sample's internal chiroptical properties itself. Thus, a molar ellipticity ( $\Delta\epsilon$ ), defined as a difference in molar extinction coefficient ( $\epsilon$ ) for left- and right-handed CPL ( $\Delta\epsilon = \epsilon_l - \epsilon_r$ ), should be considered to allow quantitative comparisons of chiroptical properties of different samples and is given by the formula

$$\Delta\epsilon = \theta/32980cl \quad (1)$$

where the path length (*l*) is in cm.

However, this is still not the true measure of the chirality under consideration, although it is by far the most commonly used parameter when discussing the nature of a particular system or comparisons therewith. This is because the intensity of the CD signal is also dependent on the oscillator strength of the originating transition (i.e., the strength of the corresponding UV–vis signal); thus, to obtain a measure of chirality that is independent of all light absorption processes, the anisotropy factor (*g*) is used,

$$g = \Delta\epsilon/\epsilon \quad (2)$$

where  $\epsilon$  is the molar extinction coefficient.

Alternatively, the *g* factor can be calculated for samples of unknown concentrations by considering the optical densities (od).

$$g = \Delta\text{od}/\text{od} \quad (3)$$

where od is the magnitude of the UV–vis signal in arbitrary units of a spectrophotometer and  $\Delta\text{od} = \theta/32980$ .

As mentioned above, the molecular origin of the CD signals is the preferential left- or right-handed absorption of the electronic transitions ( $\Delta\epsilon = \epsilon_l - \epsilon_r$ ). For common organic molecules, the  $n\text{--}\pi^*$  transitions occur at ca. 290–300 nm, which is lower in energy than the simple olefinic and benzenoid  $\pi\text{--}\pi^*$  transitions occurring at ca. 200 nm and 220–280 nm, respectively, while more extended (and conjugated)  $\pi$ -electron systems, such as fused aromatics, display absorptions of progressively lower energies. The observation of Cotton effects arising from the transitions of  $\sigma$  electrons is less commonly studied, as these typically arise at  $\lambda < 200 \text{ nm}$  and are often masked by the solvent.

Thus, the simplest example of a CD spectrum is that of a chiral molecule with a single chromophoric substituent. This will show a single positive or negative monosignate Cotton effect, which corresponds in general to an absorption band in the UV–vis spectrum. Determining whether a particular enantiomer produces a positive or negative ECD is currently nontrivial and requires DFT level calculations that become increasingly difficult with conformational flexibility, overlapping of different transitions, and the number of chromophores due to coupling effects (see below). However, in certain supramolecular systems, inspecting the signs and characteristics of the Cotton effects led to empirical rules that allow the chirality and the spatial conformation of guests within a chiral supramolecular complex to be determined. A celebrated example of this was the "Sector rule" for phenyl derivatives included within  $\beta$ -cyclodextrin's chiral cavity. According to this rule proposed by Kajtar et al.,<sup>20</sup> if the electronic transition of the guest chromophore is aligned parallel to the axis of symmetry of the cyclodextrin cavity, the sign of the corresponding Cotton effect will be positive,

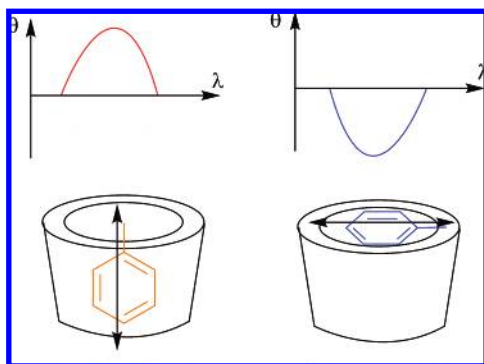


**Figure 2.** Schematic representation of the "Sector rule".

while if the transition is aligned perpendicular to the cavity axis, the CD sign will be negative, as shown in Figure 2.

However, the class of CD spectra that has proven to be by far the most powerful investigative and diagnostic tool with chiral supramolecular systems is that possessing bisignate Cotton effects. These arise when there is through-space coupling between the various chromophores' electronic transitions within the supramolecular system to produce bisignate CD signals that have either first-positive and second-negative (positive chirality) or first-negative and second-positive (negative chirality) Cotton effects for the corresponding coupling, with convention stating that the first Cotton effect is always that of the lowest energy and defines the chirality. The fundamental principles that govern how the relative energies and spatial orientation of a pair of optically active transitions relate to the observed couplet in the CD spectra were first postulated by Harada and Nakanishi.<sup>21</sup> This treatment, known as the exciton chirality method, has proven to be powerful and versatile, being applied to the rationalization and application of numerous conventional and supramolecular systems, in particular to the absolute configuration determination of the whole or part of the system (see section 3). The essential features of this method are that the total amplitude of a bisignate CD signal is inversely proportional to the square of the interchromophoric distance and is proportional to the square of the extinction coefficient of the coupled chromophores. It should be noted that the exciton chirality method was devised on the basis of the theory of exciton coupling, which postulates that the exciton interaction between the two chromophores splits the excited state into two energy levels known as Davydov splitting<sup>22</sup> using a chiral bischromophoric molecular system.<sup>23</sup> A schematic representation of the coupling electronic transitions and the observed relationship between the prominent features (maxima, minima, and crossover points) of the CD signal and their originating UV-vis transitions are shown in Figure 3.

In Figure 3a, we see two pairs of electronic transitions coupled in either a right-handed (clockwise) or left-handed (anticlockwise) fashion that lead to first-positive/second-negative and first-negative/second-positive bisignate CD signals, respectively (only a positive couplet is shown in Figure 3b). The experimentally measured intensities of the positive and negative extrema are not always equal for various reasons (for example, experimental and instrumental errors and the influence of other closely located transitions), and thus, for meaningful comparisons with related bisignate CD signal(s), a total CD amplitude ( $A$ ) value is often used (where  $A$  is the sum of the maximum intensities of each Cotton effect in the couplet). The  $A$  value may be positive or negative to denote the system's sense of chirality as judged by the first

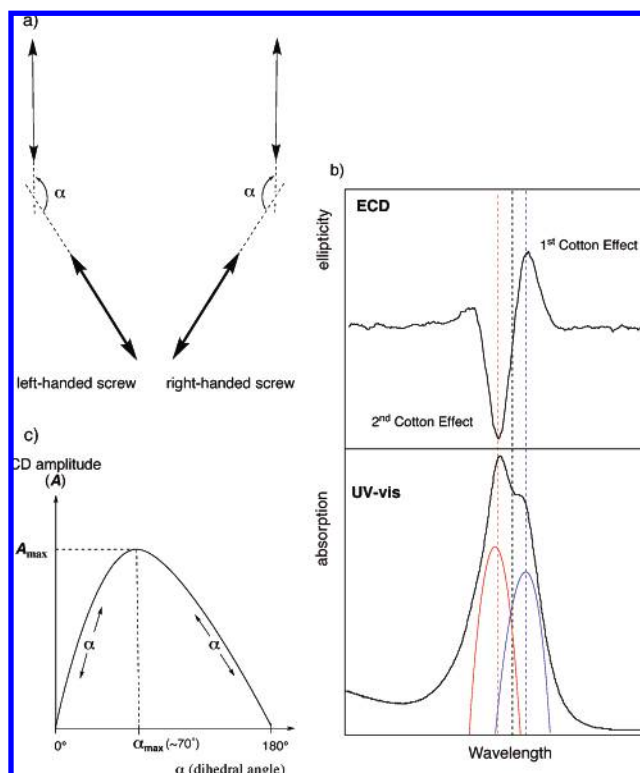


**Figure 3.** Schematic representation of the coupling electronic transitions (a), the relationships between the absorption and CD spectra (b), and the CD amplitude dependence on the dihedral angles between the corresponding coupling electronic transitions (c).

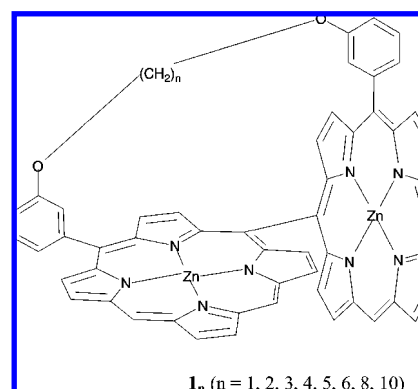


**Figure 4.** General structure of the meso-meso-linked diporphyrins.

Cotton effect sign. The  $A$  value as shown in the case of simple dibenzoates has a parabolic dependence on the dihedral angle between the coupling transitions, with zero values at  $0^\circ$  and  $180^\circ$  and a maximum value at  $\sim 70^\circ$  (Figure 3c).<sup>21</sup> The resulting parameters ( $\alpha$ , slope, intensities, etc.) are not quantitatively the same for all chiral systems, although they are broadly similar and generally applicable, as shown below.

The validity of this theoretical consideration of how the magnitude of the Cotton effects is dependent upon the intertransition angle can be experimentally shown from data published by Osuka and co-workers for a series of rigidly meso-meso-linked diporphyrins;<sup>24</sup> see Figure 4.

In this system, the interporphyrin angle, and, thus, the interelectronic transition angle (in this case, the coupling B-transitions are perpendicular to the bond linking the two porphyrins), is systematically varied by changing the number of linking methylene groups in the molecular strap. The interporphyrin angles were determined by MM2 molecular modeling calculations and consideration of X-ray structures,

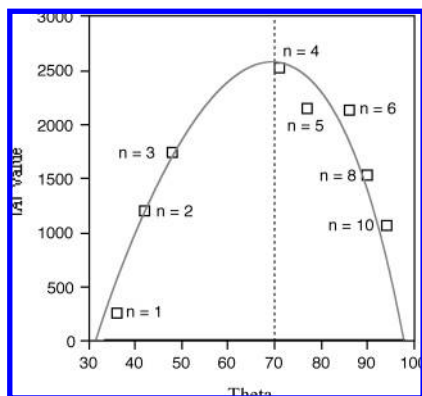


**Figure 5.** Experimental CD amplitude dependence upon the dihedral angles between the corresponding electronic transitions of meso-meso-linked diporphyrins.

which are plotted against their corresponding  $A$  values in Figure 5.

Here, we see a clear experimentally obtained parabolic dependence, with the  $A$  values increasing from **1**<sub>1</sub> to **1**<sub>4</sub>, reaching a maximum at  $\theta = 70^\circ$ , and then reducing systematically from **1**<sub>5</sub> to **1**<sub>10</sub>. This result is in accordance with exciton coupling theory, as discussed previously, and also agrees with the calculations reported by Mason et al.<sup>25</sup> from studies on 9,9'-bianthryl derivatives, where  $\theta_{\text{max}}$  was found to be between 65 and 70°.

Appreciation of this angular dependence of the  $A$  value for bisignate CD signals has been widely used to investigate various molecular properties such as intramolecular/intermolecular conformations and substituent sizes<sup>26</sup> as well as the effects of solvent,<sup>27</sup> among others.

Another key factor that influences the  $A$  value magnitude is that of intertransition distance. This dependence is illustrated in the work of Matile et al.,<sup>28</sup> who studied how the  $A$  values arising from pairs of chromophores separated by rigid spacer molecules varied with distance and chromophore's extinction coefficient; see Figure 6.

A cursory consideration of these results shows that, as expected, the magnitude of the  $A$  value falls away with

increasing interchromophore distance (as seen for other systems);<sup>29</sup> however, it is clearly not simply inversely proportional to the square of the interchromophoric distance as predicted by theory. This highlights the difficulty of isolating the effect of solely one influence and, in this case, probably arises from the varying intertransition angles. Importantly, though, switching the chromophore from porphyrin ( $\epsilon = \text{ca. } 350\,000 \text{ cm}^{-1} \text{ M}^{-1}$ ) to dimethylaminobenzoate ( $\epsilon = \text{ca. } 50\,000 \text{ cm}^{-1} \text{ M}^{-1}$ ) resulted in a reduction of the  $A$  value magnitude, by as much as a 10-fold decrease for the longer distances; this is, thus, an important factor that needs to be considered when designing supramolecular systems and studying the bisignate CD couplet.

Related to ECD is circularly polarized fluorescence (CPF) as a method for investigating chirality, although this technique is much more rarely applied, especially in supramolecular systems. Essentially, CPF investigates whether the fluorescence emission from an electronically excited species is circularly polarized or not and, if so, whether it is left- or right-handed and what its magnitude is; this information is then related back to the chiral structure of the excited species under study. Examples of its application to systems where noncovalent interactions are important are typically in liquid crystal type.<sup>30</sup>

A related technique that is becoming more widely applied is vibrational circular dichroism spectroscopy (VCD), which arises from chiral absorptions in the infrared regions, associated with bond bending and stretching. The importance of VCD as a reliable tool for analyzing chiral conformations<sup>31</sup> and determining absolute configurations in the solution phase<sup>32</sup> has recently become well-recognized, with the method having been successively applied to a number of relatively rigid chiral organic<sup>33</sup> and bioorganic molecules,<sup>34</sup> ranging from simple alcohols<sup>35</sup> to complicated carbohydrates,<sup>36</sup> and even to larger supramolecular/helical molecules.<sup>37</sup>

The method entails a comparison of the experimental VCD spectra with those simulated from DFT calculations. The key factor that makes the application of VCD spectroscopy so challenging is that, although consideration of the calculated VCD spectra for the global minimum conformation may

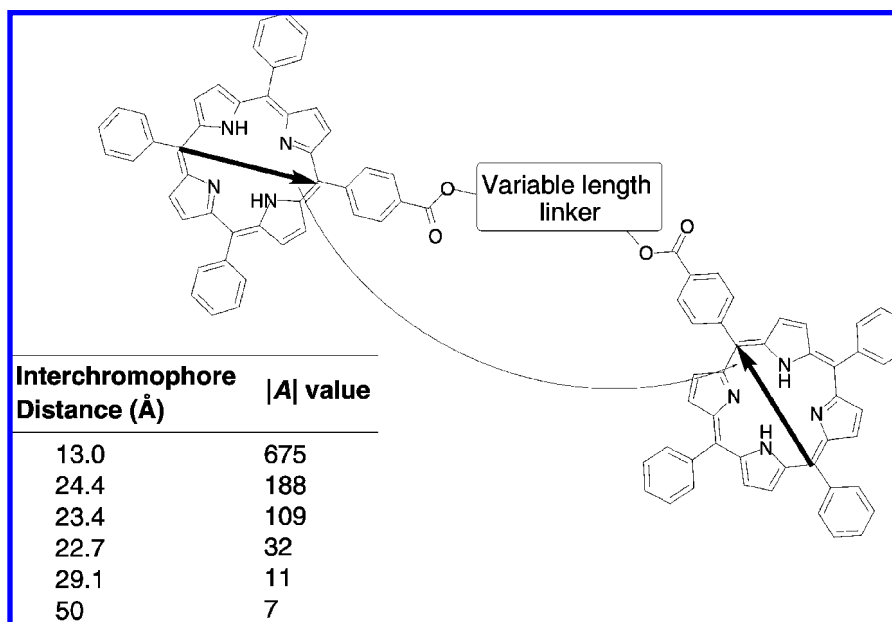


**Figure 6.** General formula of the bisporphyrins separated by the variable-length linkers and the  $A$  value-interchromophore distance relationship.



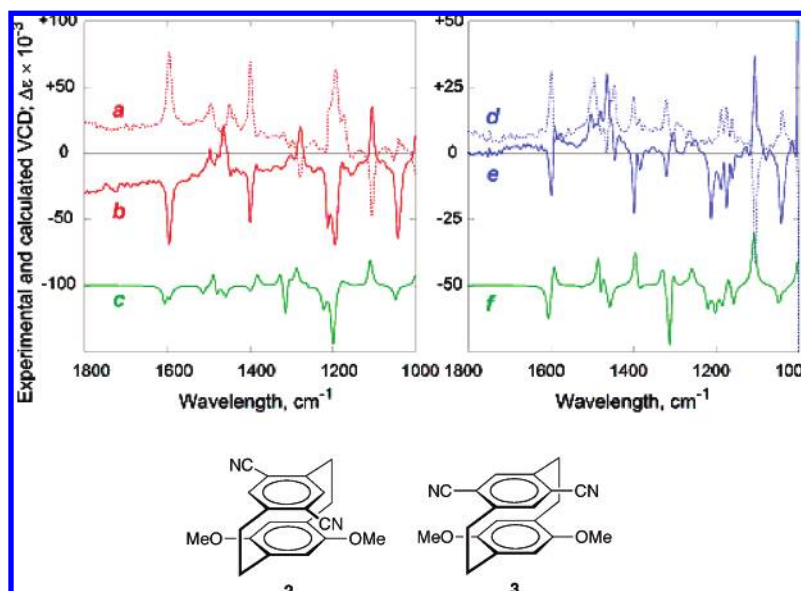


**Figure 7.** Structures and experimental VCD spectra of (+)- and (–)-**2** (a and b, correspondingly) and (+)- and (–)-**3** (d and e, correspondingly) and calculated spectra of (4*S<sub>p</sub>*,12*S<sub>p</sub>*)-**2** and (4*R<sub>p</sub>*,12*S<sub>p</sub>*)-**3** (c and f, correspondingly). Reprinted with permission from Furo, T.; Mori, T.; Wada, T.; Inoue, Y. *J. Am. Chem. Soc.* **2005**, 127, 8242. Copyright 2005 American Chemical Society.

result in overall spectral profiles that are broadly coincident, many minor (but important) peaks are only reproduced on taking into account conformers that are a minor percentage of the whole population. In such cases where molecules exist as a number of conformations, the theoretical VCD spectrum is calculated for each and then an overall spectrum is generated from a combination of the individual spectra weighted by the population of all possible conformations; because of this, highly dynamic supramolecules are a particularly challenging target.

ECD spectra have also been used in the assignment of absolute configurations by a similar comparison of theoretical and experimental spectra.<sup>38</sup> However, the theoretical ECD spectrum involves the calculation of an excited state, which is, in general, less reliable and requires a much higher theory level and/or larger basis sets. Thus, the results for the theoretical ECD were often unsatisfactory and less conclusive with respect to the assignment of absolute configurations, but some recent work has shown that progress is possible in this area.<sup>39</sup> In contrast, the calculation of VCD intensities, only depending on the electronic ground state, is more accessible and reliably performed by conventional (and less time-consuming) DFT methods.

Instrumental and theoretical advances in VCD spectroscopy are enabling the elucidation of the absolute configuration and conformations of chiral organic and biological molecules in solution of even greater degrees of complexity. Indeed, it has been shown that the absolute configuration may be correctly determined by VCD methods in cases where conventional exciton coupling theory fails to do so.<sup>40</sup> Possessing a rigid skeleton and substituents, the absolute configurations of donor–acceptor [2.2]paracyclophanes **2** and **3** were analyzed by both VCD–DFT and ECD exciton chirality methods; see Figure 7.

In particular, on considering the coupling of the electronic transitions, the exciton chirality method predicts that the (–)-optical isomers of **2** and **3** should be (4*S<sub>p</sub>*,12*S<sub>p</sub>*)-**2** and (4*S<sub>p</sub>*,12*S<sub>p</sub>*)-**3**, respectively. However, combined VCD–DFT analysis (at the B3LYP/6-31G(d) level) suggests the same diastereomer for **2** but the opposite (4*R<sub>p</sub>*,12*S<sub>p</sub>*) diastereomer

for **3** (as determined by the matching of the experimental and theoretical VCD spectra in Figure 7). This prediction was indeed found to be the case on elucidation of the single-crystal X-ray structures. The failure of exciton coupling theory in this case is believed to arise from boat-type deformations and the electronic charge-transfer interactions between the aromatic moieties.

At the current time, the application of this technique to supramolecular systems is limited because of the difficulties of calculating all of the possible conformations. However, in view of the continued growth of computing power and the rapid development in theory, it is anticipated that such analysis will become increasingly important in chiral supramolecular chemistry.

### 3. Chirality Sensing and Induction in Convergent Host–Guest Assemblies

Chirality sensing within supramolecular systems may be grouped in numerous ways, for instance, according to the structure of their constituents, the form of chirality generated, or the application of the system; however, we shall now consider chiral assemblies whose intermolecular interactions are designed to be convergent and, thus, form discrete supramolecular species, in which one chiral component induces chirality in an achiral counterpart(s), and consequently how this may be used for chirality-sensing purposes.

#### 3.1. Target-Specific Sensors

One of the most common aims in this area is the rational design of a receptor for a specific guest that will allow chiral information to be transferred and subsequently “read-out”. An early example of such a bespoke supramolecular chirality-sensing system that also allows the study of the factors influencing the chirality induction is that of the axially linked 2,2′-biphenol-based system designed to interact with chiral cyclic diamines (Figure 8).<sup>41</sup>

Here, these 2,2′-biphenols are in a dynamic equilibrium between one of either two chiral conformations and are, consequently, racemic. The design of the host is rationalized, in that compounds **4** and **5** are predominantly used as the



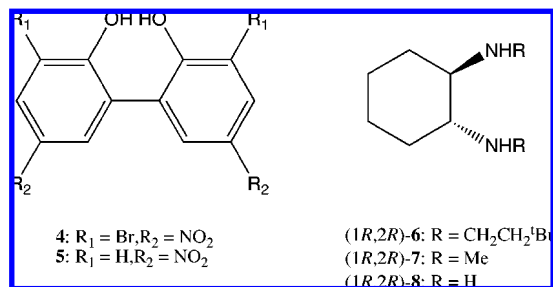
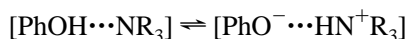


**Figure 8.** Structures of the biphenol hosts (**4**, **5**) and diamine guests (**6**–**8**).

nitro substituents that makes the transition moment larger and, thus, more conformationally sensitive, also moving it to a lower energy and so into a less occupied region of the spectrum. It is this sort of holistic consideration of the host sensor, binding, signal, and readout that is needed for smart design of practical sensors.

On addition of the bulky diamine (1*R*,2*R*)-**6** to **4**, the UV–vis peak at 310 nm is diminished and a new peak arises at 360 nm; concurrently, the CD spectrum becomes active, generating a negative bisignate signal that corresponds to an anticlockwise coupling of the electronic transitions and, thus, *M*-helicity (with the antipodal (1*S*,2*S*)-**6** inducing the signal of the opposite sign). This chiral complex was found from UV–vis and <sup>1</sup>H NMR experiments to possess a 1:1 stoichiometry with a high binding constant of >10<sup>6</sup> M<sup>−1</sup>. Thus, the binding of the two chirally orientated amino groups to the host's hydroxyls forces the two phenols into *M*-helicity as a result of the geometric and electronic requirements of the hydrogen bonding as well as the chiral steric interactions between the host and the guest. Further studies show a crucial dependence of the magnitude of chirality induction on the covalent structure and, thus, on the aforementioned steric effect of the guest. If the magnitude of the first Cotton effect is used as a measure of chirality induction, then we see the following tendency: R = CH<sub>2</sub>CH<sub>2</sub><sup>t</sup>Bu (**6**) (Δε = −1.1 cm<sup>−1</sup> M<sup>−1</sup>), R = Me (**7**) (Δε = 0.7 cm<sup>−1</sup> M<sup>−1</sup>), and R = H (**8**) (Δε = 0.4 cm<sup>−1</sup> M<sup>−1</sup>). This trend clearly shows that, in this case, the larger the size of the substituents at the binding site, the greater the steric clash with the racemic host and, thus, the greater the subsequent chirality induction. Such close steric contacts are confirmed by the intermolecular nuclear Overhauser effects (NOEs) between the <sup>t</sup>Bu groups of **6** and the aromatic ring protons of the host. Importantly, however, the largest substituent in **6** gives the opposite chirality to that induced by **7** and **8** of the same chirality. The mechanism by which such an effect arises was not discussed in this article, but detailed mechanistic studies of chirality inversion by substituent sizes in the case of a different supramolecular system can be found in section 6.

An interesting extension to this work is the observation of proton-transferred hydrogen bonding occurring at low temperatures and the effect that this has on the supramolecular structure and its chiroptical properties.<sup>42</sup> In this case, the hydrogen bonding is in a tautomeric equilibrium that can be represented by



which has been observed before<sup>43</sup> and, because of the presence of charged groups, is expected to significantly effect the geometric and energetic features of the hydrogen-bonding system.

Thus, on lowering the temperature of a solution of **6** and **4** in toluene to −80 °C, a new absorption band at 412 nm is observed that arises from the phenolate formed on proton transfer. The appearance of the new phenolate band was found to be critically dependent on the molar ratio of **6** and **4**, i.e., no band was observed for ratios of 0–1, but above 1.2 equiv of **6**, the new phenolate band was progressively more present. On determination of the stoichiometry of the new species by Job plot analysis, it was found to be 2:1 with respect to **6** and **4**. Accompanying the appearance of the new UV–vis band was a new bisignate CD signal in the same λ = 380–470 nm region; this displayed the same molar ratio dependence, with no optical activity for this region observed below 1 equiv of guest. For (1*R*,2*R*)-**6**, the new bisignate signal of the resulting supramolecular complex also exhibits negative chirality in the same manner as that observed for the 1:1 species.

Remarkably, it was found that, by manipulating the above equilibrium, chirality can be induced by addition of an *achiral* amine. From previous experiments, it was seen that, on cooling a 1:1 solution to −40 °C, no chirality induction at the phenolate band was observed. However, on addition of 1 equiv of the achiral diisopropylamine and subsequent cooling of the solution to this temperature, chirality induction at the phenolate region was observed as a result of the formation of a 1:1:1 ternary species with CD intensity up to half that observed for the 1:2 at −80 °C. It is surmised that, while the 1:1 species at −40 °C is chiral (as seen from weak CD signals at ca. 360 nm), the magnitude of the electrostatic charges at the amine and hydroxy groups is not sufficient to induce proton transfer; however, on addition of diisopropylamine, which binds to one of the amines of **6**, this enhances the positive charge of the nitrogen so to facilitate the proton transfer to the negative phenol oxygen and subsequent chirality transfer.

Recently, the rational design of sensors for sugar-based guests (simple sugars, saccharides, and carbohydrates) has been of increasing interest, driven particularly by greater appreciation of the importance of sugar-moiety recognition in biomolecular events such as cell–cell interactions and in carbohydrate transport and recognition.<sup>44</sup> Additionally, sensing of saccharides is crucial for some therapeutic approaches,<sup>45</sup> as well as in diagnostic contexts such as in the inability of current enzymatic protocols to sense unnatural L-glucose arising from blood vessel damage.<sup>46</sup> Inspired by the X-ray structures of saccharide–protein complexes showing the protein's binding of the sugar moiety by multiple hydrogen bonds,<sup>47</sup> a number of artificial sugar host molecules have been developed, though not necessarily with a specific consideration of the chirality of the system.<sup>48</sup>

In general, one of the most common approaches to the rational design of host sensors for the recognition and analysis of chiral guests is that of designing a size-specific cavity that is functionalized with groups that are complementary with the interacting groups of the guest (for example, for the most efficient hydrogen bonding), so providing an enthalpic driving force for binding, as well as chromophores that are brought into a chiral conformation by the transfer of chiral information from the guest by electronic and steric influences, thus giving access to techniques such as ECD, VCD, and CPF.

An elegant example of such a host designed for saccharide sensing is that of the bis[(pyrrolyl)ethynyl]naphthyridine (**9**) and bis[(indolyl)ethynyl]naphthyridine (**10**) systems developed by Chou, Chen, and co-workers (Figure 9).<sup>49</sup>

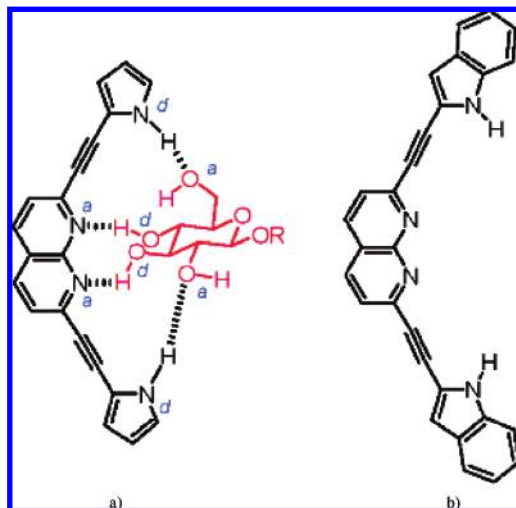


**Figure 9.** Structures of the intermolecular complex of **9** with alkyl  $\beta$ -D-glucopyranoside via quadruple hydrogen bondings (a) and **10** (b). Reprinted with permission from Fang, J.-M.; Selvi, S.; Liao, J.-H.; Slanina, Z.; Chen, C.-T.; Chou, P.-T. *J. Am. Chem. Soc.* **2004**, *126*, 3559. Copyright 2004 American Chemical Society.

In these systems, the molecular cleft is lined with a conjugated donor–acceptor–acceptor–donor moiety that is complementary to the acceptor–donor–donor–acceptor orientation of the OH groups of octyl  $\beta$ -D-glucopyranoside (**11**), which is the primary guest under study; as a result, it allows discrimination between this and other saccharide guests that have less favorable OH groups' orientations. On addition of 1 equiv of **11** to **9**, dramatic shifts of the pyrrole NHs ( $\Delta\delta = 1.4$  ppm) are observed that are found to arise from a 1:1 complex with a binding constant of ca.  $2 \times 10^4$  M $^{-1}$ , with  $\Delta H^\circ$  and  $\Delta S^\circ$  parameters of  $-51.4$  kJ mol $^{-1}$  and  $-91.1$  J mol $^{-1}$ , respectively, showing that this is a predominantly enthalpy-driven process that is able to overcome the considerable loss of entropy. UV–vis titrations of **9** and **10** showed clean isobestic points on addition of **11** at 415 and 426 nm, respectively. Subsequent fitting of the  $[A_o/(A - A_o)]$  absorbance data against the inverse concentration of **11** gave

clear linear fittings, further confirming the 1:1 host–guest ratio. The selectivity of the **9** and **10** hosts for various saccharide guests was investigated by comparison of their binding constants; see Figure 10.

The differences in affinities nicely illustrate how only small changes to the relative positions of the interacting groups of the host and guest dramatically affect the binding selectivity and, consequently, the degree of chirality transfer. The only difference between octyl- $\beta$ -D-glucopyranoside (**11**) and octyl- $\beta$ -D-galactopyranoside (**12**) is the orientation of the 4-OH group, which leads, however, to a 3-fold drop in the binding constant, presumably as this is now orientated in a less-available position for hydrogen bonding with **9**. The complete removal of one of the OH groups in octyl- $\beta$ -L-fucopyranoside (**13**) further decreases the binding constant, while that of the five-membered ring  $\beta$ -D-ribofuranoside (**14**) is again lower, which is perhaps not unexpected owing to its starkly different covalent structure. It should be noted that, while the absolute magnitudes of the binding constants were different for **9** and **10**, the relative trends between guests were the same, indicating that the same binding mechanism is active but with slightly different energies due to the electronic differences between the pyrrole and indole rings.

The CD experiments were carried out using **10** because of the higher extinction coefficient of indole compared to pyrrole, thus giving it a greater sensitivity. On addition of **11**, first positive and second negative (344 and 317 nm, respectively) bisignate Cotton effects are observed in the indole region of the spectrum (also, a positive Cotton effect arising from the naphthyl core is found at 442 nm). Using the exciton coupling theory approach, this result means that the main-axis transitions of the two indole moieties have been brought into a clockwise orientation by the binding of the chiral guest, and the assembly now possesses *P*-helicity. Analogously, binding of the enantiomeric **15** results in a mirror image CD spectrum and *M*-helicity. However, the difficulty in understanding the detailed chirality-induction mechanism is realized by comparing the *A* values of octyl- $\beta$ -D-glucoside (**11**) and octyl- $\beta$ -D-galactoside (**12**); even

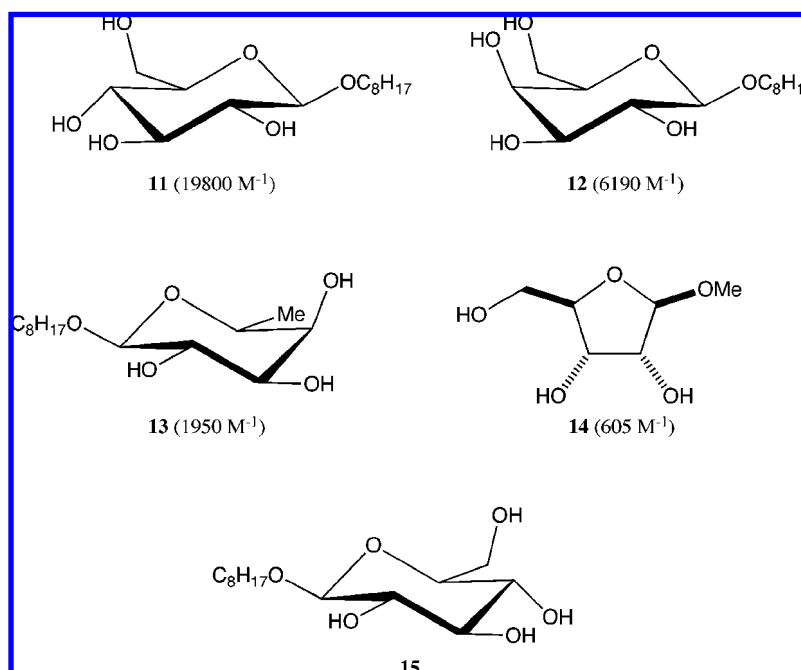


**Figure 10.** Structures of the saccharide guests (**11**–**15**) and their binding constants upon interaction with **9** (shown in brackets).

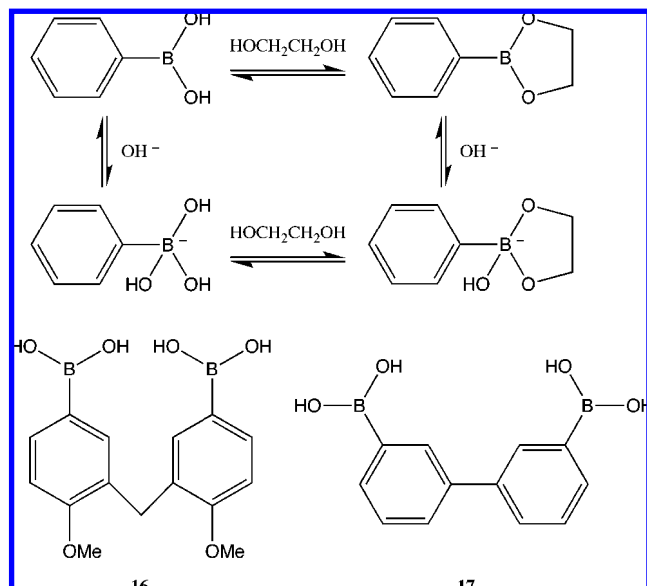


**Figure 11.** Schematic representation of the interactions between boronate and 1,2-diol (top) and structures of the diboronate hosts (**16** and **17**).

though they are both D-saccharides, they have opposite  $A$  values of  $-17\,400$  and  $+40\,100\text{ deg cm}^2\text{ dmol}^{-1}$ , respectively. Further, it may seem logical that the stronger binding constant would give rise to the greater magnitude of chirality induction; however, in this case, the binding constants for **11** and **12** with **10** are  $11\,700$  and  $7\,940\text{ M}^{-1}$ , respectively. Thus, this illustrates that, to fully understand the chirality-induction process, so to make a rational and robust supramolecular chirality sensor, all the influencing factors such as steric effects, solvent, structure, etc. must be considered; see section 5.

As seen above, it is the ability to utilize the association strength and geometric characteristics of noncovalent interactions that allows binding of guests in specific chiral conformations, leading to through-space coupling of the electronic transitions, which can then be interpreted on the basis of either positive or negative chirality by the exciton coupling method. However, one factor that places a severe restriction on the effectiveness of electrostatic noncovalent interactions is competition for the donor and acceptor sites by, typically, polar media or solvents acting as competitive binders; indeed, the addition of even small amounts of such a solvent can reduce the percentage of bound guest to unusable amounts. This is particularly so for water and, consequently, makes chirality sensing of important biological-based guests with a methodology that resembles their native environment problematic at best.

Such a scenario is found in the discriminatory sensing and analysis of mono- and disaccharides. Clearly, it is through the hydroxyl groups of the saccharides that interaction with the host must occur, but this interaction will be negligible in bulk aqueous solution because of the aforementioned solvent competition. To overcome this problem, Shinkai and co-workers utilized the reaction between diboronate acids and the 1,2- or 1,3-diol moieties of monosaccharides and disaccharides that results in the formation of boronate esters.<sup>50</sup> This is apparently a covalent process and is, thus, not susceptible to the water competition as a hydrogen-bond-based system would be. Crucially, though, it is a reversible process that occurs on a fast time scale and is considered to be noncovalent by the authors; see Figure 11.

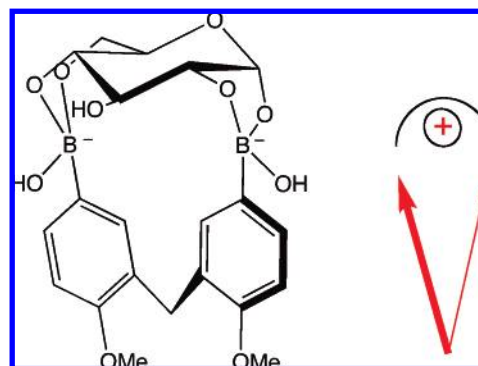


**Figure 12.** Schematic representation of the complex between **16** and D-glucose and the resulting clockwise orientation of the coupling transitions in **16**.

Compound **16**, which has two boronic acid groups that are at the correct distance (ca.  $6\text{ Å}$ ) and angle to interact with the 1,2-diol and 4,6-diol moieties in monosaccharides, was shown to form 1:1 complexes with glucose, mannose, galactose, and talose, which were CD active and for which the chirality could be rationalized by the bisignate Cotton effects observed. D-Glucose gave positive chirality, with L-glucose showing a corresponding negative chirality; all other D-saccharides gave positive chirality, except D-galactose, which was negative; see Figure 12.

The origin of the induced chirality of these saccharides was elucidated by <sup>1</sup>H NMR and CD techniques to arise from the linking of the two molecules by the formation of the aforementioned boronate esters between the two boronic acid groups of the host and the 1,2-diol and 4,6-diol moieties of the guest. It is then the transfer of chirality from the chiral saccharide part of the macrocycle to the achiral host that induces a unidirectional twist between the two phenyl groups from which bisignate Cotton effects are observed; see Figure 12.

The nature of the chirality-induction process in these macrocycle structures was further investigated. Studies that looked at the effect of blocking, removing, or inverting the optimal orientation of the saccharides' OH groups that interact with the boronic acid showed that any of these manipulations to the covalent structure resulted in either a reduction in the magnitude of the induced chirality or a CD silent spectrum if a 1:1 macrocycle cannot be formed due to the incorrect relative orientations of the boronic acid and the OH groups. For instance, fructose has a 1,2-diol pointing upward and a 3,4-diol pointing downward, making it geometrically impossible to form two boronate esters in a 1:1 complex, and is correspondingly CD inactive. This phenomenon was found to be due to the formation of a 1:2 complex resulting in each saccharide molecule being bound by only a single bond to **16**. Consequently, instead of its chirality being effectively transferred to the achiral host through the "two-point" interaction of the macrocycle, the "one-point" attached D-galactose molecules are more-or-less free to rotate in space and, thus, rotate away from the host, so making the mechanism for chirality transfer less efficient.

The host molecule **17** was designed along the same fundamental principles, but with the sensing of disaccharides in mind. Here, the boronic acid moieties are further apart (between  $7.4$  and  $9.2\text{ Å}$ ) and are well-matched to the distance between the 1,2-diol and the 4'-OH and 5'-OH groups of disaccharides. For D-maltose, first negative and second positive bisignate Cotton effects were observed, which



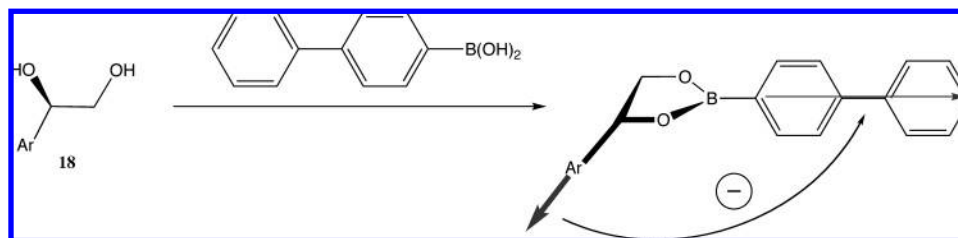


**Figure 13.** Interaction of chiral 1-arylethane-1,2-diols (**18**) with 4-biphenylboronic acid and the resulting complex exhibiting an anticlockwise orientation of the coupling transitions in the case of the (*R*)-**18**.

correspond to an anticlockwise orientation of the electronic transitions of **17** in the complex. However, D-cellobitose and D-lactose induced positive and negative chirality, respectively, while D-saccharose showed no CD signal at all due to the more distant 1,2-diol and 4'-OH and 5'-OH groups of this saccharide.

This work, particularly for disaccharides, shows that, while the approach of using the formation of boronate esters is successful in both allowing the host–guest complexation of saccharides in water and with subsequent chirality induction (with structure dependence), the specific chiral outcome is less predictable.

The approach for developing chirality-sensing systems via the formation of boronate esters was further pursued by the group of Rosini, who used the formation of structurally well-defined assemblies between chiral 1-arylethane-1,2-diols (**18**) and 4-biphenylboronic acid to produce a system that was consistently able to predict the guest chirality, albeit with structurally more simple guests than those studied by Shinkai; see Figure 13.<sup>51</sup>

It was consistently found that **18** gave a negative couplet for *R* absolute configuration at C<sub>1</sub>, with positive chirality observed for their (*S*)-antipodes. This result arises from two main factors: (i) the structural rigidity imposed on the system by the five-membered ring of the boronate ester, along with the fact that the guests are themselves quite inflexible, keeping the two long-axis transitions in a consistent conformation between the guests; and (ii) the rotation of the molecules on either side of the five-membered ring is along the long transition axis (i.e., the C<sub>1</sub>–C<sub>4</sub> axis of the phenyl rings), which also keeps the system conformationally consistent; additionally this has the effect that the transitions perpendicular to the long axis do not contribute to the CD spectra, as they are cancelled through rotational averaging.

Saccharide sensing continues to be of significant interest, with the sensors increasing in complexity and sophistication. A recent example is found in the work of Reinhoudt and co-workers in which they report the first example of a saccharide sensing system in which the sensor itself is a supramolecular assembly.<sup>52</sup> The system is based on a series of tetra-rossette assemblies comprising 15 components formed from 3 calixarene tetramelamines (**19**) and 12 barbituric acid (**20** and **21**) or cyanuric acid (**22**) derivatives, and it possesses 72 cooperative hydrogen bonds (Figure 14). This type of supramolecular assembly has been extensively studied by this group,<sup>53</sup> although in contrast to the saccharide sensing systems discussed previously, this approach is studied in CHCl<sub>3</sub> so to maintain the integrity of the hydrogen bond network.

Thus, in the absence of any chiral influence, the tetra-rossette **19**<sub>3</sub>·(**20**)<sub>12</sub> assembly exists as a racemic mixture of (*P*)- and (*M*)-enantiomers. It was found that, on addition of 10 equiv of *n*-octyl-β-D-glucopyranoside (**23**) to a CHCl<sub>3</sub> solution of

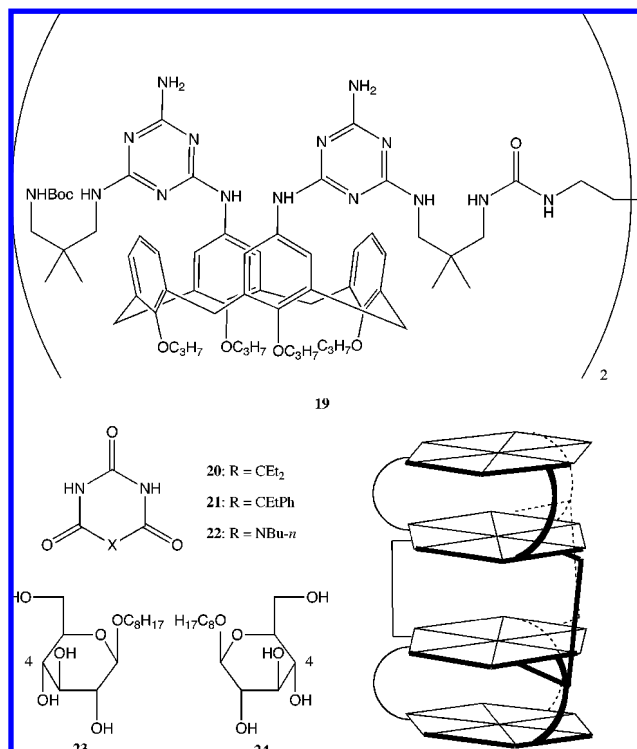


**Figure 14.** Structures of the tetra-rossette building blocks (**19**–**22**) and saccharide guests (**23**, **24**), and schematic representation of the tetra-rossette assembly.

**19**<sub>3</sub>·(**20**)<sub>12</sub>, the appearance of new <sup>1</sup>H NMR signals for the NH group of a urea moiety at a Δδ = 0.05 ppm from the original indicates the preferential inclusion of **23** into one of the tetra-rossette isomers (*P* and *M*), so forming an excess of one diastereomeric complex with a 1:1 stoichiometry as determined by Job plot analysis. Crucially, these signals were only seen for groups on the second and third floors of the assembly, showing that **23** is included solely in-between these floors. Additional computational studies reveal that the hydroxyl group at the 4-position of **23** interacts with the urea carbonyl group of the host and that, for the mismatch enantiomer **24**, its alkyl chain is orientated in a way that results in unfavorable steric hindrance that disrupts the hydrogen-bonding network of the rosette's second floor. This induction of diastereomeric excess (de) into the system means that it is now optically active and can be analyzed by CD methods. This optical activity is seen in the Cotton effects at ~290–310 nm, i.e., a negative Cotton effect for **23** binding and positive for **24**, revealing *M*- and *P*-helicity, respectively. The binding constants for these two guests were found to be ~20 M<sup>-1</sup>, and because the *P* and *M* forms are in dynamic equilibrium, this leads to a ca. 9% de in the helical conformation favored by the guest under consideration. If such systems are to become useful sensors, then they must



show selectivity, which is indeed seen here, as it is found that the  $\alpha$ -isomer of **23** does not show any binding to the host. Another approach for increasing the binding (and, thus, chirality transfer) discrimination of the saccharides is to preinduce the helical chirality in the host. This approach is achieved here by the covalent appending of (*R*)-phenylethylamine to the calixarene components of the host, so inducing *M* helicity. Thus, on addition of the mismatch saccharide guest **23**, no changes in the  $^1\text{H}$  NMR spectrum were observed, while **24** resulted in shifts of the second and third floor urea NH groups of  $\Delta\delta = 0.1$  ppm. Interestingly, on addition of **24**, no further changes to the CD spectrum were found, showing that the steric host–guest interactions arising from the guest binding do not further enhance the unidirectional twist, presumably, as the additional steric interactions are not sufficient to overcome the internal strain already present in the system.

### 3.2. Induction via Cavity Encapsulation

The binding of saccharides and the sensing of their chirality has also been targeted via guest encapsulation in an achiral cavity and subsequent chirality transfer. One elegant approach is that of the systems devised by Inouye et al.<sup>54</sup> On the basis of previous work in which tris(ethynylpyridine) hosts were used as receptors in which the chiralities of ribofuranosides, deoxyribofuranosides, and glucopyranosides were sensed,<sup>55</sup> they used the ethynylpyridine unit as a starting point in the synthesis of a poly(*m*-ethynylpyridine) polymer using the Sonogashira acetylene coupling method,<sup>56</sup> resulting in a clean polymer **25** that comprised at least 72 pyridine moieties with a molecular weight of ca. 4500. From NMR analysis, free **25** in chloroform was found to exist in a disordered conformation and was shown from the concentration-independent UV–vis maxima (275 and 323 nm) to not undergo any intermolecular association at least up to  $\leq 1.0 \times 10^{-3}$  M.

On incremental addition of a  $2.0 \times 10^{-3}$  M solution of **26** to a  $1.0 \times 10^{-3}$  M solution of **25**, the UV–vis absorption intensities at 275 and 323 nm decreased with increasing **26** concentration as a result of the formation of a well-ordered helical conformation encapsulating the saccharide guest; see Figure 15.

The nature of the chirality induction and how the achiral host senses differently the chiral structure of a range of saccharides (Figure 16) was investigated by CD analysis. On addition of a  $2.0 \times 10^{-3}$  M solution of **26** to a  $1.0 \times 10^{-3}$  M solution of **25**, an induced CD spectrum with multiple Cotton effects was observed in the polymer absorption region with the maximum intensity (negative) at  $\lambda = 340$  nm. The generation of an opposite positive Cotton effect at 340 nm on the addition of the antipodal saccharide of **26** showed that the induced chirality indeed originates from chirality transfer from the saccharide to the polymer. Chirality was also induced by similar saccharides but with differences in the Cotton effects due to their differing structures; i.e., **27** also gives rise to a negative but weak Cotton effect at ca. 340 nm, while **28**, **29**, and **30** result in positive signals. The chirality-transfer mechanism active here is via the hydrogen-bonding interaction between the saccharide's OH groups and the pyridines of the polymer; this supposition is confirmed by the CD silence on addition of **31**, which is unable to form hydrogen bonds because of the blocking methyl groups.

A more detailed understanding of the supramolecular chirality-transfer process was obtained by comparison of the

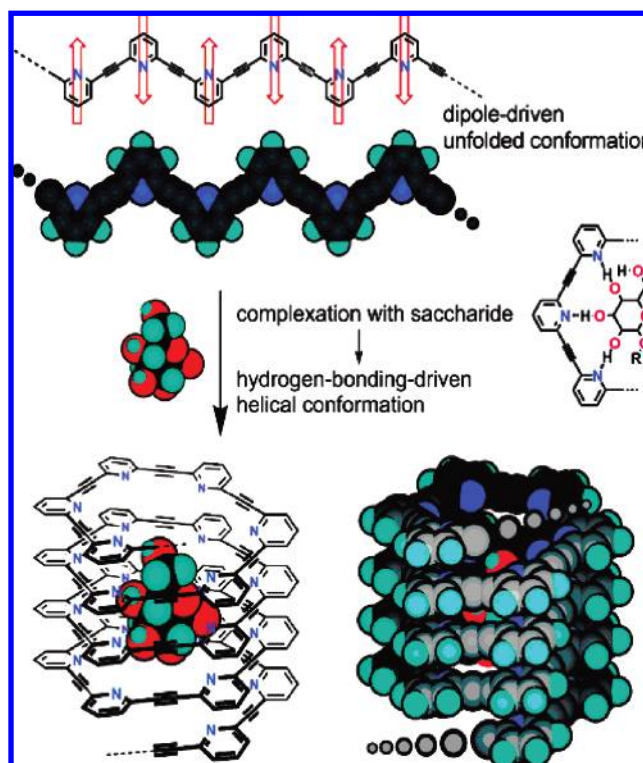


**Figure 15.** Conformational change of **25** upon complexation with a saccharide. Reprinted with permission from Inouye, M.; Waki, M.; Abe, H. *J. Am. Chem. Soc.* **2004**, 126, 2022. Copyright 2004 American Chemical Society.

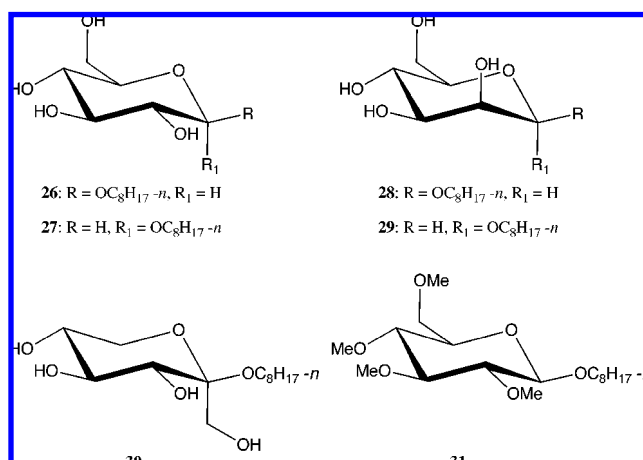


**Figure 16.** Structures of the saccharide guests (**26**–**31**).

degree of chirality induction with the length of the host and, thus, the extent of its ability to adopt a helical structure. It was found that six ethynylpyridine units are needed to adopt one helical turn and that intramolecular  $\pi$ – $\pi$  interactions occur at oligomeric lengths greater than the 12-mer. Further chirality induction only occurred for oligomers greater than a 12-mer; thus, the first chirally active species is the 18-mer, indicating that three complete helical turns are required to successfully encapsulate the saccharide guest and, thus, allow chirality transfer (the binding constant for the 24-mer and **26** was found to be  $(1.2 \pm 0.4) \times 10^3 \text{ M}^{-1}$ ). Obtaining a 1:1 stoichiometry from the associated Job plot disproved the presence of additional intermolecular chiral influences at this concentration range.

A less recent, but successful, approach to utilizing supramolecular systems based on the resorcinol–dodecanal cy-

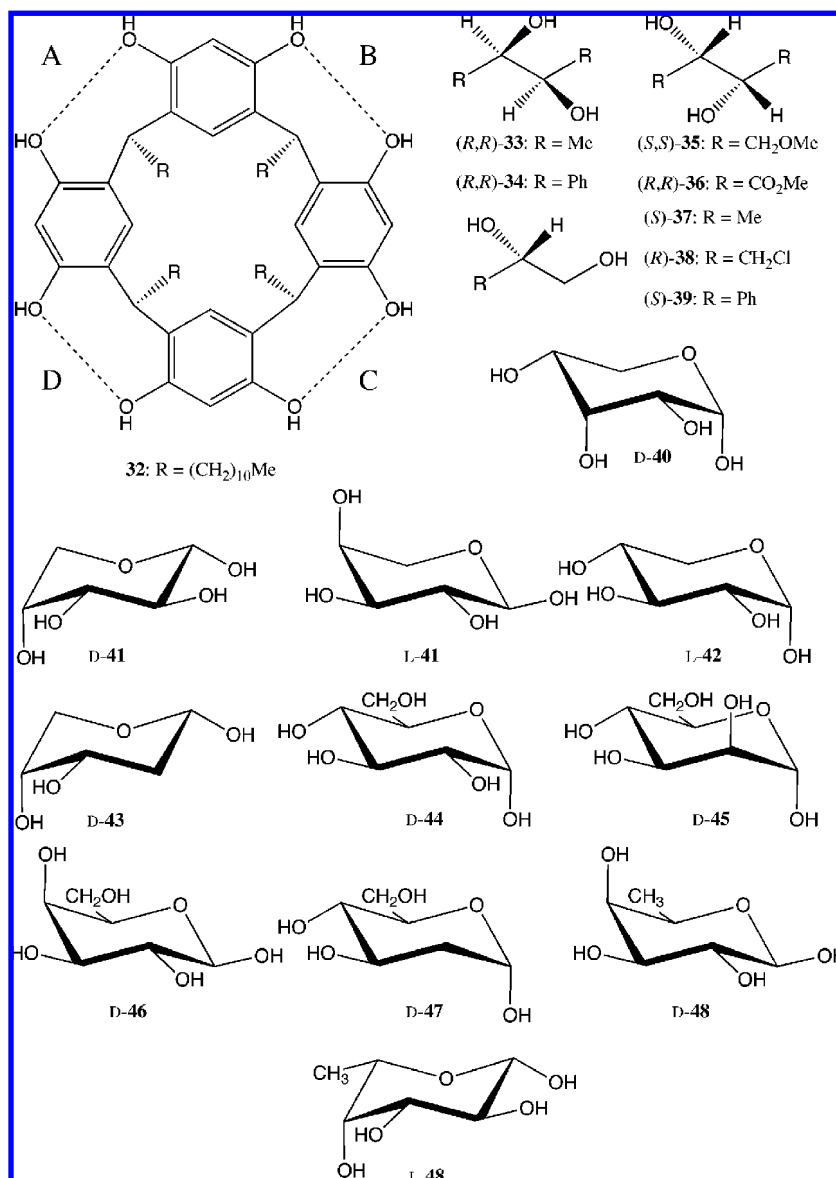


**Figure 17.** Structures of the cyclotetrameric host (**32**) and various guests (**33–48**).

clotetramer **32** for chirality sensing of diols and saccharides (Figure 17) by inclusion-type guest binding can be found in the work of Aoyama and co-workers.<sup>57</sup>

The structure of **32** is that of a bowl whose conformation and structural rigidity arise from the four concerted intramolecular hydrogen bonds between the *ortho*-hydroxyl substituents. These alcohol functionalities also act as the binding sites for the guests and for *cis*- and *trans*-1,2-cyclohexanediol. The mode of interaction was found to be via multiple hydrogen bonding to just one of the four binding sites between adjacent phenyl rings (A, B, C, and D), and not between two of these sites, as might be expected.<sup>58</sup> This consideration is extended to the acyclic diols (**33–39**), and as a result, it can be seen that the guest's OH groups must adopt a *syn-gauche* conformation in order to maximize these hydrogen-bonding interactions; it is found that this is achieved when the guests are in a pseudoequatorial (E) or pseudoaxial (A) conformation. However, on consideration of steric constraints of these two conformations, it is found that the pseudoaxial conformation results in unfavorable steric clashes with the hydrogen-bonding site in comparison to the pseudoequatorial conformation (Figure 18), and thus,

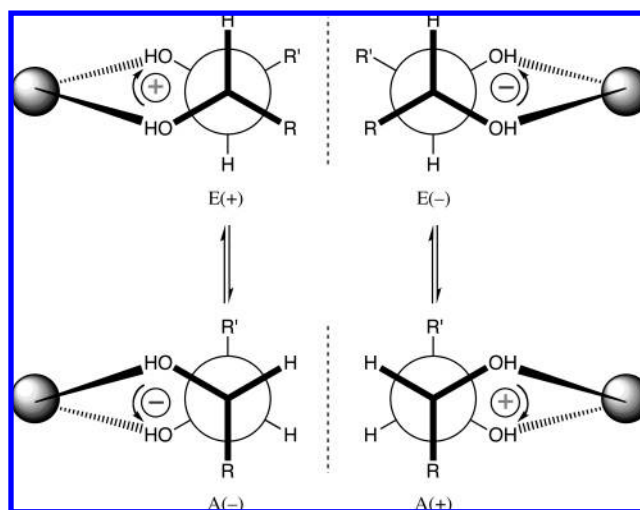


**Figure 18.** Host-guest binding modes and directions of chirality of the two C–OH bonds.

in general, it is the pseudoequatorial conformation that is favored.

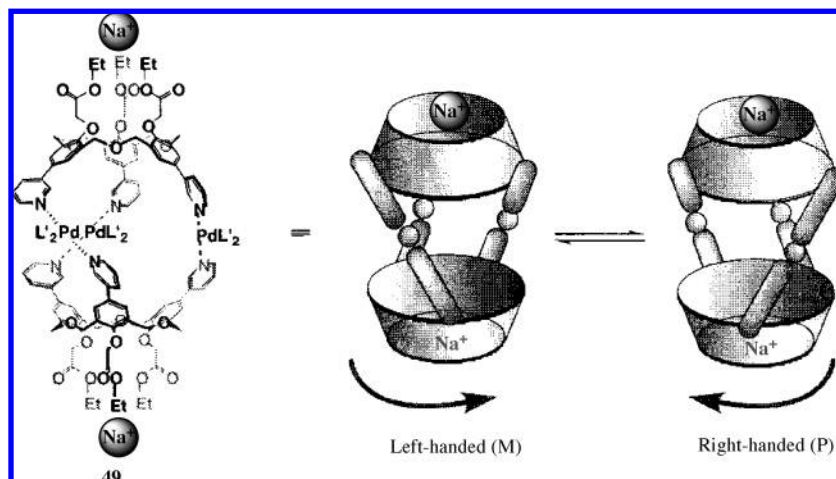


**Figure 19.** Structure and enantiomeric equilibrium of **49**. Reprinted in part with permission from Ikeda, A.; Udzu, H.; Zhong, Z.; Shinkai, S.; Sakamoto, S.; Yamaguchi, K. *J. Am. Chem. Soc.* **2001**, *123*, 3872. Copyright 2001 American Chemical Society.

From Figure 18, the orientation between the two hydroxyl binding groups can be seen, either clockwise (termed positive) or anticlockwise (termed negative); thus, there are four possible chiral conformations E(+), E(−), A(+), and A(−). When the expected chiral conformation is compared to the chirality produced in the real system, as defined by the first Cotton effect, a correlation is found: those conformations expected to be positive give rise to negative chirality in the supramolecular system, and those thought to be negative give positive supramolecular chirality. This is opposite to that expected from exciton coupling theory.

Although the rationale for this opposite-sense relationship is not addressed by the authors, it should be considered that the bisignate signal in the CD spectra originate from the aromatic region and, as such, from the resorcinol host and not the guest itself. Thus, it may be speculated that the mechanism by which the diol guest transfers its chirality to the host results in the sum of the orientations of the four aromatic moieties being opposite that of the guest.

A second class of guests studied was the sugars **40–48**. These are found to interact with **32** in a different manner to the aforementioned diols, in that they simultaneously bind to two of the adjacent binding sites (A and C or B and D) through the cis 1-OH and 4-OH groups<sup>59</sup> and not just to one site. The crucial structural feature of the guest that dictates the sense of chirality transfer for these guests is the conformation of the pyranose ring, either *C1* or *1C*. The equilibrium between these gives the following relation for the guests, i.e., D-guest-*C1* and L-guest-*1C* are enantiomers (as are D-guest-*1C* and L-guest-*C1*). The outcome of the subsequent host–guest interactions is that guests with a preferential *C1* conformation give rise to positive chirality and those with preferential *1C* give a negative chirality, which is not dependent on the guest's D/L configuration. The observed chirality induction arises from the asymmetric deformation in the relative orientations of the host's four aromatic groups, although the exact geometry and detailed mechanism has not been determined.

Though the above-mentioned work is now more than 15 years old, the study and application of calixarenes and their derivatives to supramolecular chirality have continued to evolve, producing more complex and elegant systems.<sup>60</sup> Such an example is found in the recent work of Shinkai and co-workers.<sup>61</sup> Here, we see the formation of a molecular capsule that consisted of three components. First, Na<sup>+</sup> ions bind to

the lower rim of the calix[3]arene, which brings it into a bowl conformation; second, these preorganized species then dimerize via Pd<sup>II</sup> bridges formed between the three 3-pyridyl groups of each calix[3]arene (Figure 19). The cavity formed in **49** is quite substantial, being able to successfully bind [60]fullerene.<sup>62</sup>

As can be seen in Figure 19, this capsule **49** exists in a dynamic equilibrium between two enantiomers (*P* and *M*). The potential for such a unidirectional screw sense is due to the twists of the 3-position substituted pyridines arising from minimization of the internal steric strain upon capsule formation and is not found for the analogous 4-pyridine system. Further confirmation of the existence of two enantiomers was provided by measuring the NMR spectra in the presence of the chiral shift reagent, Pirkle's reagent (*R*)- or (*S*)-2,2,2-trifluoro-1-(9-anthryl)ethanol, resulting in a splitting of the pyridyl's 6-H into two peaks of 1:1 intensity.

To induce chiral selectivity, (*S*)-2-methylbutylammonium triflate (*S*-**50**) was added as a guest, to form two diastereomers *P*-**49**·*S*-**50** and *M*-**49**·*S*-**50**. Subsequent NMR studies showed that the guest is indeed included inside the cavity and that the complexation–decomplexation is slow on the NMR time scale, although the de could not be determined directly from the NMR spectra due to the small induced chemical shifts, because the guest does not exert a strong shielding/deshielding effect. However, on the addition of the aromatic Pirkle's reagent, a de of 40% was determined.

Further, the CD spectra of the **49**·*S*-**50** assembly was obtained, resulting in a first negative–second positive Cotton effect, with a crossover point at 280 nm; however, determination of the helicity (*P* or *M*) of the de complex was not achieved because of the more complicated nature of this chromophoric system.

An additional class of supramolecular system in which the transfer of chirality may be observed to occur via an encapsulation process is rotaxanes. These are composed of three basic components: a macrocyclic ring host, a linear thread guest, and two bulky stopper groups attached to the thread, which (if large enough) precludes decomplexation (dethreading) of the guest, resulting in a mechanically locked species; see Figure 20. While the host and guest are not in equilibrium in the conventional sense observed for other supramolecular systems (i.e., the equilibrium between the bound and unbound states), neither are they covalently attached, and as such, they are in equilibrium between the



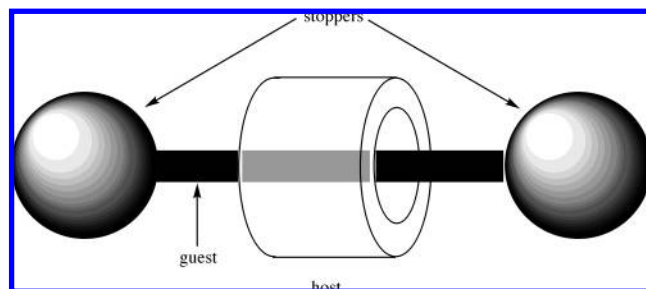


**Figure 20.** Schematic representation of the rotaxane structure.

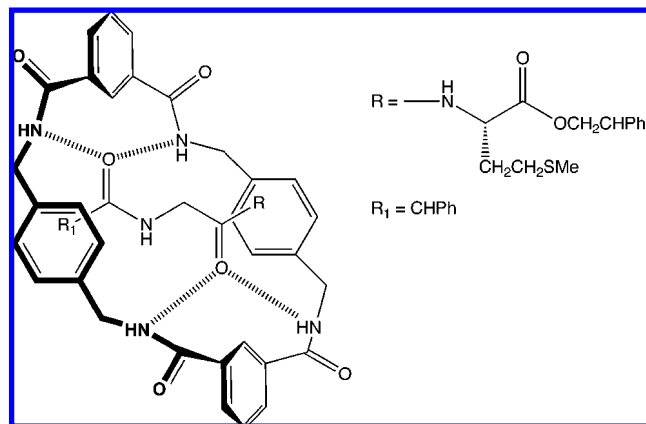


**Figure 21.** Structure of rotaxane **51**.

various conformations possible. Thus, these conformations, and so the rotaxane's structural and chiroptical characteristics, can be altered by manipulation of the intermolecular non-covalent interactions between the host and the guest.

The supramolecular nature of these systems has been extensively investigated, particularly by the groups of Stoddart<sup>63</sup> and Vögtle.<sup>64</sup> The aspect of chirality has also been considered, with studies dealing with planar chirality,<sup>65</sup> catalysis,<sup>66</sup> and separation<sup>67</sup> being reported. Recent work by Leigh and co-workers on peptide-based rotaxanes with chirality that is "on-off" switchable and invertable and with controllable magnitude of intermolecular interactions via solvent and temperature manipulation is particularly instructive.<sup>68</sup> The essential structures of the mechanically interlocked rotaxanes are shown in Figure 21 and are formed via a hydrogen bond-directed five-component synthesis.

Initially, it is crucial to note the absence of any chirality in the aromatic regions of the individual host and thread in **51**. This effect is straightforward for the host because it possesses no chiral centers or other asymmetry elements. On the other hand, the threads all possess a point-chirality center; however, because of the considerable distance between this center and the aromatic moieties, there is no asymmetry transfer between them, resulting in a CD silent aromatic region. However, on the formation of the rotaxanes, this region becomes CD active, with its sign and magnitude mutable, as mentioned previously.

First, the effect of changing of the environment via solvent composition was investigated. This was undertaken by varying the ratio of  $\text{CHCl}_3$  (non-hydrogen-bond competitive) to MeOH (hydrogen-bond competitive) in a mixed-solvent approach; see Figure 22a.

In pure  $\text{CHCl}_3$ , a strongly negative Cotton effect is seen at ca. 245 nm (below 230 nm, the solvent absorbs strongly); on stepwise addition of MeOH, the Cotton effect is seen to reduce in intensity and finally become positive.

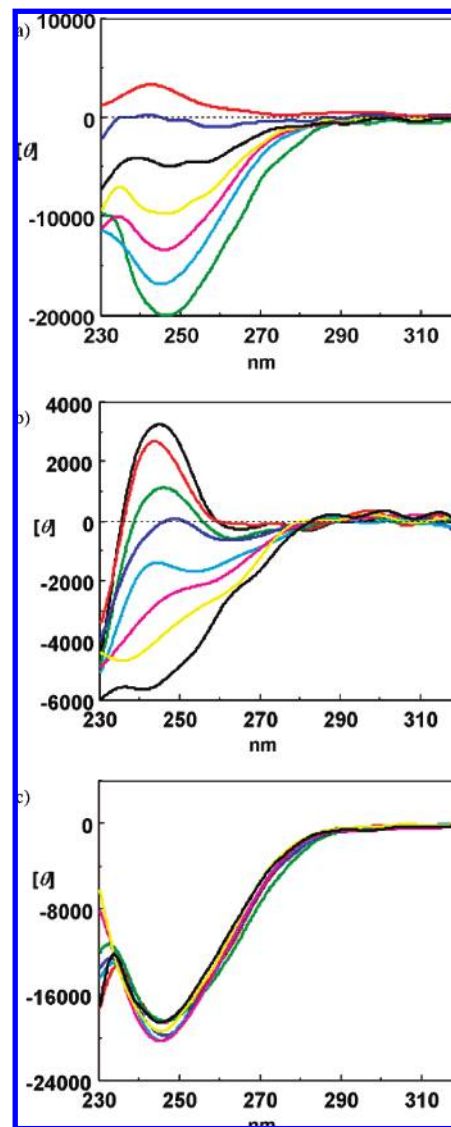


**Figure 22.** Solvent-dependent (a) and VT (b, c) CD spectra of **8**: (a) in  $\text{CHCl}_3$  (green), 1:1  $\text{CHCl}_3/\text{MeOH}$  (cyan), 2:3  $\text{CHCl}_3/\text{MeOH}$  (magenta), 1:2  $\text{CHCl}_3/\text{MeOH}$  (yellow), 1:5  $\text{CHCl}_3/\text{MeOH}$  (black), 1:10  $\text{CHCl}_3/\text{MeOH}$  (blue), and MeOH (red); (b) in MeOH and (c) in  $\text{CHCl}_3$  at 263 K (black), 273 K (red), 283 K (green), 293 K (blue), 303 K (cyan), 313 K (magenta), 323 K (yellow), and 333 K (black). Reprinted with permission from Asakawa, M.; Brancato, G.; Fanti, M.; Leigh, D. A.; Shimizu, T.; Slawin, A. M. Z.; Wong, J. K. Y.; Zerbetto, F.; Zhang, S. *J. Am. Chem. Soc.* **2002**, 124, 2939. Copyright 2002 American Chemical Society.

As a point of zero chirality induction occurs, it is noted, as stated by the authors, that the system may switch off and on in either a positive or negative direction. However, of perhaps greater insight is the observation of how the CD intensity varies in a nonlinear manner with solvent composition. In comparison to pure  $\text{CHCl}_3$ , a 1:1 mixture with MeOH results in only a 15% reduction in CD intensity, yet the 17% change on going from 87% MeOH to pure MeOH (which are almost identical in bulk polarity and dielectric constant) results in a switch from  $-5\,590$  to  $+3\,390 \text{ deg cm}^2 \text{ dmol}^{-1}$ . It is likely that this nonlinearity arises from differential degrees of specific interactions between the individual solvents and the rotaxane. This proposition is further supported by comparison of the variable-temperature CD spectra obtained in pure  $\text{CHCl}_3$  and MeOH (see Figure 22 parts b and c). In  $\text{CHCl}_3$ , it can be seen that there is



essentially no change over the temperature range studied, due to the fact that  $\text{CHCl}_3$  does not effectively compete for the rotaxane's hydrogen bonding. In MeOH, at higher temperatures, a strong negative Cotton effect is observed; however, lowering the temperature causes a reduction in the negative intensity, until it goes through zero intensity at ca. 293 K, with further decreases in the temperature giving rise to a strongly positive signal. The rationale of this is that, at lower temperatures, MeOH can form strong interactions with the rotaxane's hydrogen-bonding sites, but as the temperature increases and the entropy term plays a more important role in the complexation thermodynamics, MeOH molecules are released (desolvated) to obtain more freedoms and to give a positive entropy change, thus giving rise to the observed chirality reduction—inversion phenomenon. Subsequent analysis of the structure by computational and X-ray methods reveals an interesting structural origin of the chirality in the aromatic region, in that the chirality originates from the phenyls of the two stopper groups. One of the isophthaloyl units of the macrocycle is found adjacent to the hydrogen of the chiral center, which is then locked in place by four intercomponent hydrogen bonds (in  $\text{CHCl}_3$ ) and, consequently, restricts the motional freedom of the stoppers in a chiral manner. This is elegantly shown by replacing the four stopper phenyls with cyclohexane moieties, which results in a CD silent aromatic region. Removal of the macrocycle aromatic groups results in a shift of the CD signal to a higher energy but not its disappearance; thus, it is shown, unexpectedly, that, although these aromatic groups contribute to the energetics of the system, they do not contribute to the observed CD signal.

#### 4. Enantiodiscriminating Host–Guest Systems

In comparison to the previous sections here, we are not primarily concerned with the generation of chirality in an intrinsically achiral molecule(s) but rather with the discrimination between two enantiomers by a supramolecular system. This effect is typically achieved by different asymmetric 3D arrangements of the interacting groups (hydrogen bond, aromatic, charge–charge, hydrophobic, steric interactions, etc.) in space between a chiral host and each of the two different enantiomeric guests, thus forming diastereomers. It is conventional wisdom that, in supramolecular enantiodiscriminating systems, the minimum requirement for achieving enantiodiscrimination is the presence of three-point intermolecular interactions between the host and the guest, although the question of what is the ideal number of interacting sites in an enantiodiscriminating supramolecular system is more difficult to answer and rarely discussed.

##### 4.1. Insights into Controlling Parameters in Enantiodiscriminating Systems

An instructive example of an enantiodiscriminating host–guest system in which the host comprises a number of rationally designed functional moieties is found in the work of Schrader and co-workers, which centers on the application of bisphosphonate esters as the principle binding moiety for amino alcohols and diammonium guests.<sup>69</sup> In the case where the bisphosphonate esters are attached to a spirobisindane skeleton, two distinct and preorganized hosts are attained: (i) cleftlike **52**, which provides an unhindered approach for the guest's cationic groups to the phosphonate groups of the

host, and (ii) **53** in which the cleft is blocked by the introduction of a mesitylene spacer (Figure 23).

The bulkiness of the mesitylene group is desirable because its steric constraints preclude rotation within the cleft and, as such, give greater chemoselectivity in the guest binding, which is crucial to the host's enantiodiscriminating ability. In terms of chemoselectivity, it is the matching of the distances between the guest's two ammonium groups and the host's phosphonates that dictates the binding efficiency. For host **52**, guests whose  $\text{N}^+\cdots\text{N}^+$  distance is two or three atoms (diaminocyclohexane and His, respectively) form 1:1 complexes, while for host **53**, they are only able to form 2:1 species because they are too short to span the bulky mesitylene group. Longer guests, such as Lys and Arg (five and six atoms, respectively), form 1:1 species with **53**. It is found that, for these 1:1 complexes, modest enantioselectivity is obtained (17 and 33% for Arg and Lys, respectively). It is postulated that the mesitylene group is crucial to this effect because it provides a critical third point of interaction to facilitate the enantiodiscrimination. The origin of the interaction is suggested to be hydrophobic in nature; however, electrostatic effects such as  $\text{C}-\text{H}\cdots\pi$  interactions also cannot be ruled out.

This complex interplay between various factors that control the binding and enantiodiscrimination is, to a greater or lesser degree, present in all such supramolecular systems. Consequently, the rational application of these effects leading to the modification of a system may result in enhanced enantiodiscriminating properties. This situation can be seen in the manipulation of the host's flexibility, size, and number of interacting sites in the imidazole-containing cyclophane receptors of You et al., which were used to bind a series of methyl ester derivatives of amino acids (Figure 24).<sup>70</sup>

Clearly, acyclic **54** is more flexible than **55–58** and, as a result, lacks the degree of preorganization that is often an important aspect in host–guest systems and likely suffers from a significant loss of entropy on binding. This loss makes the association process less favorable in comparison to those of macrocyclic **55–58**; indeed, the reported binding constants for **54** are  $<100 \text{ M}^{-1}$  for the D- and L-enantiomers of Phe-OMe, while those for **55–58** are typically 3–5 times higher. Further, it is important to consider how the comparative openness of the macrocyclic structures of the hosts affects the accompanying  $K_D/K_L$  ratio. For **54**, the  $K_D/K_L$  ratio is 1.12, while for **55**, **56**, **57**, and **58**, the values are 3.33, 2.33, 2.00, and 1.40, respectively (the mean magnitude of the binding constants for the enantiomeric pairs also falls in this order). In comparison to **54**, the alkyl linker of **58** closes the open structure, thus reducing flexibility and enhancing the preorganization, although the  $K_D/K_L$  ratio is not vastly different. In **57**, the 1,4-substituted phenyl group not only is more rigid in comparison to **58** but also its quadrupolar electrostatic distribution opens up the potential for intermolecular interactions such as  $\pi-\pi$ , cation– $\pi$ , and  $\text{CH}-\pi$  with the guest, which leads to the observed enhancement of the  $K_D/K_L$  ratio. This result again highlights that, for enantiodiscriminating purposes, having enough stereomatching interaction sites between the host and the guest (at least three) is a crucial factor. Moving to the 1,3-substituted phenyl-linking group in **56**, the further increase can likely be attributed to a reduced cavity size leading to a better fit, thus making the enantiodiscriminating complement of interactions more effective. Finally, the addition of a heteroatom in **55** as the 1,3-substituted pyridine results in a marked jump in

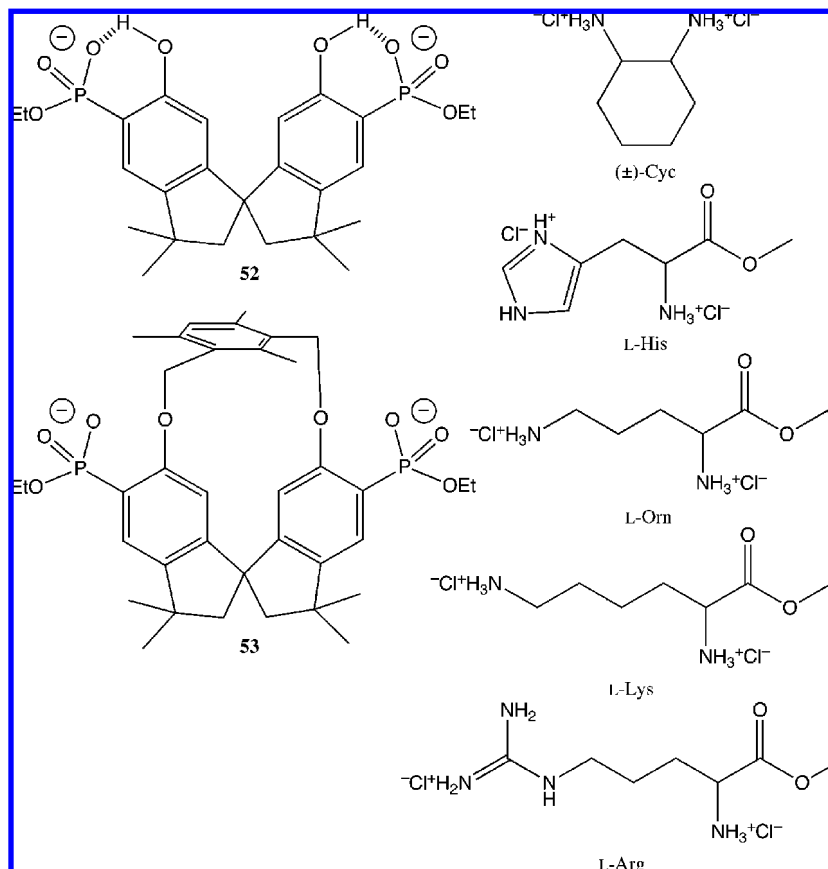


**Figure 23.** Structures of the hosts (52 and 53) and corresponding guests.

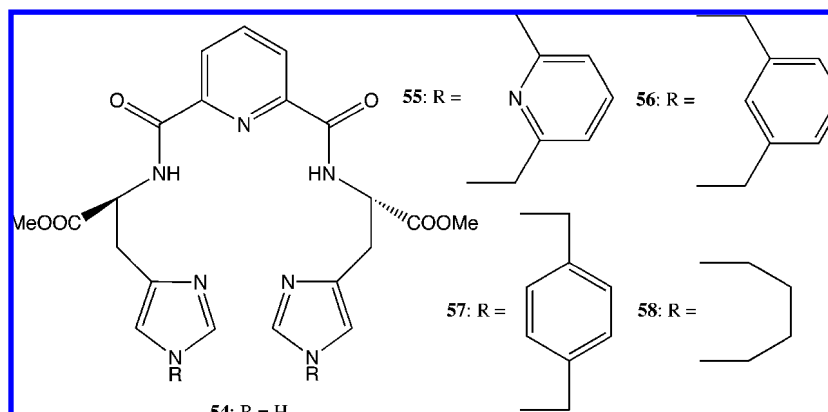


**Figure 24.** Structures of the hosts (54–58).

the  $K_D/K_L$  ratio to 3.33, although whether this is due to a change in the charge distribution in the  $\pi$  systems or to a specific interaction of the nitrogen is unclear but again highlights the need to optimize the intermolecular interactions. Further confirmation of the effect of intermolecular interactions is found in the higher binding constants and  $K_D/K_L$  ratios of guests that contain aromatic side chains and, thus, have the potential for  $\pi$ – $\pi$  interactions (Trp-OMe and Phe-OMe) in comparison to those that contain aliphatic side chains (Ala-OMe, Val-OMe, and Leu-OMe).

The facile detection of chirality and discrimination between enantiomers is a fundamental function of a chirality sensor and is conventionally achieved by measuring the circular dichroism of the resulting host–guest complex. Clearly, in some cases where the quantitative degree of chirality discrimination is not so important as knowing which enan-

tiomer is present, direct visual detection, for instance, color is highly desirable. The determination of the outcome of supramolecular events by color change has been a topic of some interest and has been used to discriminate guest lengths,<sup>71</sup> anion and cation binding,<sup>72</sup> and enantiodiscrimination.<sup>73</sup> The group of Fuji has constructed several smart supramolecular hosts that combine the application of a number of different functional moieties to produce an enantiodiscriminating color read-out.<sup>74</sup> The hosts 59–62 (Figure 25) comprise two crown ethers to allow the binding of suitably sized diamines (one amine to each crown ether), chiral substituents (all of *S* configuration) to provide a means of enantiodiscrimination, and a phenolphthalein to give a visual response to the corresponding binding.

On determination of the binding constants by the Rose–Drago method<sup>75</sup> and the accompanying (*R*)- or (*S*)-ligand

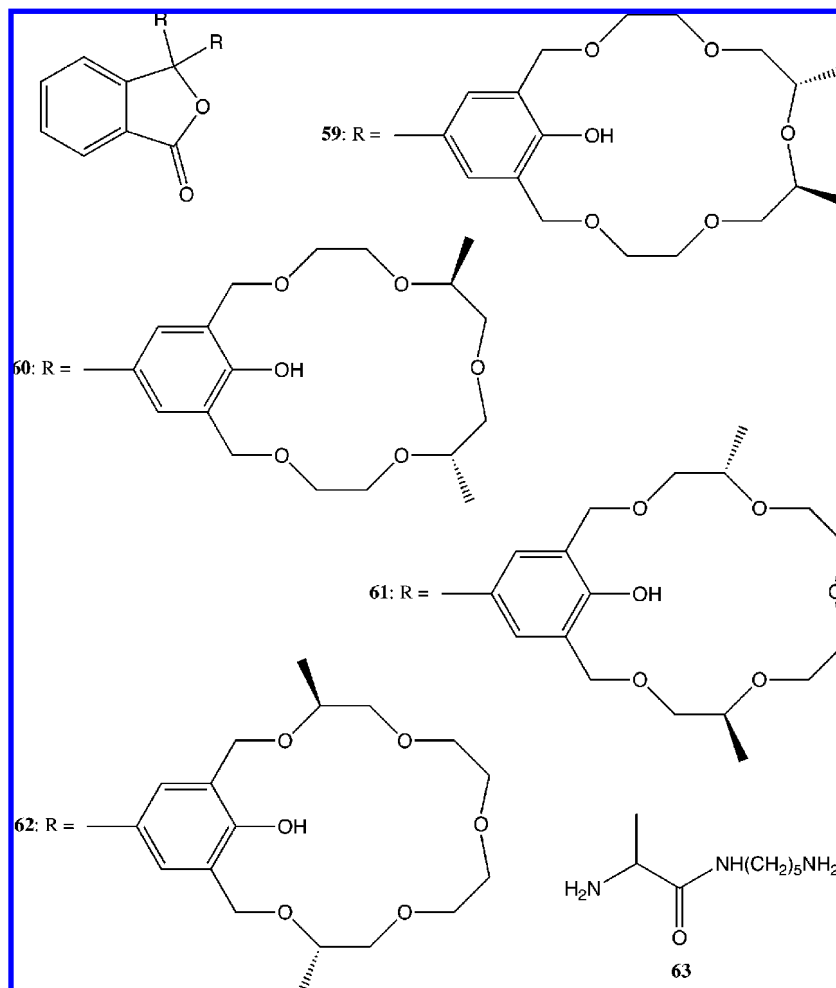


**Figure 25.** Structures of the hosts (59–62) and corresponding guest (63).

**Table 1. Apparent Association Constants of 59–62 with (*R*)- and (*S*)-63 ( $K_R$  and  $K_S$ , Respectively)<sup>74</sup>**

host	$K_R$	$K_S$	$K_{\text{large}}/K_{\text{small}}$
59	2334	1554	1.5
60	378	62	6.1
61	148	328	2.2
62	262	214	1.2

preference, the relation of these stereoselectivities to the position of the chiral methyl groups reveals the enantiodiscrimination mechanism (see Table 1).

Because of low predicted binding constants, a large excess of *N*-ethylpiperidine was added to the solution to enhance the binding and promote color outputs via the formation of a ternary supramolecular species. As seen from Table 1, host **59** gives the strongest binding, but with only a small degree of enantiodiscrimination; conversely, **60** shows a reduced magnitude of binding but with significantly different affinities for the (*R*)-**63** and (*S*)-**63** enantiomers. It is this difference that allows the visual distinction of the guests: a clear solution for host **60** + guest (*S*)-**63** and a purple solution for host **60** + guest (*R*)-**63**. The origin of the enantiodiscrimination lies in consideration of the two critical interactions present in the system: the guest–crown ether interactions that dominate the overall binding, and the differential chiral steric interactions between the  $\alpha$ -amino substituents and the methyl substituents of the crown ether; see Figure 26.

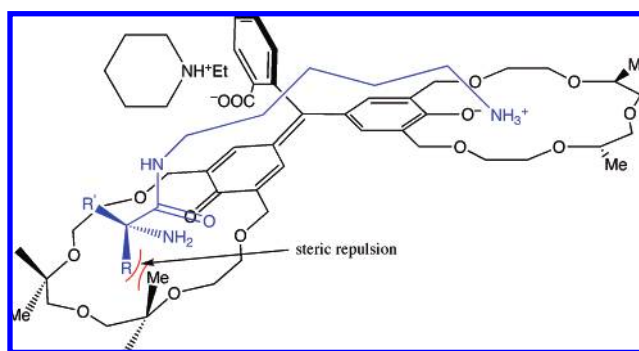


**Figure 26.** Proposed colored complex of **60** and **63** in the presence of *N*-ethylpiperidine.

Thus, in the case of host **59**, the methyl groups are distant from the guest and, thus, the degree of discrimination is low. However, for host **60**, the closer approach of the guest's substituents to the methyl group is clearly optimal for enantiodiscrimination with the  $K'_{\text{large}}/K'_{\text{small}}$  rising to 6.1. The methyl-influenced mechanism is further supported by the inversion of the enantiopreference for host **61**. Because of the Cahn–Ingold–Prelog priority rules for enantiomer assignment, the methyl group at the 5-position (*S* absolute configuration) in host **61** is orientated away from the guest (in comparison to that in host **60**, which is orientated toward the guest; Figure 26), which results in (*S*)-**63** being able to minimize most the steric clash and, thus, to have the higher

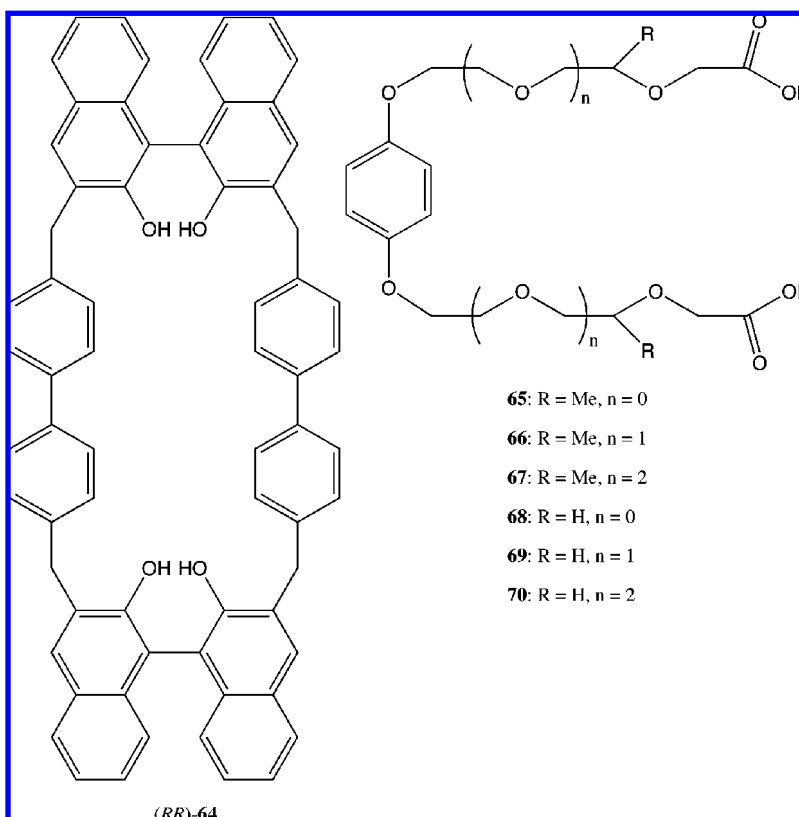


**Figure 27.** Structures of the host (**64**) and corresponding guests (**65–70**).

binding constant. On moving to host **62**, the situation reverts back to that found in host **61**, exhibiting almost negligible enantiodiscrimination because of the too-distant location of the corresponding methyl groups at the 4-positions.

The effect of the position of chiral methyl group(s) on enantioselective properties of host–guest systems is also observed in the [2]pseudorotaxane system studies by Stoddart et al.<sup>76</sup> and shown in Figure 27.

The chirality of the host arises from the incorporation of two enantiopure binaphthyl groups whose chiral integrity is maintained by the steric clashes between the naphthyl groups preventing atropisomeric racemization, while the guest's chirality is due to methyl substitution of the guest's polyether backbone, with the distance of this substitution from the central aromatic group being of crucial importance. On mixing of equimolar amounts of host **64** with guests **65–67** in MeCN, “threading” of the guests through the host's center occurs, resulting in [2]pseudorotaxane structures that are stabilized predominantly by interactions between the  $\pi$ -electron-rich hydroquinone and  $\pi$ -electron-deficient paraquat moieties. It is also this interaction that results in the weak charge-transfer band in the UV–vis spectra at wavelengths between 420 and 500 nm. UV–vis titration experiments were also used to obtain the binding constants for the different diastereomers (Table 2) that reveal the effect of the guest's methyl group position.

For the same guest chirality, the binding constant is seen to increase with the length of the polyether backbone; this is due to enhancement of the mechanical interlocking effect with increasing length. However, the opposite trend can be observed for the enantioselectivity. Thus, for the shortest backbone length (**65**), the chiral methyl groups are closest to the cyclophane host and, thus, the chiral steric interactions are strongest with a  $K_{a(RR)}/K_{a(SS)} = 3.3$ , showing that the

**Table 2.** Association Constants ( $K_a$ ) and Free Energies ( $\Delta G$ ) of (RR)-**64** with (RR)- and (SS)-guests (**65–67**)<sup>76</sup>

guest	$K_a$	$-\Delta G$	$K_{a(RR)}/K_{a(SS)}$	$\Delta\Delta G$
(RR)- <b>65</b>	5 000	5.1		
(SS)- <b>65</b>	1 530	4.4	3.3	0.7
(RR)- <b>66</b>	7 230	5.2		
(SS)- <b>66</b>	2 450	4.6	3.0	0.6
(RR)- <b>67</b>	10 100	5.5		
(SS)- <b>67</b>	8 930	5.4	1.1	0.1

orientation of the methyl groups in the (S,S)-enantiomer results in an unfavorable high energy conformation. However, as this distance increases, these interactions reduce in magnitude and, for guest **67**, result in a  $K_{a(RR)}/K_{a(SS)}$  ratio of just 1.1. Interestingly, the CD spectra of complexes of host **64** with chiral guests **65–67** show almost identical changes to those for complexes with the achiral equivalents **68–70** in the 340–600 nm range (paraquat region), i.e., gradual disappearance of the band at 380 nm, an increase of the 340 nm transition, and an isobestic point at 350 nm. This similarity between the chiral and achiral guests suggests that the geometries of the [2]pseudorotaxanes at the core region differ little in the corresponding host–guest complexes, although this does not tell us about the relative differences in the guest conformations.

Further study considering the subtle interplay between the intermolecular interactions and steric effects in an enantio-discriminating system is found in the work of Ahn and co-workers.<sup>77</sup> Particularly, a crucial role of the  $\pi$ – $\pi$  and hydrogen-bonding interactions in the chiral molecular recognition in various host–guest systems was well-demonstrated, which is interesting in that the host receptor system is based around a  $C_3$ -symmetric molecule (Figure 28).

The specific importance relating to  $C_3$ -symmetry is that, as noted by the authors, typically the chiral hosts are applied to



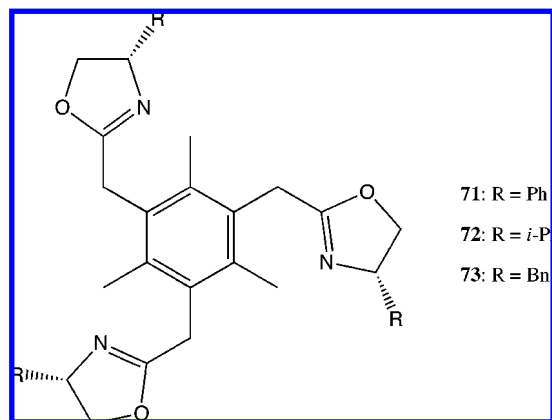


**Figure 28.** Structures of the hosts (**71–73**).

enantiodiscrimination possess  $C_1$ - or  $C_2$ -symmetry (as seen for the examples cited in this review) and that previous attempts to base such hosts around higher symmetries ( $C_3$  and  $D_3$ ) were difficult, resulting in unsuccessful enantiodiscrimination of the  $\alpha$ -chiral primary organoammonium ( $RR_2R_2CNH_3^+X^-$ ). It has been suggested<sup>78</sup> that the rationale for this is that, on complexation, the host–guest interactions provide “three equal steric barriers” on each side of the host, thus precluding enantiodiscrimination; thus, there will be little steric or electronic difference between the diastereomeric complexes and, consequently, little enantiodiscrimination. However, it was found that, for aromatic  $\alpha$ -chiral primary organoammonium guests bound by host **71**, good levels of enantiodiscrimination were obtained that could be rationalized by consideration of the intermolecular interactions in a “three-body” manner. From  $^1H$  NMR analysis of guest extraction (from a guest’s  $D_2O$  solution with a host  $CDCl_3$  solution) and isothermal titration calorimetry (ITC) experiments, the nature of the binding can be seen to be driven by a favorable enthalpy change arising from the hydrogen-bonding, cation– $\pi$ , and  $\pi$ – $\pi$  interactions, with an accompanying unfavorable reduction in entropy. The crucial contribution made by the  $\pi$ – $\pi$  interactions between the guests and the oxazoline R substituents (observed from close contacts in the X-ray structures) can be inferred by considering the related hosts **72** and **73**, which do not possess aromatic R substituents (as in the case of **72**) or where aromatic substituents are not directly attached to the oxazoline ring (as in the case of **73**), are much less effective in extracting the guests out of aqueous solution, and show poor enantioselectivity.

If the relative spatial arrangement of the guest substituents and the host oxazoline groups is considered (Figure 29), the aforementioned three-body interaction rationalization of the enantiodiscrimination can be understood.

Thus, if the two-body interactions between the substituent pairs (R and S), (R and M), and (R and L) are considered, little steric or electronic difference exists between them and, consequently, enantiodiscrimination is expected to be small-to-absent. However, if they (particularly the steric strain between the  $\pi$ – $\pi$  interacting oxazolines and aromatic guest) are considered as a three-body case, the interactions in the two diastereomeric complexes are now no longer identical and provide a rationale for the enantiodiscrimination (see circled areas of Figure 29b). Such different steric strains can be seen for the crystal structures of the diastereomers of the **71** and  $\alpha$ -phenylethylamine complexes, with the (*R*)-enantiomer-containing complex (major) showing a bond angle

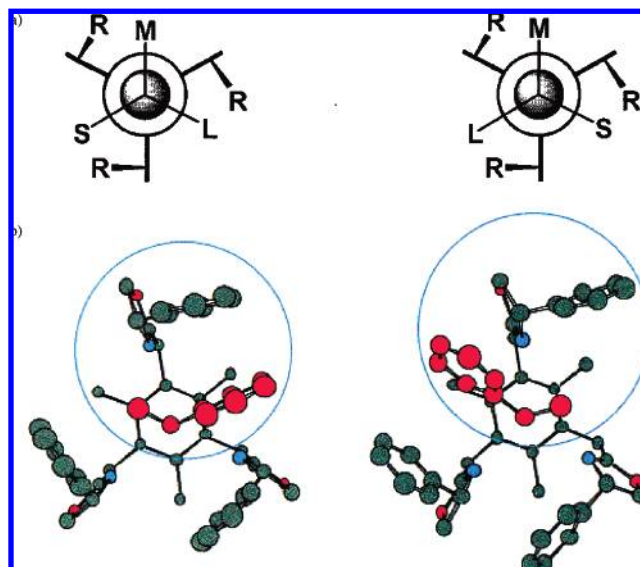


**Figure 29.** Schematic representation of diastereomeric complexes between host (**71–73**) and (*R*)- and (*S*)- $\alpha$ -phenylethylamine (on the left and right, correspondingly): S = small, M = medium, and L = large substituents (a) and the corresponding X-ray crystal structures in the case of the host **71** (b). Reprinted with permission from Kim, S.-G.; Kim, K.-H.; Jung, J.; Shin, S. K.; Ahn, K. H. *J. Am. Chem. Soc.* **2002**, *124*, 591. Copyright 2002 American Chemical Society.

between the L and M substituents of  $109.4^\circ$ , while the (*S*)-enantiomer-containing complex (minor) shows  $114.1^\circ$ . Thus, the minor complex suffers greater steric strain and is consequently disfavored, a result that correlates with the enantioselective extraction experiments in which the *R*:*S* ratio is 71:29.

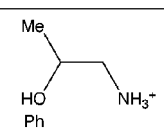
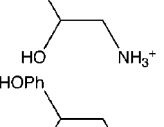
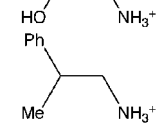
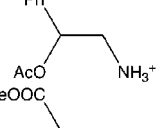
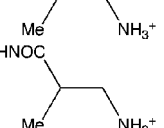
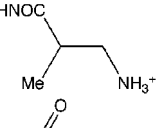
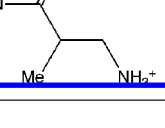
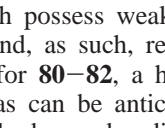
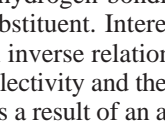
The function of **71** as an enantiodiscriminating host was further extended to include  $\beta$ -chiral primary ammonium guests, whose activity arises from the presence of a three-center (bifurcated) hydrogen bond between host and guest,<sup>79</sup> with the enantioselectivities determined also by extraction experiments from  $D_2O$  into  $CDCl_3$ ; see Table 3.

As discussed previously, the cavity created by the phenyl-substituted oxazoline pendent arms in **71** provides a  $C_3$ -symmetric environment that enables enantiodiscrimination for  $\alpha$ -chiral primary organoammonium guests; however, in this case, it can be seen that the  $\beta$ -substituted guests may occupy one of three “chiral sectors”, and if free rotation of the substituents is possible, no enantiodiscrimination can be expected; see Figure 30a.

To overcome this problem, Ahn and co-workers have utilized guest molecules whose  $\beta$ -substituent is able to form a bifurcated hydrogen bond with an ammonium hydrogen that is already participating in a hydrogen-bond interaction with the host’s oxazoline ring (Figure 30b). This yields a five-membered ring arrangement that locks the guest’s orientation and so greatly reduces the rotation, the result of which is that the chiral host may now differentiate between the enantiomers of the guests.

This function can be seen in the results of Table 3; **74**, **75**, and **76** all show significant enantioselectivities (in favor of the (*R*)-isomer) because they possess a  $\beta$ -hydroxy group that is able to act as a hydrogen-bond acceptor. However, when this functionality is replaced by the non-hydrogen-bonding methyl group of **77**, the resulting extraction is racemic, giving strong indication that the proposed mechanism is active. The enantioselectivity returns for **78** and

**Table 3. Selective Binding of **71** toward Ammonium Salts of  $\beta$ -Chiral Amines (**74**–**82**)<sup>79</sup>**

racemic guest	enantioselectivity	extraction (%)
 <b>74</b>	63:37	50
 <b>75</b>	75:25	60
 <b>76</b>	72:28	40
 <b>77</b>	50:50	97
 <b>78</b>	58:42	72
 <b>79</b>	58:42	71
 <b>80</b>	71:29	<5
 <b>81</b>	61:39	10
 <b>82</b>	83:17	<5

**79**, which possess weaker hydrogen-bond acceptors than **74**–**76** and, as such, result in a lower enantioselectivity. Finally, for **80**–**82**, a higher degree of enantioselectivity returns, as can be anticipated by the participation of the stronger hydrogen-bonding acceptor present in the carboxamide substituent. Interestingly, this appears to be, qualitatively, an inverse relationship between the magnitude of the enantioselectivity and the percentage extraction. It is possible that this is a result of an additional loss of entropy on binding arising from the bifurcated hydrogen bond.

Structural confirmation of the presence of the bifurcated hydrogen bond was obtained from X-ray crystallography. On consideration of the sum of the bifurcated bond angles ( $\theta + \theta' + \alpha = 347.7^\circ$  for **83**) (Figure 31), it can be seen that the four atoms are nearly coplanar, which is a suggested prerequisite for bifurcated hydrogen bonds.<sup>80</sup>

From molecular modeling experiments, a rationale for the steric nature of the enantiodiscrimination can be made. It is found that, because of the orientation of the phenyl groups of the host, there is a greater steric clash between the  $\beta$ -hydrogen of the (*S*)-enantiomer in comparison to the (*R*)-enantiomer, when the guest's internal conformation is fixed by the bifurcated hydrogen bond. This steric clash destabilizes the diastereomer formed from the (*S*)-enantiomer. In the case of **77** where there is no hydrogen-bond acceptor, the  $\beta$ -substituent is able to rotate and, thus, there is no preference between the enantiodifferentiating steric interactions with the host's phenyl groups; consequently, enantioselectivity is not expected, as observed in Table 3.

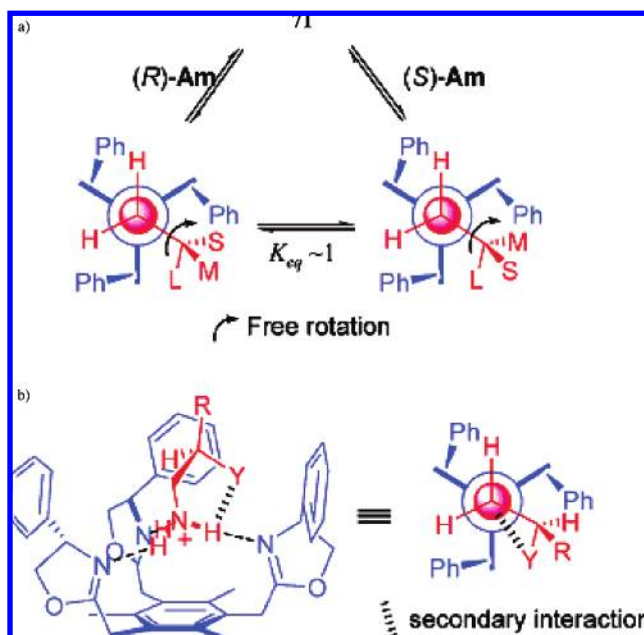


**Figure 30.** Schematic representation of diastereomeric inclusion complexes between **71** and  $\beta$ -chiral primary ammonium ions (Am) with secondary interactions. Reprinted with permission from Kim, S.-G.; Kim, K.-H.; Kim, Y. K.; Shin, S. K.; Ahn, K. H. *J. Am. Chem. Soc.* **2003**, *125*, 13819. Copyright 2003 American Chemical Society.

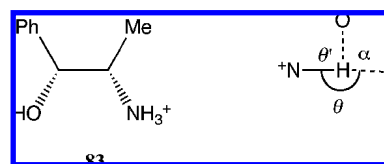


**Figure 31.** Structure of **83** and schematic representation of the bifurcated H-bonds in the complex (**71**–**83**).

## 4.2. Enantiodiscrimination Detection by Fluorescence

It is worth discussing at this point the detection of chirality, and particularly enantiodiscrimination, in supramolecular systems by fluorescence spectroscopy. The versatility of this method arises from a number of its characteristics: (i) the detection modes, i.e., quenching or enhancement of the fluorescence signal, measurement of its lifetime, and interpretation of the fluorescence anisotropy; and (ii) its experimental nature, in that it can be performed in real-time, the amount of required sample is in the micromolar region or below, and the instrumentation is typically standard, inexpensive laboratory equipment. The main, but obvious, limitation is that a suitable fluorophore(s) is required on either host or guest.

The mechanistic origin of fluorescence emission, briefly, occurs via an initial molecular absorption of light, typically, by the  $\pi$ – $\pi^*$  transitions in organic molecules, on a  $10^{-15}$  s time scale to the higher vibrational levels in the electronically excited singlet states; there is subsequent fast internal relaxation to the lowest vibrational level of the first excited singlet state ( $S_1$ ) over a  $10^{-14}$ – $10^{-11}$  s time period; fluorescence emission down to the ground state then occurs on the  $10^{-9}$ – $10^{-7}$  s time scale (Kasha's rule). Because of the duration over which the fluorescence decay occurs, it is extremely sensitive to molecular features such as structural conformations and rigidity, intra- and intermolecular interactions and energy transfer, and electron transfer.

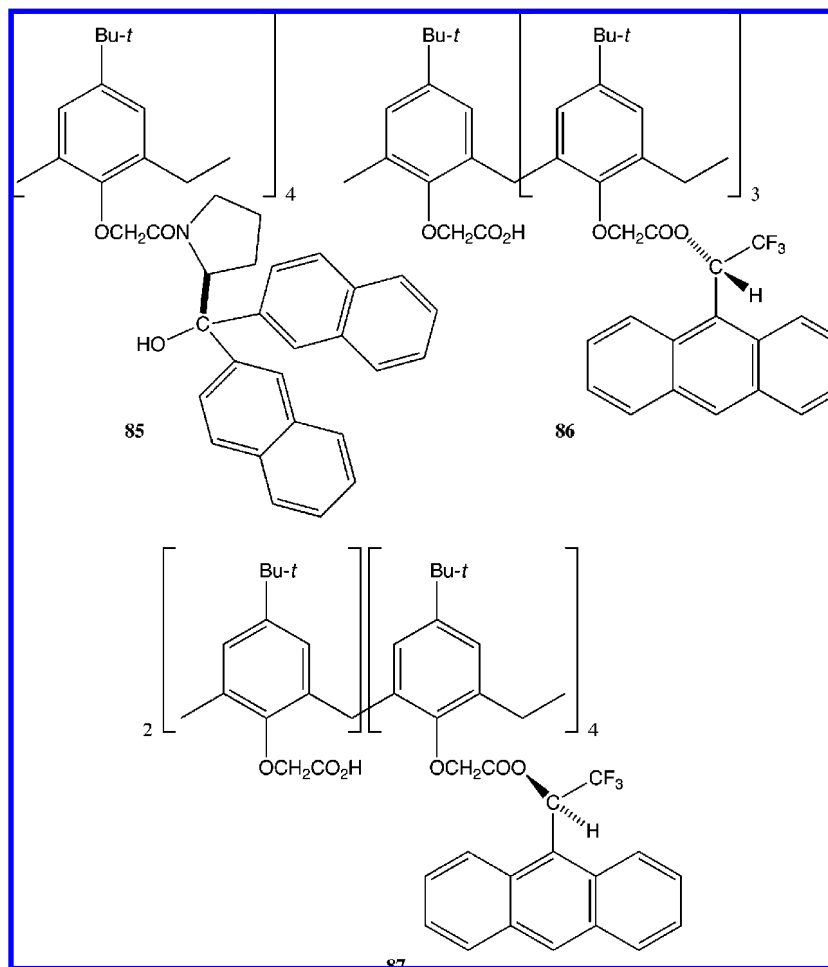


**Figure 32.** Structures of the hosts (85–87).

In terms of supramolecular chirality sensing, the issue that we are concerned with here is the application of fluorescence-based host (or guest) molecules to discriminate between guest (or host, correspondingly) enantiomers. In this light, the host molecule must possess a suitable binding site for the guests, as well as a fluorophore component. To date, reports of successful enantiodiscriminating host–guest systems have included a variety of macrocycles (fluorophore-modified calixarenes, cyclodextrins, and crown ethers),<sup>81</sup> dendrimers,<sup>82</sup> and oligomers.<sup>83</sup> A particularly complete cataloguing of the above and additional bespoke systems can be found in a recent review published by Pu.<sup>84</sup>

In terms of the quantitative analyses of these systems, the most powerful and widely applied analytical treatment is the Stern–Volmer equation,<sup>85</sup> described below,

$$I_0/I = 1 + K_{SV}[Q] \quad \text{for systems with one binding site} \quad (4)$$

$$I_0/I = 1 + K_{SV}[Q]^2 \quad \text{for systems with two binding sites} \quad (5)$$

where  $I_0$  is the emission intensity of the fluorophore in the absence of a quencher,  $I$  is the emission intensity in the presence of a quencher, and  $[Q]$  is the concentration of the quenching species.  $K_{SV}$  is the Stern–Volmer constant; for dynamic quenching, this is related to  $K_{SV} = k_q\tau_0$  ( $k_q$  = fluorescence quenching rate constant and  $\tau_0$  = fluorescence lifetime in the absence of quencher); for static quenching,

$K_{SV}$  represents the association constant of the fluorophore and the quenching species.<sup>85</sup>  $K_{SV}$  is, therefore, a measure of quenching efficiency or sensitivity to the quencher concentration. Thus, if a fluorescing system is governed by the Stern–Volmer relationship, the plot of  $I_0/I$  against  $[Q]$  will be linear with a gradient of  $K_{SV}$  and a y-axis intercept of 1.

There are many studies and reviews detailing the chemistry of chiral recognition in fluorescing species (see references above); therefore, here we shall focus on two enantiodiscriminating systems that highlight well the supramolecular aspects of the process, one concerning the application of the Stern–Volmer relationship and the other concerned with drawing inferences from enhanced fluorescence activity.

The Stern–Volmer relationship has been used for determination of the enantiomeric purity in a number of systems.<sup>86</sup> Because  $K_{SV}$  is a measure of quenching efficiency, a large value for this parameter equates to a sensitive response. Ideally, therefore, the aim is to obtain a sensor host molecule that displays a large  $K_{SV}$  magnitude with one enantiomer and zero for its antipode (no quenching effect), and subsequently to employ this material as an optical enantioselective sensor. Such a calixarene-based supramolecular system was employed by Diamond and co-workers for the enantiomeric-composition determination of a series of chiral amines.<sup>81c</sup> In this, the authors give key features for any successful enantiodiscriminating fluorescent host, including the following: (i) the host must possess suitable intermolecular interacting moieties (hydrogen bonds, charges, aromatic/polar

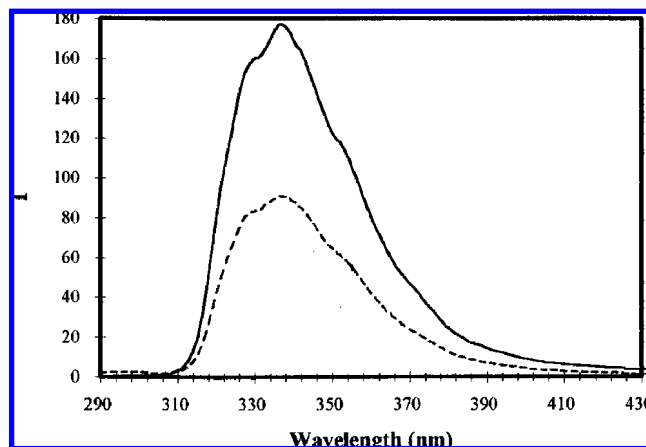


**Figure 33.** Emission spectra of **85** ( $2 \text{ mM dm}^{-3}$ ) in the presence (dashed line) and in the absence (solid line) of  $0.33 \text{ M}$  racemic **84** using an excitation wavelength of  $274 \text{ nm}$ . Reprinted with permission from Grady, T.; Harris, S. J.; Smyth, M. R.; Diamond, D. *Anal. Chem.* **1996**, *68*, 3775. Copyright 1996 American Chemical Society.

groups, etc.) to facilitate supramolecular association; (ii) there must be preorganization of the host so to provide a basis for enantioselectivity; and (iii) the result of the binding event must produce an observable signal.

In this work, they looked at the differences in the quenching efficiency caused by (*R*)- and (*S*)-1-phenylethylamine (**84**) on three lower-rim fluorophore-appended calixarene hosts **85**, **86**, and **87**; see Figure 32.

In this case, the host calixarene's chirality arises from point-chiral centers on the fluorophores, with the chiral centers being at a position  $\beta$  to the naphthyl groups in **85** and  $\alpha$  to the anthryl groups in **86** and **87**. Initial experiments indeed showed that racemic **84** has a fluorescence quenching effect on **85**; see Figure 33.

The degrees of enantioselectivity for **85**, **86**, and **87** were assessed by seeing how the  $K_{SV}$  constant (i.e., the slope in the Stern–Volmer plot) varied on addition of (*R*)- and (*S*)-**84** to each host; see Figure 34.

From parts b and c of Figure 34, it is clear that there is essentially no difference in the slope gradients, and therefore, it was stated that hosts **86** and **87** do not possess (any measurable degree of) enantiodiscriminating ability. On the other hand, host **85** in Figure 34a shows significant differentiation between the fluorescence quenching observed for the (*R*)- and (*S*)-**84** enantiomers, with  $K_{SV}$  values of  $0.052$  and  $0.028$ , respectively.

The linear and different relationships between the quenchings of the two enantiomers allow host **85** to function as a sensor for enantiomeric composition. This application is possible by relating the  $K_{SV}$  value of an unknown sample to a graph calibrated to the % enantiopurity from previous experiments. However, this approach requires a number of measurements to establish the  $K_{SV}$  value. If, on the other hand, the concentration of the sample is known, then the intensity of a single fluorescence measurement can be correlated with the enantiomeric composition, by relating this measurement to a calibration graph where the intensity is plotted against a known enantiomeric composition of certain concentration.

The crucial role of the calixarene scaffold is clearly seen when the effect of the ligand quenching on just the naphthylprolinol fluorescent label is investigated, as this results in no enantiodiscrimination and nonlinear slopes,

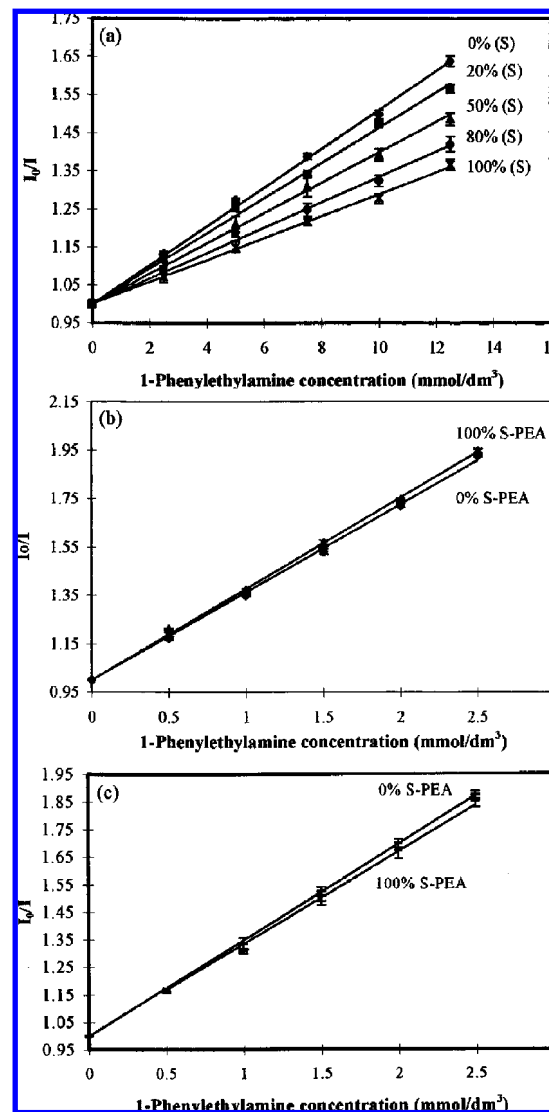


**Figure 34.** Stern–Volmer plots for the fluorescence quenching of **85** (a), **86** (b), and **87** (c) upon addition of **84** containing 0–100% of the (*S*)-form. Reprinted with permission from Grady, T.; Harris, S. J.; Smyth, M. R.; Diamond, D. *Anal. Chem.* **1996**, *68*, 3775. Copyright 1996 American Chemical Society.

indicating that the Stern–Volmer relationship is no longer obeyed. The important point here is to determine what is the supramolecular nature of the calixarene's function. Insight into this is obtained from UV–vis and molecular mechanics simulations. While the UV–vis spectra of **86** and **87** (with **84**) are simple additions of the components, this is not so for the spectrum of the **85** complex. This difference is likely due to the formation of a ground-state complex with **85**, while those with **86** and **87** are predominantly formed in the excited state. The calculation of the energy-minimized structure of **85** shows that the naphthyl substituents form a crowded arrangement at the lower rim; however, the anthryl moieties in **86** are quite distant from each other (Figure 35), which is reflected in the relative distances between the chiral centers for **85** and **86**,  $9.06$  and  $13.56 \text{ \AA}$ , respectively.

Thus, in **85** there is a well-defined chiral environment, provided by the calixarene scaffold, for interaction with **84**. Calculation for **87** was not performed because of its greater size, but it is well-known that such calix[6]arenes are considerably more flexible than their calix[4]arene counterparts. On consideration of the interaction with **84**,



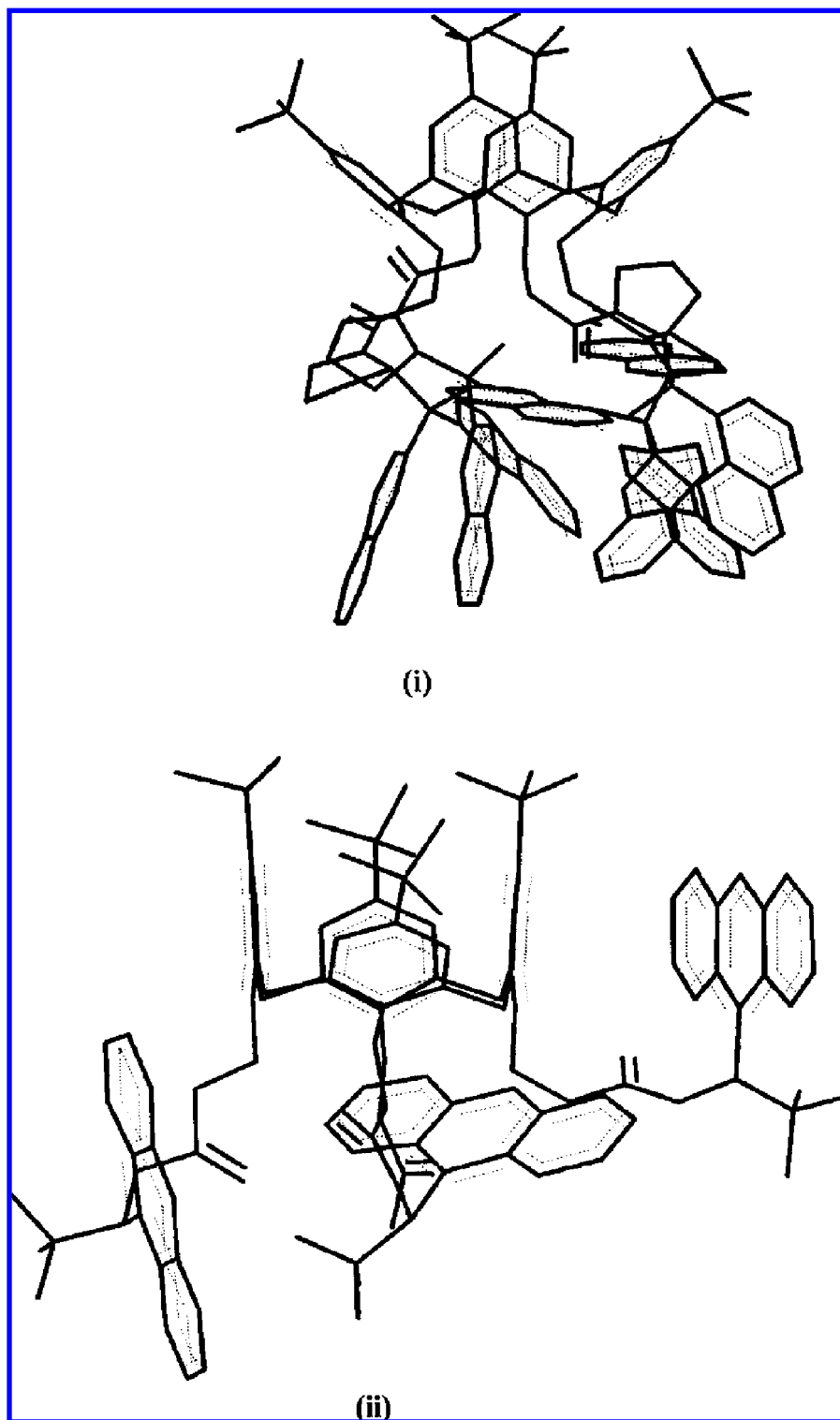


**Figure 35.** Energy-minimized structures of **85** (i) and **86** (ii) obtained using molecular mechanics in Hyperchem v. 4.0. Reprinted with permission from Grady, T.; Harris, S. J.; Smyth, M. R.; Diamond, D. *Anal. Chem.* **1996**, *68*, 3775. Copyright 1996 American Chemical Society.

two main features are observed. First, for **85**, the basic binding is facilitated by a three-point interaction consisting of a  $\pi$ – $\pi$  interaction between the phenyl and naphthyl moieties, a hydrogen bond between the amine and hydroxyl group, and a C–H to O=C interaction. This combination has the effect of strongly locking in the guest. Second, the relative positions of the guest's methyl group are found to be directed toward the host's interior for the (*R*)-enantiomer and more to the exterior for the (*S*)-enantiomer; it is this

difference that is believed to, largely, account for the enantiodiscrimination.

A different application of fluorescence spectroscopy to enantiodifferentiation is found in the work of Li et al., who investigated the effect of the interaction between the macrocycle **88** and mandelic acid; see Figure 36.<sup>87</sup> Here, it is the fluorescence emission arising from the formation of the excimer complex that acts as the probe for rationalizing the enantioselective binding.

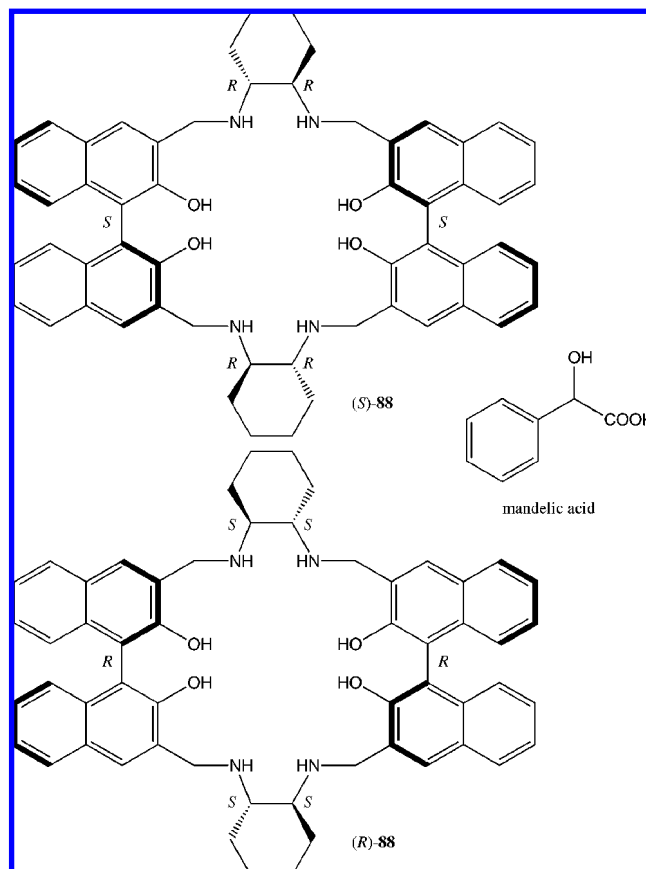


**Figure 36.** Structures of the hosts (*(S)*- and *(R)*-**88**) and mandelic acid.

In macrocycle **88**, the binaphthyl groups act as both chiral source (along with that provided by the cyclohexyl moiety) and fluorophore, with the alcohol and amine functional groups providing suitable points for intermolecular interactions. The interaction between mandelic acid and **88** only occurs in the excited state and can be observed by comparing the UV–vis and fluorescence spectra. In the UV–vis spectra, there is almost no difference between the spectra of free and bound **88** and none between the complexes with the two enantiomers of mandelic acid. However, the fluorescence spectra of **88** (at  $1 \times 10^{-5}$  M) with mandelic acid (at  $5 \times 10^{-4}$  M) show a dramatic response with an excimer emission at ca. 370 nm. Importantly, though, this response is highly chirally dependent; thus, for *(S)*-**88**, there is almost no fluorescence observed for *(R)*-mandelic acid, but for *(S)*-mandelic acid there is a strong fluorescence signal that is 20 times stronger than that for the free host. The true enantioselective nature of this system is shown on considering *(R)*-**88**, which, conversely, shows no signal for *(S)*-mandelic acid but a strong emission for *(R)*-mandelic acid.

The differing effects of the two enantiomers and the dynamic competitive binding between them can be seen in the relationships shown in Figure 37. Curve a shows the  $I/I_0$  ratio of *(R)*-**88** in the presence of enantiomeric mixtures ranging from pure *(R)*- to pure *(S)*-mandelic acid. In comparison, curve b shows the  $I/I_0$  ratio for solutions containing enantiopure *(R)*-mandelic acid whose concentrations are identical to that of *(R)*-mandelic in the mixture used in curve a. The larger values obtained for the enantiopure experiment reflect the competitive binding between the stronger-binding *(R)*-mandelic acid and the weaker-binding *(S)*-mandelic acid. The initial slow increase in  $I/I_0$  at low *(R)*-mandelic

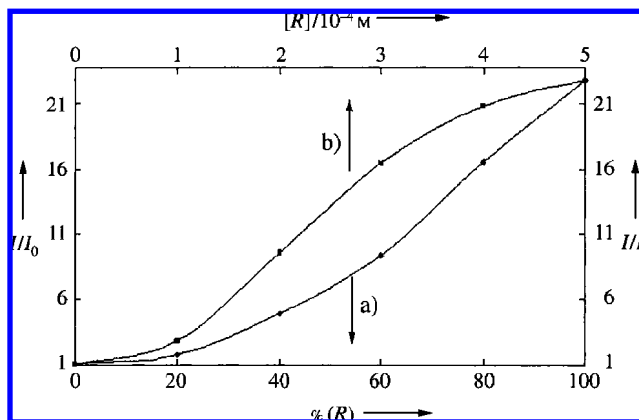


**Figure 37.** Fluorescence enhancement of *(R)*-**88** in the presence of mandelic acid at various compositions of the *R* and *S* enantiomers (a) and the optically pure *(R)*-mandelic acid (b). Reprinted with permission from Li, Z.-B.; Lin, L.; Pu, L. *Angew. Chem., Int. Ed.* **2005**, *44*, 1690. Copyright 2005 Wiley-VCH Verlag GmbH & Co.

concentrations and the later faster increase also reflect the greater binding constant for the *(R)*-guest/*(R)*-host pairing, as detailed above.

The nature of the actual binding mechanism, although not studied in detail by the authors, is likely to be via excited-state  $\pi$ – $\pi$  interactions with some assistance by inclusion into the host's cavity facilitated by hydrogen-bonding interactions between the guest's alcohol and acid groups and the host's alcohol and amine substituents; however, the lack of any significant change in the UV–vis spectra suggests that the  $\pi$ – $\pi$  interactions are not a major contribution, at least in the ground state. The hydrogen bond's influence is demonstrated by seeing how using *O*-acetyl mandelic acid (in which the alcohol group is protected) affects the excimer emission; the result is that no fluorescence is observed showing the crucial contribution of the hydrogen bond.

Recent developments have shown the application of fluorescence anisotropy to the study of enantiodifferentiating systems; an early study was the fluorescence anisotropy arising from the interaction of an anthryl-based probe with DNA,<sup>88</sup> but in particular, the rigorous work of McCarroll et al. has developed this approach to allow accurate thermodynamic parameters to be obtained.<sup>89</sup> Critical to utilizing the fluorescence anisotropy measurements is the realization that this is a measure of the rotational motion of the molecule; although there are other factors, it is this motion that dominates the depolarization of fluorescence. Thus, if a host is free in solution, it will possess a fluorescence anisotropy according to its size; however, if it then interacts with a guest molecule, the effective size of the assembly will increase and so change the rate of rotation. It follows that if there are two enantiomers interacting with a host, the effective size of the assembly will be a function of the binding strength of each, and thus, we may expect different fluorescence anisotropies for each diastereomeric complex, with the stronger binder producing a larger size and presumably a slower rotational correlation time, which will result in a higher anisotropy value. Indeed the potential of this branch of fluorescence spectroscopy lies in that, as following the anisotropy, we are only looking at the controlling parameters that are chiral in origin, and thus, changes observed in the spectra are related to these and not to other achiral events.

In their initial work, McCarroll et al. derived a term of “chiral selectivity”,  $\beta$ , and tested it with the data from the interaction of various chiral guests with a chiral surfactant

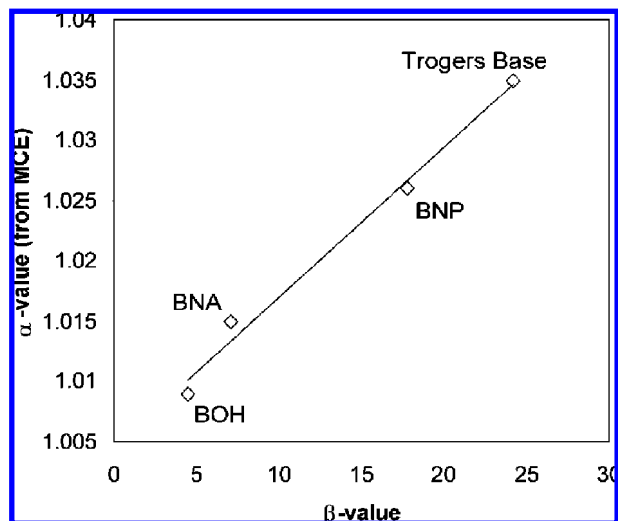


**Figure 38.** Plot of the correlation between the  $\beta$ -values derived from fluorescence anisotropy measurements and  $\alpha$ -values obtained from micellar capillary electrophoresis (MCE) experiments (BNP = 1,1-bi-2-naphthyl-2,2-diylhydrogenphosphate; BNA = 1,1-bi-2-naphthyl-2,2-diamine; BOH = 1,1-bi-2-naphthol). Reprinted with permission from McCarroll, M. E.; Billiot, F. H.; Warner, I. M. *J. Am. Chem. Soc.* **2001**, *123*, 3173. Copyright 2001 American Chemical Society.

in its micelle form, poly(sodium undecanoyl-L,L-leucylleucinate) (poly-SULL).

Initially, the presence of the enantioselective interactions were observed for a 1,1'-binaphthyl guest and poly-SULL host assembly, with the (*R*)-guest giving an anisotropy value of 0.1132 and the (*S*)-guest yielding 0.0991. However, repeating the experiments with an achiral surfactant analogue gave the same anisotropy values for both enantiomers.

To be able to make more direct comparisons between different systems, the above-mentioned  $\beta$  term was introduced to remove the complications arising for the other nonenantioselective terms.

$$r_S/r_R = \left[ \frac{3 \cos^2 \beta - 1}{2} \right] \quad (6)$$

where  $r_S$  and  $r_R$  are the anisotropy factors for the (*R*)- and (*S*)-enantiomers, respectively.

To test this hypothesis, the  $\beta$  values obtained for the guests were plotted against the chiral selectivities determined by micellar capillary electrophoresis and defined as  $\alpha$ , where  $t_S$  and  $t_R$  values are the corrected retention times.

$$\alpha = \frac{t_S}{t_R} \quad (7)$$

The graph shown in Figure 38 shows a very good correlation between the two and gives a strong validation of the  $\beta$  term approach as a measure of the differing chiral interactions between the enantiomers of the different hosts and guests.

From this linear relationship, it is then possible to derive an equation that gives the difference in the free energy of association between the two enantiomers.

$$\Delta(\Delta G)_{S,R} = -RT \ln(m\beta + 1) \quad (8)$$

This approach was extended by further work of McCarroll et al.<sup>89</sup> to include consideration of the actual binding constant, thus leading to a method for obtaining good estimations for

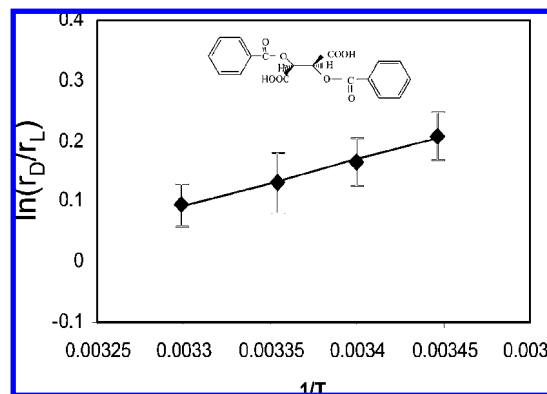


**Figure 39.** Temperature-dependent fluorescence anisotropy of the enantiomers of *O,O'*-dibenzoyl tartaric acid in the presence of  $\beta$ -cyclodextrin. Reprinted with permission from Xu, Y.; McCarroll, M. J. *Phys. Chem. B* **2005**, *109*, 8144. Copyright 2005 American Chemical Society.

values of  $\Delta\Delta H^\circ$ ,  $T\Delta\Delta S^\circ$ , and  $\Delta\Delta G^\circ$  for enantioselective host–guest events. From first principles, eq 9 is obtained and used to determine the thermodynamic parameters for the binding in a number of host–guest systems.

$$\ln\left(\frac{r_{av,R}}{r_{av,S}}\right) = \frac{-\Delta\Delta H^\circ}{RT} + \frac{\Delta\Delta S^\circ}{R} + \ln\left(\frac{r_{b,R}}{r_{b,S}}\right) + \ln\left(\frac{(K_S[S] + 1)}{(K_R[S] + 1)}\right) \quad (9)$$

Thus, from this, a plot of  $\ln(r_{av,R}/r_{av,S})$  against  $1/T$  will give a linear response where the gradient is equal to  $\Delta\Delta H^\circ/R$  and the intercept is  $\Delta\Delta S^\circ/R$ ; the remaining constant is expected to approach zero in most cases.

The result of this analysis for  $\beta$ -cyclodextrin with the two enantiomers of *O,O'*-dibenzoyl tartaric acid is shown in Figure 39. Although not shown here, the positive slope for the variation of the anisotropy with  $1/T$  indicates that, as expected, the binding constants are stronger at lower temperatures, with the D enantiomer's more positive slope indicating that it has a greater enthalpy of interaction with  $\beta$ -cyclodextrin in comparison to its L counterpart. The thermodynamic parameters extracted from Figure 39 are as follows:  $\Delta\Delta H^\circ = -6.37 \text{ kJ mol}^{-1}$ ,  $T\Delta\Delta S^\circ = -6.03 \text{ kJ mol}^{-1}$ , and  $\Delta\Delta G^\circ = -0.33 \text{ kJ mol}^{-1}$ , thus showing that the D-preference in this case is enthalpically driven but is almost totally cancelled out by the entropic loss of a similar magnitude.

## 5. External and Internal Controlling Factors

Clearly, in dynamic supramolecular systems, the exact structural and chiral state of a system, and consequently its physical–chemical properties and associated functionality, can be effected by various factors beyond the covalent composition of the assembly. In this section, the nature and outcomes of a number of controlling factors such as the choice of solvent, temperature, and phase, which are of key importance for supramolecular interactions, are considered, although other potential influences, such as electron mediation,<sup>90</sup> optical properties,<sup>91</sup> pressure,<sup>92</sup> and pH/ionic strength,<sup>93</sup> also exist.

### 5.1. Solvent as an Active Component in Supramolecular Chirality

A thorough understanding of the effect of solvent(s) on a molecular system requires a small conceptual leap and has

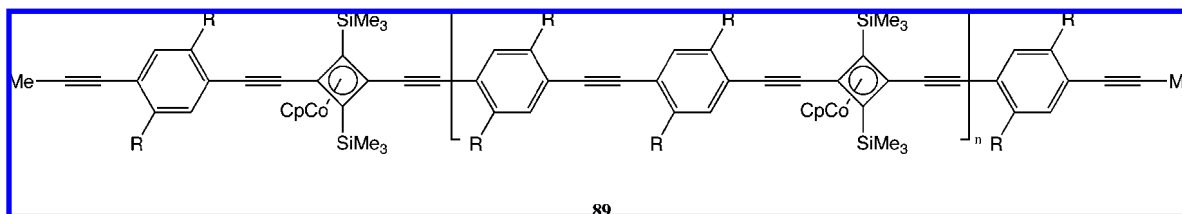


**Figure 40.** Structure of **89** ( $R = (S)$ -2,7-dimethyloctyl).

been often overlooked and not appreciated in many studies concerning supramolecular chirality. The key realization is that the solvent is molecular in origin and, as such, will interact with a solute according to the characteristics that govern noncovalent intermolecular interactions and associations. Indeed, it should be realized that the relationship between the solute (even one) and solvent molecules in solution is a supramolecular one; thus, when appropriate, we must think in supramolecular terms to understand the resulting molecular and bulk solution properties of the system.

Studies investigating the effect of solvent on the chirality of a supramolecular system can loosely be grouped into two sets: (i) those whose activity apparently arises from the influence of bulk solvent properties such as the dielectric constant and (ii) those whose activity can be seen directly to arise from the interaction of the solvent with the supramolecular system at the molecular level, with the system's properties understood by considering the solvent as another component in the dynamic supramolecular assembly.

#### 5.1.1. Solvent Influence on Chirality Magnitude

The bulk action effect of a solvent on the chirality of a supramolecular system often arises from the different solubilities that a molecule has in various solvents and the structural changes that these differences impose on the solute. This effect can be exemplified by three papers by the groups of Steffen,<sup>94</sup> Redl,<sup>95</sup> and Iarossi.<sup>96</sup> In the first paper, by Steffen et al.,<sup>94</sup> the polymer **89** (Figure 40) is found to be soluble in chloroform but much less so in methanol, and the effect of the composition of chloroform/methanol ratios on the chirality induction observed in the CD spectra is determined.

Up to 50% MeOH, no CD intensity is observed; however, above 50%, a negative bisignate CD signal appears, which crosses the  $x$ -axis at ca. 380 nm. The origin of this signal is believed to be due to intermolecular aggregation of the polymers as their solubility in the solvent is reduced with increasing methanol content. Indeed, this reduced solubility ultimately results in precipitation of the polymers above 70% methanol and an accompanying reduction in the CD intensity. In the second paper, by Redl et al.,<sup>95</sup> the low solubilizing power of methanol can again be shown to have structural consequences for the solute that ultimately affect the degree of chirality in the system.

In this system, porphyrin moieties are appended to a cellulose polymer backbone **90** (Figure 41); the chiral result is that, in tetrahydrofuran (THF), a negative bisignate CD signal is observed to be centered at ca. 420 nm, resulting from an anticlockwise orientation of the porphyrin chromophores, with the difference between the corresponding Cotton effects being ca. 10 nm. In comparison, the couplet for the corresponding methanol solution is ca. 30 nm; this arises from the greater structural rigidity of the cellulose–porphyrin polymer due to its lower solubility in methanol

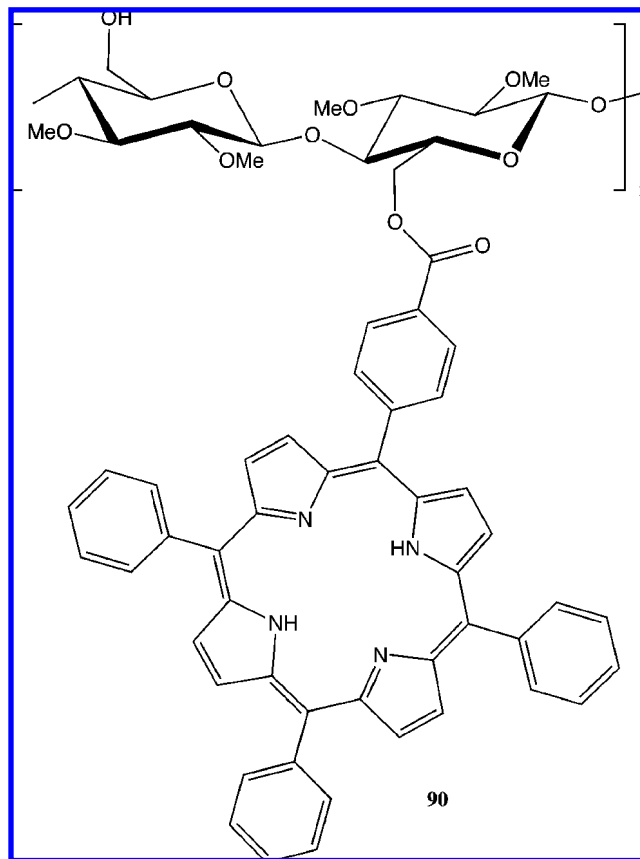


**Figure 41.** Structure of **90**.

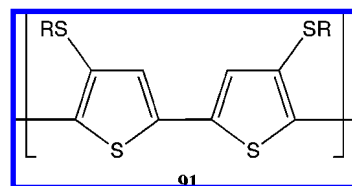


**Figure 42.** Structure of **91** ( $R = (S)$ -CH<sub>2</sub>CHMeEt).

compared to THF. The final example here of the bulk solvent effect on a system's chirality is found in the work of Iarossi et al. and shows the effect of good (chloroform) and poor (methanol and  $n$ -hexane) solvents on the overall structure of a thiophene-based conducting polymer **91** (Figure 42) and the degree of its chirality.<sup>96</sup>

In pure chloroform, the absorption maxima in the UV–vis spectrum occurs at 469 nm and is associated with the  $\pi$ – $\pi^*$  transitions, with the CD spectrum being inactive. On initial addition of methanol at a 10:1 ratio, there is no change in either spectra. However, on increasing the methanol content to 8:2, the UV–vis absorption is red-shifted and displays three bands at 530, 565, and 623 nm; in concert with this is the appearance of a negative bisignate CD signal that possesses two negative maxima and one positive



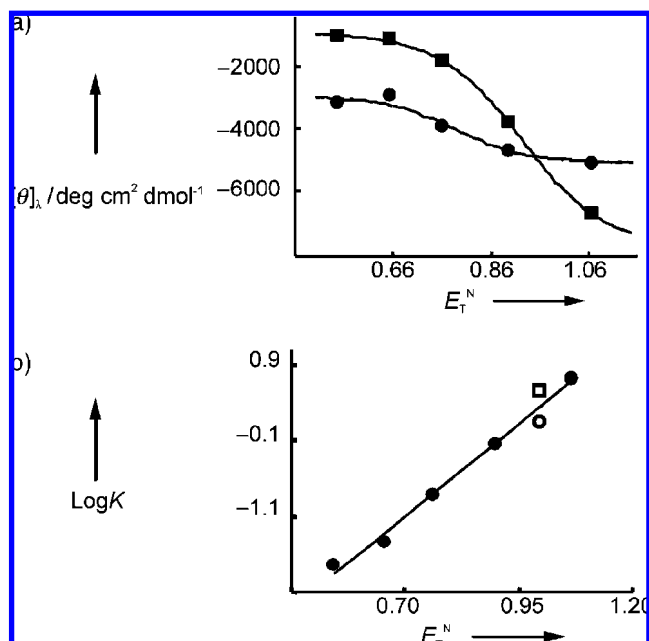


**Figure 43.** Plot of the mean residue ellipticity of **92** at 208.5 (circles) and 222 nm (squares) as a function of the empirical solvent polarity parameter  $E_T^N$  (a) and linear correlation between the  $\alpha$ -/ $3_{10}$ -helix equilibrium constant ( $\text{log } K_{\alpha/3_{10}}$ ) and  $E_T^N$  (b). Reprinted with permission from Pengo, P.; Pasquato, L.; Moro, S.; Brigo, A.; Fogolari, F.; Broxterman, Q. B.; Kaptein, B.; Scrimin, P. *Angew. Chem., Int. Ed.* **2003**, *42*, 3388. Copyright 2003 Wiley-VCH Verlag GmbH & Co.

maximum. The maximum in CD intensity occurs at a 7:3 chloroform/methanol ratio and then decreases; however, this is accompanied by a change in the UV-vis spectra, which reveals that, at the higher methanol content (ratios of 6:4 and above), a different overall structure of the polymer is induced. Thus, we see that the solvent not only modulates the degree of chirality in the polymer but also causes the overall structural type to change, with accompanying further changes in CD intensity. A similar effect of chirality magnitude modulation by solvation, ultimately resulting in a more general change in structure, is seen in work by Kawasaki et al., who investigated the changes in chirality and structure of melamine-cyanuric supramolecular membranes in water/ethanol mixtures.<sup>97</sup>

The preceding work mainly dealt with the bulk solvent effects of two markedly different solvents (mainly in terms of their respective solvating abilities for the solute). This idea can be extended by considering how a measure of the solvent's polarity may affect the basic structure and chirality of a system. In the paper by Scrimin and co-workers, the solvent's polarity (as described by the parameter  $E_T^N$ )<sup>98</sup> is related to the proportion of  $\alpha$ -helix and  $3_{10}$ -helix for a particular peptide, **92**, (Ac-[Aib-L-( $\alpha$ Me)Val-Aib]<sub>2</sub>-L-His-NH<sub>2</sub>).<sup>99</sup> The solvents chosen are hexafluoroisopropanol (having the highest  $E_T^N$  value of 1.086), 2,2,2-trifluoroethanol, methanol, ethanol, and isopropanol (having the lowest  $E_T^N$  value of 0.546). It is found that, in more polar solvents, the  $\alpha$ -helix predominates, with the less polar solvents resulting in a  $3_{10}$ -helix. The relationship between the CD intensity and the  $E_T^N$  value is clearly nonlinear (see Figure 43a) and arises from the different degrees of contribution made by the two helical types; with the  $3_{10}$ -helix, CD maxima derive from the  $n-\pi^*$  transitions, and with the  $\alpha$ -helix, maxima derive from the  $\pi-\pi^*$  transitions. However, as can be seen from Figure 43b, the relationship between the

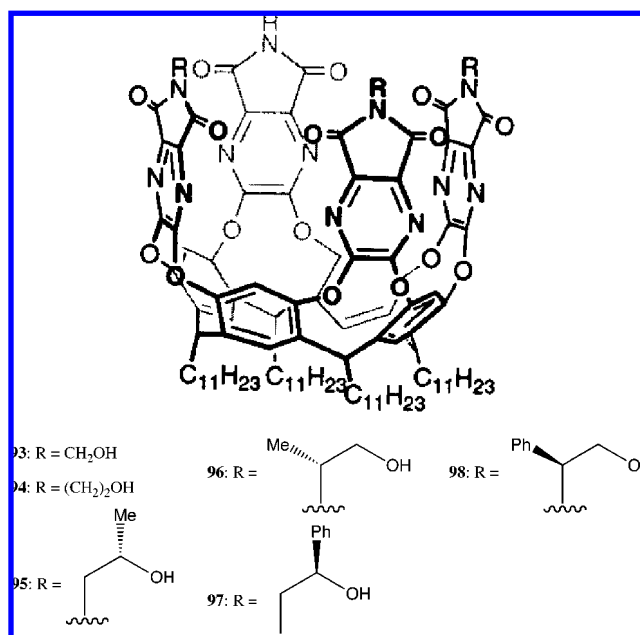


**Figure 44.** Structures of the resorcinarene host (**93–98**). Partly reprinted with permission from Saito, S.; Nuckolls, C.; Rebek, J., Jr. *J. Am. Chem. Soc.* **2000**, *122*, 9628. Copyright 2000 American Chemical Society.

logarithm of the equilibrium constants ( $\text{log } K_{\alpha/3_{10}}$ ) and  $E_T^N$  is linear, giving a strong indication that it is the polarity of the solvent that is the driving force.

As with the previously discussed work, the detailed molecular origin of the mechanism by which the helical transformation takes place is not addressed. Interestingly, however, it is noted that on transformation from the  $\alpha$ -helix to the  $3_{10}$ -helix, the number of intramolecular hydrogen bonds increases from 5 to 6, which suggests that there could be more competition for hydrogen-bonding sites with the more polar solvents. Accompanying this observation, the pitch is found to decrease because of changes in the lateral interactions between the amino acid side chains.

In the work described previously, the solvent effects on the systems' chiroptical properties have been almost exclusively considered as a bulk property effect, and, as such, are discussed in these terms. In the preceding work, we considered supramolecular chiral systems in which the nature of the solvent's control of the chirality can be rationalized by analyzing the solvent's interaction with the solute molecules in specific intermolecular interaction terms.

The chiral resorcinarene hosts **93–98** by Rebek and co-workers are such a case; see Figure 44.<sup>100</sup> Structurally these capsule-like hosts form two different conformations (Figure 45); the addition of chiral appending substituents (in **95–98**) results in a predominance for one over another, and as a result, a bisignate CD signal is observed to be centered at 300 nm in CHCl<sub>3</sub> solution. The nature of the cavities allows complexation of a number of small guests, such as norbornene.

It is found, however, that the magnitudes of the CD spectra are diminished on addition of MeOH to the CHCl<sub>3</sub> solution. The rationale for this is that the MeOH competes with the guest for the host's intramolecular hydrogen bonds. Also, from <sup>1</sup>H NMR experiments, decapsulation of the guest is observed on the addition of methanol, because of the aforementioned solvent competition. Crucially, the molecular nature of the solvent effect can be seen by increasing the

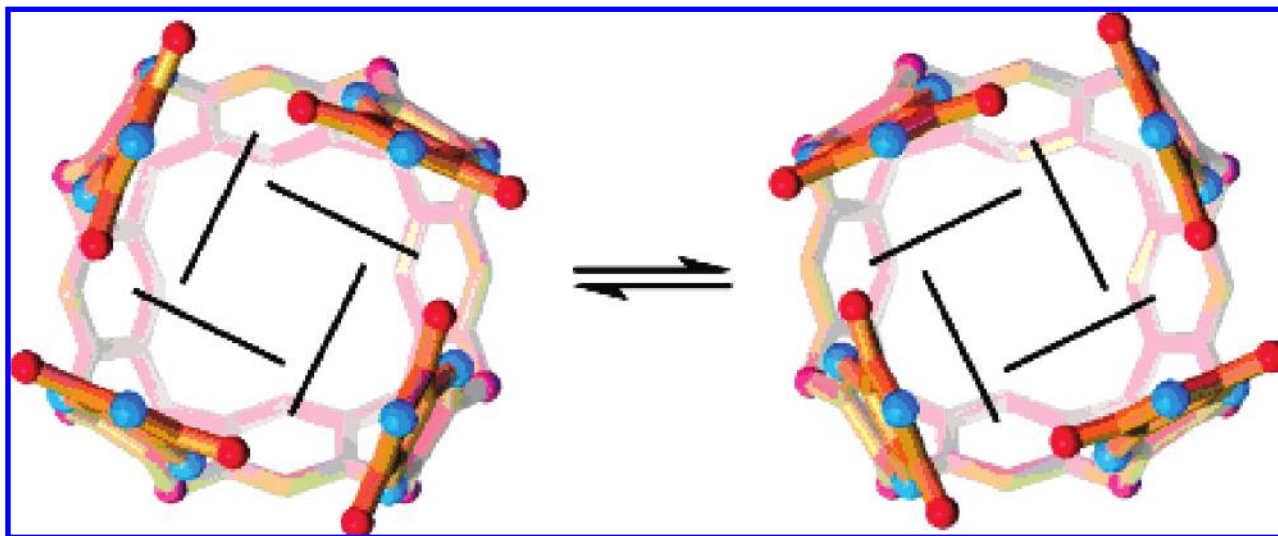


**Figure 45.** Depiction of the equilibrium between the two enantiomeric folded forms of the vase-lake conformation. Reprinted with permission from Saito, S.; Nuckolls, C.; Rebek, J., Jr. *J. Am. Chem. Soc.* **2000**, 122, 9628. Copyright 2000 American Chemical Society.

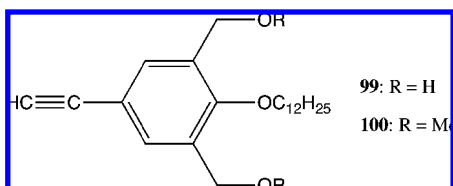


**Figure 46.** Structures of the monomers (**99**, **100**).

steric bulk of the host's substituents. This increase helps to resist the competition by the MeOH for the host's intramolecular hydrogen-bonding sites by increasing the steric hindrance for the approach of the solvent molecules. Specifically, **96** (smaller Me substituent) requires 30% MeOH for decomplexation of the guest, while **97** (larger Ph substituent) requires 60% MeOH addition.

This inter- versus intramolecular competition for hydrogen-bonding sites between the solute and the solvent can be seen to be crucial for the functioning in many important systems. For instance, in the sense-selective helical polymerization reactions studied by Aoki et al.,<sup>101</sup> in this, they looked at the role played by the *ortho*-hydroxymethyl substituents on the chirality of poly(phenylacetylene) polymers formed from monomers **99** and **100** catalyzed with (*R*)-1-phenylethylamine as a chiral cocatalyst; see Figure 46.

It was postulated that there were intramolecular hydrogen bonds involving the *ortho*-hydroxymethyl substituents; to test this, increasing amounts of dimethyl sulfoxide (DMSO) were added to a solution of poly-**99** in CCl<sub>4</sub>. As the ratio of DMSO was gradually increased, the bisignate CD signal between 430 and 310 nm gradually decreased in intensity, reaching zero at a CCl<sub>4</sub>/DMSO ratio of 10:1. Accompanying this decrease is a gradual shift in the OH vibrational band (3300 cm<sup>-1</sup>) in the infrared spectra to larger values, which indicates the gradual weakening on the hydrogen bonds, which can be expected from the conversion from intra- to intermolecular hydrogen-bonding interactions. To further test the hypotheses that the polymer's intramolecular hydrogen bonds were crucial to its chiral integrity and that the DMSO solvent was indeed a competing component in a supramolecular assembly, copolymers of **99** and **100** were synthesized with increasing ratios of **100**. The critical point here is that **100** has its *ortho* hydrogen-bonding ability blocked by the

conversion of the hydroxyls to methoxy groups. Thus, as the ratio of **100/99** in the copolymer increases, the magnitude of the chirality correspondingly decreases, as the intramolecular hydrogen bonds are less and less present to stabilize the chiral conformations. At a **100/99** ratio of 53:47, no optical activity is observed.

So far, we have considered the solvent effect, mainly, in terms of dielectric constants and hydrogen-bonding ability; however, in the work by Ogoshi and co-workers, using the dielectric-like solvent polarity parameter  $E_T(30)$ ,<sup>102</sup> the contribution of the solvents' polarizability was investigated.<sup>103</sup>

The system studied is a series of zinc bilinone derivatives (**101**, **102**, and **103**), that can form either a *P*- or an *M*-helix, with the magnitude of the diastereomeric preference determined, initially, by the chiral auxiliary; see Figure 47.

The CD spectra always have a first positive–second negative bisignate CD signal showing that the *P*-helix predominates in the equilibrium; there was found to be a good linear relationship between the absolute bisignate CD signal magnitude  $|\Delta\epsilon|$  and the diastereomeric excess (de) as determined from <sup>1</sup>H NMR.

On comparing the  $-\Delta G^\circ$  value for the *M*-to-*P* conversion (essentially the stability of the major conformer) with the  $E_T(30)$  values in different solvents (cyclohexane, CHCl<sub>3</sub>, benzene, THF, CH<sub>2</sub>Cl<sub>2</sub>, acetone, and MeCN), a reasonable linear correlation was found, with the solvents of higher  $E_T(30)$  values giving a greater  $-\Delta G^\circ$  for **101** and **102** but with almost no effect for **103**. This can be rationalized by considering the electrostatic interactions occurring between the phenyl groups and the bilinone framework in polar solvents for **101** and **102**, which cause significant steric interactions between them and, thus, greater chirality induction. However, in **103**, where there is no group with a polarizable  $\pi$ -electron system (such as the phenyl group in **101** and **102**) with which the solvent can interact, the effect of the different  $E_T(30)$  value solvents is minimal.

As mentioned previously, the authors consider another mechanism by which the solvent may interact with the bilinone. This is to look at how the change in chirality magnitude can be understood in terms of the solvents' polarizability. Again, a linear correlation is found between

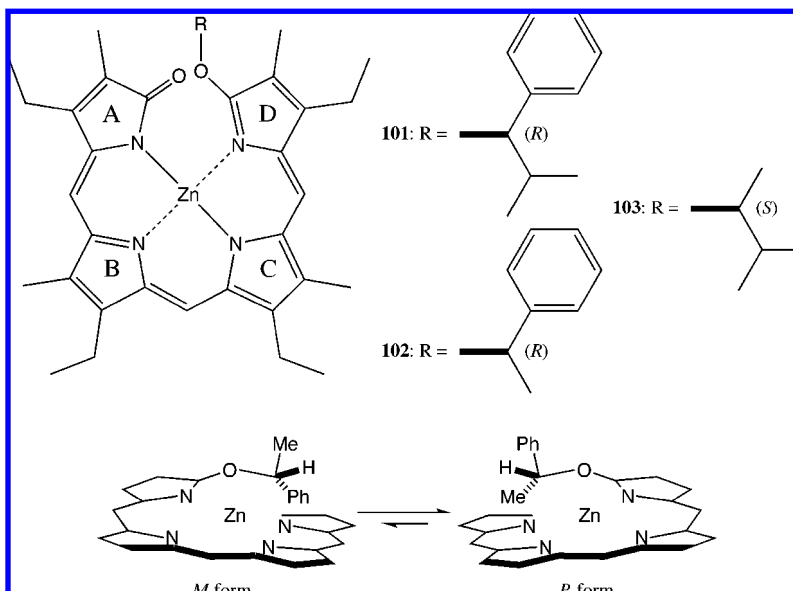


**Figure 47.** Structures of the Zn bilinones (**101**–**103**) and schematic representation of the equilibrium between the P- and M-helical structures in **102**. The four pyrrole rings are designated as A, B, C, and D.

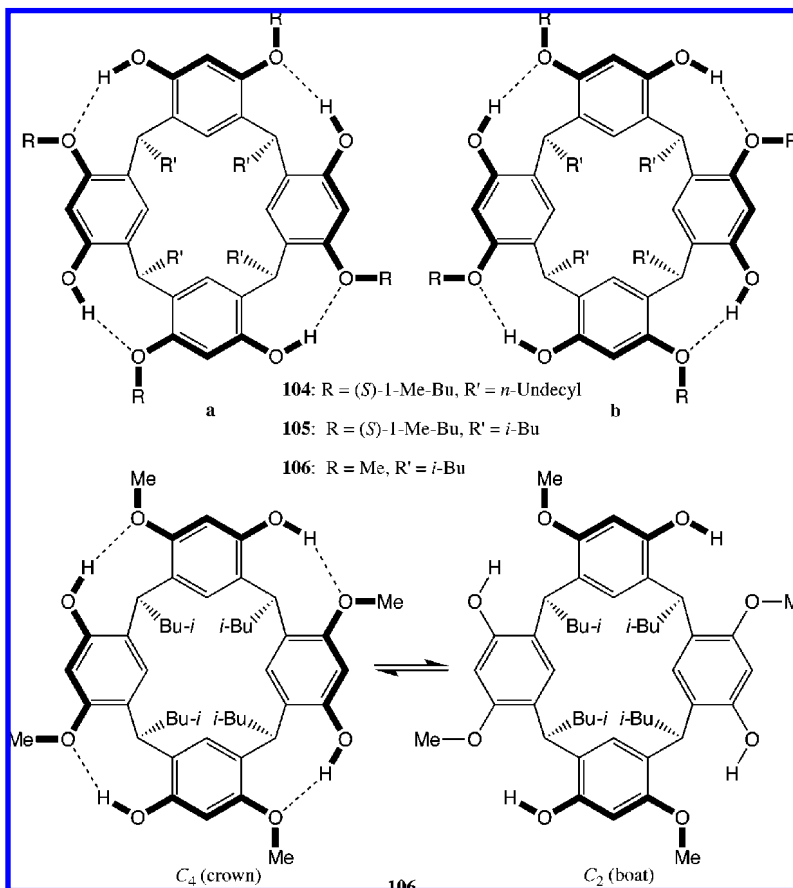


**Figure 48.** Structures of the calix[4]arenes (**104**–**106**) and equilibrium between crown and boat conformations of **106b**.

the solvent's polarizability and the  $-\Delta G^\circ$  value, with solvents of small polarizability (MeCN and acetone, polarizabilities of 4.41 and 6.39 Å<sup>3</sup>, respectively) giving higher  $-\Delta G^\circ$  values than those of larger polarizability (benzene and cyclohexane, polarizabilities of 10.3 and 10.9 Å<sup>3</sup>, respectively). Thus, it is postulated that, in more polarizable solvents, the bilinone molecule is solvated mainly through dispersion forces, and this weakens the van der Waals interactions between ring A of bilinone and its chiral auxiliary, resulting in a weaker

intramolecular interaction and, thus, a lower magnitude of optical activity.

A detailed example of how a solvent can affect the degree of chirality of a system and its molecular origin is found in the work of Schiel et al.<sup>104</sup> In this work, the solvent-controlled interconversion between the crown and boat conformations in an inherently chiral calix[4]arene (Figure 48) and the associated chiral changes are investigated, highlighting the supramolecular nature of its mechanism.

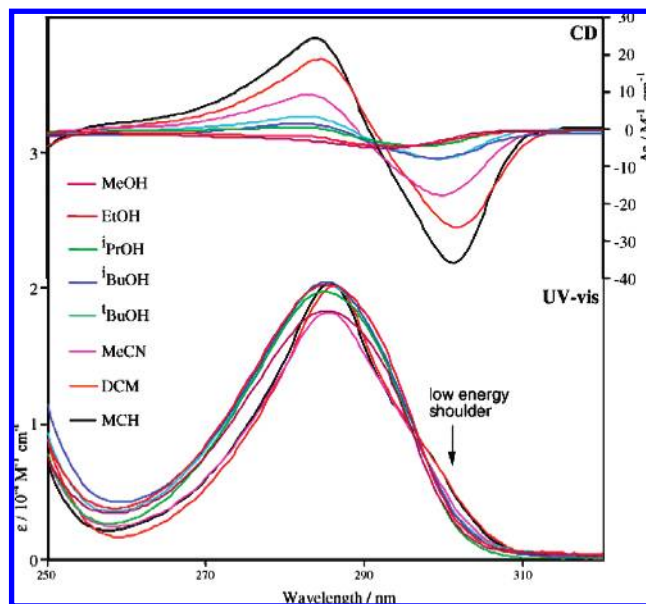


**Figure 49.** UV-vis and CD spectra of **104a** with various solvents. Reprinted with permission from Schiel, C.; Hembury, G. A.; Borovkov, V. V.; Klaes, M.; Agena, C.; Wada, T.; Grimme, S.; Inoue, Y.; Mattay, J. *J. Org. Chem.* **2006**, *71*, 976. Copyright 2006 American Chemical Society.

In less polar solvents (i.e., those with low hydrogen-bonding ability such as methylcyclohexane (MCH)), **104**–**106** are found to exhibit a first negative–second positive bisignate CD signal centered at ca. 295 nm. This result arises because the intramolecular hydrogen bonds between the aromatic substituents form a concerted ring and allow through-space coupling between the electronic transitions. However, as the solvent is changed to more polar/more hydrogen-bonding ones, the bisignate CD signal is gradually replaced by a positive monosignate one. Detailed consideration relates the structure of the solvents to the absolute magnitude of chirality induction ( $|\Delta\epsilon|$ ) and finally to the structural changes in the calix[4]arene; see Figure 49.

Thus, in the case of **104** with MCH, this is a low-polarity solvent with no hydrogen donor/acceptor atoms (e.g., N, O, S, etc.); consequently, this promotes the intramolecular hydrogen-bond-stabilized crown conformation giving a  $|\Delta\epsilon|$  value of  $-60.0 \text{ cm}^{-1} \text{ M}^{-1}$ . As the solvent is changed to  $\text{CH}_2\text{Cl}_2$  and then to MeCN, the magnitude of the bisignate CD signal is reduced to  $|\Delta\epsilon| = -45.0$  and  $-26.8 \text{ cm}^{-1} \text{ M}^{-1}$ , respectively. This reduction shows that these solvents are more able to compete for the calix[4]arene's hydrogen-bonding sites, with MeCN been more effective than  $\text{CH}_2\text{Cl}_2$ . The next three solvents,  $t\text{BuOH}$ ,  $i\text{BuOH}$ , and  $i\text{PrOH}$  (affording  $|\Delta\epsilon|$  values of  $-11.4$ ,  $-9.4$ , and  $-4.9 \text{ cm}^{-1} \text{ M}^{-1}$ , respectively), are worth considering more closely.  $t\text{BuOH}$ , bearing an effective hydrogen-bonding moiety, further reduces the bisignate chirality, but not so much as  $i\text{BuOH}$ . This difference between the two butanol isomers is believed to be due to the lower steric hindrance posed by the isobutyl configuration compared to the *tert*-butyl group when trying to approach the calix[4]arene. The slightly smaller  $i\text{PrOH}$  solvent correspondingly is less sterically restricted and, consequently, reduces the bisignate CD signal to approaching zero. Finally, on use of EtOH and MeOH solvents, there is only a monosignate Cotton effect and the conformation of the calix[4]arene is now wholly boat, with the calix[4]arene's aromatic substituents now participating effectively in solely

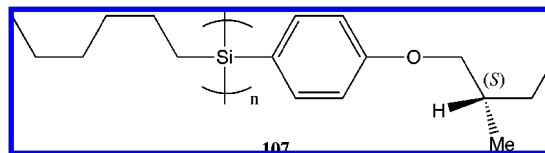


**Figure 50.** Structure of **107**.

intermolecular hydrogen bonds with the EtOH or MeOH solvent.

Finally, a demonstration of how the solvent acts as an active molecular participant in a supramolecular assembly is found in the variable-temperature (VT) CD experiments of calix[4]arene **105a** in  $t\text{BuOH}$ . At 348 K, the CD spectrum is a strong bisignate type, showing that the crown conformation (and, thus, the intramolecular hydrogen bonding) is dominant. As the temperature is reduced, the magnitude of the bisignate CD signal is also reduced, until finally, at 248 K, only a monosignate spectrum remains. The rationale for these changes is that, as the temperature is reduced, the binding constant between the calix[4]arene and  $t\text{BuOH}$  is increased, until it is eventually high enough to overcome the steric hindrance of the aromatic substituents and cause complete disruption of the intramolecular hydrogen-bonding network.

### 5.1.2. Solvent-Mediated Chirality Inversion

Further to the above effects on the magnitude of the induced chirality, it is also possible to switch the sign of chirality in supramolecular systems via solvent manipulation of the interactions occurring within the assembly. Work by Nakashima et al.<sup>105</sup> utilizing a series of poly(alkylarylsilane)s concerning mixed-solvent mediated chirality induction and inversion is particularly interesting as it highlights a critical dependence on the order in which the polymer is exposed to different solvents. The poly(alkylarylsilane) **107** considered here (Figure 50), while possessing point chirality, is optically inactive in the region of 250–450 nm in THF or toluene solution when it is molecularly dispersed due to equal amounts of *P*- and *M*-screw structures in dynamic equilibrium.

However, on the addition of a poor solvent, such as MeOH, optical activity is observed in the CD spectra, although this only occurs at above a 70:30 THF/MeOH ratio. Interestingly, this system displays an unusual phenomenon of the chirality-inversion effect that is dependent upon the method by which polymer is exposed to the different solvents. The two methods are as follows: method I, methanol added to a bulk THF solution of the polymer; method II, a THF solution of the polymer is added to bulk methanol. The relationship of the induced chirality with the THF/MeOH ratio and the solvent addition method is shown in Figure 51.

To determine the origin of the chirality, the solutions were filtered through either a  $5 \mu\text{m}$  or  $0.5 \mu\text{m}$  filter; for the  $5 \mu\text{m}$  case, a CD spectrum was still observed, but this was not the case for the  $0.5 \mu\text{m}$  filter. This effect shows that the origin of the chirality, in the wavelength range considered, is due to intermolecular aggregation of individual polymer molecules.

In the polymer solution produced via method I at 55:45 THF/MeOH ratio, a first positive–second negative bisignate CD signal is observed. However, via method II at the same 55:45 ratio, this is switched to a first negative–second positive. It is concluded that, in methods I and II, the physical–chemical characteristics of the microenvironments



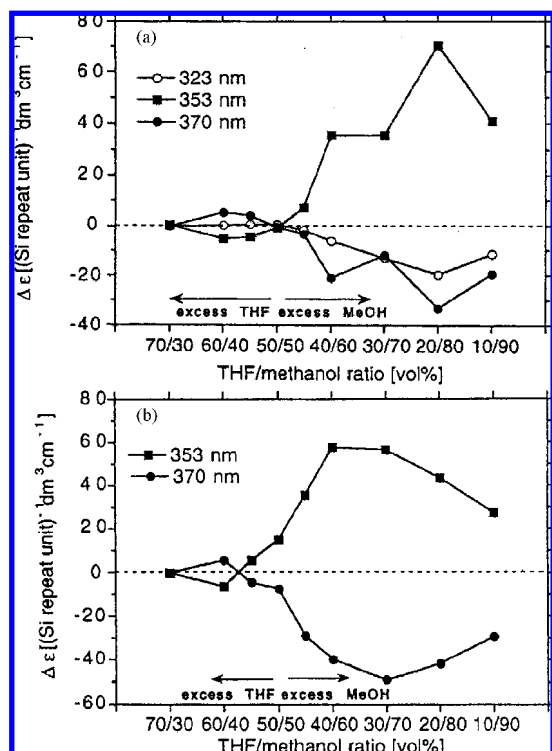


**Figure 51.** Plots of CD intensities of **107** aggregates prepared by methods I (a) and II (b) at various THF/MeOH ratios at 20 °C. Reprinted with permission from Nakashima, H.; Fujiki, M.; Koe, J. R.; Motonaga, M. *J. Am. Chem. Soc.* **2001**, *123*, 1963. Copyright 2001 American Chemical Society.

(such as the polarity) that the polymer is initially exposed to, as chirality is generated via intermolecular associations, are different. As a result, the authors suggested that the “seed” polymer aggregates formed by each method are of different conformations and result in the observed opposite chirality signs. In a model proposed by Nakanishi and Berova,<sup>106</sup> the handedness of a superhelix can be found to be dependent on the ratio between the polymer’s helical screw pitch ( $p$ ), the helical diameter ( $d$ ), and  $\pi$  (3.142) (for  $p/d < \pi$ , a right-handed screw is expected, and for  $p/d > \pi$ , a left-handed screw is expected). In this case, it is suggested that  $p$  is most influenced by the solvent, with its value becoming smaller as the polymer shrinks and folds in poor solvents.

A conceptually interesting solvent-dependent chirally inverting system is the polymer-based system reported by

Novak and co-workers<sup>107</sup> Here, we see a helix-sense selective synthesis of a chiral anthryl-based polymer, poly[*N*-(1-anthryl)-*N'*-octadecylcarbodiimide] **108**, that is regio- and stereoregular with a chiral catalyst based on a binaphthyl titanium alkoxide; see Figure 52.

The result of this is a polymer that, while possessing no chiral centers, is chiral as a result of its intramolecular conformation. This phenomenon is evident in the negative Cotton effect arising in the 300–450 nm region of the CD spectrum in THF at 298 K. Intriguingly, on sequential addition of toluene, the negative Cotton effect is first diminished and then inverts to give a weaker but positive Cotton effect (Figure 53); this switching is shown to be reversible.

Three proposals for the change in structure that causes the chirality inversion are suggested, i.e., (i) helix inversion, (ii) imine inversion, and (iii) rotation around the *N*-anthracene bond. The imine and helix inversions are ruled out as these are believed to be responsible for racemization, and this takes ca. 100 h at 353 K, but the chirality inversion takes place at 312 K in <1 min. Thus, the rotation around the *N*-anthracene bond is believed to be the major contribution, a supposition supported by a red shift in the UV–vis spectra over the switching region relating to different conformations of the anthryl moieties. However, this is not unambiguously proven, and no detailed mechanism of the solvent-mediated mechanism is suggested.

Solvent-mediated chirality inversion is also seen in the dendrimers **109** and **110** of Hofacker and Parquette; see Figure 54.<sup>108</sup> In these compounds, the chirality throughout the dendrons can be understood to arise from chiral steric interactions between the pentaethylene glycol terminal substituents that are propagated through the generations.

Dendron **109** gives a negative bisignate CD signal (*M* helicity), centered at ca. 316 nm, in both THF and H<sub>2</sub>O, that arises from the  $\pi$ – $\pi^*$  transitions of the anthranilate moieties. However, while the second-generation dendron **110** also gave a negative bisignate CD signal in THF, it was found to have switched to a positive bisignate CD signal in aqueous media, thus giving *P*-helicity. The corresponding UV–vis and CD spectra over the 10<sup>−4</sup>–10<sup>−6</sup> M concentration range were found to be invariant, thus precluding aggregation as an influencing factor on the chirality inversion. This switching results in a change in the relative chiral orientation of the anthranilate moieties, as shown in Figure 55.

Complementary IR experiments in THF/H<sub>2</sub>O mixed solvents reveal that, on increasing the content of H<sub>2</sub>O, the

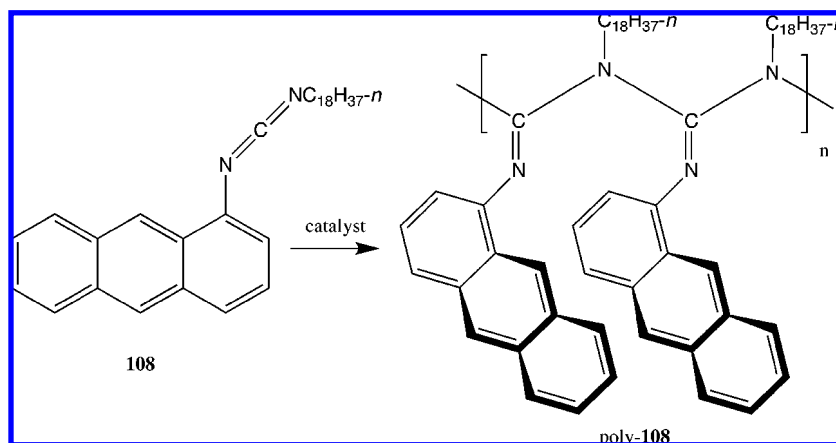


**Figure 52.** Schematic representation of obtaining poly-**108** from **108**.

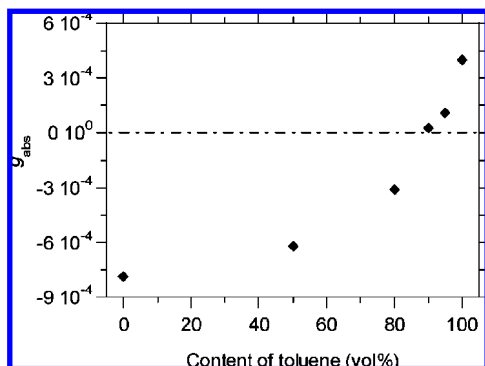


**Figure 53.**  $g_{\text{abs}}$ -values at 380 nm of poly-**108** in toluene/THF at 25 °C. Reprinted with permission from Tang, H.-Z.; Boyle, P. D.; Novak, B. M. *J. Am. Chem. Soc.* **2005**, *127*, 2136. Copyright 2005 American Chemical Society.

pentaethylene glycol groups undergo a gauche-to-anti conformational shift about the C–O bond, which is believed to result in a change in chiral steric interactions that leads to the switch in handedness. Additionally, a Monte Carlo conformational investigation of **110** in a GB/SA solvation model<sup>109</sup> results in an *M*-helix predicted for **110** in CHCl<sub>3</sub> (a model for THF) and a *P*-helix in H<sub>2</sub>O, which agrees with the CD experimental results from solution and also with the gauche-to-anti changes seen in the IR data. Thus, here we see a chirality-inversion phenomenon that is solvent mediated but rationalized in terms of the effect of the bulk solvent.

Work that considers the solvent effect at a molecular level is that of Lightner and co-workers,<sup>110</sup> which is concerned with how the variation in solvent composition affects chirality inversion and magnitude in the tetrapyrrole-like bilirubin system. This study finds that, in most solvents, including those as diverse as benzene, methanol, and *N*-methylformamide, an intramolecular hydrogen-bonded structure is formed that has either *M*- or *P*-helicity.<sup>110b</sup> For **111**, in such solvents as mentioned previously, there is a preference for *P*-helicity that arises from the chiral steric interactions between the two methyl substituents at the  $\beta$  position to the carboxylic acid

group (Figure 56); the result of this is that a first positive–second negative bisignate signal is seen in the CD spectrum arising from the coupling between the two electronic transitions, directions of which are shown in Figure 56.

The critical effect of the intramolecular hydrogen bonds is seen on the addition of DMSO, which successfully competes for the hydrogen-bonding sites, resulting in a reduction in the magnitude of the Cotton effects.

Another interesting finding was that, on stepwise addition to the original solvent of an amine (e.g., *n*-propyl-, di-*n*-propyl-, and tri-*n*-propylamine) as a cosolvent, the negative CD couplet gradually diminished and finally inverted to give a positive bisignate CD signal (Figure 57). The physical interpretation of this is that the orientation of the electronic transitions from the two dipyrinone moieties has switched from a clockwise to anticlockwise direction; see Figure 56.

The order of inversion efficiency was secondary > primary > tertiary amine in CHCl<sub>3</sub> (although this is, to a degree, found to be solvent dependent). The underlying mechanism is believed to be an acid–base reaction with the propionic acid group. Crucially, the amine remains coordinated to the acid moiety in some sort of ion–ion assembly (as deprotonation with the noncoordinating tetra-*n*-butylammonium hydroxide gave no inversion) and likely results in a new steric mode of intermolecular interaction that yields chirality inversion.

This is conceptually interesting in that amines are used as a cosolvent, particularly because amines are normally considered as ligands and not solvents in such systems. Thus, because the amine, with its well-known hydrogen-bonding/ coordinating ability, is treated as a cosolvent, it forces us to remember that solvents should always be considered in terms of their potential for interaction with the solute and its corresponding supramolecular effect on any related properties.

Recently, an important contribution to understanding the molecular-based mechanisms of solvent mediation of chirality control in supramolecular systems was made by our group, in which the solvent is considered explicitly as another

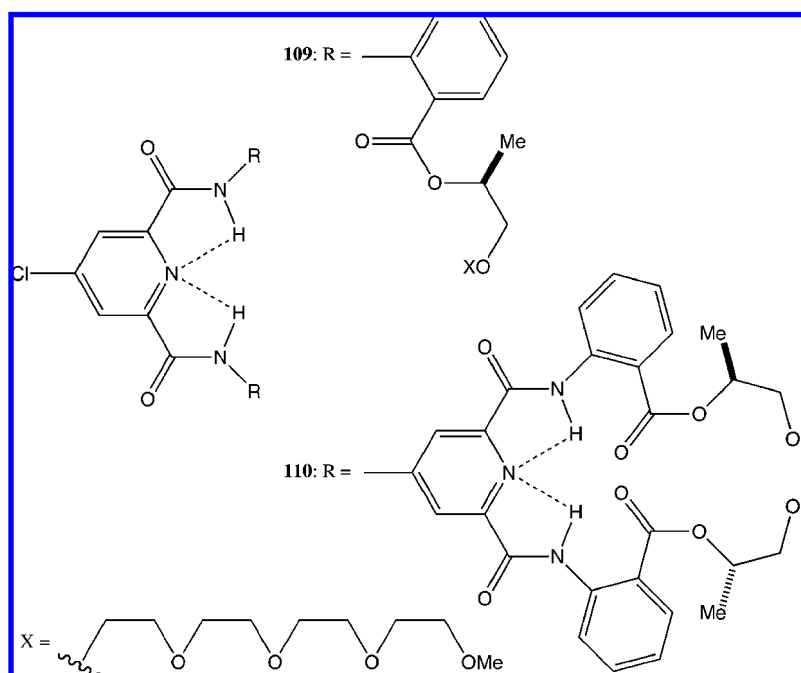


**Figure 54.** Structures of the dendrimers (**109** and **110**).

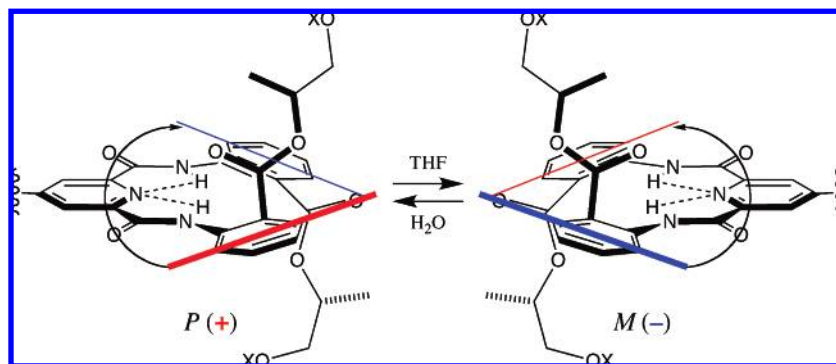


**Figure 55.** Schematic representation of the  $\pi$ - $\pi^*$  electronic transition direction in **110** in THF and  $\text{H}_2\text{O}$ .

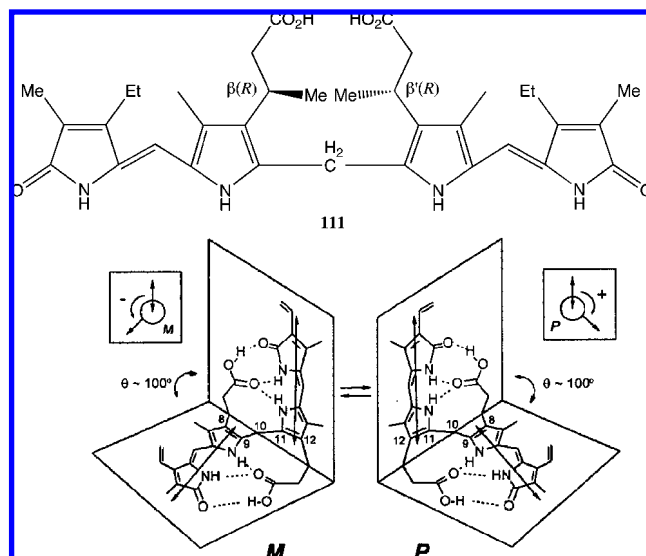


**Figure 56.** Structure of **111** and schematic representation of the most stable (enantiomeric) conformations of bilirubin (M and P) with the approximate orientation of the electric dipole moments associated with the dipyrinone long-wavelength transitions. Reprinted in part with permission from Boiadjev, S. E.; Lightner, D. A. *J. Am. Chem. Soc.* **2000**, *122*, 378. Copyright 2000 American Chemical Society.

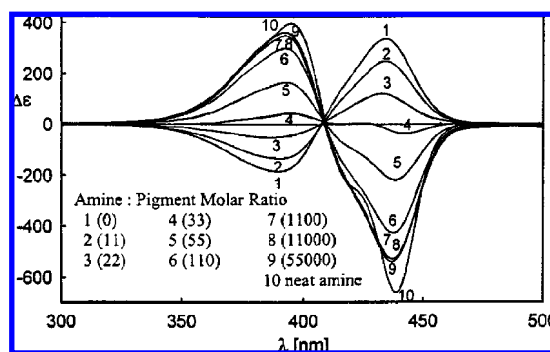


**Figure 57.** Changes in the CD spectrum of **111** upon sequential changing from pure  $\text{CHCl}_3$  solvent to pure  $n\text{-Pr}_2\text{NH}$  solvent. Reprinted with permission from Boiadjev, S. E.; Lightner, D. A. *J. Am. Chem. Soc.* **2000**, *122*, 378. Copyright 2000 American Chemical Society.

component in the whole assembly. Thus, in this work, it was determined how different solvents, considered in terms of their electrostatic distribution and size (i.e., their ability to interact with the solute molecules), mediated changes in chirality magnitude and chirality sign.<sup>27a,111</sup>

Particularly, the insight into the nature of the solvent effect on the chirality comes from detailed studies into changes in

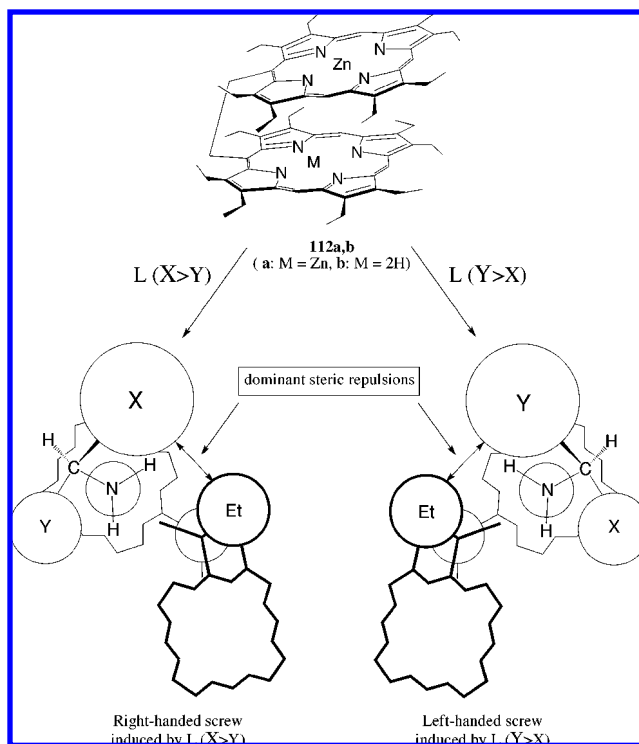


**Figure 58.** Structure of **112** and mechanism of the chirality induction upon interaction with chiral ligands.

the conformation of the supramolecular species formed between achiral bisporphyrins, **112**, and chiral ligands. The basic structural changes are shown in Figure 58 (also see section 6 for further details).

Initially, the bisporphyrin is in a folded syn conformation; then, on external ligation, this changes to the extended anti structure. Because of their close spatial proximity, the ligand's X and Y substituents can interact sterically with the neighboring porphyrin's 3- and 7-position ethyl groups. The result of these interactions is the induction of a screw (helical) structure between the two porphyrin moieties. Thus, when the bulk of the X and Y substituents are equal, it is expected that the steric interactions at the 3- and 7-positions will be equal and that no chirality is induced; however, when the substituent sizes are different, one of the screw structures (either left- or right-handed) dominates and chirality is observed. However, if the ligand is achiral, this will result in an averaging of the steric interactions and the corresponding absence of supramolecular chirality.

Initially, the solvent-effect mechanism was shown to arise from the ability of the solvent and the ligand substituents to interact in an electrostatic manner. That is, if the solvent

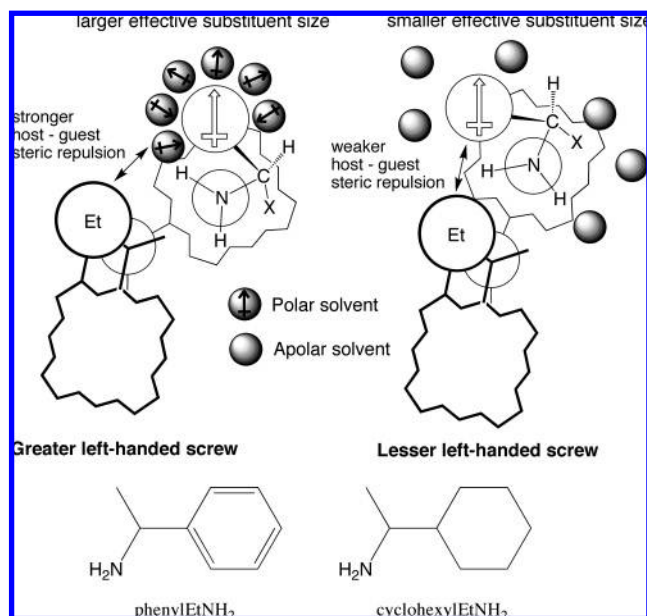


**Figure 59.** Schematic representation of the solvent effect on supramolecular chirality induction in the **112**•*L* systems and structures of phenylEtNH<sub>2</sub> and cyclohexylEtNH<sub>2</sub>.

**Table 4.** Reduction of the *A* and *g* Factor Values of **112b**•*L* in CCl<sub>4</sub> Compared to Those in CH<sub>2</sub>Cl<sub>2</sub><sup>111</sup>

<i>L</i>	% reduction ( <i>A</i> value)	% reduction ( <i>g</i> factor)
( <i>R</i> )-phenylEtNH <sub>2</sub>	59.2	59
( <i>S</i> )-phenylEtNH <sub>2</sub>	58.2	53
( <i>R</i> )-cyclohexEtNH <sub>2</sub>	32.1	33
( <i>S</i> )-cyclohexEtNH <sub>2</sub>	36.2	25

and one of the ligand's substituents have a pronounced electrostatic distribution or polarizability (such as a carbonyl or aromatic group), then these are able to interact in a supramolecular manner. This mechanism can be seen in the comparison of the chirality induction in these bisporphyrin systems, for both substituents and solvents, with and without strong electrostatic distributions and/or polarizabilities. This can be shown first by looking at the effect of polar and nonpolar solvents; see Figure 59.

The effect of the combination of the different solvents and substituents is highlighted for the changes in chirality induction in phenylEtNH<sub>2</sub> and its less polar analogue cyclohexylEtNH<sub>2</sub> (Figure 59) in both polar (CH<sub>2</sub>Cl<sub>2</sub>) and nonpolar (CCl<sub>4</sub>) solvents; see Table 4.

For the cyclohexylEtNH<sub>2</sub> ligand, the reduction in chirality on going from the CH<sub>2</sub>Cl<sub>2</sub> to CCl<sub>4</sub> is clearly less than that for its more polar phenylEtNH<sub>2</sub> analogue. The rationale for this is that there is less interaction between the cyclohexyl substituent and CH<sub>2</sub>Cl<sub>2</sub> because of the lack of complementary electrostatic distributions. In the case of the phenylEtNH<sub>2</sub> ligand in CH<sub>2</sub>Cl<sub>2</sub>, the dipole-induced dipole interactions between the solvent molecules and the phenyl ring result in a degree of association that increases the effective size of the phenyl substituent. This subsequently increases the magnitude of the steric repulsion with the adjacent ethyl group of the neighboring porphyrin moiety, so increasing the screw angle and, thus, the induced chirality. Therefore, on going to the CCl<sub>4</sub> solvent, the reduction in effective size of phenylEtNH<sub>2</sub> is greater than that for the cyclohexylEtNH<sub>2</sub> case, and consequently, the reduction in chirality is greater.

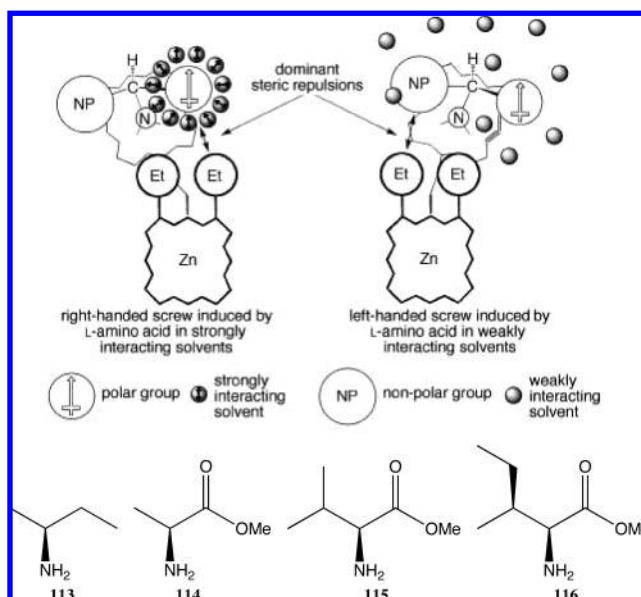


**Figure 60.** Solvent effect on the mechanism of supramolecular chirality induction in **112a**•*L* (*L* = **113**–**116**), in strongly and weakly interacting solvents, and structure of **113**–**116**. Reprinted in part with permission from Borovkov, V. V.; Hembury, G. A.; Inoue, T. *Angew. Chem., Int. Ed.* **2003**, *42*, 5310. Copyright 2003 Wiley-VCH Verlag GmbH & Co.

In subsequent work,<sup>27a</sup> this insight into the supramolecular nature of the solvent effect was taken further, with solvent shown to be understandable in a more conventional supramolecular manner, with the degree of interaction shown to be dependent on not only the electrostatic compatibility but also on its size and geometry.

In comparison to the previous work, the ligands (methyl esters of *L*-amino acids) are chosen to have two substituents at the stereogenic center of similar sizes (*C*-terminus and side-chain substituents), thus giving similar degrees of chirality-inducing steric interactions with the neighboring porphyrin. This means that even small changes to the effective size of one of the substituents by the formation of the corresponding solvent shell may result in drastic chirality modulation, such as chirality inversion; see Figure 60.

A detailed analysis investigating such inversion was performed by comparing the sign and magnitude of the induced chirality with the dielectric constant of a number of solvents; see Figure 61.

Initially, it can be seen that, for ligand **113**, the effect of the different solvents is negligible. This is because both substituents (methyl and ethyl at the stereogenic center) are nonpolar alkyl groups with which all the solvents will only weakly interact; thus, this ligand acts as a "solvent inert" reference. However, for ligands **114**, **115**, and **116**, dramatic solvent-induced changes are observed. In low  $\epsilon$  value solvents (hexane, cyclohexane, and CCl<sub>4</sub>), the interaction between the solvent and the polar methyl ester substituent is rather small and the alkyl group of larger effective size controls the induced negative chirality. However, for benzene, although it has a very similar  $\epsilon$  value to the previous solvents, the induced optical activity is dramatically switched to positive values. This is due to the pronounced electrostatic distribution possessed by this aromatic solvent, which allows it to strongly interact with the polar methyl ester substituents, so increasing their effective sizes to be greater than the alkyl groups. Upon increasing the  $\epsilon$  values in polar media, the solvent molecules are able to dipole-dipole interact with



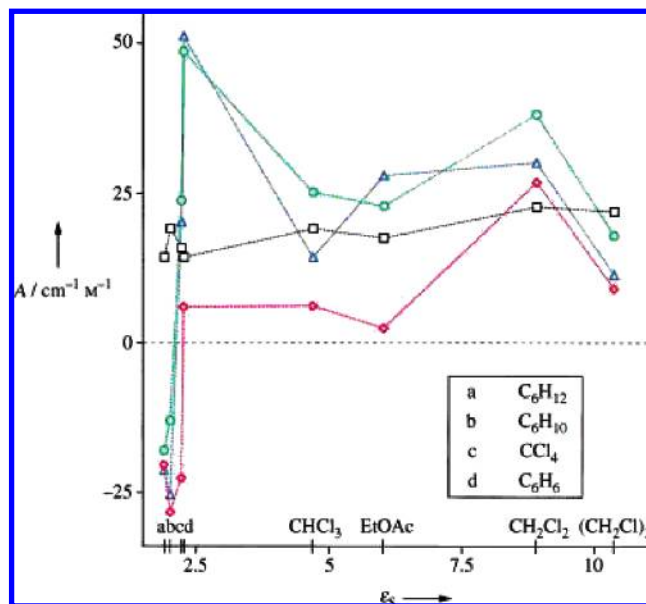


**Figure 61.** Dependence of the CD amplitude of **112a**·*L* (black, *L* = **113**; red, *L* = **114**; green, *L* = **115**; and blue, *L* = **116**) upon the dielectric constant of the solvent used. Reprinted with permission from Borovkov, V. V.; Hembury, G. A.; Inoue, T. *Angew. Chem., Int. Ed.* **2003**, 42, 5310. Copyright 2003 Wiley-VCH Verlag GmbH & Co.

the ester group of the amino acid derivatives, thus increasing the corresponding effective size of this group and switching the dominant stereogenic interactions that result in the chirality inversion.

The geometric influence of the solvent can be seen on consideration of the effect of dichloroethane. In this solvent, even though it possesses the highest  $\epsilon$  value used in this study, the induced chirality is reduced in comparison to  $\text{CH}_2\text{Cl}_2$  and the prevailing trend. This is believed to be due to its larger size that disallows efficient packing of the solvent molecules around the polar substituent, thus attenuating its effective-size enhancement in comparison to its  $\epsilon$  value.

## 5.2. Influence of Temperature on Supramolecular Chirality

Because supramolecular assemblies are dynamic multi-component systems whose intermolecular structures, and thus properties and functions, arise from the information encoded into the component molecules; any external influence that disrupts or influences this is of critical importance. Clearly, for such species held together by weak intermolecular interactions, temperature will be a key factor. The specific influences discussed here are as follows: the conceptually straightforward thermal disruption of assemblies, the more complex cases of macromolecular phase changes, and the changes in the controlling influence of the entropic and enthalpic contributions.

### 5.2.1. Temperature-Induced Monodisperse-to-Supramolecular Transitions

The subtleties of intermolecular interactions and the effect increasing the systems thermal energy are well-highlighted in work by van Herrikhuyzen et al.<sup>112</sup> In this, they observed how a slight change in the orientation of the hydrogen-bonding amide group dramatically influences the chiral supramolecular outcome of the assembly and how temperature variations differentially affect the observed optical activity.

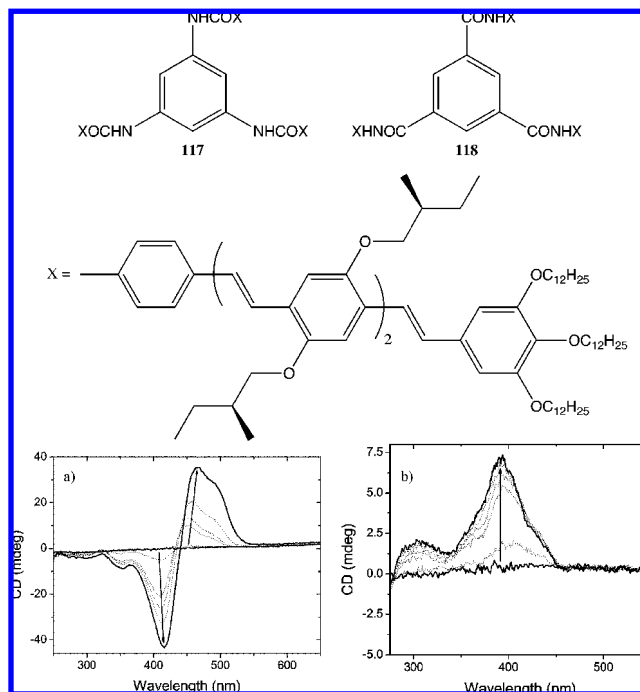


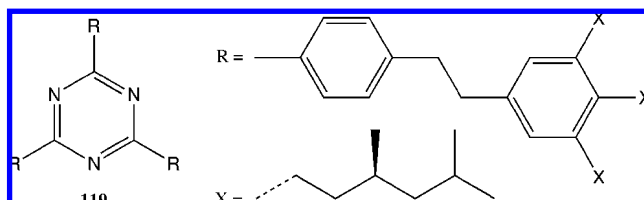
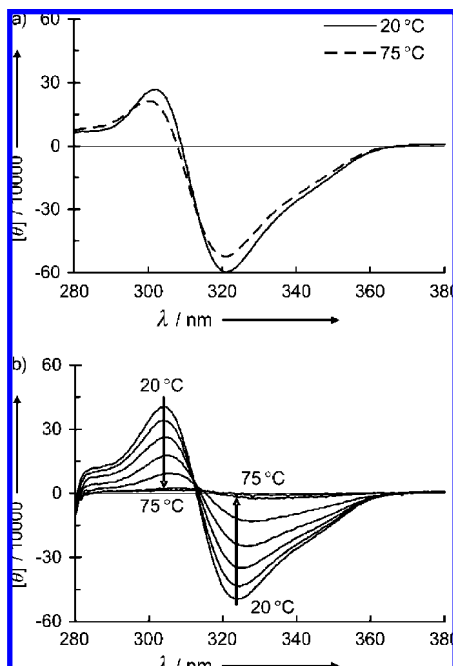
**Figure 62.** Structures and various temperature CD spectra of **117** (a) and **118** (b). Reprinted in part with permission from van Herrikhuyzen, J.; Jonkheijm, P.; Schenning, A. P. H. J.; Meijer, E. W. *Org. Biomol. Chem.* **2006**, 4, 1539. Copyright 2006 The Royal Society of Chemistry.

Two disklike 1,3,5-benzenetricarboxamide-based molecules, **117** and **118**, were found to form divergent assemblies in methylcyclohexane along the  $C_3$  axis. It should be noted here that, apparently, a small difference in the covalent structure of the two, i.e., the switching of the amide bond direction, resulted in dramatic differences in the supramolecular chirality, specifically, a positive bisignate CD signal for **117** and a positive monosignate Cotton effect for **118** (see Figure 62).

Investigation by IR spectroscopy revealed that the N–H stretching vibrations are found at  $3422\text{ cm}^{-1}$  (**117**) and  $3225\text{ cm}^{-1}$  (**118**), revealing the absence and presence of hydrogen bonding, respectively. VT CD experiments (Figure 62) showed that, on heating the two samples from 10 to  $90^\circ\text{C}$ , it was possible to disrupt the supramolecular assembly via thermal decomposition, finally resulting in loss of all chirality in the observed region. Interestingly, this is found by comparison with the associated UV–vis spectra to be a two-stage process; first, the chiral supramolecular assembly changes to an achiral one, and second, it finally becomes monodisperse. The heating effect also helps to reveal the differences in stabilities between the two systems. For **117**, the melting temperature ( $T_m$ ) is quite sharply centered at  $50^\circ\text{C}$ , while  $T_m$  for **118** is broader and centered at  $80^\circ\text{C}$ . This investigation into the different temperature effects suggests that the contribution of the amide hydrogen bonding in **118** increases the thermal stability of the assembly.

A similar effect for a supramolecular system based on  $C_3$  symmetric molecules is found in a work of Ishi-i et al.<sup>113</sup> Among others, they have investigated the columnar-type assemblies formed by **119**, which possesses a chiral center on each of its pendent alkyl chains; see Figure 63.

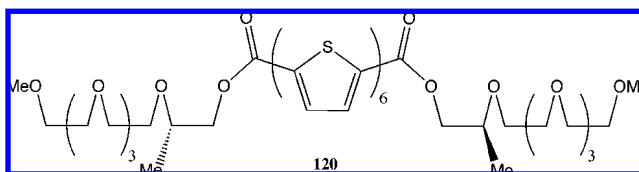
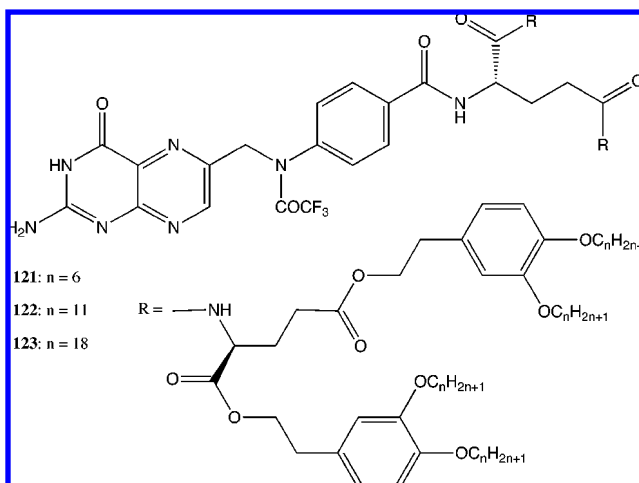
The stability of these aggregates was investigated by UV–vis and CD spectroscopies. At  $20^\circ\text{C}$  in octane, a strong absorption at  $329\text{ nm}$  is observed that correlates with the

**Figure 63.** Structure of **119**.**Figure 64.** Variable-temperature CD spectra of **119** in octane (a) and *p*-xylene (b). Reprinted with permission from Ishi-i, T.; Kuwahara, R.; Takata, A.; Jeong, Y.; Sakurai, K.; Makata, S. *Chem.—Eur. J.* **2006**, *12*, 763. Copyright 2006 Wiley-VCH Verlag GmbH & Co.

presence of the columnar-type intermolecular species. On heating to 75 °C, no significant changes are observed, revealing significant structural stability. However, in *p*-xylene on a stepwise increase in the temperature to 75 °C, the 329 nm peak is diminished and a new blue-shifted one at 308 nm appears, indicating the formation of the monodisperse species. This greater ability of the aromatic *p*-xylene to disrupt the supramolecular assembly (in comparison to the saturated hydrocarbon octane) is likely due to its  $\pi$ – $\pi$  interaction with the  $\pi$ -system of **119** (in a manner similar to that described in section 5.1). VT CD experiments of **119** in octane and *p*-xylene show the critical relationship between the supramolecular structure and the induced chirality; see Figure 64.

Thus, in both cases, a negative Cotton effect is observed, arising from the intermolecular coupling of the electronic transitions, revealing *M* helicity in the assembly. Heating from 20 °C in octane only results in a marginal reduction in CD intensity. However, in a manner analogous to the VT UV–vis experiments in *p*-xylene, the CD intensity is gradually reduced as the assembly's integrity is broken down and the increasing thermal energy of the system disrupts the intermolecular interactions.

An additional effect, but one in which the structure–chirality–temperature relationship is more subtly affected by the solvent, is seen in the supramolecular aggregates formed by the chiral  $\alpha,\alpha'$ -disubstituted sexithiophene, **120** (Figure 65).<sup>114</sup>

**Figure 65.** Structure of **120**.**Figure 66.** Structures of **121**–**123**.

In *n*-butanol, the UV–vis spectrum exhibits a maximum at 403 nm, which is typical for aggregated molecules of this type,<sup>115</sup> showing an approximate 50 nm blue shift in comparison to the monodisperse state found in more polar solvents such as chloroform. When a  $2.6 \times 10^{-5}$  M solution of **120** is cooled to –10 °C, a first negative–second positive bisignate CD signal is observed, revealing intermolecular exciton coupling in an *M*-helical arrangement. Its position is also well-matched with the corresponding UV–vis transition. Interestingly, the assembly also displays strong circularly polarized fluorescence, showing that it is chiral in both ground and excited states. On heating, the supramolecular assembly is disrupted in a manner similar to that described for **119**, **118**, and **117** previously. The CD signal is diminished and finally lost by 40 °C, while the UV–vis spectra show a correlated red shift. However, when the same experiments are carried out in aqueous solution, while the CD intensity and, thus, the chiral integrity of the species is lost by 40 °C, the UV–vis and fluorescence data indicate that **120** remains in an aggregated state above this temperature. This reveals that the relationship between the temperature effect and the chirality of an assembly can be more-or-less complex depending on the exact nature of the system, both solute and solvent.

### 5.2.2. Temperature-Induced Structural Changes in Supramolecular Assemblies

In the previous section, it was seen how temperature effects could disrupt supramolecular assemblies producing monodisperse solutions and a loss of chirality. However, there is another possibility: that the temperature effect can result in the transformation from one chiral supramolecular species to another one that is still optically active but with a different structure.

Such a transformation is observed in the liquid crystalline species produced by the folic acid derivatives (**121**–**123**) studied by Kato et al. (Figure 66),<sup>116</sup> which had also previously been shown to undergo smectic-to-columnar

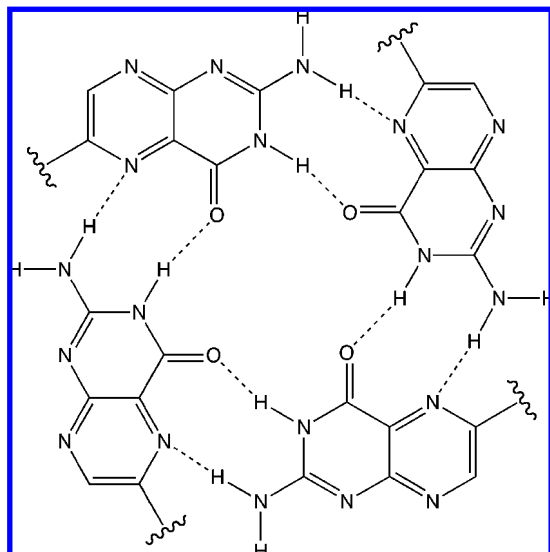


**Figure 67.** Schematic representation of tetrameric hydrogen-bonded assembly of pterin rings.

transitions induced by alkali metal salts and lipophilic solvents.<sup>117</sup>

The fundamental structural motif for the various liquid crystalline phases (which depend on a crucial 0.25 molar equiv of sodium triflate) found for these compounds is the tetrameric hydrogen-bonded assembly of pterin rings shown in Figure 67.

Analysis of the complementary VT small-angle X-ray scattering (SAXS) and VT CD experiments then reveals the temperature-controlled transitions between different phases and the effect on the supramolecular chirality; see Figure 68.

At 25 °C, **122** is in a columnar phase with an intercolumnar spacing of 55.2 Å; this corresponds to a positive bisignate CD signal with the maximum at 290 nm and the minimum at 268 nm. On heating, the intensity of this signal is gradually lost until none remains at 120 °C, although the columnar structure remains as judged from the SAXS profiles. However, at 140 °C, **122** undergoes a phase transition to a *Pm3n* cubic phase (lattice parameter of 100.0 Å) and results in a dramatic return in CD intensity with an accompanying chirality inversion producing a negative bisignate CD signal with the minimum at 358 nm and the maximum at 280 nm. Subsequent heating results in a gradual loss of the CD signal reaching zero as the cubic phase is lost, and the system becomes isotropic at 200 °C.

Thus, it is clear from this work that, as the thermal energy of the assembly changes, the intermolecular arrangement of the molecules adapts to find the energetically most favorable structure for the new conditions.

A different system is found in the nanostructures (visible by scanning electron microscopy (SEM)) formed by the self-assembly or combined-assembly of cardanyl glucosides **124** and **125**; see Figure 69.<sup>118</sup>

When **124** and **125** are combined in various ratios and subjected to a 2 day incubation, different chiral nanotube morphologies are observed: twisted ribbon, loosely coiled ribbon, tightly coiled ribbon, tubule with helical marking, and tubule without helical marking. These observations highlight the interestingly subtle supramolecular chemistry that transfers molecular chiral information to the meso/macroscopic scale. The temperature effect on the chirality and

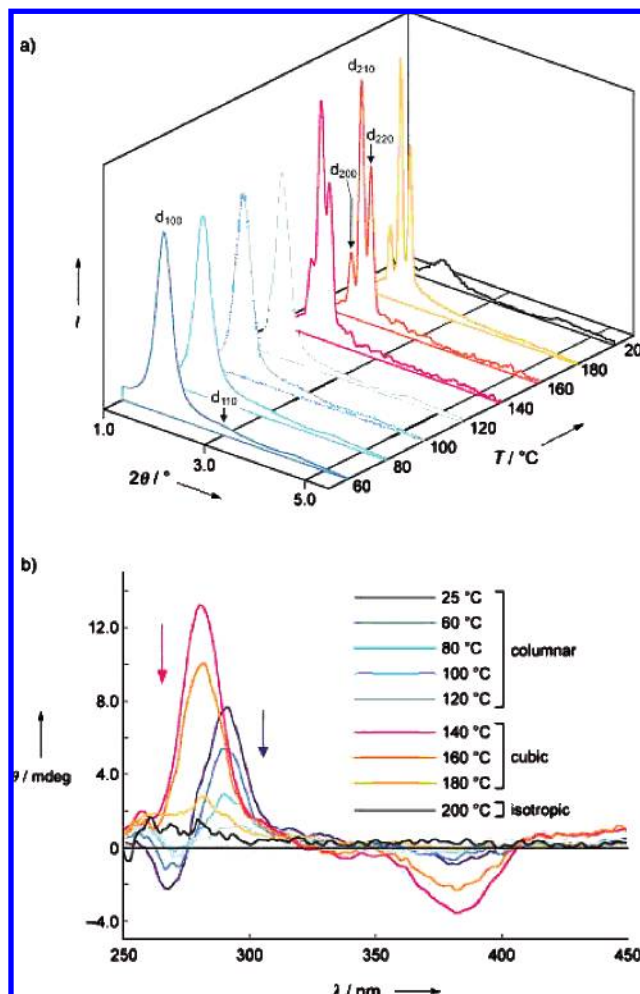


**Figure 68.** Small-angle X-ray diffraction profiles (a) and CD spectra (b) of the complex of **122**/NaOSO<sub>2</sub>CF<sub>3</sub> (1:0.25 molar ratio) on heating. Reprinted with permission from Kato, T.; Matsuoka, T.; Nishii, M.; Kamikawa, Y.; Kanie, K.; Nishimura, T.; Yashima, E.; Ujiie, S. *Angew. Chem., Int. Ed.* **2004**, *43*, 1969. Copyright 2004 Wiley-VCH Verlag GmbH & Co.

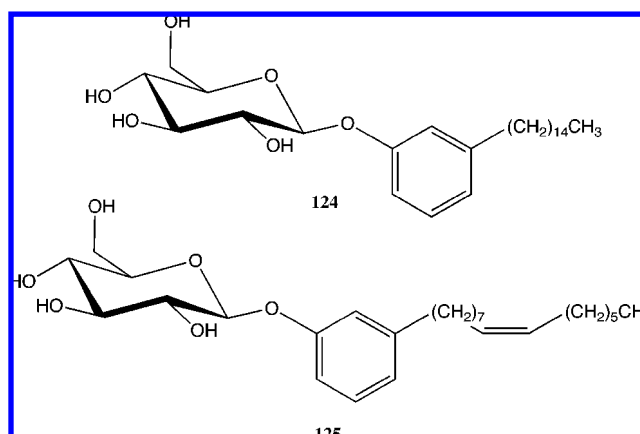


**Figure 69.** Structures of **124** and **125**.

morphology of such systems was investigated by studying the VT CD of **125** in water. At 25 °C, **125** is in a coiled helical structure with a strong negative Cotton effect at 200 nm. On heating, this is gradually reduced until, at 45 °C, an opposite and weak positive Cotton effect is observed, which correlates with a morphological switch to spherical vesicles.



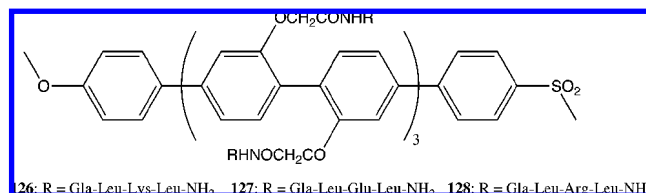


**Figure 70.** Structures of monomeric *p*-octiphenyl rods (**126–128**).

The transformation of an assembly between different forms is also well-known to occur in biomolecular species, and this realization has been used by various researchers to investigate the rational design of bio-inspired conformationally switchable chiral systems.<sup>119</sup> An example in which temperature is a crucial controlling element is found in the work of Sakai and Matile.<sup>120</sup> Here, the assembly of *p*-octiphenyl rods with six complementary tripeptide strands (**126–128**; see Figure 70) in the presence of a bilayer membrane is studied by VT UV-vis and CD measurements.

Addition of equimolar amounts of **127** and **128** to a solution containing large unilamellar vesicles from egg yolk phosphatidylcholine at 25 °C resulted in a first positive–second negative bisignate CD spectrum that is associated with a  $\beta$ -barrel structure. On raising the temperature to 70 °C, the magnitude of the Cotton effects increased but was found to be irreversible. At 90 °C, the chirality of the assembly inverted to give a weak negative bisignate CD signal, a change that is also irreversible and results in the formation of  $\beta$ -fibrils. Similar but less complex behavior is observed for the equivalent structures that comprised **126** and **127**. Here, irreversible structural changes and chirality inversion (positive-to-negative bisignate CD signals) are induced by varying the temperature from 20 to 95 °C.

Finally, chirality inversion is observed in the temperature-controlled switching between the B–Z and A–Z forms in DNA and RNA, respectively.<sup>121</sup> These are instructive supramolecular systems that well-highlight the delicate interplay between inter-/intramolecular interactions and the chirality of the structures formed, as well as how such systems may act as sensors.

The switch between the A-form of RNA and the B-form of DNA and their corresponding Z-forms is monitored by the magnitude of the fluorescence emission from a 2-aminopurine. In the A- and B-forms, the continuous  $\pi$ -stacks effectively quench the fluorescence; however, in the Z-forms, the formation of discrete four-base stacks reduces the quenching. The accompanying changes in chirality are measured by CD, and the overall results are described below in Figure 71.

Thus, for RNA at 20 °C, the right-handed A-form dominates, which gradually transforms to the Z-form by 45 °C; this is characterized by an inversion of the CD spectra at ca. 290 nm, although the negative first Cotton effect status remains unchanged. For DNA, its low-temperature structural preference is opposite to that for RNA, with the fluorescent Z-form present in comparison to the A-form for RNA. Thus, on heating, this switches to the nonfluorescent B-form.<sup>122</sup> This work elegantly shows how the chirality of the  $\pi$ - $\pi$ - and hydrogen-bond-stabilized helical structure can be dramatically switched by variation of the temperature and monitored by the fluorescence readout of the sensor.

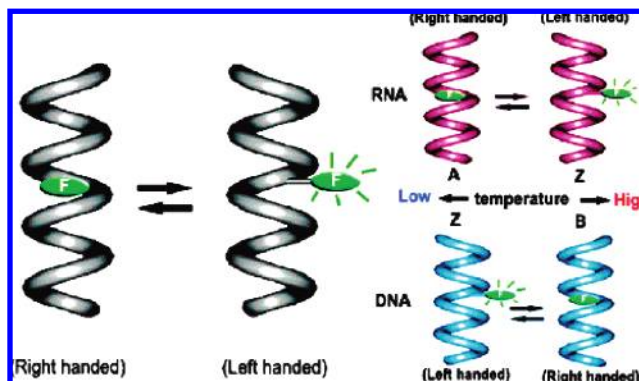


**Figure 71.** Schematic representation of the temperature-controlled RNA and DNA conformational switching. Reprinted with permission from Tashiro, R.; Sugiyama, H. *J. Am. Chem. Soc.* **2005**, *127*, 2094. Copyright 2005 American Chemical Society.

### 5.2.3. Temperature-Induced Changes in Enthalpy and Entropy Contributions

Typically, the main consideration given as to whether an intermolecular process, chiral or achiral, will proceed (and the degree to which it does) or not is often the enthalpic contribution. Specifically, the strength of the interactions that are occurring between the molecules is typically the priority issue. However, it is extremely important to realize that whether such a process is favorable will be determined by whether its change in Gibbs free energy is negative or not; this is described by the Gibbs–Helmholtz equation,  $\Delta G = \Delta H - T\Delta S$ ; thus, it is clear that there are two major terms: the enthalpy and entropy. The entropy term is clearly extremely important but is commonly not considered sufficiently. This omission is possibly because obtaining numerical data is more difficult, and the results are conceptually more challenging to rationalize. Recently, such realizations have become an issue of increasing importance in the literature.<sup>123</sup> In particular, the group of Inoue has been at the forefront of work trying to unravel the nature of the entropic control in chiral supramolecular systems.<sup>124</sup>

One of the latest papers from the Inoue group shows how, for an asymmetric reduction reaction occurring within a ternary assembly, temperature changes result in a switching between enthalpic and entropic control. The outcome is that both the degree and sign of the enantioselectivity changes.<sup>125</sup> In this NADH reaction model, a series of amino acid appended 1,4-dihydronicotinamides form a transient ternary species with methyl benzoylformate and a magnesium ion, with the product's chirality determined by which enantiotopic hydrogen at the C4 position is sterically blocked; see Figure 72.

The reactions with compounds **129–133** were carried out at temperatures between –35 and 72 °C, and the relative rate constants for the production of either *R* or *S* enantiomer were determined and plotted against the reciprocal of the temperature; see Figure 73. This reveals that the enantioselectivity formed from the reaction within the assembly is both changed in magnitude and sign (at 0 °C for **132**) by variation of the temperature. To gain further insight the differential activation, enthalpies ( $\Delta\Delta H^\ddagger$ ) and entropies ( $\Delta\Delta S^\ddagger$ ) are obtained from the differential Eyring equation,  $\ln(k_S/k_R) = \Delta\Delta S^\ddagger_{S-R}/R - \Delta\Delta H^\ddagger_{S-R}/RT$ .

It is found that the  $\Delta\Delta S^\ddagger_{S-R}$  values are not equal to zero, being –3.75 and +1.89 cal/mol for **131** and **132**, respectively. The rationale for these values is thought to be changes



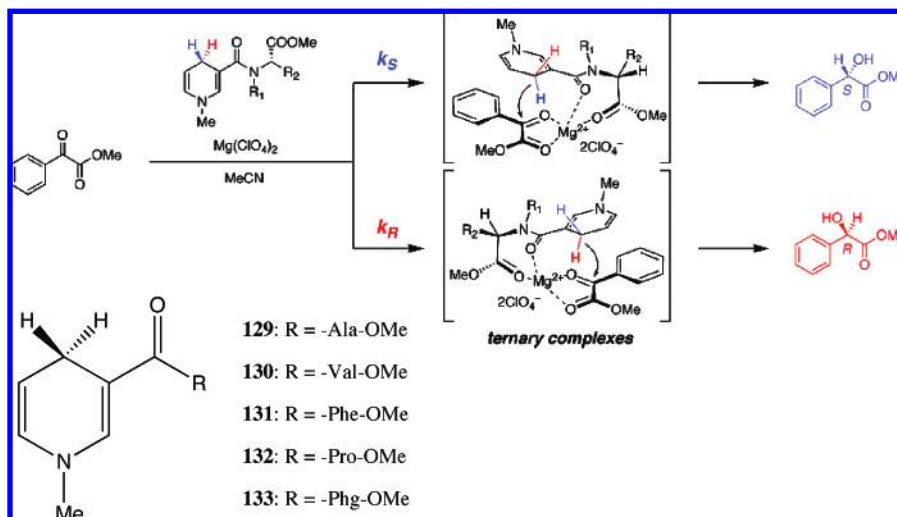


**Figure 72.** Schematic illustration of the proposed ternary complexes (or the transition states) involved in the asymmetric reduction of  $\alpha$ -ketoesters with chiral 1,4-dihydronicotinamides and structures of **129**–**133**. Reprinted in part with permission from Saito, R.; Naruse, S.; Takano, K.; Fukuda, K.; Katoh, A.; Inoue, Y. *Org. Lett.* **2006**, *8*, 2067. Copyright 2006 American Chemical Society.

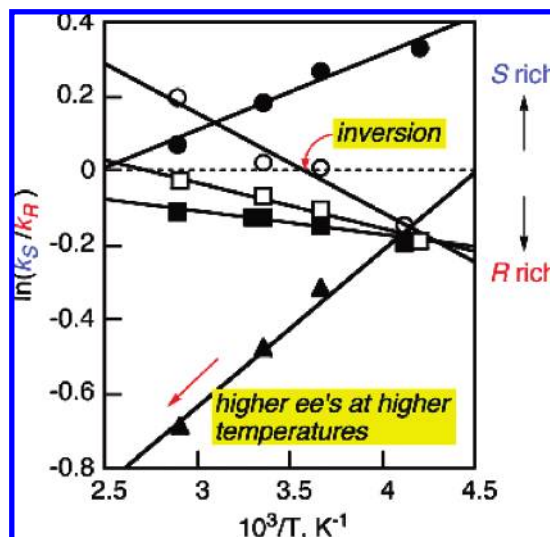


**Figure 73.** Temperature dependence of the enantioselectivity in the asymmetric reduction of methyl benzoylformate with **129** (closed circle), **130** (closed square), **131** (closed triangle), **132** (open circle), and **133** (open square). Reprinted in part with permission from Saito, R.; Naruse, S.; Takano, K.; Fukuda, K.; Katoh, A.; Inoue, Y. *Org. Lett.* **2006**, *8*, 2067. Copyright 2006 American Chemical Society.

in the activation volume, caused by the movement of the benzyl group for **131** and by a flipping action of the pyrrolidine ring for **131**. Subsequent plotting of the enthalpy–entropy compensation plot ( $\Delta\Delta S^\ddagger_{S-R}$  against  $\Delta\Delta H^\ddagger_{S-R}$ ) produced a straight line, which confirms that the enantio-differentiating mechanism does not change with the amino acid. From these results, it can be seen that the product's chirality is determined by the enthalpy term at low temperatures and by the entropy term at higher temperatures. Such a phenomenon is possible due to the flexible transition-state complex in which the intermolecular interactions between the assembly's components allow the subtle changes in conformation.

### 5.3. Influence of Phase Transitions on Supramolecular Chirality

Work from the group of Urbanová considered the changes in chirality on the solution-to-gel (sol–gel) phase transition

of the chiral brucine–porphyrin gelator (**134**) and used VCD data obtained in different solvents to investigate their origin;<sup>126</sup> see Figure 74.

In DMSO- $d_6$ , **134** forms a dark-brown solution, but on addition of CD<sub>3</sub>OD, this changes to a homogeneous organogel (starting at a 4:1 DMSO- $d_6$ /CD<sub>3</sub>OD ratio) with the same color and is found to entrap ca. 3000 CD<sub>3</sub>OD molecules per molecule of **134**. The sol–gel transition is accompanied by an inversion of the chirality associated with the  $\nu(\text{C=O})$  stretch at ca. 1665 cm<sup>−1</sup>, from a very weak negative Cotton effect to a stronger positive one at a 4:1 ratio, which then increases again in pure CD<sub>3</sub>OD. The weak negative Cotton effect correlates with that of pure brucine in the solution phase in DMSO- $d_6$ , which confirms that **134** is not able to form intermolecular associations in this solvent, likely because of effective competition for the interaction sites by the solvent. Also, it is observed that the maxima of both the IR and VCD peaks for the  $\nu(\text{C=O})$  stretch in the gel phase do not significantly alter on change of solvent composition, indicating that these sites are inside the sol clusters and not available for potential solvent interaction, and thus, this can be inferred as a requirement for gel stability. Therefore, **134** is classed as a hydrogen-bond gelator rather than a non-hydrogen-bond gelator because it is clear that these intermolecular interactions are crucial to the gel formation.<sup>127</sup> Additional to this, it was found that no gel phase was formed when benzoyl groups replaced the porphyrin moieties, with the authors proposing that  $\pi$ – $\pi$  interactions associated with the porphyrins are central to the chiral superstructures formation. The chirality to be generated in the gel phase was then directly observed by analysis of a dry gel sample by SEM. This revealed the presence of puckered fibrils of 200–250 nm diameter, with a regular right-handed helical structure.

The potential importance of the phase state is dramatically shown in work investigating lutein (Figure 75) by Zsila et al. in which changes in the chiral state are observed for monodisperse, solution supramolecular, thin film, and crystalline states.<sup>128</sup>

In acetone solution, UV–vis analysis indicates that lutein exists in a predominantly monomeric state, and no CD signals are observed in the 350–550 nm region associated with the polyene moiety ( $\pi$ – $\pi^*$  transitions), despite a molar absorp-

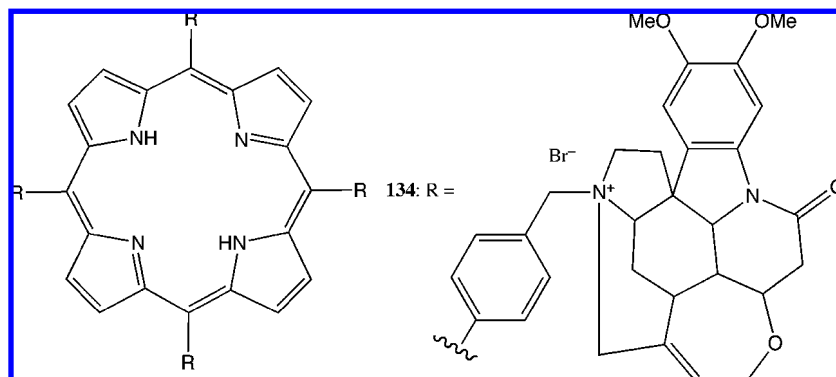


**Figure 74.** Structure of **134**.

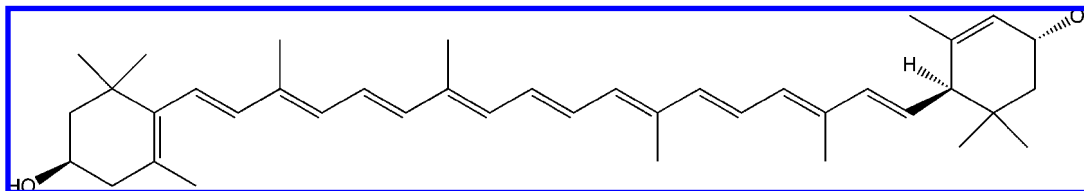


**Figure 75.** Structure of lutein.

tion coefficient of ca.  $1.2 \times 10^5 \text{ M}^{-1} \text{ cm}^{-1}$ . It also shows that chiral information from the point-chirality sources at either end is not intramolecularly transferred to the polyene. On addition of water to the acetone/lutein solution, a negative bisignate signal appears with a zero crossover wavelength of 372.5 nm. Detailed quantitative analysis of the spectral data leads to the conclusion that here the lutein exists as stacked H-type dimers (favored by the hydrophobic nature of the molecule) and, according to the exciton coupling theory, possesses left-handed orientation.

However, on a phase transition to the thin-film state, an inversion of the chirality is observed to give a positive bisignate CD signal corresponding to a right-handed orientation; see Figure 76. Investigation of the  $g$ -factors from both the aqueous acetone and the thin films give values of similar absolute magnitude,  $-5.6 \times 10^{-3}$  and  $+3.4 \times 10^{-3}$ , respectively, which suggests that the degree of chiral organization is almost the same in both phases. Subsequent CD measurements of crystalline lutein (as a KBr disk) then show another inversion of chirality (Figure 76) and a return to that found in aqueous solution that suggests a H-type intermolecular arrangement, as also found for the aqueous acetone solution.

When considering the effect of the phase (e.g., solution to solid) on the chirality generated, it is important, but often overlooked, to consider the presence of exciton coupling interactions that may occur not just from within the discrete supramolecular system that we consider in solution but also from between several such assemblies that are close enough in the solid-state structure. This principle is shown in work by our group.<sup>129</sup> In this, chirality is induced in an achiral bis(zinc porphyrin) **112a** by the addition of chiral monoamine ligands, according to the mechanism described in section 5.1.2, and the differences found between the solution and the solid phase have been investigated. For example, the (*S*)-isopinocampheylamine ligand induces in solution a positive bisignate CD signal that corresponds to a clockwise orientation between the low-energy porphyrin electronic transitions; however, in the solid state (KBr disk), this is inverted to give a negative bisignate CD signal, thus suggesting that anticlockwise orientations of the corresponding electronic

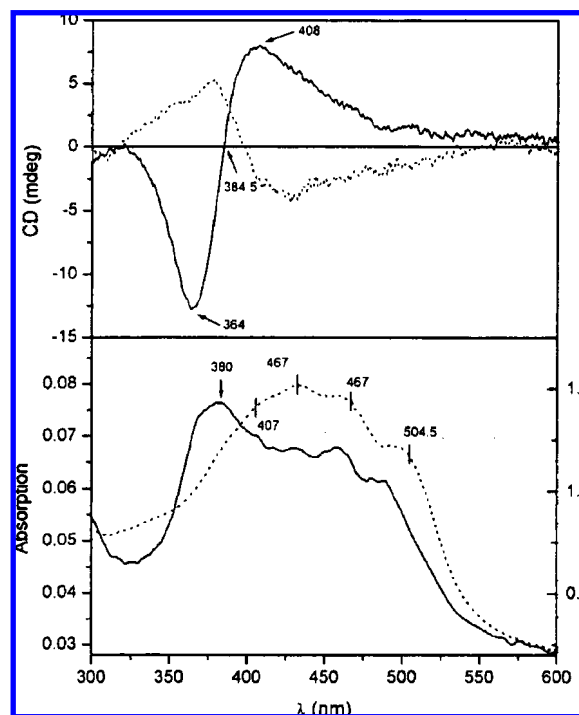


**Figure 76.** UV/vis and CD spectra of lutein film on a quartz slide (solid line) and lutein crystals in a KBr disk (dotted line, right axis). Reprinted in part with permission from Zsila, F.; Bilkádi, Z.; Keresztes, Z.; Deli, J.; Simonyi, M. *J. Phys. Chem. B* **2001**, *105*, 9413. Copyright 2001 American Chemical Society.

transitions dominate. The rationale for this interpretation is presented in Figure 77.

The analysis explains that, while the intramolecular clockwise orientation found in solution still occurs, the intermolecular anticlockwise transition couplings, which are more numerous, must be taken into account and, because of their amplification effect, result in the final observed chirality inversion. A similar amplification effect in which consideration of the intermolecular electronic transition couplings rationalize the solid-state chirality in comparison to a marginally chiral solution state was also observed for a zinc

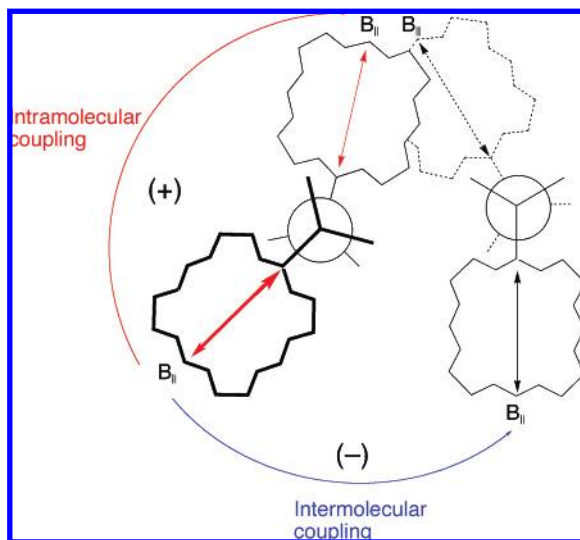


**Figure 77.** Schematic representation of the intra- and intermolecular exciton coupling in the solid state **112a·(S)-L**. Reprinted with permission from Borovkov, V. V.; Hembury, G. A.; Inoue, Y. *Acc. Chem. Res.* **2004**, 37, 449. Copyright 2004 American Chemical Society.

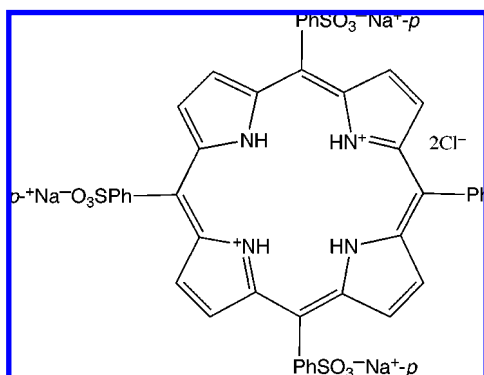


**Figure 78.** Structure of **135**.

octaethylporphyrin monomer system in the presence of enantiopure amines.<sup>130</sup>

Finally, one of the most remarkable and fascinating examples of influencing chirality by phase change is that performed by Ribó et al. Essentially, this work describes the generation of either left- or right-handed aggregates from an achiral solution by virtue of whether the solution is stirred in either a clockwise or anticlockwise direction.<sup>131</sup> In these experiments, the aggregating species are a group of diprotonated *meso*-sulfonatophenyl-substituted porphyrins, typified by **135** in Figure 78, and are designed to interact via the positively charged porphyrin ring and the negatively charged sulfonate groups.

Typical experimental details are as follows: a solution of 3  $\mu$ M **135** held at an angle of 45° or 55°, which is then subjected to rotary evaporation (25 Torr) while being stirred (600 rpm) either in clockwise or anticlockwise direction, thus generating a vortex in the solution. The resulting aggregates were analyzed by UV-vis and CD spectroscopies to give the results shown in Figure 79.

Thus, from such experiments and analysis, it is found that, reproducibly, clockwise vortices give positive chirality of the aggregates (*P*-helicity) at the Soret band (ca. 490 nm), while anticlockwise vortices give negative chirality (*M*-helicity). Although such phenomena had been reported before,<sup>132</sup> the results were disputed and attributed to linear

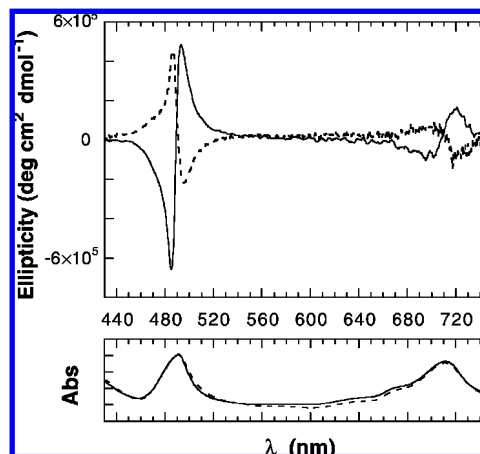


**Figure 79.** CD and UV-vis spectra of two solutions of homo-associates of **135**: clockwise (solid lines) and anticlockwise (dashed lines) vortex directions during the rotary evaporation. Reprinted with permission from Ribó, J. M.; Crusats, J.; Sagués, F.; Claret, J.; Rubires, R. *Science* **2001**, 292, 2063. Copyright 2001 American Association for the Advancement of Science.

dichroism effects.<sup>133</sup> In the present case, linear dichroism was eliminated as a contribution to the CD, and it was found that changes in the optical rotation dispersion spectra correlated with those of the CD spectra; as such, this is the first undisputed case of chirality induction of this type.

It is believed that the origin of the aggregates' chirality comes from an initial long ribbonlike J-aggregate of **135**; it is then either a left- or right-handed deviation from linearity that produces the initial chiral fluctuation as influenced by the vortex direction; see Figure 80. The aggregates are then built up by the subsequent addition of further smaller **135** assemblies, to finally give H-type bundles of J-type aggregate. It is key to realize that any additional approach by further chiral building blocks will be diastereotopic in nature and, thus, promote the buildup of homochiral assemblies. It is also believed that chiral steric hindrance arising from the aggregates provides an autocatalytic mechanism for preserving the dominant chirality while disfavoring the opposite.

In this and preceding sections, we have briefly discussed several porphyrin-based chirogenic assemblies. However, taking into account the paramount importance of porphyrinoids for chirality-sensing purposes, these systems will be discussed in the next section in more detail.

## 6. Porphyrin-Based Systems

Supramolecular systems on the basis of porphyrins so far have attracted much attention for chirality-sensing purposes, owing to their appropriate spectral and physicochemical properties, easy handling and versatile modification, direct relation to many biological processes, and wide applicability. The scientific interest in such porphyrin supramolecular systems and their effective application are well-documented in several reviews discussing this subject to a greater or lesser extent.<sup>5a,b,23c,26,134</sup> However, in contrast to the previously published reviews, this section will exclusively summarize the most important representative examples of supramolecular systems, which are able to sense different types of chirality using porphyrins as a chromophoric reporter unit and classify it into several categories according to the chirality's origin and the complexity of the supramolecular system.

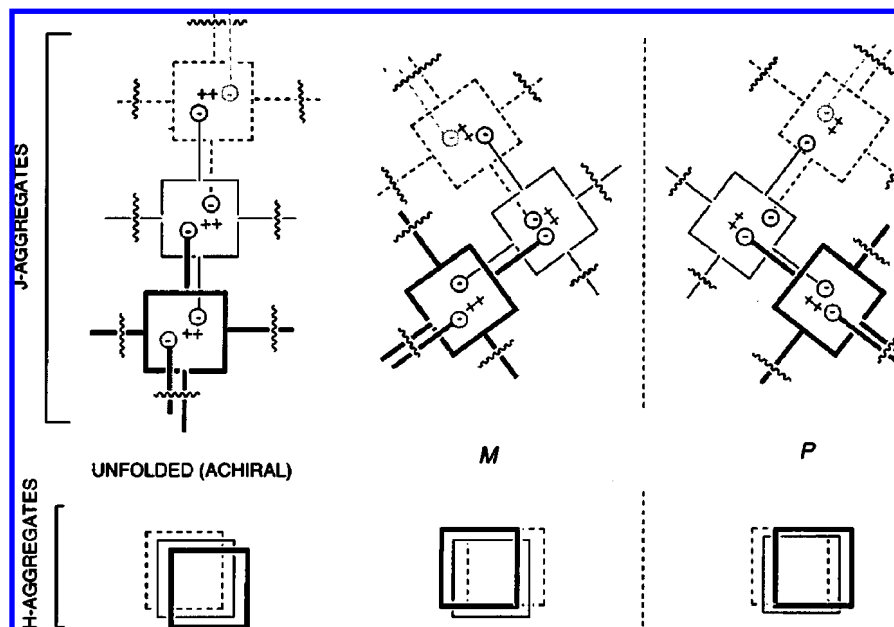


**Figure 80.** Different types of the porphyrin association. Reprinted with permission from Rubires, R.; Farrera, J.-A.; Ribó, J. M. *Chem.—Eur. J.* **2001**, 7, 436. Copyright 2001 Wiley-VCH Verlag GmbH & Co.

## 6.1. Point-Chirality Sensing

As the simplest and, thus, most easily understandable and widely applicable detection process, point-chirality sensing will be discussed first. In general, there should be clearly distinguished two processes under this term: (i) chirality sensing itself, that is, asymmetry transfer from a chiral guest to an achiral porphyrin host upon noncovalent host–guest interactions and (ii) chiral recognition that resembles the “lock and key” principle in which there is better matching between two particular enantiomeric pairs of host and guest, thus resulting in better binding interactions.

Monomeric porphyrins are the simplest chromophoric units in terms of structure; nevertheless, they can be effectively used for chirality-sensing/recognition purposes. For example, Aida's group applied a series of saddle-shaped fully substituted porphyrins **136–138** for chirality sensing of various enantiopure acids (Figure 81).<sup>6a,135</sup> The chirality-transfer mechanism is based on the equilibrium shift between the racemic mirror image forms of these porphyrins upon interaction with chiral acids via hydrogen bonding of two carboxylates to the pyrrole nitrogens from opposite sides to give a 1:2 complex (Figure 81). The resulting supramolecular complexes exhibited a noticeable induced CD signal in the region of the Soret band, the sign of which was correlated with the relative steric bulk at the asymmetric center, thus allowing the absolute-configuration determination, except in some borderline cases, when the relative size of two substituents was nearly equal. Despite the lack of a comprehensive rationale of the observed optical activity, the induced chirality was effectively used to memorize chirality (see section 7). Later, this concept was elegantly expanded to the corresponding bisporphyrin **139** (Figure 81), which resulted in significant amplification (more than 7-fold) of the optical activity ( $A = 260 \text{ M}^{-1} \text{ cm}^{-1}$  in the case of (*S*)-mandelic acid) in comparison to the corresponding monomer, owing, as assumed, to the translation of the nonplanar chirality of the porphyrin ring into the helical chirality of the entire assembly.<sup>136</sup> However, a stepwise increase of the guest concentration produced complicated changes in the CD

signals, apparently reflecting a multistep equilibrium in the binding process. Despite this complexity, **139** was suggested for use as a chirality sensor that can read out absolute structures of interacting guest molecules and transcribe them into highly amplified CD signals in the visible region.

Other examples included a group of various saccharide sensors. Shinkai and co-workers designed a simple but selective porphyrin sensor exclusively for D-lactulose on the basis of distance matching between the binding sites of this sugar and two boronic acid groups in *cis*-**140** (Figure 82) that yielded a 1:1 complex with a monosignate CD response in the Soret band region.<sup>137</sup> Further elaboration of the host structure resulted in wider sensoric applicability for different chiral guests. Particularly, a double-decker architecture of center-to-center bound bisporphyrins **141–148** (Figure 82), designed on the basis of Fe–O–Fe  $\mu$ -oxo-dimers and Ce complexes, allowed chirality sensing of saccharides (for **141**, **142**, **146**, **147**), dicarboxylic acids (for **143–145**), dianions (for **148**), and memorizing chirality (for **145**).<sup>138</sup> The generated chiral memory was remarkably preserved for 3 days at 0 °C and even for 1 year at –37 °C (see section 7). The association mechanism included the interaction of a bidentate guest with two binding groups of the neighboring porphyrin moieties, forcing these macrocycles to rotate around the central axis and subsequently to form right- or left-handed twists, depending on the guest's stereochemistry (Figure 82). This asymmetry transfer resulted in noticeable optical activity in the region of the porphyrin absorption caused by interporphyrin exciton coupling, the sign of which was essentially determined by the direction of the interporphyrin twist. The host–guest binding occurred in a highly cooperative manner, exhibiting a positive allosteric effect, and the CD response was strongly affected by the guest's structure, solvent, and pH. Interestingly, in the case of maltooligosaccharide guests, a chirality-switching effect controlled by the number of saccharide units was reported for **146**.

Amino acids are another important class of chiral compound, the chirality of which plays a vitally important role in the functioning of living organisms; therefore, several re-



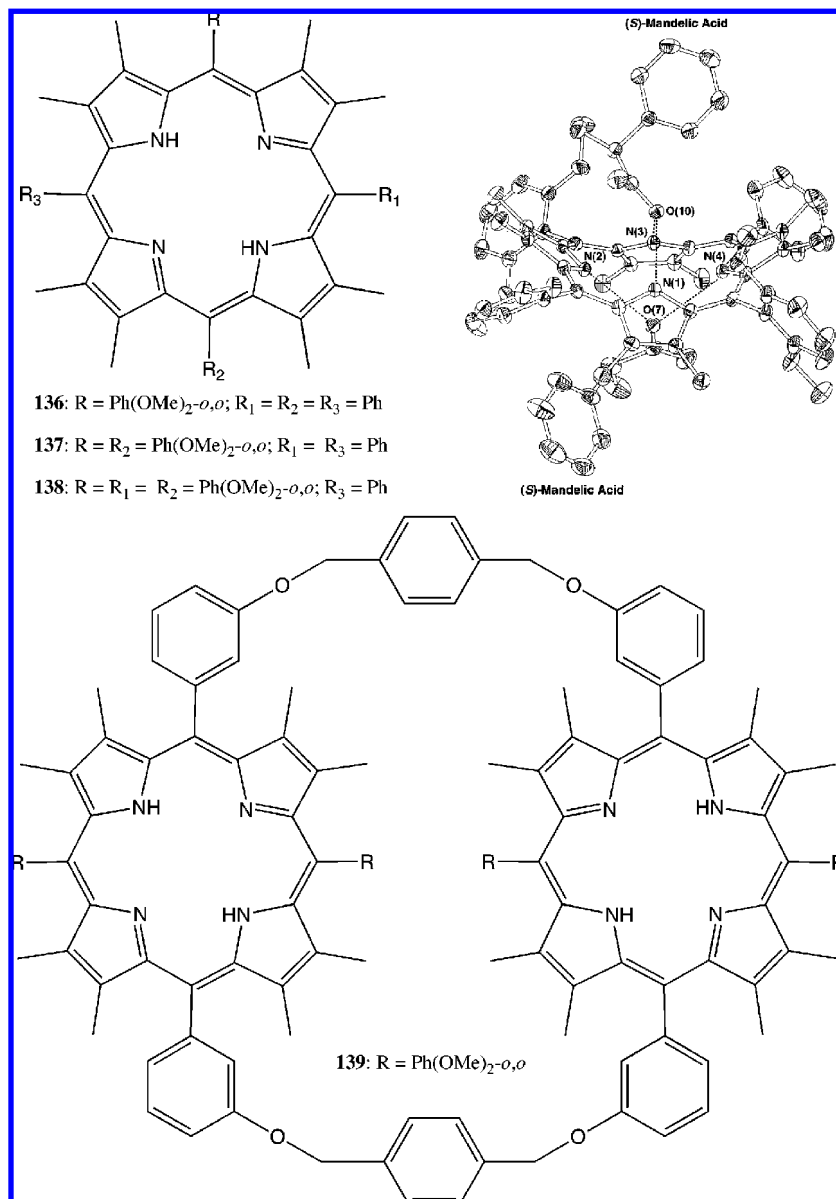


**Figure 81.** Structures of **136**–**139** and crystallographic structure of the mandelate complex of **137**. Reprinted in part with permission from Mizuno, Y.; Aida, T.; Yamaguchi, K. *J. Am. Chem. Soc.* **2000**, *122*, 5278. Copyright 2000 American Chemical Society.

search groups have been intensively investigating amino acid-based supramolecular systems. Hence, Mizutani, Ogoshi, and co-workers, using the *trans*-isomers of **149** and **150** (Figure 83), have developed a receptor for amino acids with particular selectivity found for Asp-OMe (the binding constant was found to be as large as  $6.98 \times 10^4 \text{ M}^{-1}$ ); this arises from the conformational matching of a three-point fixation mode ensured by the coordination and two hydrogen-bonding interactions.<sup>139</sup> All the systems studied exhibited a small-to-moderate negative couplet induced in the Soret region, which was suggested to originate via the porphyrin–carbonyl coupling mechanism, although other factors may also contribute. To expand the applicability of the amino acid receptors, a series of porphyrins **151** (Figure 83) were proposed for dual use: (i) in nonpolar organic solvents as the ester derivatives and (ii) in aqueous media as the hydrolyzed derivatives.<sup>140</sup> Interestingly, it was found that two driving forces competitively contribute to the binding: the electrostatic interactions upon coordination of the amino group to the Zn central ion in organic solvents (enthalpic

forces) and the host–guest dispersion interactions (an enthalpic force) along with desolvation-driven binding (an entropic force), which were dominant in water.

To sense the chirality of unprotected zwitterionic amino acids, Tamiaki et al. applied a biphasic organic solvent–water system using **152** (Figure 83) for extraction of amino acids from the aqueous phase.<sup>141</sup> The resulting 1:1 complexes gave two well-resolved CD couplets of opposite sign, which were matched to the split Soret band and Q transitions in the UV–vis spectra. The *A* value was strongly dependent upon the solvent used and the Ph ring substituents, with the highest sensitivity found for aromatic solvents and  $X = t\text{-Bu}$ . The sign of the induced CD generally followed the chirality of amino acids, though with several reported exceptions. Nevertheless, the authors suggested to use this method for determination of the absolute configuration of unprotected  $\alpha$ -amino acids. Additionally, replacement of the achiral acac external ligand with enantiopure 3-acetylcampors resulted in the corresponding chiral complexes, which in turn were applied for chirality recognition.<sup>142</sup> It was successfully

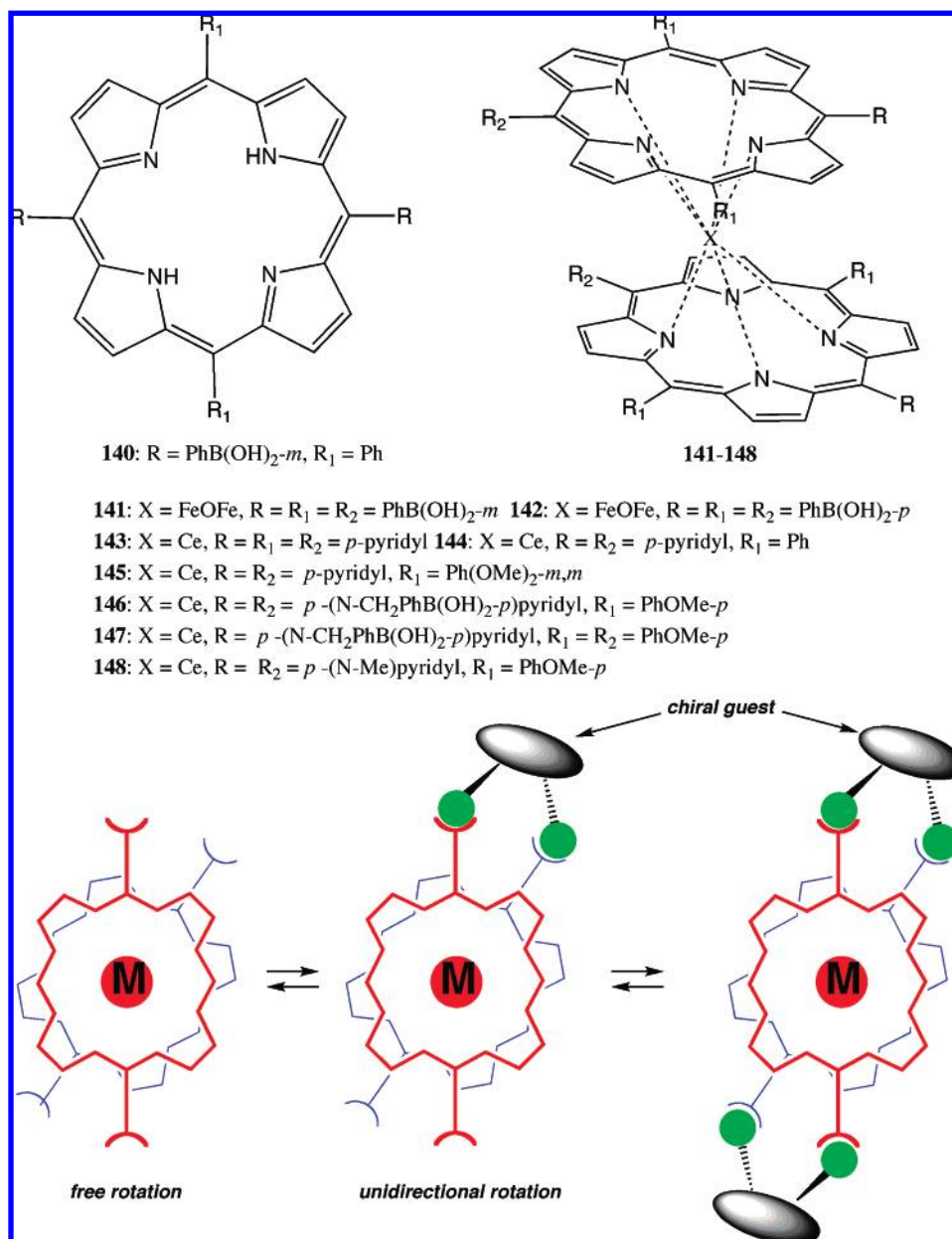


**Figure 82.** Structures of **140**–**148** and schematic representation of chirality transfer from enantiomeric guests to **141**–**148**. Reprinted in part with permission from Borovkov, V. V.; Inoue, Y. *Top. Curr. Chem.* **2006**, 265, 89. Copyright 2006 Springer-Verlag.

demonstrated by the complexation with two antipodal dipeptides, the CD response of which gave opposite bisignate couplets of different intensities depending upon the corresponding diastereomeric compositions. However, the sensitivity of this system was not high enough to detect antipodal alanines. The sensitivity of this method was further improved by using a synergistic binding approach upon incorporation of the crown ether moiety to yield **153** (Figure 83).<sup>143</sup> Co-ordination of the  $\text{CO}_2^-$  group of amino acid to the lanthanide center, as well as the  $\text{NH}_3^+$  group to the crown ether, along with an appropriate metal choice, considerably enhanced the extraction abilities and  $A$  values.

Another approach for sensing unprotected amino acids was demonstrated by Harmon and co-workers by using solid-state optical detection.<sup>144</sup> This method was based on the hypsochromic shifts in UV–vis spectra of **154** (Figure 83) immobilized as a monolayer onto a cellulose film caused by interaction with amino acids. The degree of spectral change was dependent upon the structure of the amino acid,

making it possible to quantify different amino acids in solutions, although the operating mechanism was not reported.

One of the most effective recognitions of amino acid esters with an enantioselectivity as high as 21.54 (for Phe-OMe) was reported by Zhu and co-workers upon applying the amino-acid-substituted **155**–**157** (Figure 84).<sup>145</sup> It was shown that the enantioselectivity was exponentially dependent upon the temperature and that the diastereomeric complexes exhibited different CD responses. Specifically, the CD spectrum of **155** in the presence of weakly bound L-Ala-OMe was essentially similar to that of uncomplexed **155**, yielding a single negative Cotton effect in the region of the Soret band, while strongly bound D-Ala-OMe produced a positive couplet, apparently because of the excitonic interactions between the porphyrin and the amino acid's carbonyl transitions, although this chiroptical effect was not explained.

As mentioned above, a bischromophoric (or multichromophoric) motif considerably enhances the applicability and

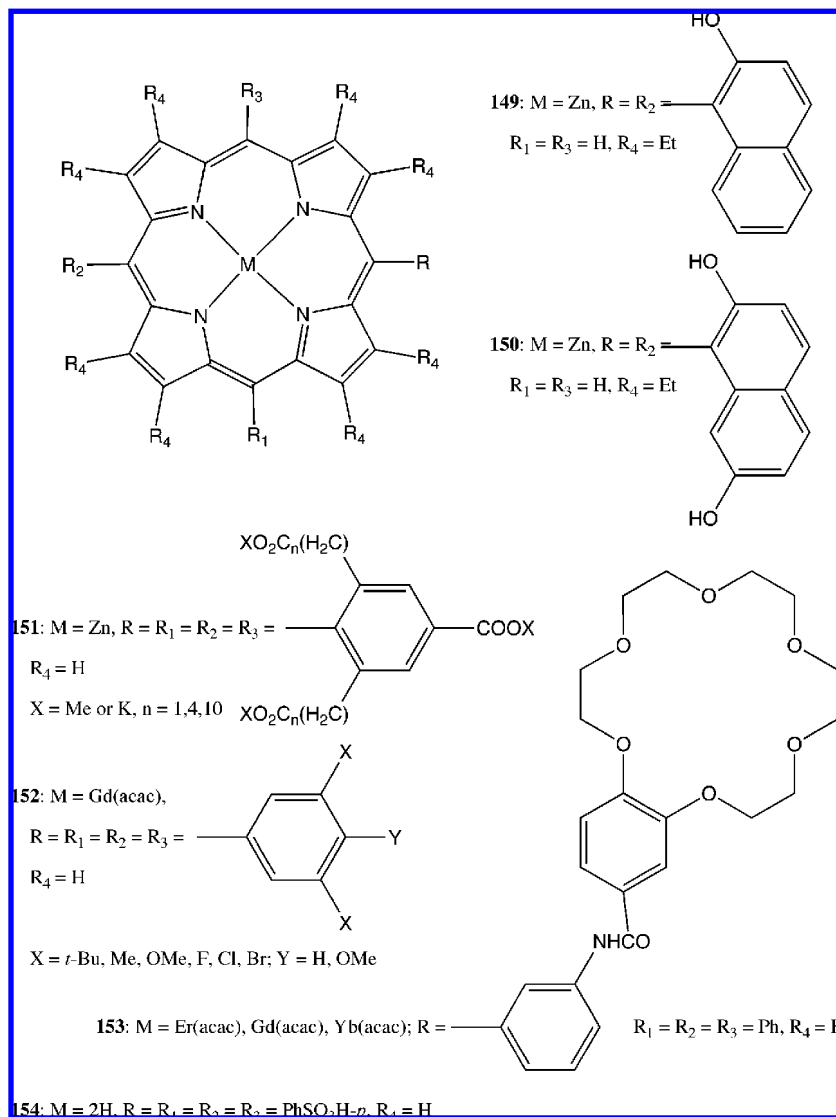


**Figure 83.** Structures of porphyrins (**149**–**154**).

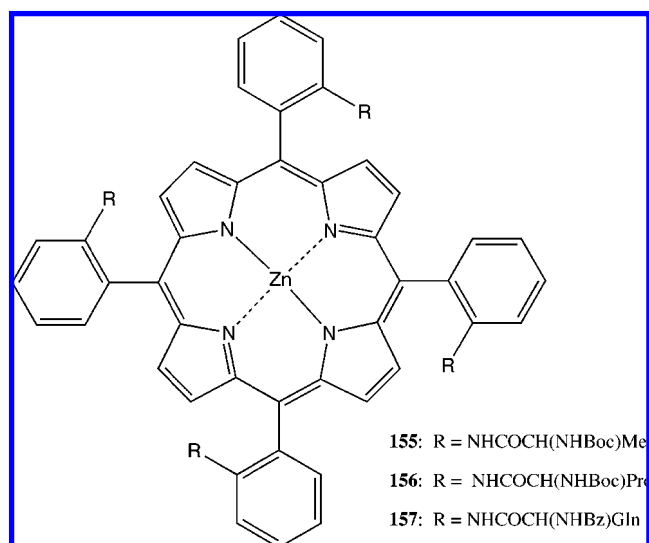


**Figure 84.** Structures of porphyrins (**155**–**157**).

sensitivity of porphyrinoid-based supramolecular systems for chirality-sensing purposes. This approach was successfully used by Durfee, Kobayashi, Ceulemans, and co-workers.<sup>146</sup> In particular, two subphthalocyanine units connected by an

(*R*)-1,1'-binaphthyl (BNP) bridge in **158** (Figure 85) produced intense CD signal in the region of the low-energy Q transitions, the complex shape of which was rationalized in terms of the excitonic interactions by analyzing band-deconvolution results. Similarly, in the case of **159** (Figure 85), a pair of phthalocyanine chromophores was brought together in a chiral arrangement by a hematoxylin bridge. The chiroptical response consisted of an intense negative-to-positive bisignate and several weak CD signals in the Q and Soret band regions arising from the excitonic interactions between the two phthalocyanines. The induced optical activity was unambiguously confirmed by *ab initio* geometry optimization combined with a Kuhn–Kirkwood coupled-oscillator mechanism, which additionally allowed determination of the absolute configuration of hematoxylin as the (**6a*S***,**11b*R***)-form. Although this method provides a powerful tool for assigning stereochemistry, the practical application is rather limited because of its overall complexity.

More effective supramolecular systems for chirality sensing were proposed by Nakanishi and co-workers on the basis of bisporphyrin host **160**, which is able to adopt a tweezer conformation upon complexation with bidentate ligands (Figure 86).<sup>7b,147</sup> The chirality-induction mechanism was found to be based upon the stereospecific differentiation of

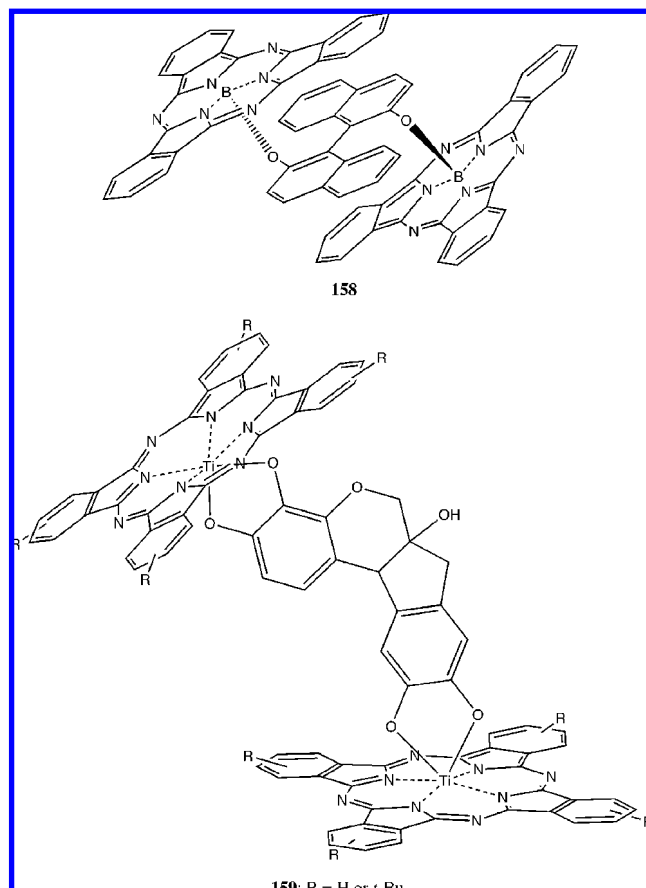


Figure 85. Structures of bisporphyrinoids (**158**, **159**).

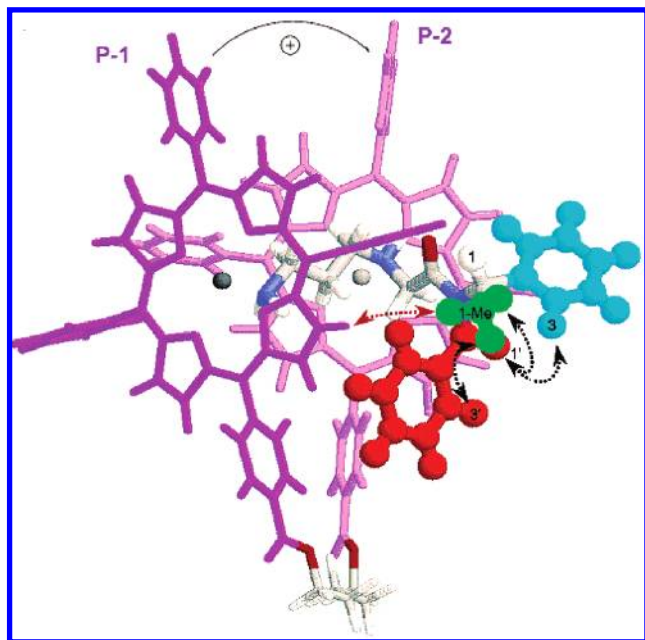


Figure 86. Molecular model of complex of **160** with a chiral guest. Reprinted with permission from Huang, X.; Fujioka, N.; Pescitelli, G.; Koehn, F. E.; Williamson, R. T.; Nakanishi, K.; Berova, N. *J. Am. Chem. Soc.* **2002**, 124, 10320. Copyright 2002 American Chemical Society.

the substituents' relative bulkiness at the asymmetric carbon by forcing the bisporphyrin to adopt, in general, the least sterically hindered conformation, although it was also reported that other factors such as hydrogen bonding, heteroatoms, solvent, etc. might affect the overall geometry

of the assembly. This resulted in formation of a directional orientation of the two porphyrins in **160**, thus inducing an exciton couplet CD, the sign of which was suggested to be used as a tool for the absolute configuration determination of various bidentate guests. In cases when the relative bulkiness could not be directly determined, molecular mechanics calculations were applied for conformational analysis to explain the observed inconsistency between the predicted and obtained chirality. However, this system cannot be directly used for sensing monodentate guests without additional synthetic modification.

To fill this gap, our group has developed a highly efficient chirality sensor on the basis of a simple ethane-bridged bisporphyrin structure **112**.<sup>26,27a,111,148</sup> In sharp contrast to the other bisporphyrin systems, this host is able to sense the chirality of not only bidentate but also monodentate guests, owing to the linkage's semiflexibility/semirigidity provided by the relatively short but sufficiently flexible ethane chain via formation of the stable extended 1:2 host–guest complexes in a cooperative manner with a Gibbs free energy ranging from  $-6.7$  to  $-8.4$  kcal mol<sup>-1</sup> for primary amines as determined by analyzing the corresponding UV–vis/CD spectral changes. The specific mechanism of chirogenesis in **112** caused by monodentate guests included competitive repulsive interactions between the two most bulky substituents at the ligand's stereogenic center and the ethyl groups of the neighboring porphyrin ring (Figure 58). The bulkiest group forced the neighboring macrocycle to move outward, thus generating a unidirectional twist, which resulted in a moderate-to-strong exciton couplet CD signal in the Soret region. The chirality sign correlated with the induced helicity, allowing straightforward determination of the absolute configuration of monodentate guests. A fully rationalized host–guest interaction mechanism allowed the detailed investigation of various external and internal factors influencing the chirality-induction processes. For example, it was shown that the *A* value was linearly dependent upon the size of the largest substituent at the stereogenic center for homologous ligands, thus allowing prediction of the induced chirality.<sup>148a,b,d</sup> Also, a decisive role of the solvent as an active part of the overall supramolecular system was clearly understood through judicious analysis of the selective solute–solvent interactions in the borderline cases where the differences between the competitive chiral interactions were small and the substituent's relative bulkiness could be modulated upon formation of a specific solvation shell (see section 5.1).<sup>27a,111</sup> Temperature was found to be another important factor controlling the chirogenic processes, considerably increasing the *A* values upon lowering the temperature via enhancing the binding affinity, thus allowing chirality induction by alcohols possessing a well-known low affinity for Zn porphyrins.<sup>148e–g</sup> However, the alcohol binding, and thus the chirality-sensing ability, was considerably increased by replacement of Zn central ion with a Mg ion.<sup>148h</sup>

Interaction of **112a** with bidentate guests resulted in the formation of extremely stable 1:1 tweezer complexes with the binding constants estimated as high as  $>10^7$  M<sup>-1</sup>. However, further increasing the bidentate guest concentration could shift the supramolecular equilibria in the majority of cases toward the extended 1:2 complex, hence allowing investigation of the corresponding stoichiometry effect.<sup>148i–k</sup> In the case of enantiomeric 1,2-diphenylethylenediamine, a remarkable phenomenon of chirality switching controlled exclusively by the stoichiometry of the supramolecular



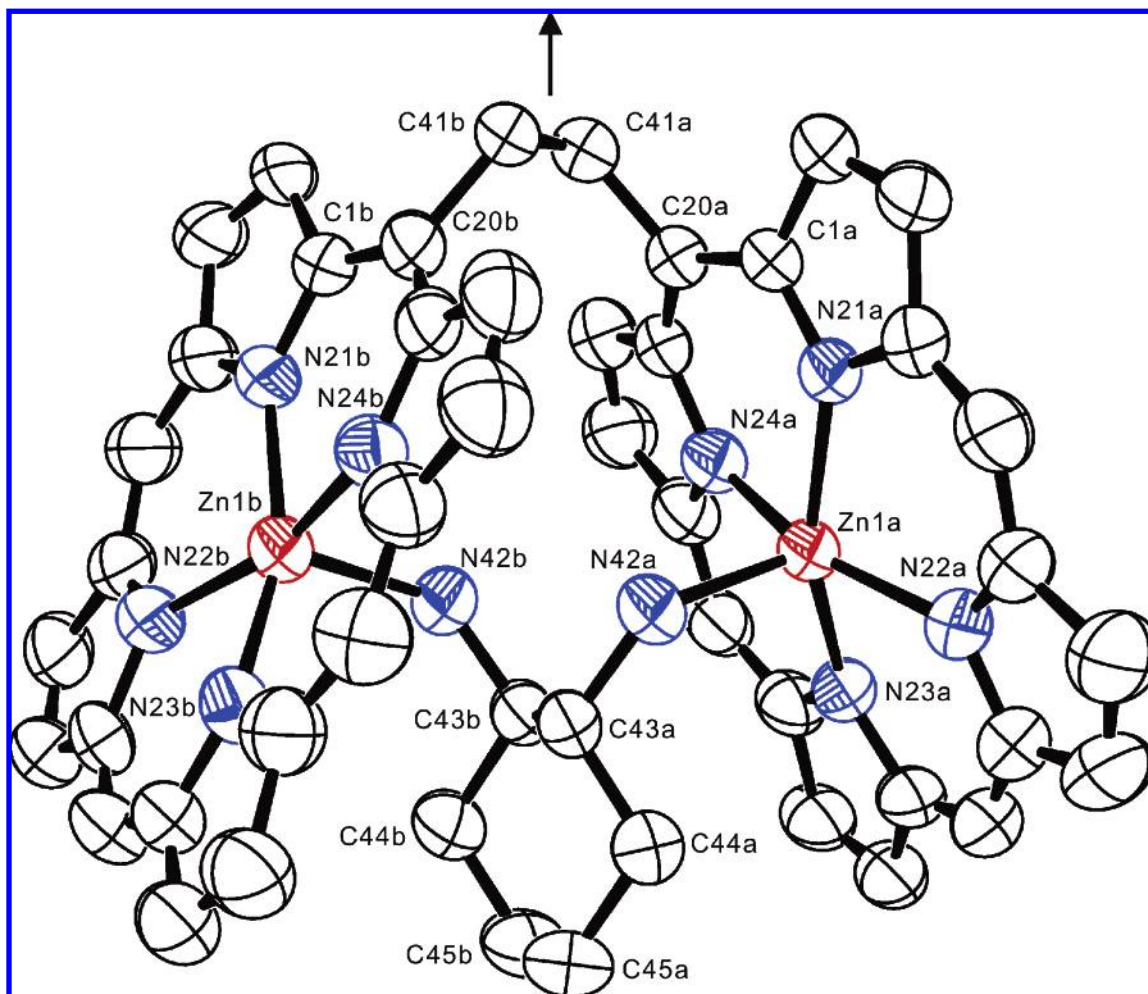


**Figure 87.** Crystallographic structure of the **112a**/(*R,R*)-DACH tweezer complex. Reprinted with permission from Borovkov, V. V.; Fujii, I.; Muranaka, A.; Hembury, G. A.; Tanaka, T.; Ceulemans, A.; Kobayashi, N.; Inoue, Y. *Angew. Chem., Int. Ed.* **2004**, *43*, 5481. Copyright 2004 Wiley-VCH Verlag GmbH & Co.

system as a result of the opposite spatial orientation of the 1:1 and 1:2 complexes was discovered. More importantly, a full and unambiguous rationalization of the induced optical activity in the bisporphyrin-based supramolecular system was achieved for the first time by using chiral 1,2-diaminocyclohexane (DACH). Particularly, on the basis of the obtained crystallographic structure of the **112a**/(*R,R*)-DACH tweezer complex (Figure 87) and the Kuhn–Kirkwood coupled-oscillator mechanism, the CD signal was assigned to be a combination of the two  $B_{||}$ – $B_{||}$  and  $B_{\perp}$ – $B_{\perp}$  homocouplings, both of which were orientated in an anticlockwise manner, thus resulting in an intense negative CD couplet ( $A = -590 \text{ M}^{-1} \text{ cm}^{-1}$ ), while the contribution of the corresponding  $B_{||}$ – $B_{\perp}$  heterocouplings was found to be negligible.<sup>39</sup> Thus, high sensitivity, full rationalization, and wide applicability for various types of guests showed that **112** could serve as an powerful tool for studying various aspects of supramolecular chirogenesis and additionally for use as a versatile chirality sensor. Furthermore, a simple modification of this structural motif, i.e., the reduction of one pyrrole ring in each porphyrin unit, also allows effective enantioselective recognition of chiral guests. Hence, enantiopure bischlorin **161** (Figure 88) exhibits a noticeably different CD response upon interaction with the corresponding antipodal amines.<sup>149</sup> The mechanism of chiral recognition is based on two-point host–guest interactions combined with the variability of the

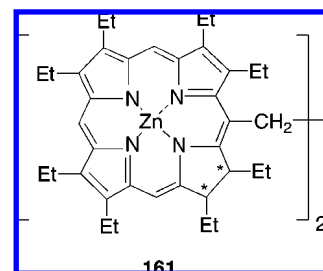


**Figure 88.** Structure of bischlorin **161**.

coupling electronic transitions of the chromophoric host, which is dependent upon the guest's stereochemistry.

Besides the point-chirality sensing discussed above, porphyrin chromophores can also be effectively used for more complicated conformational chirality sensing, as defined in section 2.

## 6.2. Chiral Conformation Sensing

This type of chirality often occurs in many natural biopolymers and superstructures (DNA/RNA, polypeptides, proteins, etc.). In order to sense such chirality efficiently, the porphyrin chromophores should be able to interact with the corresponding system to read out the chiral information. However, this is a rather arduous task because of a large

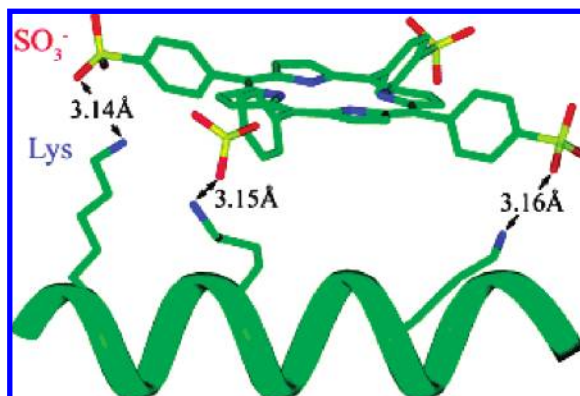


**Figure 89.** Model of a 1:1 complex of **154**/Cp3K-N. Reprinted with permission from Kovaric, B. C.; Kokona, B.; Schwab, A. D.; Twomey, M. A.; de Paula, J. C.; Fairman, R. J. *Am. Chem. Soc.* **2006**, *128*, 4166. Copyright 2006 American Chemical Society.

number of, and, in many cases, uncertainty relating to the interaction sites.

One of the successful approaches, which was able to solve this problem in the case of oligopeptides, was demonstrated by Kovaric et al.<sup>150</sup> It was shown that anionic **154**, upon electrostatic interactions with the lysine residues of a designed peptide, Cp3K-N, induces a coiled-coil structure, resulting in a tightly bound porphyrin–peptide pair of 1:1 stoichiometry (Figure 89), which produces optical activity in the Soret region.

Another example of peptide sensing was shown by Mihara and co-workers, who applied the coordination properties of Zn and Fe complexes of mesoporphyrin IX (MP) to construct a supramolecular system on the basis of  $\alpha$ -helical peptide dendrimers conjugated with porphyrins.<sup>151</sup> The metalloporphyrins were bound to a designed hydrophobic pocket of the peptide units containing the histidine residue to deploy a porphyrin parallel to the helix axis, resulting in an intense CD response in the Soret region, which was heavily dependent upon the particular dendrimer generation. A negative couplet observed for the lower-generation dendrimers ( $n = 4$ ) transformed into a single positive Cotton effect (for  $n = 8, 16$ ) followed by the partial regeneration of a low-energy negative Cotton effect. While the observed chiroptical properties were not discussed in detail, these systems were applied for peroxidase-like activities (for FeMP), which were suppressed with dendrimer growth, and photoinduced energy and electron transfer (for ZnMP), which in contrast was accomplished more effectively as the dendrimer generation increased, reflecting denser packing of the porphyrins.

Fukushima used a chiral template based on a  $\beta$ -sheet of poly(Glu-Val-Lys-Val) to investigate chirality induction in porphyrin aggregates consisting of **154**.<sup>152</sup> Upon electrostatic interactions between the porphyrin and the polypeptide, several optically active aggregates are apparently formed, which resulted in the appearance of two negative well-separated CD couplets and a negative monosignate CD signal in the region of Soret and Q bands, respectively. The chiroptical properties were controlled by the host–guest ratio, pH, and ionic strength. The CD amplitudes were enhanced upon decreasing pH, and interestingly, the chirality sign could be even switched at high salt concentrations, indicating a spatial rearrangement of the coupling electronic transitions within the aggregates, apparently via modulation of the electrostatic interactions between the porphyrins and the polypeptide; however, the exact mechanism was unknown.

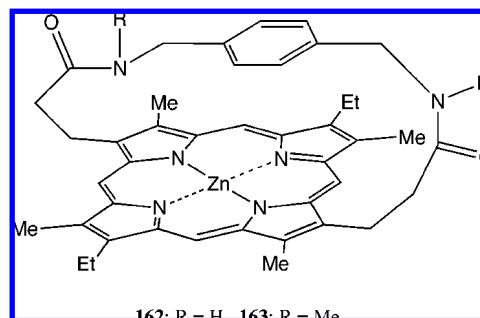


**Figure 90.** Structures of **162** and **163**.

Further insight into the self-assembly of **154** onto polylysine was gained by Purrello, Periasamy, and co-workers.<sup>153</sup> This system also exhibited efficient chirality transfer from the polypeptide matrix to the porphyrin J-aggregates. This process was controlled by pH and rationalized in terms of the monomer–aggregate equilibrium, which was shifted toward the aggregation state at low pHs because of the protonation of polylysine. Additionally, it was reported that metalation could strongly affect the aggregation behavior and, consequently, the chiroptical properties: the corresponding Zn complex presumably favored the face-to-face arrangement, yielding a complicated multicomponent CD signal, with the hexacoordinate Sn complex exhibiting the strong resistance toward aggregation. Another attractive development for the polypeptide matrix was a combination of cationic and anionic porphyrins.<sup>154</sup> Particularly, **154** and various metal complexes of 5,10,15,20-tetra(4-*N*-methylpyridyl)porphyrin (TMP) formed stable chiral aggregates on polyglutamic acid, resulting in a strong chiroptical response in the Soret region ( $A = 2500 \text{ cm}^{-1} \text{ M}^{-1}$  for the Zn complex). Using CuTMP promoted further stability of this heteroporphyrin assembly, allowing the chiral information to be memorized even when the chiral matrix was disrupted by raising the pH. The chiral memory was retained for several days, decreasing only by 30% in  $\sim 4$  weeks owing to the kinetic inertness of the aggregates (see section 7).

In studies of more complex supramolecular structures based on proteins, the role played by porphyrins is clearly switched from the host to the guest. Thus, Larsen and co-workers investigated the self-assembled complexes between either uroporphyrin (UP) or 5,10,15,20-tetra(4-carboxyphenyl)porphyrin (CPP) and cytochrome *c*.<sup>155</sup> The complex formation involved electrostatic interaction between carboxylic groups of these porphyrins and a region of the positively charged lysine residues located on the protein's exterior, leading to the positive and negative CD couplets observed for UP and CPP, correspondingly, after subtraction of the protein background. The induced CD was speculated to be a result of exciton coupling between the intrinsic protein heme and the bound porphyrins that are orientated differently on the surface. Although this chiroptical distinction was not amply rationalized, the authors linked this behavior to the corresponding excited-state properties, such as difference in the fluorescence quenching and significant triplet-state quenching of UP, resulting in the intercomplex photoinduced electron transfer with a rate constant of  $1.8 \times 10^6 \text{ s}^{-1}$ .

A different type of binding mode was tested by Aida and co-workers for the enantioselective reconstitution of apocytochrome *b*<sub>562</sub> with chiral porphyrins **162** and **163** (Figure 90).<sup>156</sup> Highly preferential binding of the (*R*)-enantiomers (as large as by a factor of 30) not only allowed effective

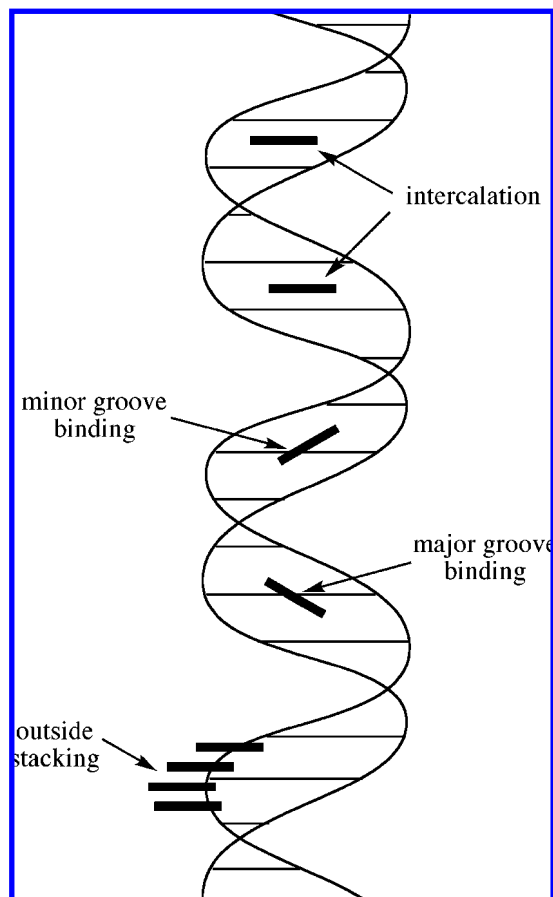


**Figure 91.** Schematic representation of three possible binding modes for the DNA/RNA-porphyrin complexes.

optical resolution of the corresponding racemic mixture but also produced essentially different CD responses in the Soret region: a relatively small monosignate positive Cotton effect for the Zn complex of (*R*)-**162** and an intense bisignate positive couplet for (*S*)-**162**. The origin of this dissimilarity was assumed to be a different planarity of the reconstituted porphyrins, with greater conformational distortion suggested for the unfavorable (*S*)-**162** resulting in intramolecular exciton coupling between the phenylene and porphyrin chromophores.

In the case of polynucleotides, since the phosphate residues produce negative charge around DNA/RNA, cationic porphyrins may serve as the best-suited guests for assembly with these double-helical structures. It is widely acknowledged that there are three major host–guest interaction modes for the DNA/RNA complexes: intercalation between base pairs, binding to major or minor grooves, and outside stacking. These have been well-established and are dependent upon the porphyrin and DNA/RNA structures and media (Figure 91).<sup>134g,h,q,v,157</sup> The chiroptical response from these complexes is also known to reflect the orientation of porphyrin electronic transitions in relation to the chirally arranged bases of nucleic acids and/or coupling between the porphyrin chromophores stacked in a chiral fashion along the double helix, with the intercalation mode inducing a negative CD, the external binding resulting in a positive CD of larger intensity, and the aggregation producing a bisignate exciton couplet in the region of the porphyrin Soret band. Taking into account these general principles and the vast number of publications in this area, we shall only discuss several selected results obtained recently, which indicate modern research trends.

Binding studies on the TMP structural motif, which was originally applied to the interaction with natural DNA,<sup>157</sup> have been successfully continued to gain a deeper insight into the association mechanism and possible applications. Particularly, McMillin's group, using various DNA hairpins, made an important mechanistic conclusion that the dG–dC pairs promoted intercalation of TMP and CuTMP, thus inducing a negative CD signal due to the robust hydrogen-bonding framework, which was able to compensate for the steric hindrances imposed by the bulky porphyrins, while porphyrins bound externally to hairpins with stems enriched with dA–dT pairs were documented with positive CDs.<sup>158</sup> Using the CD signatures along with other spectroscopic methods, the two modes (intercalation and external binding) of complexation of TMP with free and encapsulated DNA of T7 bacteriophage were established.<sup>159</sup> It was found that the presence of the protein capsid in the phage particle did not prevent the porphyrin–DNA interactions, which could also have important implications for photodynamic therapy. Insertion of Co or V=O into the central metal ion position of TMP resulted in a single binding mode in the major groove of calf thymus DNA, apparently due to the nonplanarity of the porphyrin ring, as was reported by Barnes and Schreiner on the basis of a positive CD in combination with other optical spectra.<sup>160</sup> Besides the DNA binding, the TMP interaction with RNA and DNA–RNA hybrid duplexes was tested by Uno et al.<sup>161</sup> The induced CD suggested two preferential binding modes: the external self-stacking of TMP along the RNA duplexes, resulting in a bisignate exciton-coupling-type signal, and intercalation into the DNA–RNA hybrids, generating a negative CD. The RNA behavior, in particular, was explained in terms of the unfavorable conformations of the base pairs for the intercalation binding arising from their considerable displacement from the helical axis. Further transformations of the DNA host revealed that introduction of the third strand to form the corresponding triplexes inhibited the formation of the TMP–DNA assemblies as monitored by CD spectroscopy.<sup>162</sup>

Along with metalation, the porphyrin structure itself is another important factor for controlling the binding mode. For example, modified TMP upon placing the *N*-Me group at the corresponding meta-position facilitated the stacking mode of interaction between the porphyrin and poly-(d(A–T)<sub>2</sub>) as reported by Kim and co-workers.<sup>163</sup> Moreover, an interesting effect of time-dependent chirality inversion was observed for this system, likely due to structural reorganizations within the complex, although no rationale was presented so far. On the other hand, removal of two 10,20-meso-substituents of TMP (**164**) in its meta-modified derivative drastically switched the mechanism of interaction with DNA.<sup>164</sup> Surprisingly, they bound to DNA exclusively via intercalation, irrespective of the base composition, apparently due to the reduction of the porphyrin's bulkiness. However, the loop sequence should also be considered, as was demonstrated by **164** upon interaction with DNA hairpins.<sup>165</sup> Further modification of the porphyrin periphery (introduction of two Ph groups at the 10,20-meso-positions of **164**) led to another phenomena of chirality switching controlled by ionic strength: a negative CD couplet induced by extended assemblies of this porphyrin on poly(rA) at low salt concentration was gradually changed into the mirror-imaged signal, probably as a result of the helical sense inversion of porphyrin aggregates.<sup>166</sup> Also, this porphyrin in combination with AuTMP was proposed by Pasternack



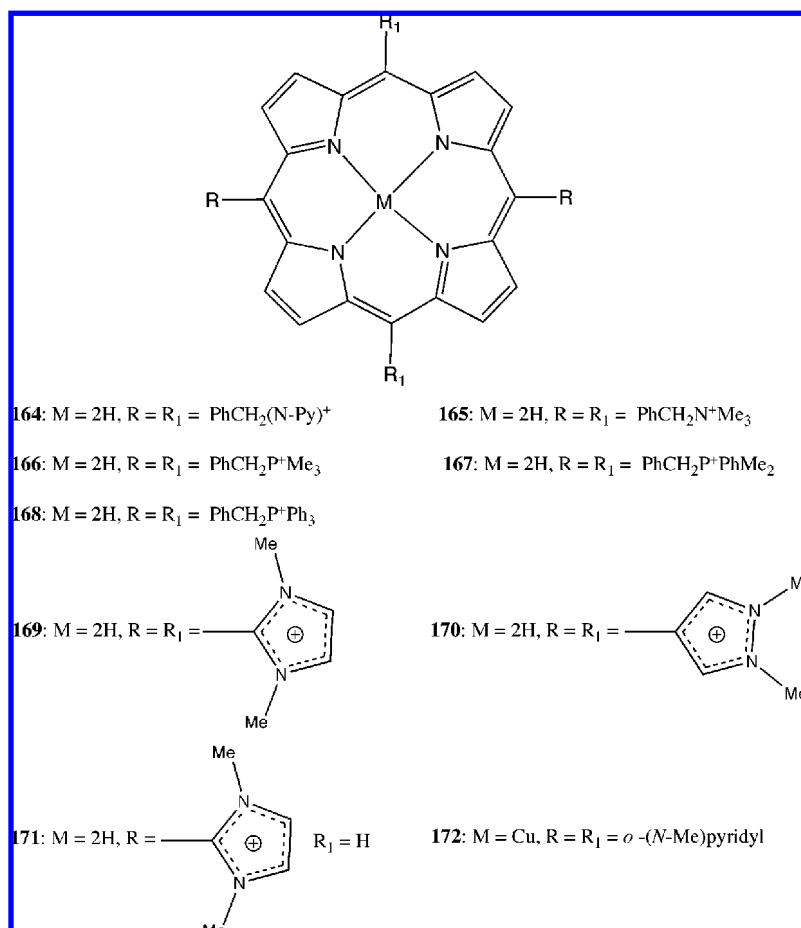


**Figure 92.** Structures of **164**–**172**.

and co-workers as a convenient supramolecular control of the size and extent of porphyrin assemblies on DNA, owing to its ability to aggregate at high salt concentration and the predominant intercalation behavior of AuTMP.<sup>167</sup>

Replacing the Me groups of TMP with  $-\text{CH}_2\text{PhB}(\text{OH})_2-o$  offered an effective sugar control of the porphyrin–DNA interactions, as reported by Shinkai and co-workers.<sup>168</sup> Essentially, while this porphyrin interacted with a duplex via intercalation with poly(dGdC) or the outside binding to poly(dAdT) and calf thymus DNA, the addition of saccharide dissociated the porphyrin–DNA complex through the saccharide-binding ability of boronic acid moieties, as indicated by the corresponding CD changes. Another modification such as attachment of polyethylenimine enhanced the porphyrin binding ability to DNA by creation of multiple cationic charges,<sup>169</sup> while ferrocenyl substitution resulted in effective control of the interaction mode with DNA by ionic strength: intercalation and outside binding at the low and high salt concentration, respectively, as indicated by the switching of a negative induced Cotton effect to a positive one.<sup>170</sup> These systems were also applied for DNA photocleavage<sup>169</sup> and photoinduced electron transfer.<sup>170</sup>

In order to apply a 5,10,15,20-tetraphenylporphyrin (TPP) structural motif for DNA binding studies, positive charges were introduced by modification with amine or phosphorus groups to yield **164**–**168** (Figure 92).<sup>171</sup> On the basis of the induced CD, the authors concluded that none of these porphyrins could intercalate, apparently because of their excessive bulkiness. The amine-containing **164** and **165** bound mainly to the outside surface of DNA with a positive Cotton effect as the major component of the CD. The

phosphorus-containing **166** exhibited a rather more complicated CD profile, with a lower-energy negative couplet and a higher-energy positive Cotton effect depending upon the molar ratio and ionic strength, and was likely a result of the combination of various binding modes. More bulky **167** and **168** tended to form extended assemblies on the nucleic acid's surface as judged by the conservative CD signals. These porphyrins were also tested for singlet oxygen generation ability considering the potential photodynamic therapy applications. Another type of cationic porphyrin was produced by Akutsu, Tjahjono, and their co-workers through the attachment of diazolium rings at the meso-position to give **169**–**171** (Figure 92).<sup>172</sup> It was confirmed by CD analysis that **169** bound outside to the minor groove of calf thymus DNA, while **170** intercalated apparently due to the steric hindrances imposed by the bulkier dimethylimidazole groups in **169**. This suggestion was further confirmed by partial switching of the binding mode to the intercalation upon removal of the two meso-substituents in **171**.

A useful approach for anionic porphyrin introduction onto the DNA matrix via heteroporphyrin aggregates was proposed by Liu and co-workers.<sup>173</sup> Specifically, it was shown that a mixture of **154** with TMP resulted in formation of the heteroaggregates stacked along the DNA surface with the aggregation mode and CD behavior controlled by the molar ratio of the porphyrins. The same system was studied in thin-film conditions in the presence of poly(allylamine hydrochloride) to yield well-detected J-aggregates characterized by low-energy transitions in the Soret band region, which generated a corresponding positive CD couplet. Surprisingly, **154** alone was able to interact with the DNA films to form



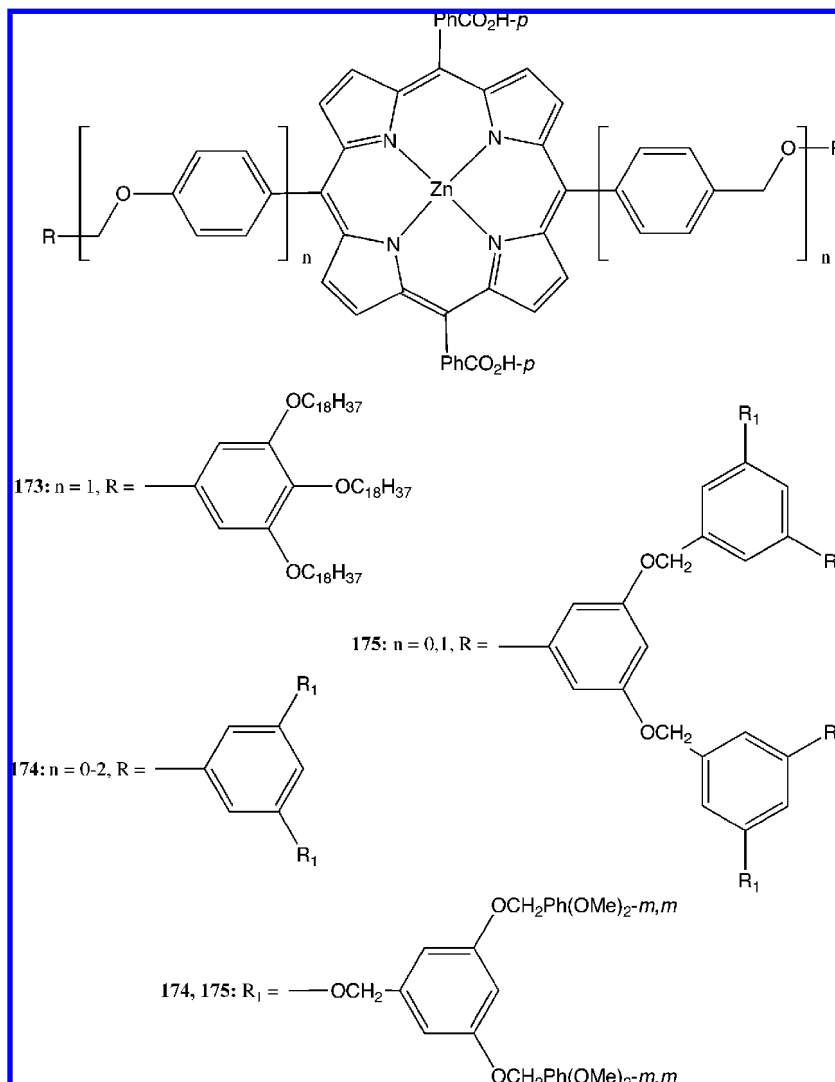


**Figure 93.** Structures of **173–175**.

the time-dependent H- and J-types of aggregates, as suggested by the authors. However, the complexity of the observed CD changes makes it difficult to dwell on the proposed interaction mechanisms exclusively. It is worth noting that another anionic porphyrin with four nido-carboranyl groups attached to *p*- or *m*-positions of TPP exhibited a tendency to form chiral aggregates on DNA under physiological conditions, although the chiroptical details were not presented.<sup>174</sup>

In the above-mentioned systems, the Soret band region was commonly used for the CD investigations of the porphyrin–DNA interaction processes. However, it is well-known that porphyrin chromophores possess quasi-allowed low-energy Q absorptions as well, for which the electronically excited-state configuration differs from that of Soret band. This stimulated Schreiner and co-workers to study the Q region upon the DNA binding.<sup>175</sup> They demonstrated that the CD behavior of the Q band of two typical porphyrins, i.e., intercalated PtTMP and outside-bounded **172**, was essentially the same as that of the Soret band transitions, showing two pairs ( $Q_0$  and  $Q_1$ ) of Cotton effects of the same sign: negative for PtTMP and positive for **172**, thus allowing the Q-band CD signature to be also used for determination of the binding mode. In addition to the strong asymmetry fields induced by chiral molecules and supramolecular systems, porphyrin chromophores were found to be very

sensitive even to the relatively weak asymmetry fields induced by the macroenvironment.

### 6.3. Macroenvironmental Chirality Sensing

One of the most representative examples of macroenvironmental chirality is a directional stirring or vortex. Thus, Ribó and co-workers reported an intriguing phenomenon of such chirality sensing using the J-aggregates of **154** and related *meso*-sulfonatophenyl substituted porphyrins by vortex motion during the aggregation process caused by the intermolecular association between the positively charged porphyrin ring and the negatively charged sulfonate groups.<sup>131,176</sup> While without stirring equal amounts of left- and right-handed aggregates were formed, upon stirring, the porphyrins were arranged with a unidirectional helical orientation with about 85% probability, having the helicity dependent upon the vortex (i.e., stirring) direction. Clockwise and anticlockwise stirring generated right- and left-handed chirality, respectively, that corresponded to a strong positive and negative CD couplet in the porphyrin absorption region as a result of the interchromophoric exciton coupling. While the detailed mechanisms of the chirality induction and amplification remains unclear, it was suggested that the chiral vortex acted at the mesoscale level upon the kinetically controlled growth of the supramolecular assembly and

spontaneous symmetry-breaking processes in the diffusion-limited generation of the high-molecular-weight homoassociates. This assumption was further supported by the direct visualization of 3D homochiral helices using atomic force microscopy.

A similar approach was undertaken by Aida and co-workers to induce chirality in the hydrogen-bonded J-aggregates of dendritic **173**–**175** (Figure 93) by spin-coating technique.<sup>177</sup> The chirality sign was also governed by the spin direction with clockwise and anticlockwise rotation generating positive and negative exciton couplets, respectively, while the CD intensity was strongly affected by the structure of dendritic periphery with the largest  $A$  value detected for **174** ( $n = 1$ ). While the origin and driving forces of this phenomenon have yet to be rationalized, the generation of these 2D supramolecular sheets, which adopt a twisted geometry relative to one another upon rotational force, was proposed. The examples described in this section clearly demonstrate the prime importance and pivotal role of porphyrin chromophores for sensing different types of chiral influences via the supramolecular interactions.

## 7. Supramolecular Systems with Chiral Memories

Central to the observed chiral effects in the above work is the concept of the “molecular chiral source” that interacts with the achiral substrate via supramolecular noncovalent interactions to produce a chiral species whose properties, as we have seen, can be an end in themselves, or as a diagnostic tool for analysis of the chiral inductor. However, until recently, it was unquestioned that such chiral supramolecular systems had a mandatory requirement that they must be composed of (at least) two species: chiral and achiral (in which chirality is induced). However, this dictum was dispelled by the work of Aida and colleagues who showed the conceptually new phenomenon of “chirality memory”, which is a supramolecular system in which chirality was first induced and then shown to retain its chirality even when the chiral information source was removed and all the components of the system are (from a configurational viewpoint) achiral.

The basis of Aida and co-workers' research is a series of saddle-shaped fully substituted porphyrins (**136**–**138**) (see Figure 81) whose nonplanarity derives from the steric repulsion among the neighboring substituents and results in two enantiomeric forms, which rapidly interconvert to yield a racemic mixture.<sup>6a,135</sup> This equilibrium was shifted to one particular chiral conformation upon interaction with various enantiopure carboxylic acids via hydrogen bonding of two carboxylates to the pyrrole nitrogens of the porphyrin ring from opposite sides, giving 1:2 complexes as mentioned previously. Thus, on the addition of, for example, (*R*)-mandelate, two diastereomeric complexes are formed, with the favorable species existing in a diastereomeric excess of >98%. This complex formation results in the observation of strong induced bisignate CD signals in the region of the Soret band (although the authors did not discuss the electronic origin of the observed optical activity). The mechanism of the chirality transfer, as determined from X-ray studies, is via steric hindrance minimization, in which unfavorable steric interactions between the guest's largest substituent and the most bulky part of the porphyrin (i.e., the *o*-dimethoxyphenyl group) are reduced by orientation of the guest's substituent away from this and over the porphyrin's smaller *meso*-phenyl moiety.

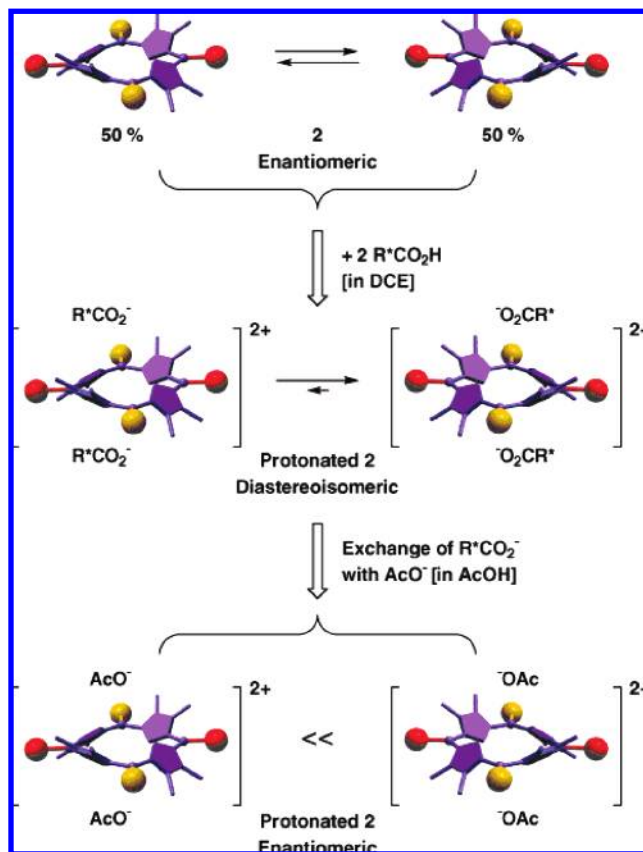


**Figure 94.** Schematic representation of chirality transfer and memory events with saddle-shaped chiral porphyrin. Reprinted with permission from Mizuno, Y.; Aida, T.; Yamaguchi, K. *J. Am. Chem. Soc.* **2000**, *122*, 5278. Copyright 2000 American Chemical Society.

Remarkably, when the porphyrin–mandelate complex is dissolved in achiral AcOH, which displaces the two chiral acids, the complex retains its chirality (and is now enantiomeric, having no chirality-inducing source) as observed by not only the retention of the Cotton effects but also their enhancement (Figure 94). Thus, these complexes have a memory for the chirality of the species that induced the system's asymmetry after the removal of these inductor molecules. The memory effect arises from that fact that the chiral–achiral ligand substitution is under kinetic control and that the acid switch occurs before racemization (macroscopic inversion) can take place. This racemization half-life was found to be substantial, temperature dependent, and 200 h at 23 °C, with the activation parameters being  $\Delta G^\ddagger = 26.1 \text{ kcal mol}^{-1}$ ,  $\Delta H^\ddagger = 29.1 \text{ kcal mol}^{-1}$  and  $\Delta S^\ddagger = 10.6 \text{ cal K}^{-1} \text{ mol}^{-1}$ .

Shinkai and co-workers also developed a supramolecular chirality memory system **145** (Figure 82) that took the concept to a new level of elegance, producing a system that could memorize the chirality of the complex even when the chiral source had been removed and not replaced<sup>138c</sup> with an achiral “clip” molecule (as in the case of Aida and co-workers). The mechanism of chirality induction was unambiguously established and discussed previously (see section 6).

The chiral-memory generation was achieved by the addition of an excess of pyridine that successfully competes for the ligand's binding sites, resulting in the free (unbound) porphyrin. Subsequently, it was found that chirality of the system, as determined from the CD spectra, is retained/memorized (although at a reduced level). The origin of this

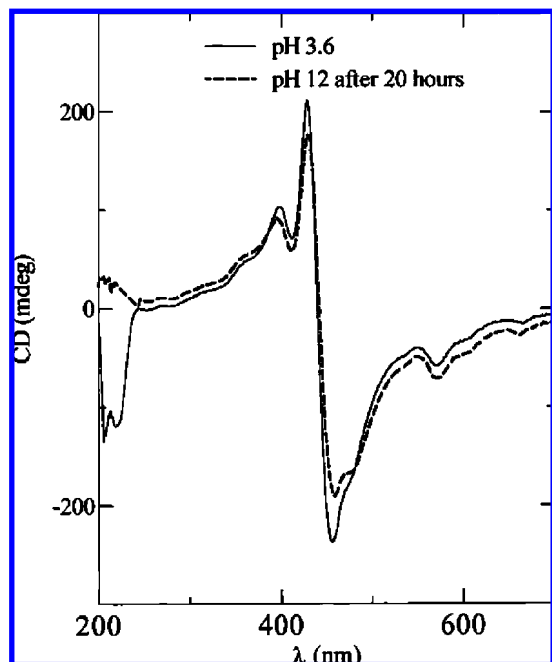


**Figure 95.** CD spectra of (full line) a solution of CuTMP-154 (4 mM each) in the presence of poly-L-glutamate (400 mM) at pH 3.6 and (dotted line) the same solution at pH 12. Reprinted with permission from Purrello, R.; Raudino, A.; Scolaro, L. M.; Loisi, A.; Bellacchio, E.; Lauceri, R. *J. Phys. Chem. B* **2000**, *104*, 10900. Copyright 2000 American Chemical Society.

memory is in the steric hindrance between the 3,5-dimethoxyphenyl groups of the neighboring porphyrins, which inhibits rotation and, thus, racemization. This rotation was found to have first-order kinetics ( $\Delta G^\ddagger = 23.0 \text{ kcal mol}^{-1}$ ,  $\Delta H^\ddagger = 18.1 \text{ kcal mol}^{-1}$ , and  $\Delta S^\ddagger = -16.4 \text{ cal K}^{-1} \text{ mol}^{-1}$ ) and was remarkably preserved for 3 days at 0 °C and for 1 year at -37 °C and was calculated to last for  $1.9 \times 10^6$  years at -100 °C.

Purrello et al. reported a number of self-assembly systems that possess a chirality-memory effect. Here, initial work showed the formation of aggregates between the cationic porphyrin CuTMP, anionic porphyrin **154**, and either L- or D-polyglutamic acid acting as a chiral matrix.<sup>154c</sup>

Upon the formation of a binary self-assembled system between CuTMP and an enantiopure polyglutamic acid, an induced CD was observed and ascribed to monomer aggregation of the CuTMP molecules onto the  $\alpha$ -helix structure of the matrix. This chirality was, however, lost on lowering the pH to ca. 4, which is associated with the transformation of the polyglutamic acid from  $\alpha$ -helix to a random-coil conformation. Conversely, the induced CD obtained from the corresponding CuTMP, **154**, and polyglutamic acid ternary complex shows a remarkable memory effect, in that, even when the conformation of the polyglutamic acid is switched to a random coil by raising the pH to 12 (as observed by the disappearance of the polymer matrix CD band at ca. 200 nm), the porphyrin assemblies retain their chirality; see Figure 95.

Indeed, these complexes were found to be stable for several months, with only a 30% decrease in CD intensity over a 4 week period. The stability of these ternary species is believed to arise from highly cooperative interactions within the aggregates between the oppositely charged porphyrins, although neither a detailed conformational structure for the assembly nor a rationale of the electronic transition's

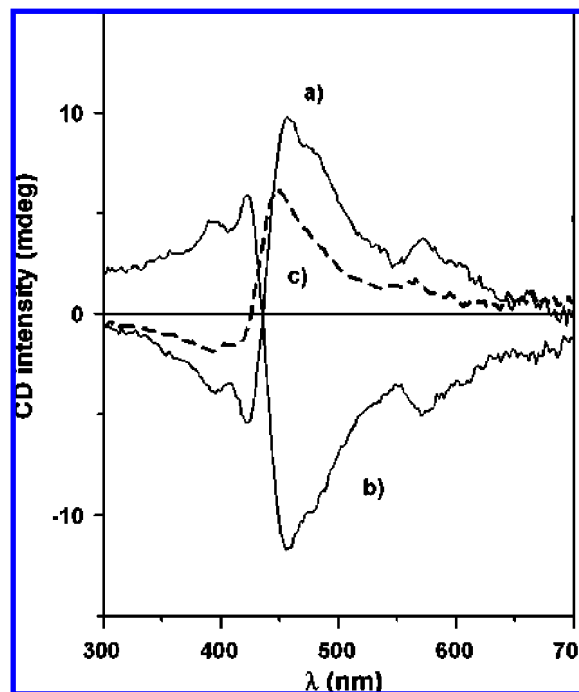


**Figure 96.** CD spectrum of **154** and CuTMP in ultrapure Millipore water in the presence of (a) L-Phe, (b) D-Phe, and (c) after the removal of the L-enantiomer. Reprinted in part with permission from Lauceri, R.; Raudino, A.; Scolaro Monsù, L.; Micali, N.; Purrello, R. *J. Am. Chem. Soc.* **2002**, *124*, 894. Copyright 2002 American Chemical Society.

chiral origins have been suggested, although these are admittedly complex tasks. This memory was also found to be stable to the addition of a competing and antipodal chirality source. Thus, it was seen that addition of a 1 mM (a 5-fold excess) solution of poly-D-glutamate to the CuTMP/**154**/poly-L-glutamate species results in complete retention of the first negative–second positive bisignate Cotton effects arising from the porphyrin's Soret band.

Purrello and co-workers also reported a similar self-assembly memory system based upon the aggregation of the oppositely charged CuTMP and **154**, but this time in the presence of enantiopure aromatic amino acids.<sup>178</sup> As can be seen from Figure 96, the addition of a 1:1 solution of the two porphyrins ( $2 \times 10^{-6} \text{ M}$  each) to a  $8 \times 10^{-3} \text{ M}$  solution of L-Phe results in a first positive–second negative bisignate CD signal (with D-Phe giving the mirror image).

The induced chirality was found to arise from a template effect of Phe clusters (ca. 60 nm at 30 °C as determined by dynamic light scattering), with the size of the clusters varied by the temperature (specifically, decreasing with increasing temperature) and sensed by the degree of chirality induced in the porphyrin aggregates, i.e., reduced induced CD intensity with increasing temperature. As found previously, a remarkable long-lasting chirality-memory effect, expressed in terms of CD signal retention, was observed upon removing the phenylalanine chiral source template clusters by ultrafiltration; see Figure 96c.

The origin of the growth of these chiral porphyrin aggregates is found to be via an initiation role of the Phe clusters, which seed assemblies of porphyrin clusters existing at a concentration of  $6 \times 10^{-13} \text{ M}$  (with each assembly composed of  $2 \times 10^6$  porphyrin molecules), consequently allowing a 100% enantiospecific self-propagation of the aggregation process. This process is a good example of a

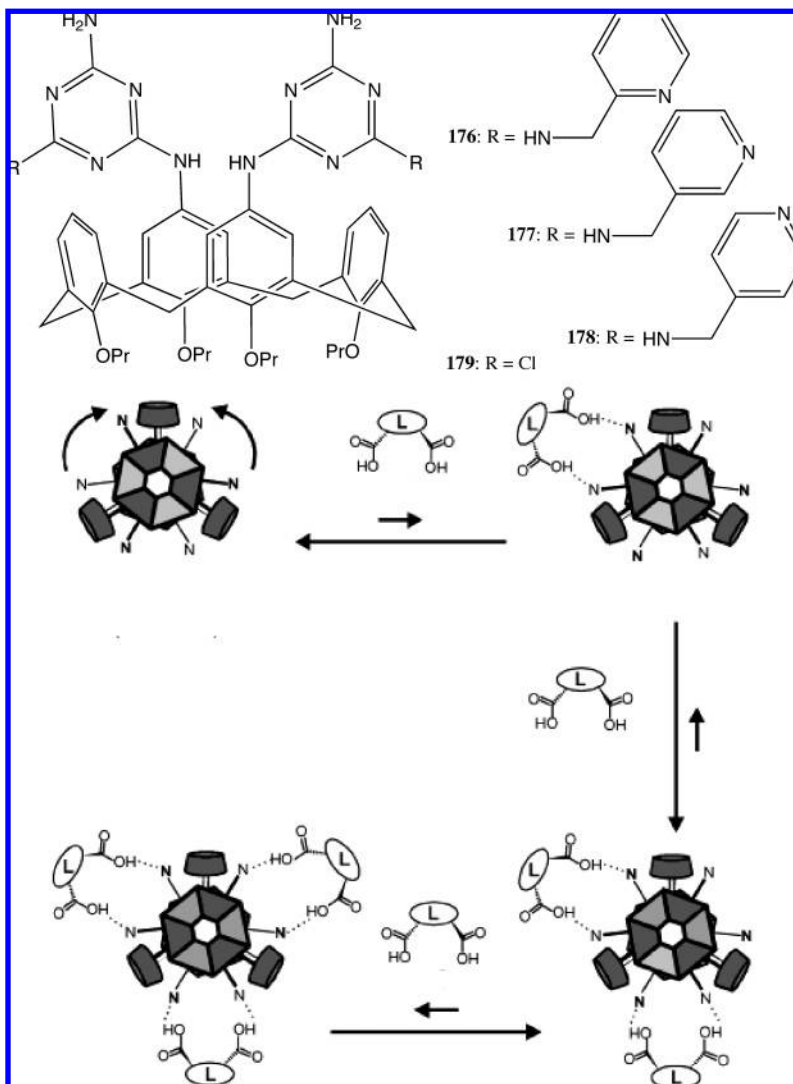


**Figure 97.** Structures of calix[4]arenes **176–179** and schematic representation of the cooperative interactions with **L-180**. Reprinted in part with permission from Ishi-i, T.; Crego-Calama, M.; Timmerman, P.; Reinhoudt, D. N.; Shinkai, S. *J. Am. Chem. Soc.* **2002**, *124*, 14631. Copyright 2002 American Chemical Society.

smart chirogenic supramolecular system that displays chirality induction, memory, and amplification.

Reinhoudt and co-workers further investigated the nature of the chirality-memory concept, based on their extensive work on self-assembled double rosettes formed from three calix[4]arene dimelamines and six cyanurates and bound together by 36 cooperative hydrogen bonds (**176–179**; see Figure 97).<sup>179–181</sup> It was previously found that these supramolecular assemblies form a racemic mixture of (*P*)- and (*M*)-enantiomers that could be separated as diastereomers by using chiral barbiturates to create diastereomers, with the chiral barbiturates then replaced with achiral cyanurates to give the enantiomerically pure species.<sup>5c,8b</sup>

They subsequently found that appending each calix[4]arene moiety with two 2-pyridyl functionalities, attached to opposite phenyl rings, allowed the pyridyl groups to interact with external chiral dicarboxylic acids.<sup>182</sup> Thus, when 3 equiv of an enantiopure dicarboxylic acid, such as the dibenzoyl tartaric acid (**180**), are added to the racemic rosette, there exists the potential for diastereomers to be formed. Each diacid binds via interaction with two of the six 2-pyridyl moieties, which from Corey-Pauling-Koltun (CPK) model analysis was found to be across the two halves of the rosette in a cliplike manner; see Figure 97.

Results show that this interaction amplifies the interconversion between the less-favorable *P*-helicity and the more-favorable *M*-helicity (for **L-180**), resulting in a maximum of 90% de achieved within 15 h of addition. On removal of the chiral diacid by addition of ethylenediamine, the enantiopure supramolecular assembly was produced, exhibiting significant chirality memory, with a racemization half-life of 1 week at 20 °C or 1 year at 0 °C. Thus, we again see the phenomena of a supramolecular chiral species in which none of the components are themselves chiral and whose enantiomeric integrity is maintained via an extensive cooperative network of supramolecular interactions.

In contrast to the examples above whose systems rely, initially, on a chiral source and whose memory is then maintained by intermolecular interactions, Raymond and co-workers took the chiral-memory concept a stage further and developed an elegant example where the generation, memory, and application of the chirality is achieved without the use of a chiral source.<sup>183</sup> In this case, the supramolecular species is a tetrahedral structure composed of four metal (Ga) centers and six achiral ligands; see Figure 98. This [Ga<sub>4</sub>L<sub>6</sub>]<sup>12-</sup> species forms spontaneously in solution to yield a racemic mixture of the ΔΔΔΔ and ΛΛΛΛ enantiomers with each ligand coordinating to two metal ions.



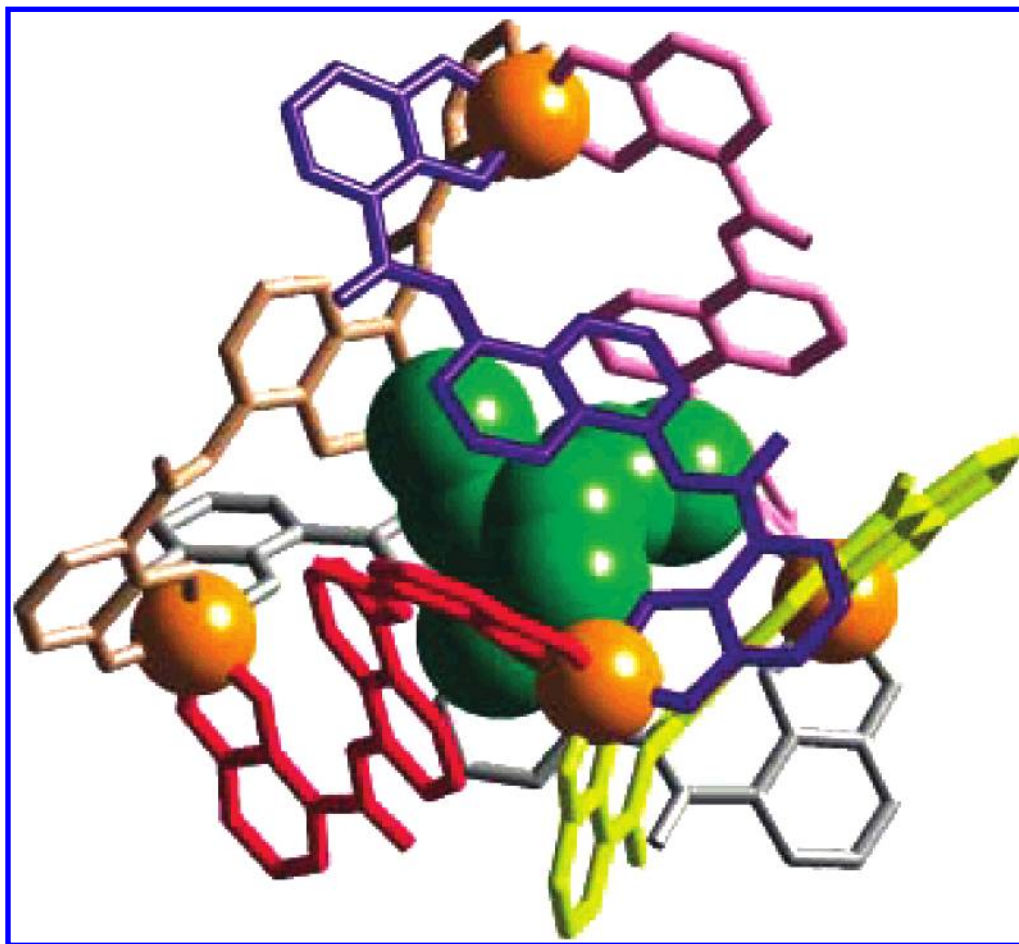


**Figure 98.**  $M_4L_6$  tetrahedral assembly composed of biscatecholamide ligands and octahedrally coordinated metal ions. The structure encapsulates guests such as  $Et_4N^+$  ions. Reprinted with permission from Ziegler, M.; Davis, A. V.; Johnson, D. W.; Raymond, K. N. *Angew. Chem., Int. Ed.* **2003**, 42, 665. Copyright 2003 Wiley-VCH Verlag GmbH & Co.

On separation of these enantiomers (the separation is achieved using chiral counteranions and subsequent resolution of the diastereomers then exchanging for achiral counteranions), the chirality of the enantiomers is found to be highly robust and retained its enantiopurity for 8 months, even after extended boiling. Critically, it is observed that the chirality is maintained even though partial ligand dissociation of the complex occurs over the time scale of a few seconds.

In a remarkable further work, Raymond and co-workers devised an experiment to show, as they say, that the chirality of the assembly is a property of the structure itself and not of its constituent components. This is a concept that flies in the face of the accepted wisdom of “preprogrammed” self-assembly arising inherently from the structures of the molecular components. In this experiment, a second bidentate ligand ( $L^2$ ) of a similar coordination chemistry but different geometrical preference was taken, which when complexed on its own with Ga, forms a helical  $[Ga_2L_3]^{6-}$  structure. However, when these two species ( $[Ga_4L_1]^{12-}$  and  $[Ga_2L_3]^{6-}$ , 5.5 mM each) were added together into a  $D_2O$  solution and heated at 75 °C, the stepwise substitution of the  $L^1$  ligand was observed (by  $^1H$  NMR monitoring of  $Et_4N^+$  encapsulated in the central cavity) to give a mixture of  $[Et_4N \subset Ga_4L^1_n L^2_{6-n}]^{11-}$  species, with little left of the initial compound after 24 h. The stepwise replacement did not compromise either the structure or the chiral memory of the initial tetrahedral geometry, with complete retention of the

$\Delta\Delta\Delta\Delta$  configuration as observed by the unchanging CD spectra over the 24 h period.

The origin of these phenomena arises from the coexistence of the structural rigidity conferred on the species by its extensive coordination network (interactions) and the lability of the individual components whose kinetic characteristics make ligand substitution possible while not allowing complete dissociation and, thus, racemization and memory loss. As observed by Purrello,<sup>184</sup> this is an example of dynamic structural and chiral memory, in contrast to other examples in this area that may be regarded as static, and that may allow this system to perform in catalytic cycles.

This insight by Purrello was soon realized in further work by Raymond and co-workers, making use of the 350–500 Å<sup>3</sup> cavity to encapsulate a substrate for catalysis in a cationic 3-aza-Cope rearrangement.<sup>185</sup> A range of enammonium substrates of varying sizes and shapes were found to be well-encapsulated, and it was found that the reaction proceeded within the cavity. The effect on the rate of reaction was measured; in all cases, it was found that binding by the  $[Ga_4L_1]^{12-}$  complex enhanced the rate constant by up to 854 times. Further analysis revealed that this enhancement originates from the bound substrate conformation resembling that of the chairlike transition state, which consequently decreases the entropic barrier to rearrangement. This behavior is found to be truly catalytic (rather than just rate enhancing) as the rearranged product equilibrates with the bulk solution, where it undergoes hydrolysis, thus freeing the cavity for

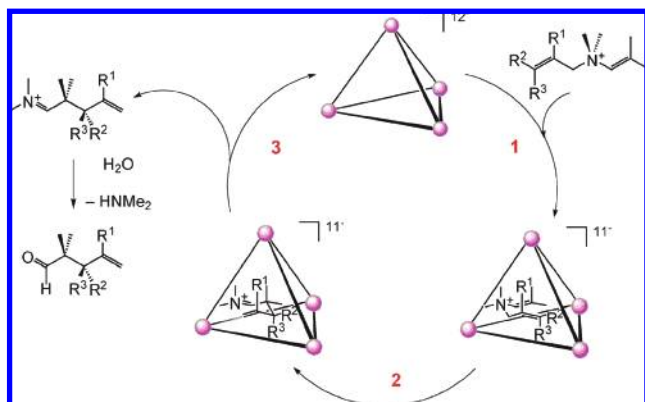


**Figure 99.** Proposed catalytic cycle for the cationic 3-aza-Cope rearrangement. Reprinted with permission from Fiedler, D.; Bergman, R. G.; Raymond, K. N. *Angew. Chem., Int. Ed.* **2004**, *43*, 6748. Copyright 2004 Wiley-VCH Verlag GmbH & Co.

further substrate binding and enabling catalytic turnover; see Figure 99.

Although this particular reaction is not chiral, this work clearly shows the potential for the application of the chiral-memory approach, as the chiral catalyst formed without any “expensive” chiral source, which is a very attractive feature for technological applications.

Finally, in this section, we consider the chiral memory observed in the polymer-based system developed by Yashima and co-workers.<sup>7c,186</sup> Although a more extensive examination of the chirality-sensing nature of these helical polymers can be found in section 10, we can see an early example of how the utilization of chirality induction and kinetic control produces a chiral supramolecular system with its own distinct memory characteristics,<sup>4c</sup> which has subsequently been applied to catalytic processes.

The basis of this work is the polymer *cis-trans*-poly((4-carboxyphenyl)acetylene) (**181**), which, although containing short helical sections, has many reversal points and is, as such, achiral and CD inactive. By noting that the helicity of various biological macromolecules is controlled to a degree by the homochirality of their constituent components, it was shown that, on the addition of the primary amine (*R*)-1-(1-naphthyl)ethylamine ((*R*)-**182**), helical chirality was induced, with the induced CD sign depending upon the chirality of the ligand (Figure 100). The origin of this induction was found to be via interaction between the ligand’s amine functionality and the polymer’s 4-carboxyphenyl moiety. The dynamic nature of this induced chiral system was shown by disruption of the helical structure by addition of trifluoroacetic acid and subsequent addition of a ligand, (*S*)-2-amino-1-propanol, of opposite chirality that generated the opposite-handed helix. Such a dynamic nature is of critical importance for engendering the ability on the helical system to memorize its chirality.

Thus, when a 50 equiv excess of the achiral 2-aminoethanol was added to the helical **181**/*(R)*-**182** complex, replacing the chiral (*R*)-**182** ligand, almost no loss in the intensity of the induced CD was observed. An interesting effect of “chirality repair” was found when the **181**/2-aminoethanol solution was physically separated from (*R*)-**182** by gel permeation chromatography. After separation, the helix still showed the memory of its induced chirality but with an induced CD intensity of 87% of its original value ( $[\theta]_{374} = 2.8 \times 10^4 \text{ deg cm}^2 \text{ dmol}^{-1}$ ); however, after 13 days at ambient temperature, the dynamic nature of the polymer–

ligand interactions had allowed the chiral intensity to recover to  $[\theta]_{374} = 2.7 \times 10^4 \text{ deg cm}^2 \text{ dmol}^{-1}$ , thus showing one of the great strong points of the supramolecular approach in general.

In a polymeric system they developed, Yashima and co-workers show how this chiral memory can then be “stored” via the enantioselective esterification of a chiral phosphorus center controlled by chirality transfer from the helicity of the molecule to the prochiral phosphorus center (Figure 101).<sup>187</sup> Thus, chirality is induced in the phosphonic acid methyl ester bearing helical poly(phenylacetylene) in a manner analogous to that seen above for **181**; then, in a standard reaction with diazomethane, esterification is achieved. This process was found to occur with modest ee values ranging from 2.1 to 15% depending on the exact polymer type, chiral inductor ligand, and temperature (with lower ee found at lower temperatures), with the mechanism believed to arise from the hindered approach of the diazomethane due to the helical structure. Further work investigating the chiral-memory effect can also be found in the work of Kubo et al., who have utilized a bisporphyrin system connected by a crown ether.<sup>188</sup>

## 8. Direct Chirality Observation on Surfaces

Supramolecular sensing and communication of chiral information has, hitherto, been largely confined to the solution phase; however, recently, there has been a great increase in the observation and rationalization of the chiral behavior on two-dimensional surfaces. Because of the divergent nature of the intermolecular interactions, it is possible to generate a hierarchically structured surface where the chirality is propagated from the molecular up to the macro(supra)molecular level. This has allowed determination of the conformation and chirality of individual molecules,<sup>189</sup> generation and control of large divergent supramolecular systems, and understanding of how intermolecular and molecular-surface interactions underpin the formation processes<sup>190</sup> leading to functional devices at the nanometer scale.<sup>191</sup> This has been made by the molecular-level and even atomic-level resolution now possible by microscopy techniques such as scanning tunneling microscopy (STM) and atomic force microscopy (AFM), with accompanying support from lower-resolution techniques such as transmission electron microscopy (TEM) and scanning electron microscopy (SEM).

Detailed and insightful work in this area was recently reported by Raval and co-workers for a system comprising (*R*)- and (*S*)-alanine chemisorbed onto a Cu(110) surface.<sup>192</sup> In this study, they make the definition that such surfaces can be classified into two groups: (1) “weakly adsorbed” systems, in which the intermolecular interactions dominate the two-dimensional architectures, and (2) “strongly adsorbed” systems, in which both the intermolecular interactions and the molecule–metal bonding influence the architectural outcome, with the belief that strongly adsorbed systems possess a potential for greater structural and property tunability. The surface considered here was prepared by adsorption (via sublimation) of, initially, (*S*)-alanine onto the Cu(110) crystal at room temperature under ultrahigh vacuum conditions, and annealed between 400 and 430 K. When examined by STM, a perfect two-dimensional chiral assembly, with one chiral domain that is non-superimposable with its mirror image, was observed across the surface extending to the macroscopic scale (Figure 102).



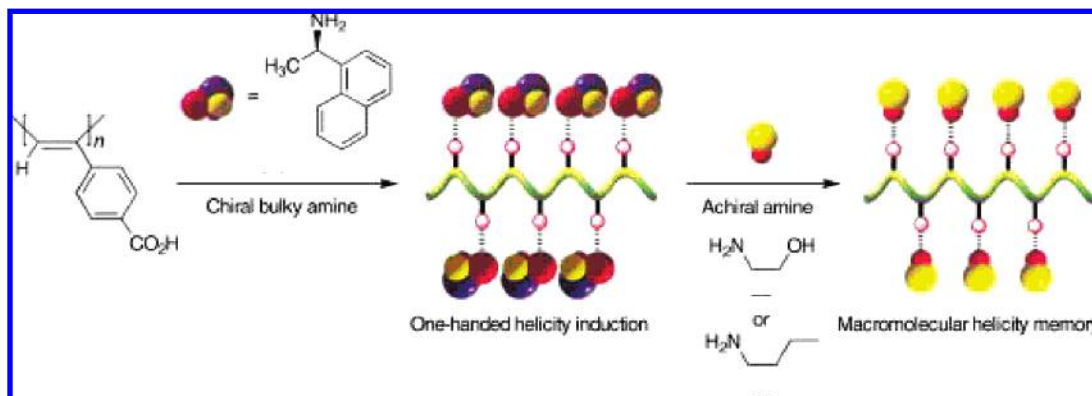


**Figure 100.** Schematic illustration of memory of macromolecular helicity concept. The macromolecular helicity induced on **181** by a chiral amine (*R*-**182**) is memorized after complete removal of the amine and replacement with achiral amines. Reprinted in part with permission from Yashima, E.; Maeda, K.; Nishimura, T. *Chem.—Eur. J.* **2004**, *10*, 42. Copyright 2004 Wiley-VCH Verlag GmbH & Co.

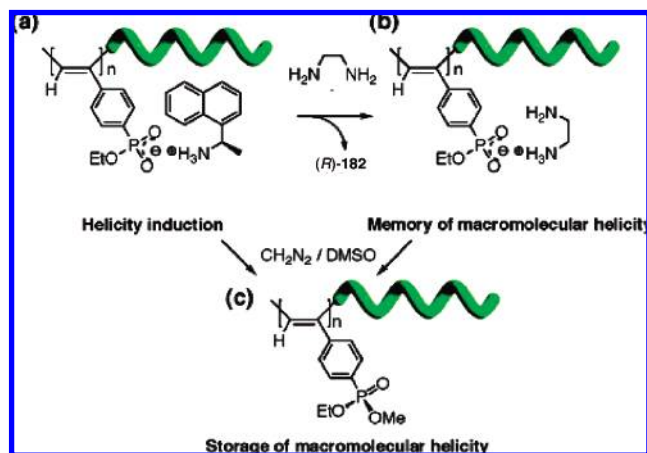


**Figure 101.** Schematic illustration of helicity induction in achiral polymer upon complexation with (*R*)-**182** (a), memory of the induced macromolecular helicity after replacement of (*R*)-**182** by achiral diamine (b), and storage of the induced helicity and helicity memory by enantioselective esterification with diazomethane (c). Reprinted in part with permission from Onouchi, H.; Miyagawa, T.; Furuko, A.; Maeda, K.; Yashima, E. *J. Am. Chem. Soc.* **2005**, *127*, 2960. Copyright 2005 American Chemical Society.

Analysis with reflection–absorption infrared spectroscopy revealed the mode of alanine bonding to the copper surface and, consequently, the mechanism by which the supramolecular chirality is sensed and transferred over the surface. It was found that the alanine at the lowest supramolecular level exists in pairs, with one molecule of the pair bound to the copper surface via both oxygens of the carboxylate and the nitrogen of the neutral amino group ( $\mu_3$ ), and the other bound via the amino group and one of the carboxylate's oxygens ( $\mu_2$ ). The consequence of these modes of interaction is that, in both cases, the methyl group is orientated upward away from the surface, which results in chiral steric interactions inducing a right-handed kink in the structure for (*S*)-alanine and an opposite left-handed kink for (*R*)-alanine. This initial level of chirality sensing is then enhanced to clusters of six or eight alanines comprising pairs of the ( $\mu_2$ )- and ( $\mu_3$ )-type molecules, bound together by a lateral tier of chiral N–H $\cdots$ O interactions (which are found close to the copper surface) and a separate chiral transverse tier of C–H $\cdots$ O interactions (that exist further from the surface) (Figure 103).

From a supramolecular point of view, the rationale for the formation of such discrete and regular clusters is interesting. Raval and co-workers suggest that this arises from

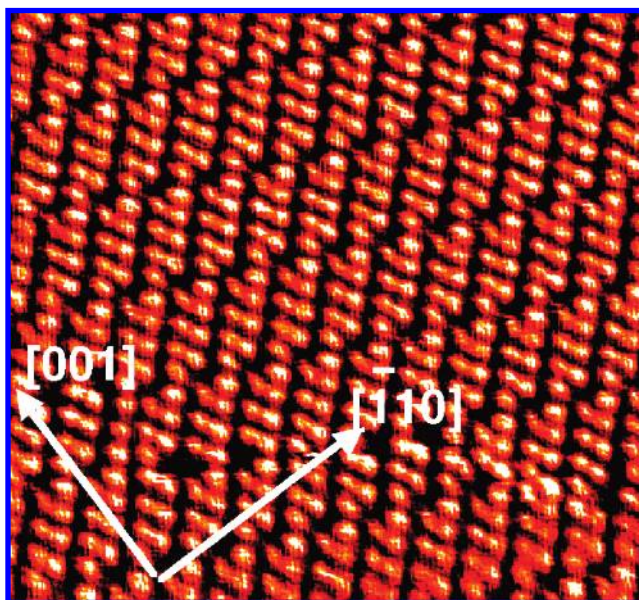


**Figure 102.** STM images showing the chiral phase of *S*-alanine adsorbed on Cu(110) obtained after annealing the room-temperature saturated surface to 403 K. Reprinted with permission from Barlow, S. M.; Louafi, S.; Le Roux, D.; Williams, J.; Muryn, C.; Haq, S.; Raval, R. *Langmuir* **2004**, *20*, 7171. Copyright 2004 American Chemical Society.

the stress of maintaining optimal intermolecular interactions that become too great at a critical cluster size, resulting in a fracturing of the assembly. Two possible scenarios from the literature are proposed for this:<sup>193,194</sup> (1) that the geometric requirements of the intermolecular interactions force the molecules into unfavorable copper bonding positions, resulting in new cluster nucleations, or (2) that the strength of the molecule–copper chemisorption causes surface reconstruction (in which the positions of the bound copper atoms are slightly shifted) of the copper atoms to allow optimization of the adsorption geometry, thus resulting in stresses in the copper–copper bonding and consequent strain breaks. A fascinating, and potentially useful, consequence of the long-range ordering of these chiral clusters are channels of bare metal that are themselves chiral; it is proposed that these chiral channels could be exploited for molecular-recognition and chiral-molecular-reaction purposes. An insightful realization arising from this is that the stresses transmitted through the surface from which these channels are formed must be themselves chiral, which has profound implications for rational chirality sensing on such surfaces. Thus, in consider-

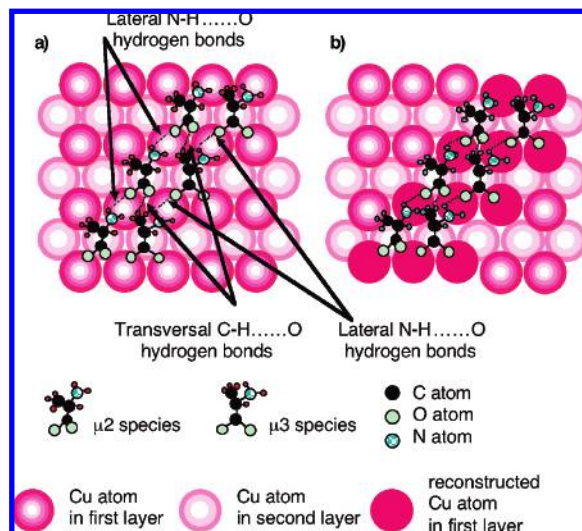


**Figure 103.** Cluster model for packs of six molecules of *S*-alanine adsorbed on the Cu(110) surface: (a) unreconstructed surface and (b) pseudo-(100) reconstructed surface. Reprinted with permission from Barlow, S. M.; Louafi, S.; Le Roux, D.; Williams, J.; Muryn, C.; Haq, S.; Raval, R. *Langmuir* **2004**, *20*, 7171. Copyright 2004 American Chemical Society.

ing the origin of the morphology and function of extended chiral arrays, both the intermolecular interactions and molecule–metal bonding are key aspects.

The transmission of chirality across an extended surface and how this is mediated by the local sensing of supramolecular/steric interactions is found in the enantiomeric surfaces reported by Fasel et al.<sup>195</sup> This work was based on their discovery that racemic mixtures of heptahelicene spontaneously form separate enantiomeric domains on a Cu(111) surface (as observed by STM methods).<sup>196</sup> Subsequently, this led to further investigation of this phenomenon by looking at the surface architectures formed by the individual enantiomers (*M*)-**183** and (*P*)-**183** (Figure 104). However, as discussed previously, the metal–molecule interactions are a critical consideration in the system, and indeed, Fasel et al. found that, on Ni(111) and Ni(100) surfaces, the subsequent low mobility of the helicenes precluded the observation of any surface chiral effects.

At 95% surface coverage by **183**, the molecules were found to form in pairs of two different triangular clusters, one comprising six molecules and the other comprising three molecules (3,6-structure), with (*M*)-**183** generating anticlockwise clusters and (*P*)-**183** generating clockwise equivalents. However, on increasing the surface coverage to 100%, the architecture was then solely composed of the three molecule clusters (3-structure). Closer inspection of the STM images reveals that, for the six-molecule cluster in the 3,6-structure, if an anticlockwise path is traced between the (*M*)-**183** molecules, it is found that each molecule is rotated at an angle of 60° to the previous one, and that each molecule in a three-molecule cluster is rotated at an angle of 120°, which Ward, in his comment,<sup>197</sup> describes as being a “gearlike” rotation.

These results show the critical dependence that the surface chirality has on the subtleties of the correlations between the chiral intermolecular interactions and their divergent transmission. Indeed, it should be noted that these helicenes possess no hydrogen bonding or strongly dipolar moieties, and as such, the chirality sensing by neighboring molecules will be via the chiral steric constraints imposed by the

helicene’s three-dimensional structure and the associated aromatic interactions.

One of the limitations/challenges in this area of research is the preparation of samples that are adequate for analysis by STM or similar techniques, often requiring ultrahigh vacuum or low-temperature conditions. Thus, with this in mind, as well as the fact that most conventional chemical reactions take place in solution, Wang and co-workers undertook to study chiral surfaces in solution by using electrochemical STM (ECSTM).<sup>198</sup> In this work, a Cu(111) surface was saturated with a solution containing 0.1 M HClO<sub>4</sub> and 0.1 M of either (*R*)- or (*S*)-2-phenylpropioamide (PPA). The subsequent ECSTM images reveal that individual molecules of (*R*)- or (*S*)-PPA are ordered in non-superimposable chiral fashions. In these results, we again see the transfer of the molecular chirality in a supramolecular fashion, thus creating enantiomeric surfaces. Indeed, the spatial resolution in these samples is such that the individual atoms are discernible, and from this, it was found that the phenyl ring lies parallel to the copper surface and in a hollow site, with the amino, carbonyl, and methyl groups in two-bridge sites. In fact, as a result of the high image quality, the chirality of the individual molecules could be directly determined from the chiral center–amine and chiral center–methyl distances, which were found to be 0.23 and 0.15 nm, respectively, for (*S*)-PPA, which correlates with the expected substitution around its chiral center.

Hitherto, we have seen a number of systems in which surface chirality is generated and studied; however, these have been characterized by the use of comparatively simple small molecules, primarily to facilitate the formation of regular, high-quality surfaces for obtaining useful images. However, if the understanding and application of chiral surface science are to progress in a manner similar to the advances made in conventional chiral supramolecular chemistry in the last 15 years, more complex and rationally designed molecular layers need to be investigated. In this light, recent work by Reinhoudt and co-workers<sup>199</sup> is particularly interesting. Highly ordered pyrolytic graphite (HOPG) is employed as a surface for assembly of the discrete 15-component supramolecular rosettes for which Reinhoudt has become well-known.<sup>200,201</sup> These are composed of melamine-substituted calix[4]arene **184** and 5,5-diethylbarbiturate (DEB) building blocks that are individually achiral and, in solution, form **184**<sub>3</sub>·(DEB)<sub>12</sub> tetra-rosette assemblies (maintained by 72 hydrogen bonds) as a racemic mixture of (*P*)- and (*M*)-enantiomers that have a diameter of 3.3 nm (Figure 105).

Because of the large depth of the surface molecular layer (ca. 3.3 nm), STM methods do not produce good images, due to an exponential tip–sample-distance dependence that results in a limiting thickness for STM.<sup>202</sup> Thus, Reinhoudt and co-workers employed AFM, which does not have such distance limitations. Initially, rows of self-assembled tetra-rosettes are found along three distinct orientations (differing by 60°), which is believed to be due to the underlying HOPG structure. Closer inspection reveals that there are two further domains of equal abundance that are orientated at 46° to the underlying HOPG structure. Further magnification reveals that the rows of the tetra-rosettes can be described by two mirror-image unit cells with areas of 10.6 nm<sup>2</sup> that correlate with the size of an individual tetra-rosette (Figure 106).

Thus, we see that the two enantiomers of the **184**<sub>3</sub>·(DEB)<sub>12</sub> supramolecular structure have spontaneously resolved to form



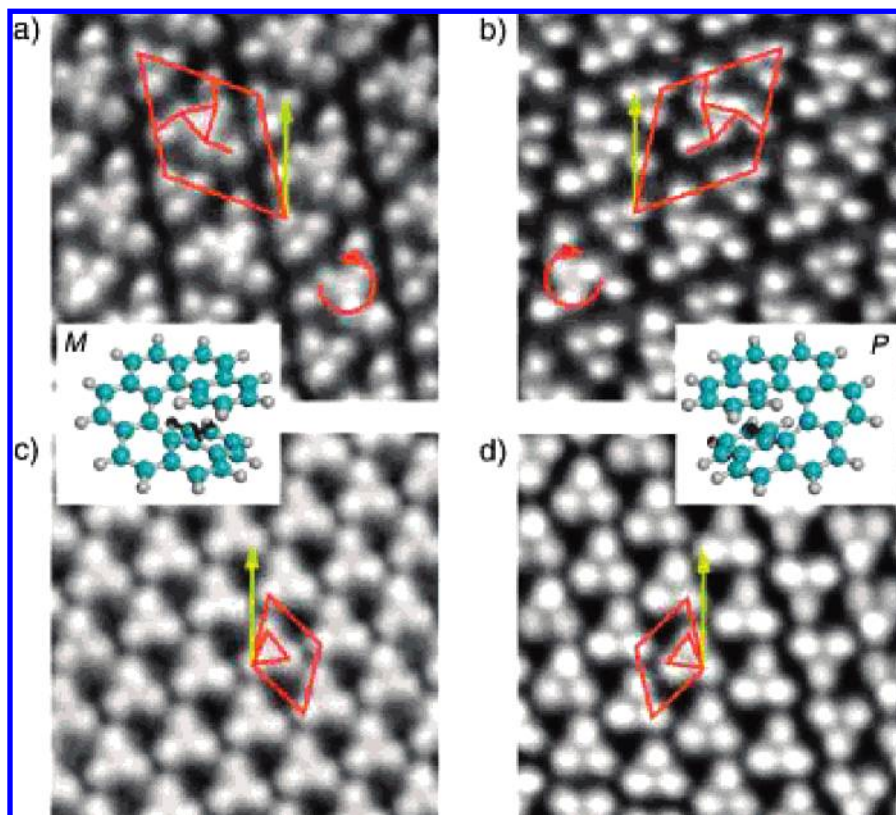


**Figure 104.** High-resolution STM images of (M)- and (P)-**183** structures (10 nm  $\times$  10 nm): (a) (M)-**183** at  $q = 0.95$ , (b) (P)-**183** at  $q = 0.95$ , (c) (M)-**183** at  $q = 1$ , and (d) (P)-**183** at  $q = 1$ . Reprinted with permission from Fasel, R.; Parschau, M.; Ernst, K.-H. *Angew. Chem., Int. Ed.* **2003**, *42*, 5178. Copyright 2003 Wiley-VCH Verlag GmbH & Co.

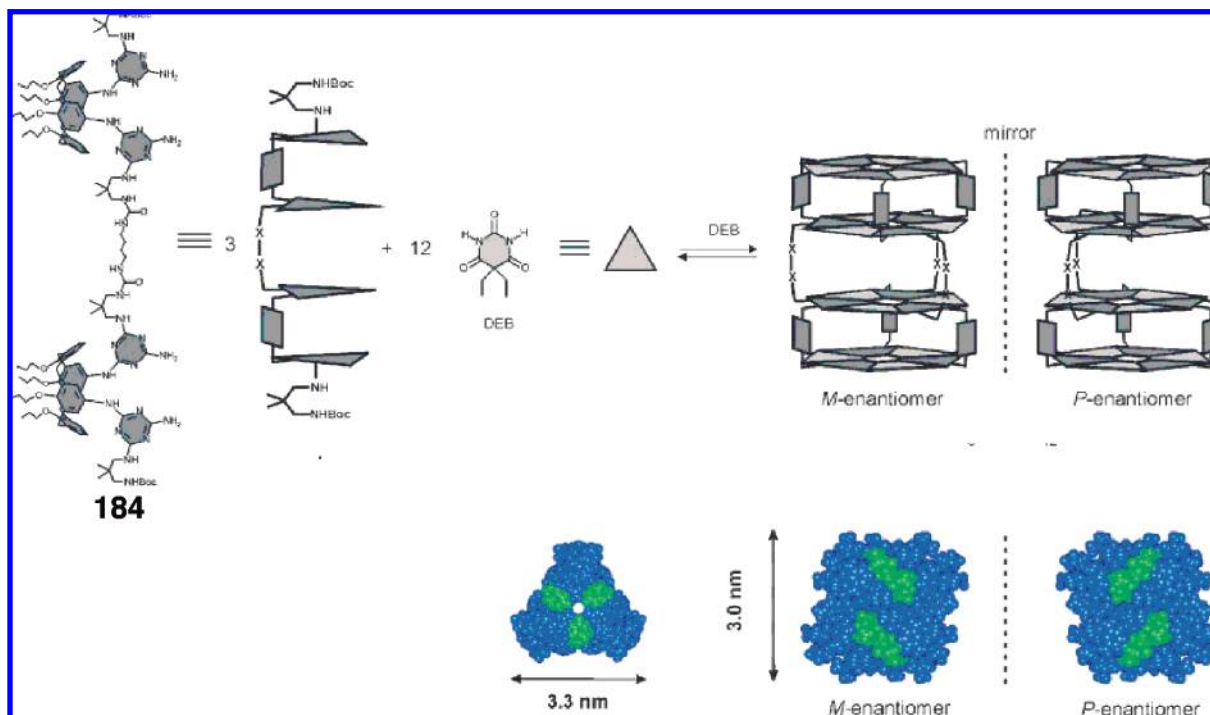


**Figure 105.** Tetraosette  $184_3 \cdot (\text{DEB})_{12}$ : structure (top, left) and schematic structure of both enantiomers (top, right), gas-phase minimized structure in top view (bottom, middle), and side-view structure of both enantiomers (bottom, right) including typical dimensions. Blue color denotes dimelamine calix[4]arene derivatives, while green color denotes DEB. Reprinted in part with permission from Schönherr, H.; Crego-Calama, M.; Vancso, G. J.; Reinhoudt, D. N. *Adv. Mater.* **2004**, *16*, 1416. Copyright 2004 Wiley-VCH Verlag GmbH & Co.

separate enantiomeric domains of *P*- and *M*-helicity, although it was not possible to assign the chirality to the individual domains. Unlike the previous examples of chiral surfaces, the detailed effect of the HOPG surface and the nature of

the supramolecular chirality propagation across the surface were not discussed, presumably because of the more-complex interactions involved and the lower image resolution. Such resolution of racemic mixtures on surfaces is not an uncom-

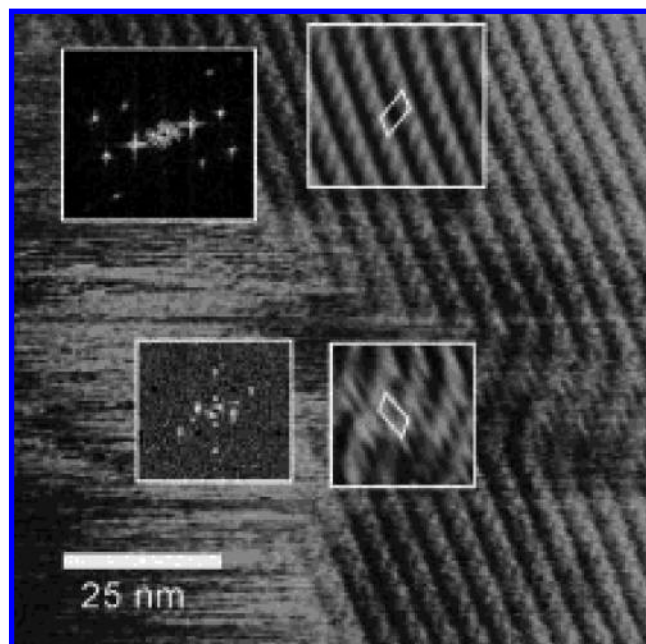


**Figure 106.** TM-AFM phase image of nanorod domains of tetraosettes **184**<sub>3</sub>·(DEB)<sub>12</sub> on HOPG (insets: 2D FFTs, left; Fourier-filtered sections, right). The unit cell of the structure observed is indicated in the corresponding Fourier-filtered sections. Reprinted with permission from Schönherr, H.; Crego-Calama, M.; Vancso, G. J.; Reinhoudt, D. N. *Adv. Mater.* **2004**, *16*, 1416. Copyright 2004 Wiley-VCH Verlag GmbH & Co.

mon phenomenon, but it may prove to be a powerful approach for the understanding and application of such complex chiral species.

## 9. Chirality in Supramolecular Polymeric Assemblies

The concept of “supramolecular polymers” is that a series of monomer molecules self-assemble under the control of intermolecular interactions in a divergent manner to produce a one-dimensional polymer. These are attractive species as their chirality, composition, and structure can be controlled by various internal (interaction strength and steric and electronic effects) and external (temperature, solvent, ligation, and pH) factors, which consequently allow a degree of rational design of their properties. Indeed, such structures have been shown to extend the properties of their supramolecular structure up to the mesoscopic level.<sup>203</sup> The work considered here investigates the nature of such assemblies and how chirality may be induced, amplified, switched, and memorized along with the mechanisms that underpin these effects.

The inspiration of nature and a desire to mimic it in the hope of further understanding biological systems and to exploit their elegant functions have long driven chemists. Drawing from the different controlling interactions that underpin the structure of DNA (interbase hydrogen bonding, base pair stacking, and the sugar–phosphate backbone), various researchers have looked to create helical self-assembling polymers that, crucially, are water-soluble. Such aqueous supramolecular structures are inherently troublesome to control in water because of the high degree of competition the water has for the hydrogen bonds that stabilize and transfer the (chiral) structural information throughout the supramolecule. Nevertheless, in recent years, a number of

groups have achieved this with chiral supramolecular systems that rationally, and elegantly, combine a number of different functional moieties to dictate structural integrity and the chiral nature of such supramolecular polymers.<sup>204</sup>

A leading group in this area is that of Meijer, who have formulated a general strategy to these ends. The approach utilizes individual monomer units that comprise three distinct moieties: (1) hydrogen-bonding groups that form the internal “base pair”, (2) an aromatic core that gives further structural integrity and promotes the vertical stacking of the monomers in water, and (3) peripheral alkane or oxyethylene chains that give solubility in water (for the oxyethylene chains) and whose chiral substituents allow transmission and amplification of the chirality through the polymer via sensing of the chiral steric fields by adjacent monomers. The components of such systems<sup>8c,205</sup> are shown in Figure 107.

Initially, it was found that all the compounds exist as monomers in dimethylsulfoxide; however, in chloroform, the self-complementary association of the ureidotriazine 4-fold hydrogen-bonding moieties was observed. This leads to the formation of discrete dimers for monofunctional **185**, and to divergent supramolecular polymers for **186** and **187**, in which each ureidotriazine group interacts with two other molecules, one above and one below, thus forming a supramolecular polymer with columnar architecture.

Studies of the chiral bifunctional compound **186b** in dodecane showed that it was CD active with the maxima of the Cotton effects correlating with the maxima in the UV–vis spectra, thus revealing that the chirality at the periphery has been transferred to a helical arrangement of the core aromatic chromophores with a preferred handedness. This is emphasized by the lack of a CD signal in the aromatic region of the spectrum for chiral **185b** that only forms discrete dimers. Such columnar arrangements were further proved by small-angle neutron scattering experiments, which gave a column radius of  $17 \pm 1$  Å for the achiral **186a**. A high stability was observed with only a 2-fold decrease in CD intensity found on reducing the concentration from  $10^{-3}$  to  $10^{-6}$  M. The helicity was lost on heating the sample, with the CD intensity almost entirely quenched over the 60–80 °C range; this is a fully reversible process (upon subsequent cooling) that shows that the denaturation is a cooperative process. The helicity was also dramatically reduced (by a factor of 10) on addition of quite small amounts of chloroform (2.6%), as this solvent effectively interacts with the chromophores and is, thus, in competition with the vertical chromophore stacking.

Compounds **188** and **187b** are water-soluble because of their oxyethylene side chains. The UV–vis spectra of **187b** in hydrogen bond-breaking solvents such as methanol, acetone, and acetonitrile, in which it exists as a monomer, has a maximum at 288 nm; however, in chloroform, leading to dimer formation, the maximum is red-shifted to 292 nm because of the hydrogen bonding. Consequently, the maximum of 292 nm obtained in water for **187b** is thought to indicate that it is also in a hydrogen-bonding situation. Monitoring the corresponding CD spectra reveals that methanol, acetone and acetonitrile solutions are CD silent, which is expected as they exist only as the monomer. Critically, however, the chloroform solution of **187b**, which was previously shown to be participating in a hydrogen-bonding dimer, is also CD inactive. This is due to the aromatic groups not coherently stacking and the corresponding formation of a random-coil supramolecular polymer. In

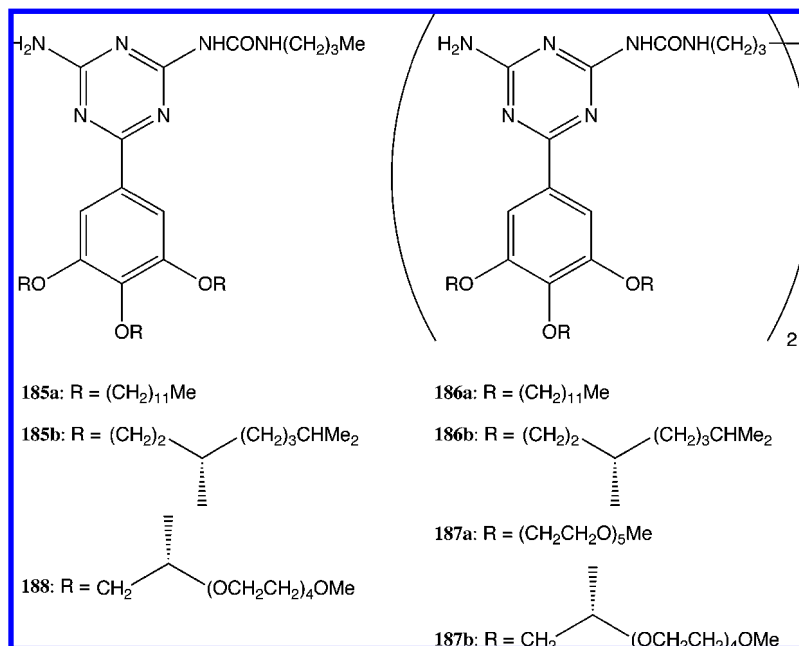
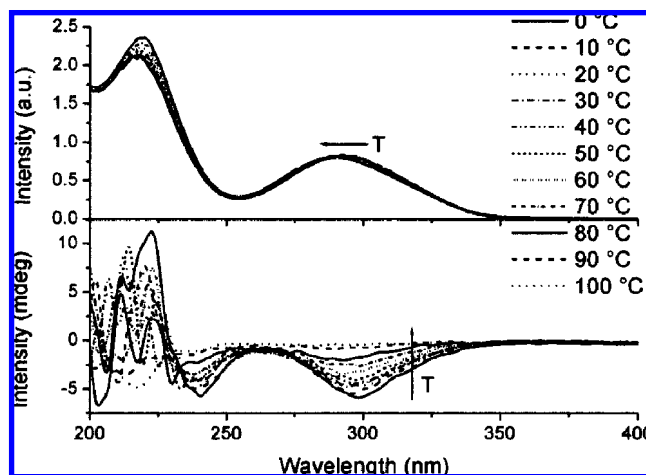


Figure 107. Structures of 185–188.



**Figure 108.** UV–vis (upper) and CD spectra (lower) of **187b** in water ( $2.4 \times 10^{-4}$  M) at different temperatures. Reprinted with permission from Brunsfeld, L.; Vekemans, J. A. J. M.; Hirschberg, J. H. K. K.; Sijbesma, R. P.; Meijer, E. W. *PNAS* **2002**, 99, 4977. Copyright 2002 the National Academy of Sciences.

water, however, a CD signal is observed at a wavelength corresponding to the UV–vis maximum. Thus, the formation of the supramolecular structure is ensured by the presence of a number of influencing structural features, the hydrogen-bonding dimerization, the hydrophobic protective core that also promotes the columnar stacking, the solvating peripheral groups, and the chiral substituents that propagate chirality through the structure.

Such chirality transfer arises from the structural adjustments made between adjacent molecules and so on throughout the polymer under the influence of the chiral steric field generated by the chiral substituents, which can be seen in the temperature dependence of the CD intensity (Figure 108). Here, we see that, on heating, the CD signal decreases in intensity until it has become zero at 90 °C, which arises from the increasing thermal motion of the helix that reduces the correlated nature of the intermolecular chiral interactions, thus decreasing the extended chiral order, eventually leading to disruption of the helix entirely at higher temperatures.

Awareness of this communication/sensing of the chirality between parts of a supramolecular structure leads to the concept of chirality amplification, that is, the induction of chirality in an achiral part of a system via chirality transfer from a “seed” chiral source molecule. Supramolecular assemblies are ideal environments for establishing and studying chiral amplification because of the potential for a convenient combination of chiral and achiral analogues within a single assembly. In the current system, such an effect is observed.

Initially, Meijer and co-workers attempted to observe chirality amplification by conducting “soldiers-and-sergeants” experiments of the type pioneered by Green et al.,<sup>206</sup> in which the changes in CD intensity are measured for a series of constant concentration solutions of **187a** and **187b**, with an increasing percentage of chiral “sergeant” molecules (**187b**). Thus, if a chiral amplification mechanism is active, a nonlinear increase of the CD intensity is expected. However, in this case, it was found that the solution’s chirality increased in a linear manner with increasing **187b** percentage concentration, showing that no chiral amplification takes place; this is believed to be due to the differing solubilities resulting in the formation of separate aggregates. Contrastingly, for an analogue of achiral **187a** and the chiral **188**, a highly nonlinear response was observed (Figure 109).

Initially, the concentrations were maintained at  $10^{-4}$  M in water; this resulted in shifting of the UV–vis maxima to 292 nm, showing hydrogen bonding, but with a silent CD spectrum because the interacting dimers are not yet aggregating. However, on raising the concentration to  $5 \times 10^{-3}$  M at 5 °C, Cotton effects appeared, which showed the aforementioned nonlinear dependence on the sergeant concentration. This demonstrates that the chirality from the enantiopure molecules transfers its asymmetry via noncovalent interactions to its neighbors, who then subsequently transmit their induced chirality to their neighbor, and so on.

A question of fundamental importance has, however, not been addressed in the discussed work. This is, what is the efficiency of the chiral amplification, i.e., how many achiral molecules can be chirally influenced by a single chiral seed



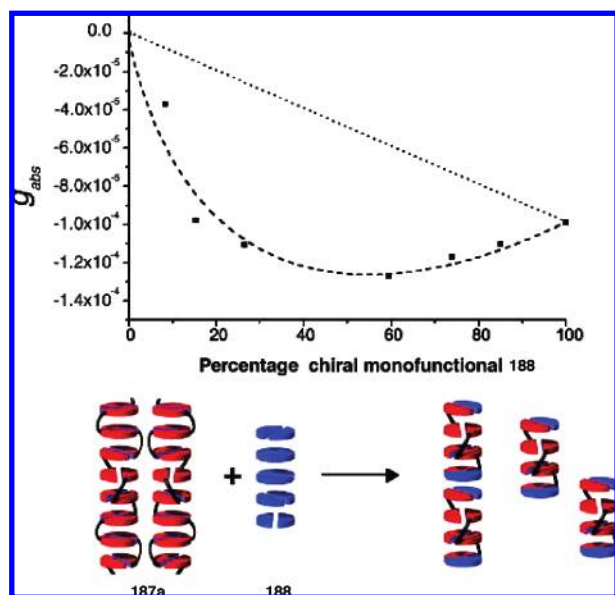


**Figure 109.** Dependence of the overall chirality on the mole fraction of chiral **188** in mixtures of **188** and achiral **187a** in water at 5 °C, expressed in terms of the  $g$  value and measured at the maximum of the Cotton effect at 287–293 nm (upper) and proposed mode of amplification of chirality (lower). Reprinted with permission from Brunsveld, L.; Vekemans, J. A. J. M.; Hirschberg, J. H. K. K.; Sijbesma, R. P.; Meijer, E. W. *PNAS* **2002**, 99, 4977. Copyright 2002 the National Academy of Sciences.

molecule? Meijer and co-workers found that, for  $C_3$ -core-based systems in nonaqueous solvents, the chirality imposed by one chiral molecule on subsequent achiral ones was 80 for an *N*-acylated 3,3'-diamino-2,2'-bipyridine system<sup>207</sup> and up to 200 for a benzene-1,3,5-tricarboxamide-based one.<sup>208</sup> They also noted that any aggregate not possessing directional secondary interactions with which to transfer asymmetry along the axis possessed considerably lower chirality amplification.<sup>209</sup>

In an extension of the previously discussed work, the determination of the chirality amplification efficiency of a supramolecular chiral helix in water was undertaken.<sup>210</sup> The covalent structure of the monomer is based on a  $C_3$  benzene-1,3,5-tricarboxamide and is designed in such a manner as to have the same elements previously used to direct the rational assembly of chiral supramolecular helices, i.e., hydrogen-bonding groups, an aromatic core to promote stacking, and peripheral oxyethylene units to ensure water solubility and to be the source of the chiral information (Figure 110).

When mixtures of **189** and **190** are dissolved in water, aggregation occurred over a period of 1.5 h as determined from the broad  $^1\text{H}$  NMR spectra, the red-shifted UV–vis spectra, and a strong luminescence, with the aggregation seen to be highly chiral from the accompanying Cotton effects in the CD spectra. When corresponding soldiers-and-sergeants experiments were undertaken at 5 °C, a nonlinear response of the  $g$  factor to the fraction of chiral **189** was seen, with the maximum chirality found at 25–30% of **189**. Using the Havinga model (which relates the binding constant to the length of assembly with the same helical pitch),<sup>207</sup> a cooperativity length (i.e., the number of achiral monomers influenced by a single chiral molecule) of 12 molecules was found, corresponding to an average of 200 monomers per helix. Interestingly, the maximum chirality for the pure chiral **189** helix is lower than those for helix mixtures with a fraction of **189** > ca. 10%; this effect is believed to be due

to more efficient packing of the achiral **190** monomers arising from the extra nine branching methyl groups in **189**, an effect also seen in polymers that show chirality transfer between achiral and chiral moieties,<sup>211</sup> showing the crucial and sensitive chirality sensing in such extended assemblies.

The soldiers-and-sergeants mechanism has been applied by the same group to create chiral supramolecular polymers that, via polymerization of appended peripheral sorbyl moieties, transfer the supramolecular helicity to the covalent polymer's backbone.<sup>212</sup> The achiral monomers are based on the benzene-1,3,5-tricarboxamide system seen above, and as a consequence of the cooperative hydrogen bonding, aromatic and van der Waals interactions form racemic columnar assemblies, with a triple-seam of hydrogen bonds along the axis of the assembly. On the addition of a small quantity of chiral sergeant molecules, chirality is induced into the structure in a nonlinear manner with a leveling-off at ~10% sergeant concentration (it is noted that antipodal sergeants produce opposite chirality). Then the sorbyl moieties undergo 1,4-polymerization as initiated by irradiation with  $\lambda = 365$  nm in the presence of 2,2-dimethoxyphenylacetophenone to produce a covalent backbone. It is found that after rigorous (postpolymerization) removal of the sergeant monomer (which has no sorbyl groups), the chirality of the, now, covalent polymer is retained.

However, the structure of the polymer was found to be disrupted by the addition of methanol, which competes for the hydrogen bonding, thus rendering the structure achiral. Remarkably, on removal of the methanol, the benzamide core of the polymer reassembles and the polymer regains its chiral structure with no loss of CD sign or intensity, which mimics a biological-like unfolding–refolding sequence, which was shown to be robust over a number of cycles (Figure 111).

Further investigation showed that the structure of the polymer is composed of a series of microstructures, an achiral zigzag part and a chiral helical part, where the chiral influence of the sergeant was transferred to the covalent backbone. The helical sections are then, to a degree, able to propagate their chirality along the column axis. This is a strong example of how the supramolecular approach and kinetic control can lead to the rational production of quite complex “conventional” materials whose structure and properties would be very difficult to obtain by other methods.

Another chirality-transfer controlling mechanism studied by this group is the “majority-rules” principle, which, again, was pioneered largely by Green and co-workers.<sup>213</sup> Thus, while the soldiers-and-sergeants principle is concerned with the influence of a small number of chiral groups over a large number of achiral ones, the majority-rules effect tries to rationalize the observation that, in a system whose basic units are all chiral, a small excess of one enantiomer leads to that species dominating the helical sense of the whole helical structure. Although observation and studies of this phenomenon have, almost exclusively, been within the field of polymers, Meijer and co-workers have recently published work where the majority-rules effect has been observed in a self-assembled helical polymer.<sup>214</sup> In this, they apply two enantiomeric  $C_3$ -symmetric molecules, similar to those seen previously but with alkyl peripheral groups, to give good solubility in nonpolar solvents, (*S*)-**191** and (*R*)-**192** (Figure 110).

CD spectra of individual enantiomers showed perfect mirror images, with a  $\Delta\epsilon$  maximum for the bipyridine at 387 nm and values of  $-33.9$  and  $32.6 \text{ cm}^{-1} \text{ M}^{-1}$  for (*S*)-



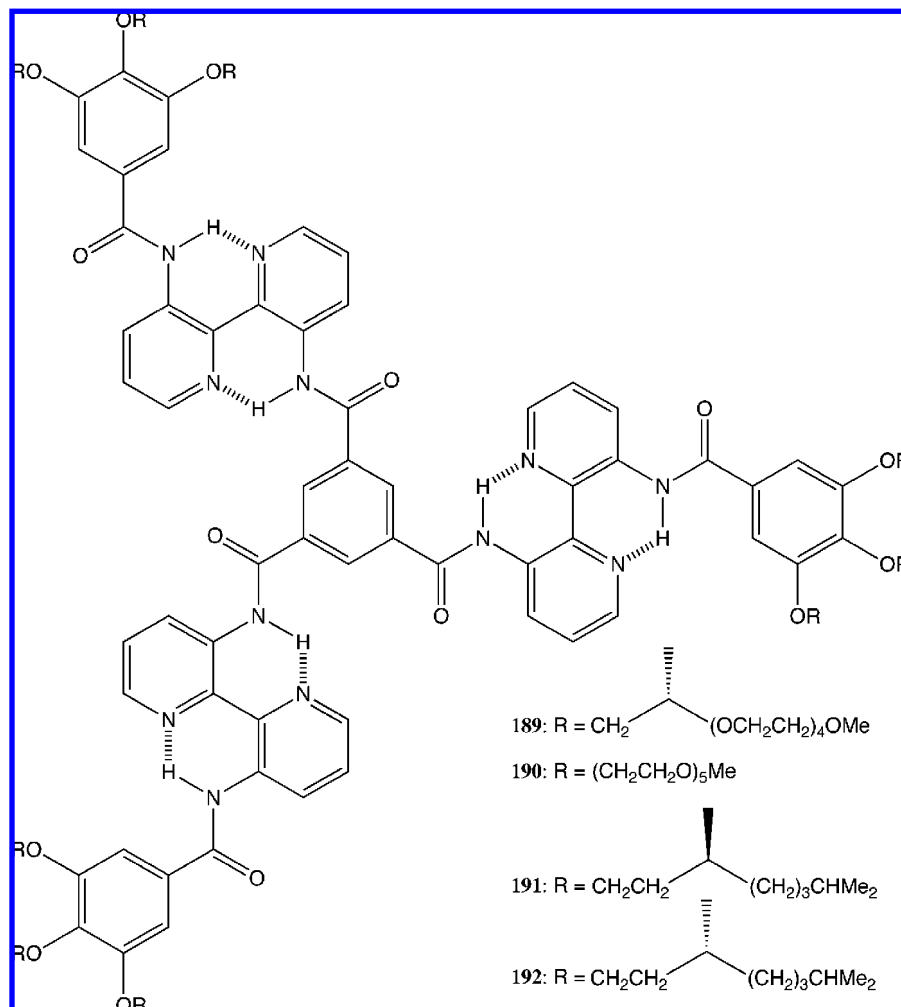


**Figure 110.** Structures of **189–192**.

**191** and (*R*)-**192**, respectively. Via monitoring at this wavelength, the *g* factor was measured at different enantiomeric excesses (0–100%), the results of which can be seen in Figure 112.

It is suggested that this dramatic nonlinearity confirms the presence of a majority-rules chirality-control mechanism, where the majority enantiomer has a greater chirality influence on the whole structure than would be expected on its percentage composition (it is additionally noted that the zero points of the *g* factor and ee are coincident).

To rationalize why, on the addition of (for example) a (*R*)-monomer into the helical structure dominated by the (*S*)-monomers, this adopts (presumably) its nonpreferred screw-sense rather than causes local helical inversion, a theoretical model developed by van Gestel<sup>215</sup> was applied. The results indicate that the free energy penalty for a monomer adopting its nonpreferred screw-sense is 0.94 kJ mol<sup>−1</sup> compared to helix reversal that amounts to 7.8 kJ mol<sup>−1</sup>. This 8× increase in the energy penalty for helix inversion gives a strong indication as to the origin of the majority-rules effect and is likely to be a factor that should be considered in related systems.

Clearly, in the cases where the monomer solution from which a supramolecular polymer is formed is not homochiral, the formation of a heteropolymer (as seen above) is not the only structural possibility. This issue has been addressed by Ishida and Aida, where they use a comparison of experimental and theoretical predictions of UV–vis and CD

responses to size-exclusion chromatography (SEC) traces to determine whether mixtures of xylene-bridged bis(cyclic dipeptides) (**193**) (Figure 113) result in homochiral or heterochiral supramolecular polymeric assemblies and how this translates into optical purity and molecular weight distribution.<sup>216</sup>

The SEC profile of *L*-**193** at 25 mM shows a typical monodisperse chromatographic profile with a broad tail, indicating a supramolecular polymer; accordingly, this is concentration dependent with the corresponding 0.5 mM *L*-**193** solution showing a sharper peak corresponding to a narrower range of lower-molecular-weight polymers. The formation of this supramolecular species is through the four hydrogen bonds that each molecule makes with its neighbors, as observed by the highly downfield-shifted amide protons at  $\delta = 9.8$  ppm in the <sup>1</sup>H NMR spectra, which can be seen to be broken by the addition of trifluoroacetic acid, resulting in the corresponding upfield shifts of the amide protons. This interaction mode is also seen in the X-ray structure of the analogous structure.

Using a theoretical prediction by Flory,<sup>217</sup> they consider three possible polymer compositions and their associated UV–vis and CD responses for a *D*-**193** enriched mixture; see Figure 114. Thus, Figure 114a shows a nonstereoselective polymerization, in which the UV–vis absorption is independent of the *L/D* concentrations, and the CD spectra solely reflect the enantiomeric purity. In the homochiral case (Figure 114b), the UV–vis is bimodal, with the split arising from

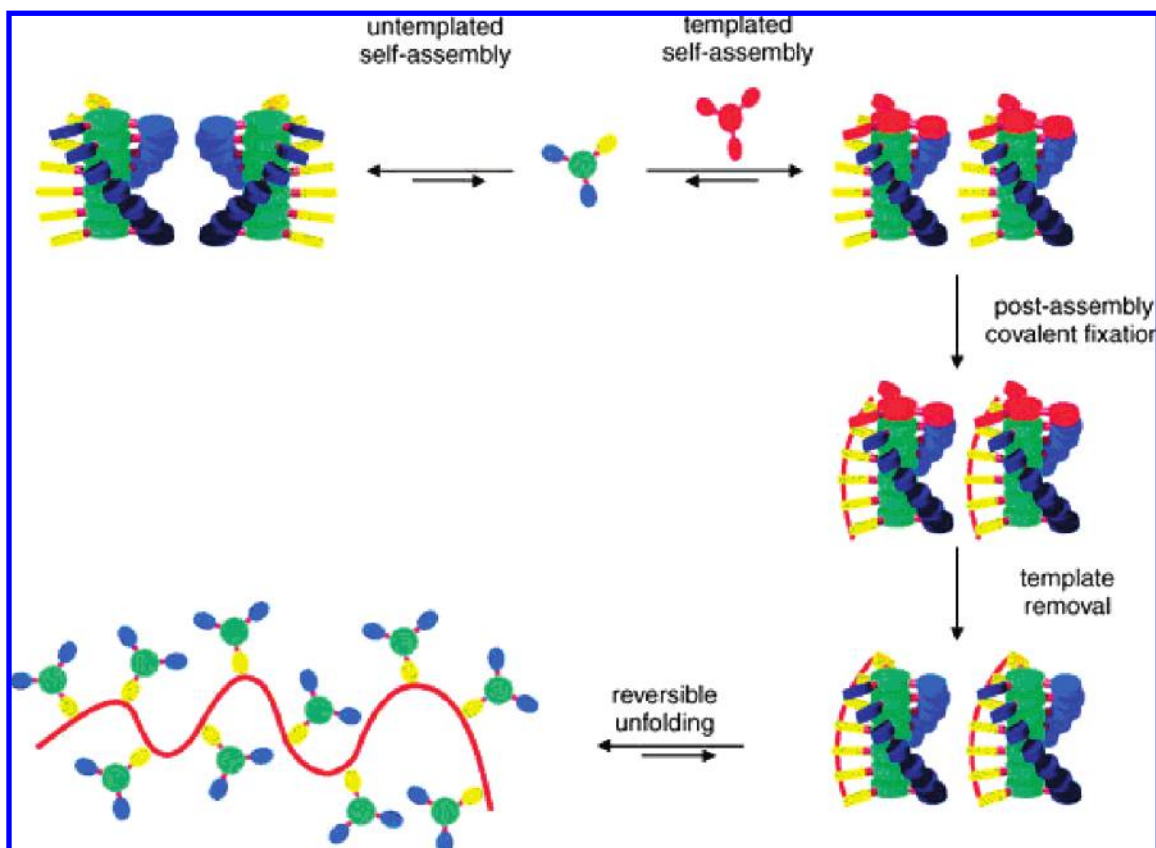


**Figure 111.** Sequence of events leading to locking of supramolecular chirality into columnar self-assemblies. Reprinted with permission from Wilson, A. J.; Masuda, M.; Sijbesma, R. P.; Meijer, E. W. *Angew. Chem., Int. Ed.* **2005**, *44*, 2275. Copyright 2005 Wiley-VCH Verlag GmbH & Co.

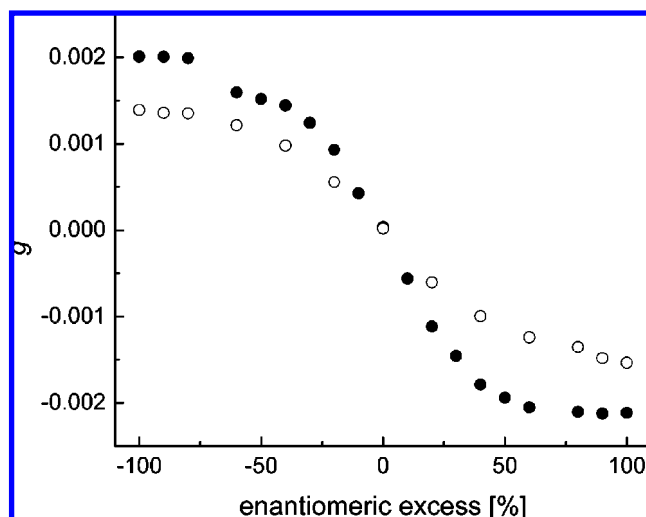


**Figure 112.** Anisotropy factor  $g$  as a function of the enantiomeric excess for mixtures of (*S*)-**191** and (*R*)-**192** at 20 °C (closed circles) and 50 °C (open circles). Reprinted with permission from van Gestel, J.; Palmans, A. R. A.; Titulaer, B.; Vekemans, J. A. J. M.; Meijer, E. W. *J. Am. Chem. Soc.* **2005**, *127*, 5490. Copyright 2005 American Chemical Society.

the higher concentration of lower-molecular-weight species due to homochiral polymer formation. The CD is expected to be truncated, with the absence of a signal from the low-molecular-weight region due to the cancelling effect of the smaller poly-L and poly-D species. In a heterochiral regime (Figure 114c), there is an excess of D-monomer, resulting in a peak at the low-molecular-weight region of the UV-vis spectra, and an absence of signal in the CD spectra for

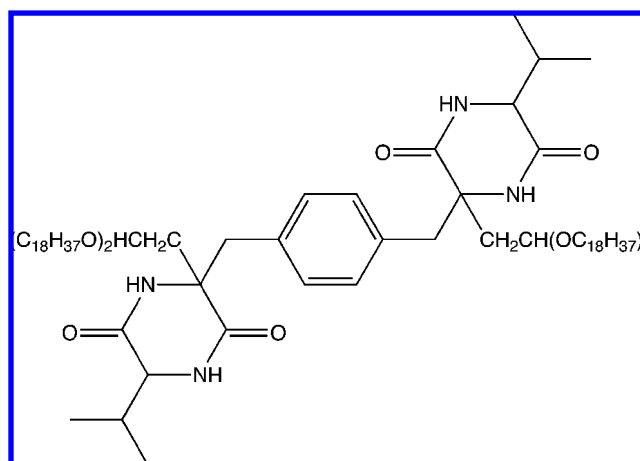


**Figure 113.** Structure of **193**.

the higher-molecular-weight region due to the cancelling effect of the equimolar amounts of poly-L and poly-D, with only the CD intensity for the monomers observed. When the SEC UV-vis and CD responses for 25 mM constant concentration solutions (varying between 100% L-**193** and 100% D-**193**) were examined, it became clear that, for this system, the homochiral (Figure 114b) supramolecular polymer formation regime is dominant, with clearly bimodal UV-vis spectra and truncated CD spectra, for the cases where there was an excess of one enantiomer. Thus, in a manner contradictory to that seen above for the “majority-rules” case of inclusion of antipodal monomers into a “largely” homochiral association, here the intermolecular sensing of the chirality between homo- and heterochiral

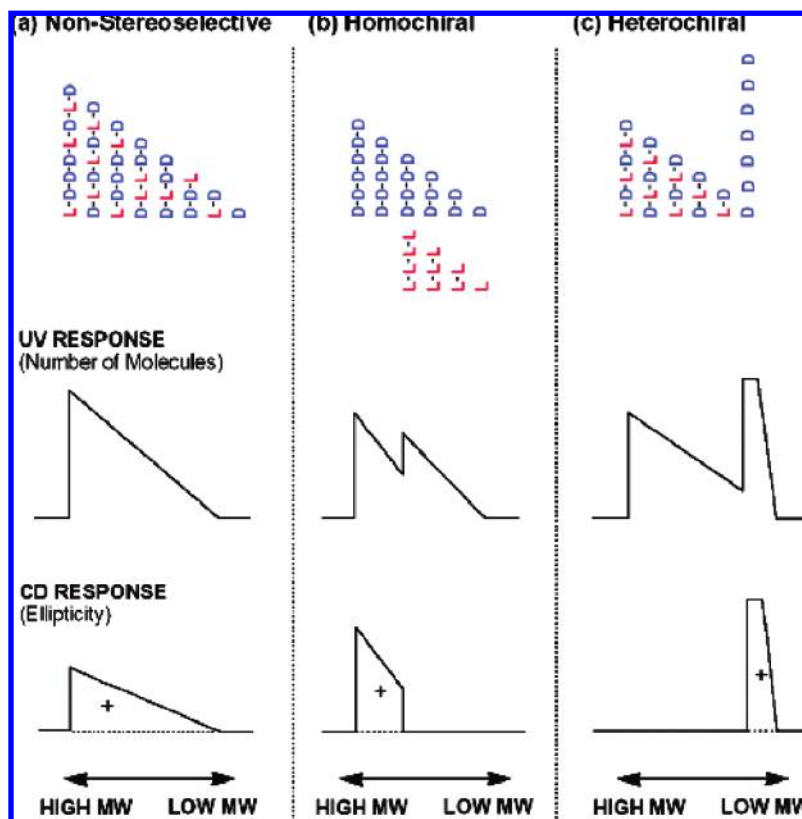


**Figure 114.** Schematic representation of SEC profiles of an enantiomerically unbalanced (D-enriched) monomer, as expected for (a) nonstereoselective, (b) homochiral, and (c) heterochiral polymerizations. Reprinted with permission from Ishida, Y.; Aida, T. *J. Am. Chem. Soc.* **2002**, *124*, 14017. Copyright 2002 American Chemical Society.

species, and the associated binding free energies, results in homopolymer formation; as a result, it was possible to separate and obtain enantiopure poly L-**193** and poly D-**193** species by the SEC method.

## 10. Chirality Sensing and Control in Polymeric Assemblies

The proceeding section considers the nature of the chirality induction based on polymers whose monomer units are covalently linked to form the backbone moiety. Although not all of these systems are strictly supramolecular, the underlying mechanisms that give rise to the chirality induction and control are noncovalent in nature, and because of the extended polymers' dynamic nature, these systems can be viewed to act with very supramolecular-like characters and offer approaches that can give further insights into how chirality is sensed by such molecular systems.

The group of Okamoto and Yashima first reported the application of supramolecular principles to chirality induction in polymeric species over a decade ago and have subsequently extended the classes of polymers used and developed a thorough understanding of their functioning.<sup>7c,186,218</sup> In this, external chiral guests interact with an achiral polymer, resulting in chirality transfer and subsequent enantioselective (*P*- or *M*-) helicity induction (Figure 115). This sequence is the foundation of the system previously discussed relating to the supramolecular-memory phenomenon (see section 7).<sup>4c,7c</sup>

Prior to this, optically active and chirally functioning polymers were mainly produced by conventional synthetic methods requiring chiral monomers and/or chiral catalysts.

Thus, the advantages of such a supramolecular approach are its adaptability without the need for derivatization and the potential for a high chirogenic efficiency (in the cases of chiral amplification).

The supramolecular polymers of the Okamoto and Yashima group, aside from their aforementioned memory properties, have been also applied as chirality sensors that can be tailored to the ligand of interest through choosing complementary pendant functional groups to match those of the ligands; specifically, **194** for acids, **195** for sugars, **196** and **197** for amines, and **198** for ammonium.<sup>219</sup>

Another active group in this field is that of Moore and co-workers, studying a number of factors that control the chiral structure of polymers that have their origin in noncovalent interactions.<sup>10a,220</sup> To this end, they have predominantly utilized a series of amphiphilic *m*-phenylene-ethynylene oligomers, which can be classified into two similar but critically different classes; see Figure 116. These are (1) the molecules of group **199**, where the aliphatic chiral side chains are the apolar moiety compared to the aromatic backbone and the polymer is soluble in lipophilic solvents, and (2) group **200**, where the relative polarity is inverted by the presence of polar chiral side chains and dissolution requires a polar solvent.

From studies of **200**, it was found that, in chloroform, the polymers were present in random conformations (i.e., no backbone helicity); however, in acetonitrile, helices were formed, as determined for the ratio of the backbone UV-vis absorbance bands at 287 and 303 nm (a higher  $A_{303}/A_{287}$  ratio indicates a greater degree of helicity). It is also necessary for the polymer to be long enough to fold back upon itself. As such, no helices were found for any polymer

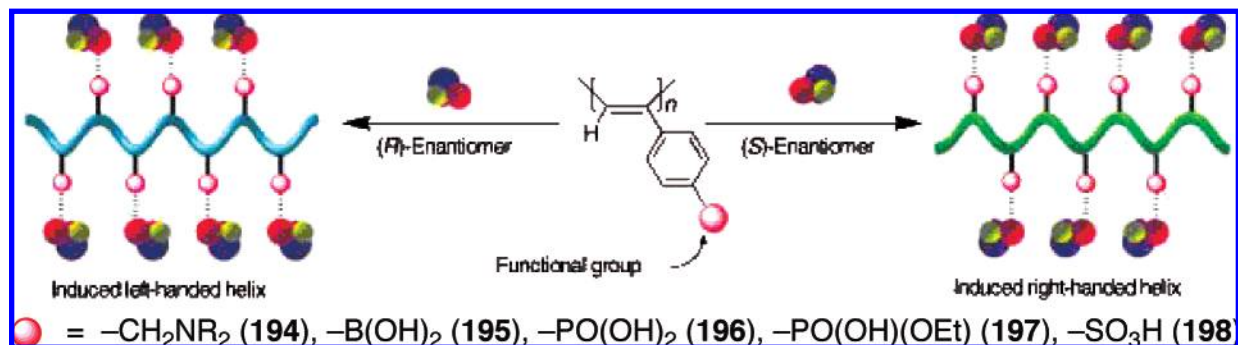


**Figure 115.** Schematic illustration of the formation of a one-handed helical structure of achiral poly(phenylacetylene)s (**194**–**198**) upon complexation with chiral compounds. Reprinted in part with permission from Morino, K.; Watase, N.; Maeda, K.; Yashima, E. *Chem. – Eur. J.* **2004**, *10*, 4703. Copyright 2004 Wiley-VCH Verlag GmbH & Co.

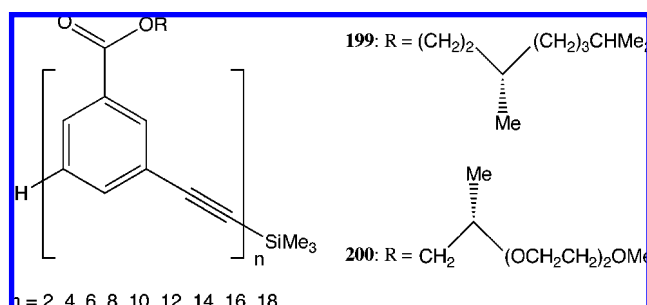


**Figure 116.** Structures of **199** and **200**.

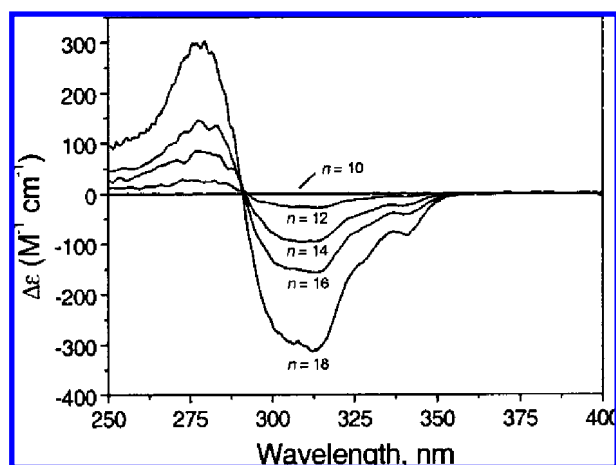


**Figure 117.** CD spectra of **199** ( $n = 10$ – $18$ ) in heptane at  $20\text{ }^{\circ}\text{C}$ . Reprinted with permission from Brunsveld, L.; Prince, R. B.; Meijer, E. W.; Moore, J. S. *Org. Lett.* **2000**, *2*, 1525. Copyright 2000 American Chemical Society.

with  $n < 10$ ; correspondingly, all species with  $n < 10$  were found to be achiral.<sup>10a</sup>

For compounds **199**, it was also found that, in chloroform, the relative intensities of the 287 and 303 nm bands showed no presence of helicity regardless of polymer length; this is believed to be because chloroform is a good solvent for all the parts of the polymer and does not facilitate any intramolecular ordering.<sup>220</sup> However, in heptane, while the  $n = 8$  and  $10$  species also show no helix formation, the sharply reduced 303 nm band for  $n = 12$ – $18$  reveals helix formation that increases in magnitude for the longer polymers. CD measurements of **199** in chloroform showed no signals in the backbone region, as expected from a random-coil conformation. This is in contrast to the CD spectra in heptane; see Figure 117. Here, we can see that, for polymers with  $n > 10$ , a clear negative bisignate couplet is evident.

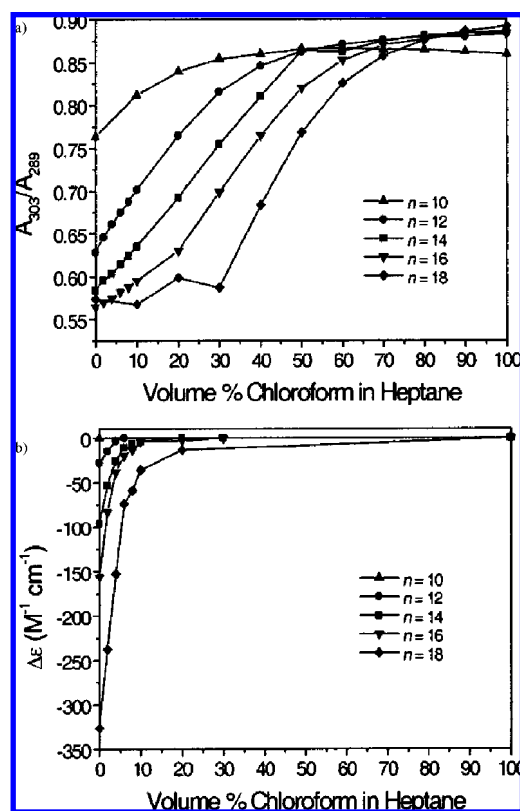


**Figure 118.** Plot of UV absorbance ratio ( $A_{303}/A_{289}$ ) (a) and CD signal at  $316\text{ nm}$  (b) for **199** ( $n = 10$ – $18$ ) vs the volume % chloroform in heptane. Reprinted with permission from Brunsveld, L.; Prince, R. B.; Meijer, E. W.; Moore, J. S. *Org. Lett.* **2000**, *2*, 1525. Copyright 2000 American Chemical Society.

The CD signal increases in magnitude with polymer length, which correlates with the onset of, and degree of, helicity in the backbone. So we may state that, for these systems, backbone order is necessary before chirality transfer can occur.

To further understand the mechanistic relationship between the chirality induction and the helix structure, CD measurements were made to see how the magnitude of chirality is related to the degree of helicity. In these, the composition of the solvent was systematically varied between 100% heptane (helix promoting) and 100% chloroform (helix precluding); see Figure 118.

From Figure 118a, we can see that helicity is entirely lost in 50–70% chloroform; however, Figure 118b shows that the polymer's backbone chirality is almost entirely quenched by 10% chloroform, or conversely, that there is a rapid



growth of chirality at high heptane ratios. Closer examination of the spectra for  $n = 16$  and 18 shows that the changes are sigmoidal. These observations reveal that the chiral intermolecular interactions between chiral centers and the backbone are of a cooperative nature. The same scenario was also observed for **200** in acetonitrile/chloroform mixed solvents, though with a longer persistence of chirality, believed to be due to the slower change in bulk solvent polarity due to the use of acetonitrile compared to heptane.

It is noted that the onset of chirality transfer for **199** and **200** occurs at different polymer lengths, i.e., at  $n > 10$  for **199** and at  $n > 8$  for **200**, which is likely to be due to the different distances that the chiral center is from the backbone, 4 bonds and 3 bonds for **199** and **200**, respectively. Thus, it can be surmised that the cooperative chiral steric field exerted by the chiral center, and its subsequent cooperative propagation along the backbone, is greater for the closer chiral center–backbone distance in **200**.

Additional insights and advances of the theory of how noncovalent interactions dictate the chirality in polymers have been achieved by the work of Fujiki and co-workers. From the study of the chiral properties of a series of polysilylene aggregates,<sup>221</sup> it was found that these underwent helical sense inversions that were dependent upon the composition of the included chiral monomer. As seen previously, the induction and propagation of chirality in achiral (supramolecular) polymers by chiral monomers has been explained using the sergeants-and-soldiers concept, with the associated Ising model predicting the extent of chiral order of a copolymer as a function of the enantiomer concentration.<sup>222</sup> However, in the cases of the random copolymers studied by Fujiki, this model was not sufficient to predict the experimental outcome. This was considered to arise from the fact that, in the polymers previously explained by the Ising model, the chiral centers of the side chains were close to the backbone and interacted directly with it, while, on the other hand, if the chiral centers were distant from the backbone, then they predominantly interact with neighboring side chains that then propagated the chirality. To take this into account,<sup>223</sup> the following basic change to an assumption made in the Ising model was suggested, i.e., that the interaction energies between chiral–chiral and chiral–achiral side-chain pairs are different (which were previously considered identical); the result of this can be seen in Figure 119.

From Figure 119, we can see that the modified Ising model predicts well the experimental outcome for both **201** (chiral center near the backbone) and **202** (chiral center distant from the backbone). Critically, however, the modified model correctly predicts the inversion of the screw sense in **202**, which the conventional Ising model does not. This result highlights the subtle differences in the noncovalent interactions between chiral, achiral, and induced-chiral species, as well as how the combination can lead to dramatic changes in the extended structure.

In a manner similar to that seen for chirality induction in supramolecular helices, Fujiki and co-workers have also exploited the supramolecular interactions between an achiral poly(*n*-hexyl-*p*-*n*-propoxyphenylsilylene) polymer host **203** (Figure 120) and chiral external ligands to understand and exploit the resulting induced chirality.<sup>224</sup>

In this system, it is found that, on interaction with chiral ligands bearing an alcohol group, a specific helicity is generated (*P* or *M*) and a bisignate induced CD signal is observed, which depends upon the structure of the ligand

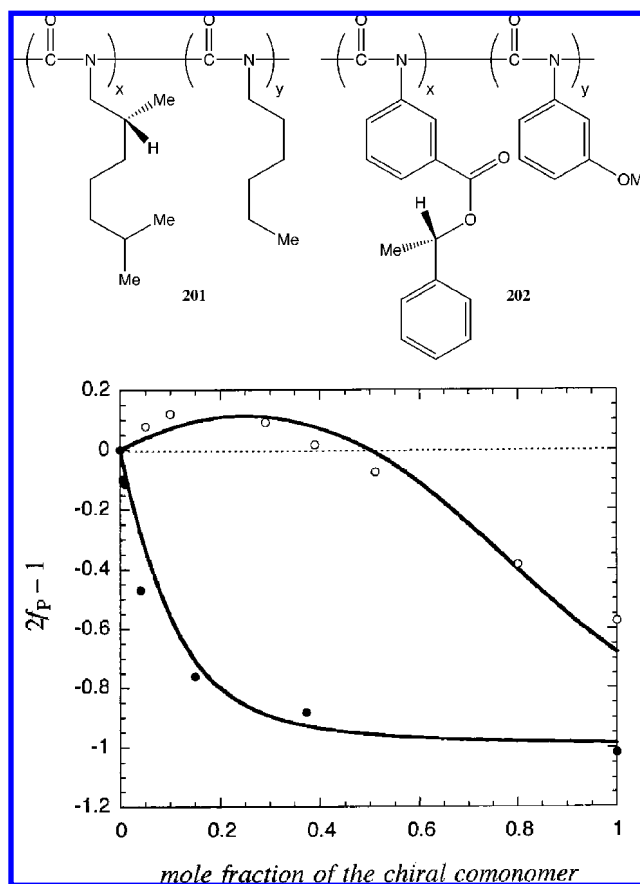


**Figure 119.** Structures of **201** and **202** and composition dependence of the enantiomer excess  $2f_P - 1$  of the P state of **201** in 20 °C chloroform (closed circles) and **202** in 25 °C THF (open circles); the solid curves calculated by the modified Ising model theory. Reprinted in part with permission from Sato, T.; Terao, K.; Teramoto, A.; Fujiki, M. *Macromolecules* **2002**, *35*, 5355. Copyright 2002 American Chemical Society.

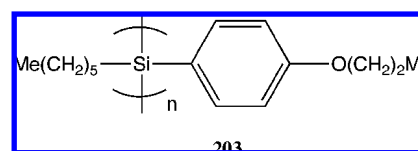


**Figure 120.** Structure of **203**.

(see Figure 121). These observations are believed to arise from weak hydrogen bonding between the alcohol of the ligand and the ether of the polymer and subsequent chiral steric interactions, as shown by the absence of an induced CD signal for the analogous poly(*n*-hexyl-*p*-*n*-butylphenylsilylene) polymer, which does not possess an ether group and, thus, lacks an interaction site.

Interestingly, **203** was found to have a linear relationship between its induced CD intensity and the ee of the chiral 2-butanol. This is notable because, as we have seen previously, nonlinear responses of the induced CD to the ee values are often found arising from the majority-rules principle, deriving from cooperative interactions between the chiral side chains. The lack of such a nonlinear effect in the current system is attributed to the weaker intermolecular interaction present in this case. However, an advantage of this mechanism is that it allows the system to act as both a chirality sensor and an ee gauge. From the study of a range of chiral alcohols, it was found that the results can be grouped into two classes. (1) On monitoring the second Cotton effect,

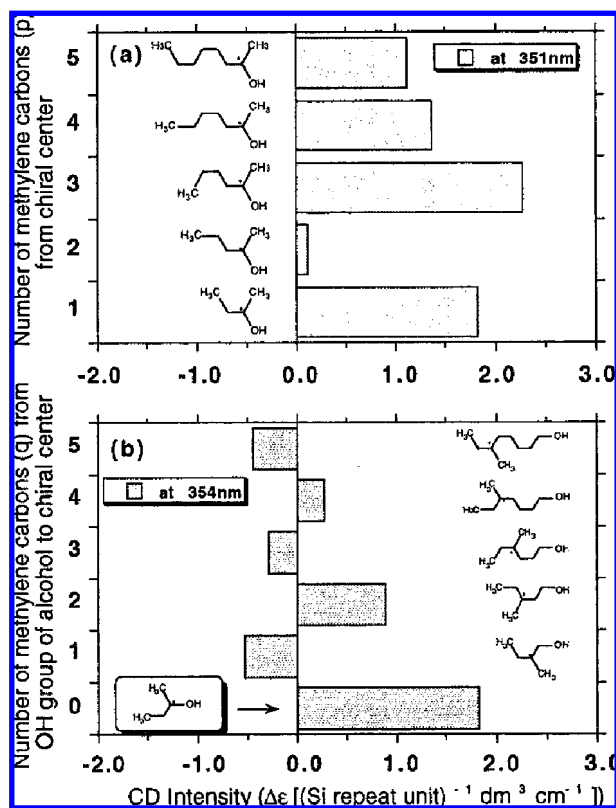


**Figure 121.** Plot of CD intensities of **203** aggregates in toluene/series of (*S*)-chiral alkyl alcohols ((a) secondary alcohols, (b) primary alcohols)/methanol mixtures at 20 °C. (For comparison, the induced CD intensity with (*S*)-2-BuOH is inserted in (b)). Reprinted with permission from Nakashima, H.; Koe, J. R.; Torimitsu, K.; Fujiki, M. *J. Am. Chem. Soc.* **2001**, *123*, 4847. Copyright 2001 American Chemical Society.

the induced chirality in secondary alcohols was found to consistently depend on the guest's absolute configuration, i.e., a positive second Cotton effect for (*S*)-enantiomers and a negative second Cotton effect for (*R*)-enantiomers (Figure 121a). (2) For primary alcohols with varying lengths of separation from the chiral center, the second Cotton effect was found to oscillate between positive for even numbers of carbons between the chiral center and the alcohol and negative for odd numbers of carbons (Figure 121b). Fujiki and co-workers stated that, from exciton theory and model studies, the inversion of the bisignate Cotton effects is due to the transition between *P*- and *M*- helices.

Clearly, there are different mechanisms operating in each case, which are believed to be similar to those previously discussed for the chirality phenomena in the **201/202** systems. The polymer helices in the secondary alcohol cases are determined by direct noncovalent interactions between the chiral center and the polymer backbone because of their close spatial proximity, while in the case of the primary alcohols, the more distant chiral centers are believed to interact with neighboring side chains, generating order that is then transferred to the backbone and propagated along its axis.

## 11. Conclusions

Chirality is one of the most fundamental issues of modern molecular science and is directly related to the functioning of living organisms and to many aspects of daily human life. Therefore, rationalizing the underpinning science of chirality induction, and the development of effective and versatile

chirality sensors, is an important task for research activities. This review demonstrates recent progress in this field with a particular emphasis on the advantages of a supramolecular approach to chirality induction and detection. There are many kinds of supramolecular systems, which are able to sense different types of chiral influences. However, despite the wide structural diversity of these assemblies and apparent attractiveness of this methodology, the detailed nature of the chirality-transfer mechanisms and the corresponding chiroptical properties of many of them have only been perfunctorily examined. Also, although supramolecular chemistry offers a unique tool for fine-tuning the chiroptical properties via various controlling factors, this opportunity has been scarcely developed. These are serious issues for designing optimal systems for chirality induction and detection, since the optical outcome of a system is directly related to the sensoric ability as a chiroptical probe. Therefore, further efforts in this field should be concentrated on closing these gaps, which should have an immediate positive impact not only in supramolecular chirality induction and sensing but also in related application areas, such as asymmetric synthesis and catalysis, medical science and pharmacology, and biomimetics and molecular devices, in which the chirogenic effects are to be exploited.

## 12. Note Added after ASAP Publication

This paper posted ASAP on December 21, 2007 with an error in reference 54. The correct version published on January 9, 2008.

## 13. References

- (1) (a) Saenger, W. *Principles of Nucleic Acid Structure*; Springer: New York, 1984. (b) Voet, D.; Voet, J.G. *Biochemistry*, 2nd ed.; John Wiley & Sons, Inc.: New York, Chichester, Brisbane, Toronto, Singapore, 1995. (c) Steed, J. W.; Atwood, J. L. *Supramolecular Chemistry*; John Wiley & Sons, Ltd.: Chichester, New York, Weinheim, Brisbane, Singapore, Toronto, 2000. (d) Kyte, J. *Structure in Protein Chemistry*; Garland Publishing, Inc.: New York, London, 1995. (e) Rodger, A.; Nordén, B. *Circular Dichroism and Linear Dichroism*; Oxford University Press: Oxford, New York, Tokyo, 1997. (f) Hsu, M.-C.; Woody, R. W. *J. Am. Chem. Soc.* **1971**, *93*, 3515. (g) Blauer, G.; Sreerama, N.; Woody, R. W. *Biochemistry* **1993**, *32*, 6674.
- (2) (a) Montanari, F.; Casella, L. *Metalloporphyrin Catalyzed Oxidations*; Kluwer: Dordrecht, The Netherlands, 1994. (b) Seo, J. S.; Whang, D.; Lee, H.; Jun, S. I.; Oh, J.; Jeon, Y. J.; Kim, K. *Nature* **2000**, *404*, 982. (c) Nimri, S.; Keinan, E. *J. Am. Chem. Soc.* **1999**, *121*, 8978.
- (3) (a) Verbiest, T.; van Elshocht, S.; Kauranen, M.; Hellemans, L.; Snauwaert, J.; Nuckolls, C.; Katz, T. J.; Persoons, A. *Science* **1998**, *282*, 913. (b) Lin, W.; Wang, Z.; Ma, L. *J. Am. Chem. Soc.* **1999**, *121*, 11249.
- (4) (a) Jha, S. K.; Cheon, K.-S.; Green, M. M.; Selinger, J. V. *J. Am. Chem. Soc.* **1999**, *121*, 1665. (b) Akagi, K.; Piao, G.; Kaneko, S.; Sakamaki, K.; Shirakawa, H.; Kyotani, M. *Science* **1998**, *282*, 1683. (c) Yashima, E.; Maeda, K.; Okamoto, Y. *Nature* **1999**, *399*, 449.
- (5) (a) Ogoshi, H.; Mizutani, T. *Acc. Chem. Res.* **1998**, *31*, 81. (b) James, T. D.; Sandanayake, K. R. A. S.; Shinkai, S. *Angew. Chem., Int. Ed. Engl.* **1996**, *35*, 1910. (c) Prins, L. J.; Huskens, J.; de Jong, F.; Timmerman, P.; Reinhoudt, D. N. *Nature* **1999**, *398*, 498. (d) Štíbor, I.; Zlatušková, P. *Top. Curr. Chem.* **2005**, *255*, 31. (e) Okamoto, Y.; Yashima, E.; Yamamoto, C. *Top. Stereochem.* **2003**, *24*, 157. (f) Kolp, B.; Viebrock, H.; von Zelewsky, A.; Abeln, D. *Inorg. Chem.* **2001**, *40*, 1196.
- (6) (a) Furusho, Y.; Kimura, T.; Mizuno, Y.; Aida, T. *J. Am. Chem. Soc.* **1997**, *119*, 5267. (b) Feringa, B. L.; van Delden, R. A.; Koumura, N.; Geertsema, E. M. *Chem. Rev.* **2000**, *100*, 1789. (c) Zahn, S.; Canary, J. W. *Science* **2000**, *288*, 1404.
- (7) (a) Baum, G.; Constable, E. C.; Fenske, D.; Housecroft, C. E.; Kulke, T. *Chem.—Eur. J.* **1999**, *5*, 1862. (b) Huang, X.; Rickman, B. H.; Borhan, B.; Berova, N.; Nakanishi, K. *J. Am. Chem. Soc.* **1998**, *120*,

6185. (c) Yashima, E.; Matsushima, T.; Okamoto, Y. *J. Am. Chem. Soc.* **1997**, *119*, 6345.
- (8) (a) Hauang, B.; Parquette, J. R. *J. Am. Chem. Soc.* **2001**, *123*, 2689. (b) Prins, L. J.; De Jong, F.; Timmerman, P.; Reinhoudt, D. N. *Nature* **2000**, *408*, 181. (c) Ky Hirschberg, J. H. K.; Brunsveld, L.; Ramzi, A.; Vekemans, J. A. J. M.; Sijbesma, R. P.; Meijer, E. W. *Nature* **2000**, *407*, 167. (d) Johnson, R. S.; Yamazaki, T.; Kovalenko, A.; Fenniri, H. *J. Am. Chem. Soc.* **2007**, *129*, 5735.
- (9) (a) Wu, C. W.; Sanborn, T. J.; Huang, K.; Zuckermann, R. N.; Barron, A. E. *J. Am. Chem. Soc.* **2001**, *123*, 6778. (b) Gin, M. S.; Moore, J. S. *Org. Lett.* **2000**, *2*, 135. (c) von Berlepsch, H.; Böttcher, C.; Ouart, A.; Burger, C.; Dähne, S.; Kirstein, S. *J. Phys. Chem. B* **2000**, *104*, 5255. (d) Moriuchi, T.; Nishiyama, M.; Yoshida, K.; Ishikawa, T.; Hirao, T. *Org. Lett.* **2001**, *3*, 1459. (e) Liu, D.; Williamson, D. A.; Kennedy, M. L.; Williams, T. D.; Morton, M. M.; Benson, D. R. *J. Am. Chem. Soc.* **1999**, *121*, 11798.
- (10) (a) Prince, R. B.; Brunsveld, L.; Meijer, E. W.; Moore, J. S. *Angew. Chem., Int. Ed.* **2000**, *39*, 228. (b) Wu, C. W.; Sanborn, T. J.; Huang, K.; Zuckermann, R. N.; Barron, A. E. *J. Am. Chem. Soc.* **2001**, *123*, 2958. (c) Nakamura, K.; Okubo, H.; Yamaguchi, M. *Org. Lett.* **2001**, *3*, 1097.
- (11) (a) Stephens, P. J.; McCann, D. M.; Stoncius, S.; Cheeseman, J. R.; Frisch, M. J. *J. Org. Chem.* **2002**, *69*, 1948. (b) Ruud, K.; Helgaker, T. *Chem. Phys. Lett.* **2004**, *352*, 533.
- (12) Herges, R.; Deichmann, M.; Wakita, T.; Okamoto, Y. *Angew. Chem., Int. Ed.* **2003**, *42*, 10, 1170.
- (13) (a) Green, M. M.; Cheon, K.-S.; Yang, S.-Y.; Park, J.-W.; Swansburg, S.; Lui, W. *Acc. Chem. Res.* **2001**, *34*, 672. (b) Yashima, E.; Maeda, K.; Nishimura, T. *Chem.—Eur. J.* **2004**, *10*, 42.
- (14) (a) Murguly, E.; McDonald, R.; Branda, N. R. *Org. Lett.* **2000**, *2*, 3169. (b) Reetz, M.; Sostmann, S. *Tetrahedron* **2001**, 2515. (c) Wood, T. E.; Thompson, A. *Chem. Rev.* **2007**, *107*, 1831.
- (15) (a) Nelson, J. C.; Saven, J. G.; Moore, J. S.; Wolynes, P. G. *Science* **1997**, *277*, 1793. (b) Yashima, E.; Maeda, K.; Nishimura, T. *Chem.—Eur. J.* **2004**, *10*, 42 and references therein.
- (16) Velders, H. A.; Hotze, A. C. G.; Haasnoot, J. G.; Reedijk, J. *Inorg. Chem.* **1999**, *38*, 2762.
- (17) Hese, D.; Hembury, G. A.; Drew, M. G. B.; Borovkov, V. V.; Inoue, Y. *J. Am. Chem. Soc.* **2001**, *123*, 12232.
- (18) Gawronski, J.; Grajewski, J. *Org. Lett.* **2003**, *5*, 3301.
- (19) Mislow, K. *Chirality* **2002**, *14*, 126.
- (20) Kajtar, M.; Horvath-Toro, C.; Kuthi, E.; Szejtli, J. *Acta Chim. Acad. Sci. Hung.* **1982**, *110*, 327.
- (21) Harada, N.; Nakanishi, K. *Circular Dichroism Spectroscopy—Exciton Coupling in Organic Stereochemistry*; University Science Books: Mill Valley, CA, 1983.
- (22) (a) Davydov, A. S. *Zhur. Ekspt. i Teoret. Fiz.* **1948**, *18*, 210. (b) Davydov, A. S. *Theory of Molecular Excitons*; Trans. Kasha, M., Oppenheimer, M., Jr., Eds.; McGraw-Hill: New York, 1962.
- (23) (a) Koreeda, M.; Harada, N.; Nakanishi, K. *J. Am. Chem. Soc.* **1974**, *96*, 266. (b) Harada, N.; Nakanishi, K. *Acc. Chem. Res.* **1972**, *5*, 257. (c) Berova, N.; Di Bari, L.; Pescitelli, G. *Chem. Soc. Rev.* **2007**, *37*, 914.
- (24) Yoshida, N.; Ishizuka, T.; Osuka, A.; Jeong, D. H.; Cho, H. S.; Kim, D.; Matsuzaki, Y.; Nogami, A.; Tanaka, K. *Chem.—Eur. J.* **2003**, *9*, 58.
- (25) Mason, S. F.; Seal, R. H.; Roberts, D. R. *Tetrahedron* **1974**, *30*, 1671.
- (26) Borovkov, V. V.; Hembury, G. A.; Inoue, Y. *Acc. Chem. Res.* **2004**, *37*, 449 and references therein.
- (27) (a) Borovkov, V. V.; Hembury, G. A.; Inoue, Y. *Angew. Chem., Int. Ed.* **2003**, *42*, 5310. (b) Steensgaard, D. B.; Wackerbarth, H.; Hildebrandt, P.; Holzwarth, A. R. *J. Phys. Chem. B* **2000**, *104*, 10379. (c) Iarossi, D.; Mucci, A.; Parenti, F.; Schenetti, L.; Seeber, R.; Zanardi, C.; Forni, A.; Tonelli, M. *Chem.—Eur. J.* **2001**, *7*, 676. (d) de Loos, M.; van Esch, J.; Kellogg, R. M.; Feringa, B. L. *Angew. Chem., Int. Ed.* **2001**, *40*, 613.
- (28) Matile, S.; Berova, N.; Nakanishi, K.; Fleischhauer, J.; Woody, R. W. *J. Am. Chem. Soc.* **1996**, *118*, 5198.
- (29) (a) Chen, S. L.; Harada, N.; Nakanishi, K. *J. Am. Chem. Soc.* **1974**, *96*, 7352. (b) Canceill, J.; Collet, A.; Jaques, J. *J. Chem. Soc., Perkin Trans. 2* **1982**, 83.
- (30) (a) Bobrovsky, A.; Shibaev, V.; Stumpe, J. *J. Phys. Chem. B* **2006**, *110*, 2331. (b) Geng, Y.; Trajkovska, A.; Culligan, S. W.; Ou, J. J.; Philip Chen, H. M.; Katsis, D.; Chen, S. H. *J. Am. Chem. Soc.* **2003**, *125*, 14032. (c) Iida, H.; Nakamura, A.; Inoue, Y.; Akagi, K. *Synth. Met.* **2003**, *135–136*, 91. (d) Bobrovsky, A.; Boiko, N. I.; Shibaev, V. P.; Wendorff, J. H. *Adv. Mater.* **2003**, *15*, 282.
- (31) (a) Nafie, L. A.; Dukor, R. K.; Freedman, T. B. In *Handbook of Vibrational Spectroscopy*; Chalmers, J. M., Griffiths, P. R., Eds.; John Wiley & Sons, Ltd.: Chichester, U.K., 2002; pp 731–744. (b) Monde, K.; Taniguchi, T.; Miura, N.; Nishimura, S.-I. *J. Am. Chem. Soc.* **2004**, *126*, 9496.
- (32) (a) Devlin, F. J.; Stephens, P. J.; Cheeseman, J. R.; Frisch, M. J. *J. Am. Chem. Soc.* **1996**, *118*, 6327. (b) Izumi, H.; Yamagami, S.; Futamura, S.; Nafie, L. A.; Dukor, R. K. *J. Am. Chem. Soc.* **2004**, *126*, 194.
- (33) (a) Devlin, F. J.; Stephens, P. J.; Besse, P. *Tetrahedron: Asymmetry* **2005**, *16*, 1557. (b) Stephens, P. J.; McCann, D. M.; Delvin, F. J.; Flood, T. C.; Butkus, E.; Stoncius, S.; Cheeseman, J. R. *J. Org. Chem.* **2005**, *70*, 3903. (c) Kuppens, T.; Langenaeker, W.; Tollenaere, J. P.; Bultinck, P. *J. Phys. Chem. A* **2003**, *107*, 542.
- (34) (a) Urbanova, M.; Pancoska, P.; Keiderling, T. A. *Biochim. Biophys. Acta* **1993**, *1203*, 290. (b) Pandya, A.; Tsankov, D.; Andrushchenko, V.; van de Sande, J. H.; Wieser, H. *Biopolymers* **2005**, *82*, 189. (c) Shanmugam, G.; Polavarapu, P. L.; Gopinath, D.; Jayakumar, R. *Peptide Sci.* **2005**, *80*, 636.
- (35) (a) Cappelli, C.; Corni, S.; Mennucci, B.; Cammi, R.; Tomasi, J. *J. Phys. Chem. A* **2002**, *106*, 12331. (b) Tarczay, G.; Magyarfalvi, G.; Vass, E. *Angew. Chem., Int. Ed.* **2006**, *45*, 1775.
- (36) (a) Petrovic, A. G.; Bose, P. K.; Polavarapu, P. L. *Carbohydr. Res.* **2004**, *339*, 2713. (b) Bose, P. K.; Polavarapu, P. L. *Carbohydr. Res.* **1999**, *322*, 135.
- (37) (a) Tsanov, D.; Krasteva, M.; Andrushchenko, V.; van de Sande, J. H.; Wieser, H. *Biophys. Chem.* **2006**, *119*, 1. (b) Buffeteau, T.; Ducasse, L.; Poniman, L.; Delsuc, N.; Huc, I. *Chem. Commun.* **2006**, 2714. (c) Wang, L. J.; Keiderling, T. A. *Biochemistry* **1992**, *31*, 10265. (d) Urbanova, M.; Setnicka, V.; Delvin, F. J.; Stephens, P. J. *J. Am. Chem. Soc.* **2005**, *127*, 6700. (e) Polyanchko, A.; Wieser, H. *Biopolymers* **2005**, *78*, 329.
- (38) (a) Stephens, P. J.; Devlin, F. J.; Cheeseman, J. R.; Frisch, M. J. *Org. Lett.* **2002**, *4*, 4595. (b) Polavarapu, P. L. *Angew. Chem., Int. Ed.* **2002**, *41*, 4544. (c) Furche, F.; Ahlrichs, R. *J. Am. Chem. Soc.* **2002**, *124*, 3804.
- (39) Borovkov, V. V.; Fujii, I.; Muranaka, A.; Hembury, G. A.; Tanaka, T.; Ceulemans, A.; Kobayashi, N.; Inoue, Y. *Angew. Chem., Int. Ed.* **2004**, *43*, 5481.
- (40) Furo, T.; Mori, T.; Wada, T.; Inoue, Y. *J. Am. Chem. Soc.* **2005**, *127*, 8242.
- (41) Mizutani, T.; Tagaki, H.; Hara, O.; Horiguchi, T.; Ogoshi, H. *Tetrahedron Lett.* **1997**, *38*, 1991.
- (42) Tagaki, H.; Mizutani, T.; Horiguchi, T.; Kitagawa, S.; Ogoshi, H. *Org. Biomol. Chem.* **2005**, *3*, 2091.
- (43) (a) Ilczyszyn, M.; Ratajczak, H. *J. Chem. Soc., Faraday Trans.* **1995**, *91*, 3859. (b) Mizutani, T.; Takagi, H.; Ueno, Y.; Horiguchi, T.; Yamamura, K.; Ogoshi, H. *J. Phys. Org. Chem.* **1998**, *11*, 737.
- (44) Davis, A. P.; Wareham, R. S. *Angew. Chem., Int. Ed.* **1999**, *38*, 2978.
- (45) (a) Feizi, T.; Mulloy, B. *Curr. Opin. Struct. Biol.* **2001**, *11*, 585. (b) Roseman, S. *J. Biol. Chem.* **2001**, *276*, 41527.
- (46) Bodenner, D. L.; Eastman, R. C. *Curr. Opin. Endocrinol. Diabetes* **1995**, *21*, 72.
- (47) (a) Lemieux, R. U. *Chem. Soc. Rev.* **1989**, *18*, 347. (b) Weis, W. I.; Drickhamer, K. *Annu. Rev. Biochem.* **1996**, *65*, 441.
- (48) (a) Mazik, M.; Bandmann, H.; Sicking, W. *Angew. Chem., Int. Ed.* **2000**, *39*, 551. (b) Benito, J. M.; Gómez-García, M.; Blanco, J. L. J.; Mellet, C. O.; Fernández, J. M. G. *J. Org. Chem.* **2001**, *66*, 1366. (c) Boner-Law, R. P.; Sanders, J. K. M. *J. Am. Chem. Soc.* **1995**, *117*, 259. (d) Anderson, S.; Neidlein, U.; Gramlich, V.; Diederich, F. *Angew. Chem., Int. Ed.* **1995**, *34*, 1596. (e) Das, G.; Hamilton, A. D. *J. Am. Chem. Soc.* **1994**, *116*, 11139.
- (49) Fang, J.-M.; Selvi, S.; Liao, J.-H.; Slanina, Z.; Chen, C.-T.; Chou, P.-T. *J. Am. Chem. Soc.* **2004**, *126*, 3559.
- (50) (a) Kondo, K.; Shiomi, Y.; Saisho, M.; Harada, T.; Shinkai, S. *Tetrahedron* **1992**, *48*, 8239. (b) Shiomi, Y.; Saisho, M.; Tsukagoshi, K.; Shinkai, S. *J. Chem. Soc., Perkin Trans. 1* **1993**, 2111. (c) Shinkai, S.; Takeuchi, M. *Trends Anal. Chem.* **1996**, *15*, 188.
- (51) Superchi, S.; Donnoli, M. I.; Rosini, C. *Org. Lett.* **1999**, *1*, 2093.
- (52) Ishi-i, T.; Mateos-Timoneda, M. A.; Timmerman, P.; Crego-Calama, M.; Reinhoudt, D. N.; Shinkai, S. *Angew. Chem., Int. Ed.* **2003**, *42*, 2300.
- (53) Mateos-Timoneda, M. A.; Crego-Calama, M.; Reinhoudt, D. N. *Chem. Soc. Rev.* **2004**, *33*, 363.
- (54) Inouye, M.; Waki, M.; Abe, H. *J. Am. Chem. Soc.* **2004**, *126*, 2022.
- (55) (a) Inouye, M.; Takahashi, K.; Nakazumi, H. *J. Am. Chem. Soc.* **1999**, *121*, 341. (b) Inouye, M.; Chiba, J.; Nakazumi, H. *J. Org. Chem.* **1999**, *64*, 8170.
- (56) Sonogashira, K. In *Metal-catalysed Cross-coupling Reactions*; Diederich, F., Stang, P. J., Eds.; Wiley-VCH: Weinheim, Germany, 1998; pp 203–229.
- (57) Kikuchi, Y.; Kobayashi, K.; Aoyama, Y. *J. Am. Chem. Soc.* **1992**, *114*, 1351.
- (58) Kikuchi, Y.; Kato, Y.; Tanaka, Y.; Toi, H.; Aoyama, Y. *J. Am. Chem. Soc.* **1991**, *113*, 1349.
- (59) Aoyama, Y.; Tanaka, Y.; Sugahara, S. *J. Am. Chem. Soc.* **1989**, *111*, 5397.



- (60) (a) Casnati, A.; Sansone, F.; Ungaro, R. *Acc. Chem. Res.* **2003**, *36*, 246. (b) Molenveld, P.; Engbersen, J. F. J.; Reinhoudt, D. N. *Chem. Soc. Rev.* **2000**, *2*, 75.
- (61) Ikeda, A.; Udzu, H.; Zhong, Z.; Shinkai, S.; Sakamoto, S.; Yamaguchi, K. *J. Am. Chem. Soc.* **2001**, *123*, 3872.
- (62) Ikeda, A.; Yoshimura, M.; Udzu, H.; Fukuhara, C.; Shinkai, S. *J. Am. Chem. Soc.* **1999**, *121*, 4296.
- (63) (a) Nepogodiev, S. A.; Stoddart, J. F. *Chem. Rev.* **1998**, *98*, 1959. (b) Raymo, F. M.; Stoddart, J. F. *Chem. Rev.* **1999**, *99*, 1643. (c) Balzani, V.; Gómez-López, M.; Stoddart, J. F. *Acc. Chem. Res.* **1998**, *31*, 405. (d) Tseng, H.-R.; Vignon, S. A.; Stoddart, J. F. *Angew. Chem., Int. Ed.* **2003**, *42*, 1491.
- (64) (a) Schalley, C. A.; Weilandt, T.; Brüggemann, J.; Vögtle, F. *Top. Curr. Chem.* **2004**, *248*, 141. (b) Schalley, C. A.; Beizai, K.; Vögtle, F. *Acc. Chem. Res.* **2001**, *34*, 465. (c) Schmieder, R.; Hubner, G.; Seel, C.; Vögtle, F. *Angew. Chem., Int. Ed.* **1999**, *38*, 3528. (d) Dunnwald, T.; Jager, R.; Vögtle, F. *Chem.—Eur. J.* **1997**, *3*, 2043.
- (65) (a) Ashton, P. R.; Boyd, S. E.; Menzer, S.; Pasini, D.; Raymo, F. M.; Spencer, N.; Stoddart, J. F.; White, A. J. P.; Williams, D. J.; Wyatt, P. G. *Chem.—Eur. J.* **1998**, *4*, 299. (b) Ashton, P. R.; Bravo, J. A.; Raymo, F. M.; Stoddart, J. F.; White, A. J. P.; Williams, D. J. *Eur. J. Org. Chem.* **1999**, 899.
- (66) Tachibana, Y.; Kihara, N.; Takata, T. *J. Am. Chem. Soc.* **2004**, *126*, 3438.
- (67) Kornýšova, O.; Šurna, R.; Snitka, V.; Pyell, U.; Maruška, A. *J. Chromatogr., A* **2002**, *971*, 225.
- (68) Asakawa, M.; Brancato, G.; Fanti, M.; Leigh, D. A.; Shimizu, T.; Slawin, A. M. Z.; Wong, J. K. Y.; Zerbetto, F.; Zhang, S. *J. Am. Chem. Soc.* **2002**, *124*, 2939.
- (69) (a) Schrader, T. *J. Org. Chem.* **1998**, *63*, 264. (b) Wehner, M.; Schrader, T.; Finocchiaro, P.; Faille, S.; Consiglio, G. *Org. Lett.* **2000**, *2*, 605.
- (70) You, J.-S.; Yu, X.-Q.; Zhang, G.-L.; Xiang, Q.-X.; Lan, J.-B.; Xie, R.-J. *Chem. Commun.* **2001**, 1816.
- (71) Fuji, K.; Tsubaki, K.; Tanaka, K.; Hayashi, N.; Otsubo, T.; Kinoshita, T. *J. Am. Chem. Soc.* **1999**, *121*, 3807.
- (72) (a) Tanaka, M.; Nakamura, M.; Salhin, M. A. A.; Ikeda, T.; Kamada, K.; Ando, H.; Shibutani, Y.; Kimura, K. *J. Org. Chem.* **2001**, *66*, 2386. (b) Niikura, K.; Bisson, A.P.; Anslyn, E. J. *Chem. Soc., Perkin Trans. 2* **1999**, 1111. (c) Miyaji, H.; Sessler, J. L. *Angew. Chem., Int. Ed.* **2001**, *40*, 154.
- (73) (a) Kubo, Y.; Maeda, S.; Tokita, S.; Kubo, M. *Nature* **1996**, *382*, 522. (b) Naemura, K.; Tobe, Y.; Kaneda, T. *Coord. Chem. Rev.* **1996**, *148*, 199. (c) Hirose, K.; Ogasahara, K.; Nishioka, K.; Tobe, Y.; Maemura, K. *J. Chem. Soc., Perkin Trans. 2* **2000**, 1984.
- (74) Tsubaki, K.; Nuruzzaman, M.; Kusumoto, T.; Hayashi, N.; Bin-Gui, W.; Fuji, K. *Org. Lett.* **2001**, *3*, 4071.
- (75) Rose, N. J.; Drago, R. S. *J. Am. Chem. Soc.* **1959**, *81*, 6138.
- (76) Asakawa, M.; Janssen, H. M.; Meijer, E.W.; Pasini, D.; Stoddart, J. F. *Eur. J. Org. Chem.* **1998**, 983.
- (77) Kim, S.-G.; Kim, K.-H.; Jung, J.; Shin, S. K.; Ahn, K. H. *J. Am. Chem. Soc.* **2002**, *124*, 591.
- (78) (a) See pages 3322–3323 in Zhang, Z. Z.; Bradshaw, J. S.; Izatt, R. M. *Chem. Rev.* **1997**, *97*, 3313. (b) Löhr, H.-G.; Vögtle, F. *Acc. Chem. Res.* **1985**, *18*, 65.
- (79) Kim, S.-G.; Kim, K.-H.; Kim, Y. K.; Shin, S. K.; Ahn, K. H. *J. Am. Chem. Soc.* **2003**, *125*, 13819.
- (80) Jeffrey, G. A.; Saenger, W. *Hydrogen Bonding in Biological Structures*; Springer-Verlag: New York, 1991; Chapter 2.2.
- (81) (a) Wong, W.-L.; Huang, K.-H.; Teng, P.-F.; Lee, C.-S.; Kwong, H.-L. *Chem. Commun.* **2004**, 384. (b) Lee, S. J.; Lin, W. *J. Am. Chem. Soc.* **2002**, *124*, 4554. (c) Grady, T.; Harris, S. J.; Smyth, M. R.; Diamond, D. *Anal. Chem.* **1996**, *68*, 3775. (d) Pagliari, S.; Corradini, R.; Galaverna, G.; Sforza, S.; Dossena, A.; Marchelli, R. *Tetrahedron Lett.* **2000**, *41*, 3691. (e) Yang, H.; Bohne, C. *J. Photochem. Photobiol., A* **1995**, *86*, 209. (f) Tundo, P.; Fendler, J. H. *J. Am. Chem. Soc.* **1980**, *102*, 1760.
- (82) (a) Pugh, V. J.; Hu, Q.-S.; Lin, P. *Angew. Chem., Int. Ed.* **2000**, *39*, 3638. (b) Gong, L.-Z.; Hu, Q.-S.; Pu, L. *J. Org. Chem.* **2001**, *66*, 2358.
- (83) (a) Ma, L.; White, P. S.; Lin, W. *J. Org. Chem.* **2002**, *67*, 7577. (b) Wang, D.; Liu, T.-J.; Zhang, W.-C.; Slaven, W. T., IV; Li, C.-J. *Chem. Commun.* **1998**, 1747.
- (84) Pu, L. *Chem. Rev.* **2004**, *104*, 1687.
- (85) Lakowicz, J. R. *Principles of Fluorescence Spectroscopy*, 2nd ed.; Kluwer, Academic/Plenum: New York, 1999.
- (86) (a) Metcalf, D. H.; Snyder, S. W.; Demas, J. N.; Richardson, F. S. *J. Am. Chem. Soc.* **1990**, *112*, 5681. (b) Yan, Y.; Myrick, M. L. *Anal. Chem.* **1999**, *71*, 1956.
- (87) Li, Z.-B.; Lin, L.; Pu, L. *Angew. Chem., Int. Ed.* **2005**, *44*, 1690.
- (88) Al Rabaa, A. R.; Tfibel, F.; Mirola, F.; Pernot, P.; Fontaine-Aupart, M. *J. Chem., Soc., Perkin Trans. 2* **1999**, 341.
- (89) (a) McCarroll, M. E.; Billiot, F. H.; Warner, I. M. *J. Am. Chem. Soc.* **2001**, *123*, 3173. (b) Xu, Y.; McCarroll, M. *J. Phys. Chem. B* **2005**, *109*, 8144.
- (90) (a) Goto, H.; Yashima, E. *J. Am. Chem. Soc.* **2002**, *124*, 7943. (b) Tucker, J.; Collinson, S. *Chem. Soc. Rev.* **2002**, *31*, 147. (c) Ori, A.; Shinkai, S. *Chem. Commun.* **1995**, 1771.
- (91) (a) Tejedor, R. M.; Millaruelo, M.; Oriol, L.; Serrano, J. L.; Alcalá, T.; Rodríguez, F. J.; Villacampa, B. *J. Mater. Chem.* **2006**, *16*, 1674. (b) Li, J.; Schuster, B.; Cheon, K.-S.; Green, M. M.; Selinger, J. V. *J. Am. Chem. Soc.* **2000**, *122*, 2603. (c) Bobrovsky, A. Y.; Boiko, N. I.; Shibaev, V. P. *Chem. Mater.* **2001**, *13*, 1998. (d) de Jong, J. J. D.; Lucas, L. N.; Kellogg, R. M.; van Esch, J. H.; Feringa, B. L. *Science* **2004**, *304*, 278.
- (92) (a) Inoue, Y.; Matsushima, E.; Wada, T. *J. Am. Chem. Soc.* **1998**, *120*, 10687. (b) Kaneda, M.; Asaoka, S.; Ikeda, H.; Mori, T.; Wada, T.; Inoue, Y. *Chem. Commun.* **2002**, 1272. (c) Kaneda, M.; Nakamura, A.; Asaoka, S.; Ikeda, H.; Mori, T.; Wada, T.; Inoue, Y. *Org. Biomol. Chem.* **2003**, *1*, 4435. (d) Yang, C.; Nakamura, A.; Fukuhara, G.; Origane, Y.; Mori, T.; Wada, T.; Inoue, Y. *J. Org. Chem.* **2006**, *71*, 3126.
- (93) (a) Angelini, N.; Micali, N.; Mineo, P.; Scamporrino, E.; Villari, V.; Vitalini, D. *J. Phys. Chem. B* **2005**, *109*, 18645. (b) Schaberle, F. A.; Kuz'min, V. A.; Borissevitch, I. E. *Biochim. Biophys. Acta* **2003**, *1621*, 183. (c) Nishino, H.; Kosaka, A.; Hembury, G. A.; Matsushima, K.; Inoue, Y. *J. Chem. Soc., Perkin Trans. 2* **2002**, 582.
- (94) Steffen, W.; Köhler, B.; Altmann, M.; Scherf, U.; Stitzer, K.; zur Loye, H.-C.; Bunz, U. H. F. *Chem.—Eur. J.* **2001**, *7*, 117.
- (95) Redl, F. X.; Lutz, M.; Daub, J. *Chem.—Eur. J.* **2001**, *7*, 5350.
- (96) Iarossi, D.; Mucci, A.; Parenti, F.; Schenetti, L.; Seeber, R.; Zanardi, C.; Forni, A.; Tonelli, M. *J. Chem.—Eur. J.* **2001**, *7*, 676.
- (97) Kawasaki, T.; Tokuhito, M.; Kimizuka, N.; Kunitake, T. *J. Am. Chem. Soc.* **2001**, *123*, 6792.
- (98) Reichardt, C. *Solvents and Solvent Effects in Organic Chemistry*; VCH: Weinheim, Germany, 1988.
- (99) Pengo, P.; Pasquato, L.; Moro, S.; Brigo, A.; Fogolari, F.; Broxterman, Q. B.; Kaptein, B.; Scrimin, P. *Angew. Chem., Int. Ed.* **2003**, *42*, 3388.
- (100) Saito, S.; Nuckolls, C.; Rebek, J., Jr. *J. Am. Chem. Soc.* **2000**, *122*, 9628.
- (101) Aoki, T.; Kaneko, T.; Maruyama, N.; Sumi, A.; Takahashi, M.; Sato, T.; Teraguchi, M. *J. Am. Chem. Soc.* **2003**, *125*, 6346.
- (102) Reichardt, C. *Chem. Rev.* **1994**, *94*, 2319.
- (103) Yagi, S.; Morinaga, T.; Nomura, T.; Takagishi, T.; Mizutani, T.; Kitagawa, S.; Ogoshi, H. *J. Org. Chem.* **2001**, *66*, 3848.
- (104) Schiel, C.; Hembury, G. A.; Borovkov, V. V.; Klaes, M.; Agena, C.; Wada, T.; Grimme, S.; Inoue, Y.; Mattay, J. *J. Org. Chem.* **2006**, *71*, 976.
- (105) Nakashima, H.; Fujiki, M.; Koe, J. R.; Motonaga, M. *J. Am. Chem. Soc.* **2001**, *123*, 1963.
- (106) Nakanishi, K.; Berova, N. In *Circular Dichroism: Principles and Applications*; Nakanishi, K., Berova, N., Woody, R. W., Eds.; VCH: New York, 1994; Chapters 5 and 13.
- (107) Tang, H.-Z.; Boyle, P. D.; Novak, B. M. *J. Am. Chem. Soc.* **2005**, *127*, 2136.
- (108) Hofacker, A. L.; Parquette, J. R. *Angew. Chem., Int. Ed.* **2005**, *44*, 1053.
- (109) Still, W. C.; Tempczyk, A.; Hawley, R. C.; Hendrickson, T. *J. Am. Chem. Soc.* **1990**, *112*, 6127.
- (110) (a) Boiadjev, S. E.; Lightner, D. A. *J. Am. Chem. Soc.* **2000**, *122*, 378. (b) Boiadjev, S. E.; Person, R. V.; Puzicha, G.; Knobler, C.; Maverick, E.; Trueblood, K. N.; Lightner, D. A. *J. Am. Chem. Soc.* **1992**, *114*, 10123.
- (111) Borovkov, V. V.; Hembury, G. A.; Yamamoto, N.; Inoue, Y. *J. Phys. Chem. A* **2003**, *107*, 8677.
- (112) van Herrikhuizen, J.; Jonkheijm, P.; Schenning, A. P. H. J.; Meijer, E. W. *Org. Biomol. Chem.* **2006**, *4*, 1539.
- (113) Ishi-i, T.; Kuwahara, R.; Takata, A.; Jeong, Y.; Sakurai, K.; Makata, S. *Chem.—Eur. J.* **2006**, *12*, 763.
- (114) Schenning, A. P. H. J.; Kilbinger, A. F. M.; Biscarini, F.; Cavallini, M.; Cooper, H. J.; Derrick, P. J.; Lazzaroni, R.; Leclère, Ph.; McDonell, L. A.; Meijer, E. W.; Meskers, S. C. J. *J. Am. Chem. Soc.* **2002**, *124*, 1269.
- (115) Katze, H. E.; Laquindanum, J. G.; Lovinger, A. *Chem. Mater.* **1998**, *10*, 633.
- (116) Kato, T.; Matsuoka, T.; Nishii, M.; Kamikawa, Y.; Kanie, K.; Nishimura, T.; Yashima, E.; Ujiie, S. *Angew. Chem., Int. Ed.* **2004**, *43*, 1969.
- (117) (a) Kato, T. *Science* **2002**, *295*, 2414. (b) Kanie, K.; Yasuda, T.; Ujiie, S.; Kato, T. *Chem. Commun.* **2000**, 1899.
- (118) John, G.; Jung, J. H.; Minamikawa, H.; Yoshida, K.; Shimizu, T. *Chem.—Eur. J.* **2002**, *8*, 5494.
- (119) (a) Renikuntla, B. R.; Armitage, S. B. *Langmuir* **2005**, *21*, 5362. (b) Lashuel, H. A.; LaBrenz, S. R.; Woo, L.; Serpell, L. C.; Kelly,



- J. W. *J. Am. Chem. Soc.* **2000**, *122*, 5262. (c) Matile, S. *Chem. Soc. Rev.* **2001**, *30*, 158. (d) Zhang, S.; Marini, D. M.; Hwang, W.; Santoso, S. *Curr. Opin. Chem. Biol.* **2002**, *6*, 865. (e) Rich, A.; Zhang, S. *Nat. Rev. Genet.* **2003**, *4*, 566. (f) Lam, S. L.; Au-Yeung, S. C. F. *J. Mol. Biol.* **1997**, *266*, 745. (g) Miyake, H.; Tsukube, H. *Supramol. Chem.* **2005**, *17*, 53.
- (120) Sakai, N.; Matile, S. *Chirality* **2004**, *16*, S38.
- (121) Tashiro, R.; Sugiyama, H. *J. Am. Chem. Soc.* **2005**, *127*, 2094.
- (122) Tashiro, R.; Sugiyama, H. *Angew. Chem., Int. Ed.* **2003**, *42*, 6018.
- (123) (a) Jadhav, V. D.; Schmidtchen, F. P. *Org. Lett.* **2006**, *8*, 2329. (b) Dunitz, J. D. *Chem. Biol.* **1995**, *2*, 709. (c) Choi, H. S.; Takahashi, A.; Ooya, T.; Yui, N. *Macromolecules* **2004**, *37*, 10036. (d) Lo Meo, P.; D'anna, F.; Gruttadauria, M.; Riela, S.; Noto, R. *Tetrahedron* **2004**, *60*, 9099. (e) Liu, Y.; Yang, Y.-W.; Cao, R.; Song, S.-H.; Zhang, H.-Y.; Wang, L.-H. *J. Phys. Chem. B* **2003**, *107*, 14130.
- (124) (a) Fukuhara, G.; Mori, T.; Wada, T.; Inoue, Y. *Chem. Commun.* **2005**, 4199. (b) Yamamura, H.; Rekharsky, M. V.; Ishihara, Y.; Kawai, M.; Inoue, Y. *J. Am. Chem. Soc.* **2004**, *126*, 14224. (c) Nishiyama, Y.; Kaneda, M.; Saito, R.; Mori, T.; Wada, T.; Inoue, Y. *J. Am. Chem. Soc.* **2004**, *126*, 6568. (d) Rekharsky, M.; Inoue, Y.; Tobey, S.; Metzger, A.; Anslyn, E. *J. Am. Chem. Soc.* **2002**, *124*, 14959.
- (125) Saito, R.; Naruse, S.; Takano, K.; Fukuda, K.; Katoh, A.; Inoue, Y. *Org. Lett.* **2006**, *8*, 2067.
- (126) Setnička, V.; Urbanová, M.; Pataridis, S.; Král, V.; Volka, K. *Tetrahedron: Asymmetry* **2002**, *13*, 2661.
- (127) Treech, P.; Weiss, R. G. *Chem. Rev.* **1997**, *97*, 3133.
- (128) Zsila, F.; Bilkádi, Z.; Keresztes, Z.; Deli, J.; Simonyi, M. *J. Phys. Chem. B* **2001**, *105*, 9413.
- (129) Borovkov, V. V.; Harada, T.; Inoue, Y.; Kuroda, R. *Angew. Chem., Int. Ed.* **2002**, *41*, 1378.
- (130) Borovkov, V. V.; Harada, T.; Hembury, G. A.; Inoue, Y.; Kuroda, R. *Angew. Chem., Int. Ed.* **2003**, *42*, 1746.
- (131) (a) Ribó, J. M.; Crusats, J.; Sagués, F.; Claret, J.; Rubires, R. *Science* **2001**, *292*, 2063. (b) Rubires, R.; Farrera, J.-A.; Ribó, J. M. *Chem.—Eur. J.* **2001**, *7*, 436.
- (132) Honda, C.; Hada, H. *Tetrahedron Lett.* **1976**, *3*, 177.
- (133) (a) Norden, B. *J. Phys. Chem.* **1977**, *81*, 151. (b) Saeva, F. D.; Olin, G. R. *J. Am. Chem. Soc.* **1977**, *99*, 4848.
- (134) (a) Borovkov, V. V.; Inoue, Y. *Top. Curr. Chem.* **2006**, *265*, 89. (b) Balaban, T. S.; Tamiaki, H.; Holzwarth, A. R. *Top. Curr. Chem.* **2005**, *258*, 1. (c) Balaban, T. S. *Acc. Chem. Res.* **2005**, *38*, 612. (d) Miyake, H.; Tsukube, H. *Supramol. Chem.* **2005**, *17*, 53. (e) Shinkai, S.; Takeuchi, M. *Biosens. Bioelectron.* **2004**, *20*, 1250. (f) Marchon, J.-C.; Ramasseul, R. In *The Porphyrin Handbook*; Kadish, K. M., Smith, K. M., Guillard, R., Eds.; Elsevier Science: New York, 2003; Vol. 11, pp 75–132. (g) Allenmark, S. *Chirality* **2003**, *15*, 409. (h) Pasternack, R. F. *Chirality* **2003**, *15*, 329. (i) Wenzel, T. J.; Wilcox, J. D. *Chirality* **2003**, *15*, 256. (j) Tsukube, H.; Shinoda, S. *Chem. Rev.* **2002**, *102*, 2389. (k) Aspinall, H. C. *Chem. Rev.* **2002**, *102*, 1807. (l) Tsukube, H.; Shinoda, S.; Tamiaki, H. *Coord. Chem. Rev.* **2002**, *226*, 227. (m) Simonneaux, G.; Maux, P. L. *Coord. Chem. Rev.* **2002**, *228*, 43. (n) Finn, M. G. *Chirality* **2002**, *14*, 534. (o) Shinkai, S.; Ikeda, M.; Sugasaki, A.; Takeuchi, M. *Acc. Chem. Res.* **2001**, *34*, 494. (p) Kobayashi, N. *Coord. Chem. Rev.* **2001**, *99*, 219–221. (q) Ogoshi, H.; Mizutani, T.; Hayashi, T.; Kuroda, Y. In *The Porphyrin Handbook*; Kadish, K. M., Smith, K. M., Guillard, R., Eds.; Academic Press: New York, 2000; Vol. 6, pp 279–340. (r) Shinkai, S.; Robertson, A. *Coord. Chem. Rev.* **2000**, *205*, 157. (s) Hartley, J. H.; James, T. D.; Ward, C. J. *J. Chem. Soc., Perkin Trans. 1* **2000**, 3155. (t) Huang, X.; Nakanishi, K.; Berova, N. *Chirality* **2000**, *12*, 237. (u) Tsukube, H.; Shinoda, S. *Enantiomer* **2000**, *5*, 13. (v) McMillin, D. R.; McNett, K. N. *Chem. Rev.* **1998**, *98*, 1201.
- (135) Mizuno, Y.; Aida, T.; Yamaguchi, K. *J. Am. Chem. Soc.* **2000**, *122*, 5278.
- (136) Mizuno, Y.; Aida, T. *Chem. Commun.* **2003**, 20.
- (137) Kijima, H.; Takeuchi, M.; Shinkai, S. *Chem. Lett.* **1998**, 781.
- (138) (a) Takeuchi, M.; Imada, T.; Shinkai, S. *Bull. Chem. Soc. Jpn.* **1998**, *71*, 1117. (b) Takeuchi, M.; Imada, T.; Shinkai, S. *Angew. Chem., Int. Ed.* **1998**, *37*, 2096. (c) Sugasaki, A.; Ikeda, M.; Takeuchi, M.; Robertson, A.; Shinkai, S. *J. Chem. Soc., Perkin Trans. 1* **1999**, 3259. (d) Sugasaki, A.; Ikeda, M.; Takeuchi, M.; Shinkai, S. *Angew. Chem., Int. Ed.* **2000**, *39*, 3839. (e) Sugasaki, A.; Sugiyasu, K.; Ikeda, M.; Takeuchi, M.; Shinkai, S. *J. Am. Chem. Soc.* **2001**, *123*, 10239. (f) Yamamoto, M.; Sugasaki, A.; Ikeda, M.; Takeuchi, M.; Frimat, K.; James, T. D.; Shinkai, S. *Chem. Lett.* **2001**, 520.
- (139) Mizutani, T.; Murakami, T.; Kurahashi, T.; Ogoshi, H. *J. Org. Chem.* **1996**, *61*, 539.
- (140) Mizutani, T.; Wada, K.; Kitagawa, S. *J. Org. Chem.* **2000**, *65*, 6097.
- (141) Tamiaki, H.; Matsumoto, N.; Unno, S.; Shinoda, S.; Tsukube, H. *Inorg. Chim. Acta* **2000**, *300–302*, 243.
- (142) Tamiaki, H.; Unno, S.; Takeuchi, E.; Tameshige, N.; Shinoda, S.; Tsukube, H. *Tetrahedron* **2003**, *59*, 10477.
- (143) Tsukube, H.; Wada, M.; Shinoda, S.; Tamiaki, H. *Chem. Commun.* **1999**, 1007.
- (144) Awawdeh, M. A.; Legako, J. A.; Harmon, H. J. *Sens. Actuator B* **2003**, *91*, 227.
- (145) Wang, C. Z.; Zhu, Z. A.; Li, Y.; Chen, Y. T.; Wen, X.; Miao, F. M.; Chan, W. L.; Chan, A. S. C. *New J. Chem.* **2001**, *25*, 801.
- (146) (a) Fukuda, T.; Olmstead, M. M.; Durfee, W. S.; Kobayashi, N. *Chem. Commun.* **2003**, 1256. (b) Muranaka, A.; Okuda, M.; Kobayashi, N.; Somers, K.; Ceulemans, A. *J. Am. Chem. Soc.* **2004**, *126*, 4596.
- (147) (a) Huang, X.; Borhan, B.; Rickman, B. H.; Nakanishi, K.; Berova, N. *Chem.—Eur. J.* **2000**, *6*, 216. (b) Kurtan, T.; Nesnas, N.; Li, Y.-Q.; Huang, X.; Nakanishi, K.; Berova, N. *J. Am. Chem. Soc.* **2001**, *123*, 5962. (c) Kurtan, T.; Nesnas, N.; Koehn, F. E.; Li, Y.-Q.; Nakanishi, K.; Berova, N. *J. Am. Chem. Soc.* **2001**, *123*, 5974. (d) Yang, Q.; Olmsted, C.; Borhan, B. *Org. Lett.* **2002**, *4*, 3423. (e) Proni, G.; Pescitelli, G.; Huang, X.; Quraishi, N. Q.; Nakanishi, K.; Berova, N. *Chem. Commun.* **2002**, 1590. (f) Huang, X.; Fujioka, N.; Pescitelli, G.; Koehn, F. E.; Williamson, V. V.; Nakanishi, K.; Berova, N. *J. Am. Chem. Soc.* **2002**, *124*, 10320. (g) Proni, G.; Pescitelli, G.; Huang, X.; Nakanishi, K.; Berova, N. *J. Am. Chem. Soc.* **2003**, *125*, 12914. (h) Ishii, H.; Chen, Y.; Miller, R. A.; Karady, S.; Nakanishi, K.; Berova, N. *Chirality* **2005**, *17*, 305. (i) Solladié-Cavallo, A.; Marsol, C.; Pescitelli, G.; Bari, L. D.; Salvadori, P.; Huang, X.; Fujioka, N.; Berova, N.; Cao, X.; Freedman, T. B.; Nafie L. A. *Eur. J. Org. Chem.* **2002**, 1788. (j) Ishii, H.; Krane, S.; Itagaki, Y.; Berova, N.; Nakanishi, K.; Weldon, P. J. *J. Nat. Prod.* **2004**, *67*, 1426.
- (148) (a) Borovkov, V. V.; Lintuluoto, J. M.; Inoue, Y. *Org. Lett.* **2000**, *2*, 1565. (b) Borovkov, V. V.; Lintuluoto, J. M.; Inoue, Y. *J. Am. Chem. Soc.* **2001**, *123*, 2979. (c) Borovkov, V. V.; Lintuluoto, J. M.; Inoue, Y. *J. Phys. Chem. A* **2000**, *104*, 9213. (d) Borovkov, V. V.; Yamamoto, N.; Lintuluoto, J. M.; Tanaka, T.; Inoue, Y. *Chirality* **2001**, *13*, 329. (e) Borovkov, V. V.; Lintuluoto, J. M.; Sugeta, H.; Fujiki, M.; Arakawa, R.; Inoue, Y. *J. Am. Chem. Soc.* **2002**, *124*, 2993. (f) Borovkov, V. V.; Lintuluoto, J. M.; Fujiki, M.; Inoue, Y. *J. Am. Chem. Soc.* **2000**, *122*, 4403. (g) Borovkov, V. V.; Hembury, G. A.; Inoue, Y. *J. Porphyrins Phthalocyanines* **2003**, *7*, 337. (h) Lintuluoto, J. M.; Borovkov, V. V.; Inoue, Y. *J. Am. Chem. Soc.* **2002**, *124*, 13676. (i) Borovkov, V. V.; Lintuluoto, J. M.; Inoue, Y. *Org. Lett.* **2002**, *4*, 169. (j) Borovkov, V. V.; Lintuluoto, J. M.; Sugiura, M.; Inoue, Y.; Kuroda, R. *J. Am. Chem. Soc.* **2002**, *124*, 11282. (k) Borovkov, V. V.; Lintuluoto, J. M.; Hembury, G. A.; Sugiura, M.; Arakawa, R.; Inoue, Y. *J. Org. Chem.* **2003**, *68*, 7176.
- (149) (a) Borovkov, V. V.; Hembury, G. A.; Inoue, Y. *J. Org. Chem.* **2005**, *70*, 8743. (b) Borovkov, V. V.; Inoue, Y. *Org. Lett.* **2006**, *8*, 2337.
- (150) Kovaric, B. C.; Kokona, B.; Schwab, A. D.; Twomey, M. A.; de Paula, J. C.; Fairman, R. *J. Am. Chem. Soc.* **2006**, *128*, 4166.
- (151) (a) Sakamoto, M.; Ueno, A.; Mihara, H. *Chem. Commun.* **2000**, 1741. (b) Sakamoto, M.; Ueno, A.; Mihara, H. *Chem.—Eur. J.* **2001**, *7*, 2449.
- (152) (a) Fukushima, Y. *Polym. J.* **1995**, *27*, 1208. (b) Fukushima, Y. *Bull. Chem. Soc. Jpn.* **1996**, *69*, 1719.
- (153) (a) Purrello, R.; Bellacchio, E.; Gurrieri, S.; Lauceri, R.; Raudino, A.; Scolaro, L. M.; Santoro, A. M. *J. Phys. Chem. B* **1998**, *102*, 8852. (b) Koti, A. S. R.; Periasamy, N. *Chem. Mater.* **2003**, *15*, 369.
- (154) (a) Purrello, R.; Scolaro, L. M.; Bellacchio, E.; Gurrieri, S.; Romeo, A. *Inorg. Chem.* **1998**, *37*, 3647. (b) Bellacchio, E.; Lauceri, R.; Gurrieri, S.; Scolaro, L. M.; Romeo, A.; Purrello, R. *J. Am. Chem. Soc.* **1998**, *120*, 12353. (c) Purrello, R.; Raudino, A.; Scolaro, L. M.; Loisi, A.; Bellacchio, E.; Lauceri, R. *J. Phys. Chem. B* **2000**, *104*, 10900. (d) Lauceri, R.; Purrello, R. *Supramol. Chem.* **2005**, *17*, 61.
- (155) Larsen, R. W.; Omdal, D. H.; Jasuja, R.; Niu, S. L.; Jameson, D. M. *J. Phys. Chem. B* **1997**, *101*, 8012.
- (156) Ishida, Y.; Konishi, K.; Aida, T.; Nagamune, T. *Chem.—Eur. J.* **1998**, *4*, 1148.
- (157) Fiel, R. J.; Howard, J. C.; Mark, E. H.; Gupta, D. N. *Nucleic Acids Res.* **1979**, *6*, 3093.
- (158) (a) Crites Tears, D. K.; McMillin, D. R. *Chem. Commun.* **1998**, 2517. (b) Eggleston, M. K.; Crites, D. K.; McMillin, D. R. *J. Phys. Chem. A* **1998**, *102*, 5506. (c) Thomas, K. E.; McMillin, D. R. *J. Phys. Chem. B* **2001**, *105*, 12628.
- (159) Zupan, K.; Herényi, L.; Toth, K.; Majer, Z.; Csik, G. *Biochem.* **2004**, *43*, 9151.
- (160) Barnes, N. R.; Schreiner, A. F. *Inorg. Chem.* **1998**, *37*, 6935.
- (161) Uno, T.; Hamasaki, K.; Tanigawa, M.; Shimabayashi, S. *Inorg. Chem.* **1997**, *36*, 1676.
- (162) Lee, Y.-A.; Kim, J.-O.; Cho, T.-S.; Song, R.; Kim, S. K. *J. Am. Chem. Soc.* **2003**, *125*, 8106.
- (163) Park, T.; Shin, J. S.; Han, S. W.; Son, J.-K.; Kim, S. K. *J. Phys. Chem. B* **2004**, *108*, 17106.

- (164) (a) Bejune, S. A.; Shelton, A. H.; McMillin, D. R. *Inorg. Chem.* **2003**, *42*, 8465. (b) Wall, R. K.; Shelton, A. H.; Bonaccorsi, L. C.; Bejune, S. A.; Dubé, D.; McMillin, D. R. *J. Am. Chem. Soc.* **2001**, *123*, 11480.
- (165) Bejune, S. A.; McMillin, D. R. *Chem. Commun.* **2004**, 1320.
- (166) Pasternack, R. F.; Gurrieri, S.; Lauceri, R.; Purrello, R. *Inorg. Chim. Acta* **1996**, *246*, 7.
- (167) Scolaro, L. M.; Romeo, A.; Pasternack, R. F. *J. Am. Chem. Soc.* **2004**, *126*, 7178.
- (168) Suenaga, H.; Arimori, S.; Shinkai, S. *J. Chem. Soc., Perkin Trans. 2* **1996**, 607.
- (169) Suenaga, H.; Nango, M.; Sugiyama, T.; Iwasaki, T.; Takeuchi, Y.; Shinkai, S. *S. Chem. Lett.* **2000**, 306.
- (170) Thornton, N. B.; Wojtowicz, H.; Netzel, T.; Dixon, D. W. *J. Phys. Chem. B* **1998**, *102*, 2101.
- (171) (a) Kubat, P.; Lang, K.; Anzenbacher, P., Jr.; Jursikova, K.; Kral, V.; Ehrenberg, B. *J. Chem. Soc., Perkin Trans. 1* **2000**, 933. (b) Kubat, P.; Lang, K.; Kral, V.; Anzenbacher, P., Jr. *J. Phys. Chem. B* **2002**, *106*, 6784.
- (172) (a) Tjahjono, D. H.; Akutsu, T.; Yoshioka, N.; Inoue, H. *Biochim. Biophys. Acta* **1999**, *1472*, 333. (b) Tjahjono, D. H.; Yamamoto, T.; Ichimoto, S.; Yoshioka, N.; Inoue, H. *J. Chem. Soc., Perkin Trans. 1* **2000**, 3077.
- (173) (a) Chen, X.; Liu, M. *J. Inorg. Biochem.* **2003**, *94*, 106. (b) Jiang, S.; Liu, M. *J. Phys. Chem. B* **2004**, *108*, 2880.
- (174) Lauceri, R.; Purrello, R.; Shetty, S. J.; Vicente, M. G. H. *J. Am. Chem. Soc.* **2001**, *123*, 5835.
- (175) Barnes, N. R.; Schreiner, A. F.; Dolan, M. A. *J. Inorg. Biochem.* **1998**, *72*, 1.
- (176) (a) Rubires, R.; Crusats, J.; El-Hachemi, Z.; Jaramillo, T.; López, M.; Valls, E.; Farrera, J.-A.; Ribó, J. M. *New J. Chem.* **1999**, 189. (b) Crusats, J.; Claret, J.; Díez-Pérez, I.; El-Hachemi, Z.; García-Ortega, H.; Rubires, R.; Sagués, F.; Ribó, J. M. *Chem. Commun.* **2003**, 1588.
- (177) Yamaguchi, T.; Kimura, T.; Matsuda, H.; Aida, T. *Angew. Chem., Int. Ed.* **2004**, *43*, 6350.
- (178) Lauceri, R.; Raudino, A.; Scolaro, M.; Micali, N.; Purrello, R. *J. Am. Chem. Soc.* **2002**, *124*, 894.
- (179) Prins, J. L.; Jolliffe, K. A.; Hulst, R.; Timmerman, P.; Reinhoudt, D. N. *J. Am. Chem. Soc.* **2000**, *122*, 3617.
- (180) Prins, J. L.; Timmerman, P.; Reinhoudt, D. N. *J. Am. Chem. Soc.* **2001**, *123*, 10153.
- (181) Prins, J. L.; Verhage, J. J.; De Jong, F.; Timmerman, P.; Reinhoudt, D. N. *Chem.—Eur. J.* **2002**, *8*, 2302.
- (182) Ishi-i, T.; Crego-Calama, M.; Timmerman, P.; Reinhoudt, D. N.; Shinkai, S. *J. Am. Chem. Soc.* **2002**, *124*, 14631.
- (183) Ziegler, M.; Davis, A. V.; Johnson, D. W.; Raymond, K. N. *Angew. Chem., Int. Ed.* **2003**, *42*, 665.
- (184) Purrello, R. *Nat. Mater.* **2003**, *2*, 216.
- (185) Fiedler, D.; Bergman, R. G.; Raymond, K. N. *Angew. Chem., Int. Ed.* **2004**, *43*, 6748.
- (186) (a) Yashima, E.; Matsushima, T.; Okamoto, Y. *J. Am. Chem. Soc.* **1995**, *117*, 11596. (b) Yashima, E.; Maeda, K.; Nishimura, T. *Chem.—Eur. J.* **2004**, *10*, 42.
- (187) Onouchi, H.; Miyagawa, T.; Furuko, A.; Maeda, K.; Yashima, E. *J. Am. Chem. Soc.* **2005**, *127*, 2960.
- (188) (a) Kubo, Y.; Ohno, T.; Yamanaka, J.-I.; Tokita, S.; Iida, T.; Ishimura, Y. *J. Am. Chem. Soc.* **2001**, *123*, 12700. (b) Kubo, Y.; Ishii, Y.; Yoshizawa, T.; Tokita, S. *Chem. Commun.* **2004**, 1394.
- (189) (a) Lopinski, G. P.; Moffatt, D. J.; Wayner, D. D. M.; Wolkow, R. A. *Nature* **1998**, *392*, 909. (b) Böhringer, M.; Schneider, W. D.; Berndt, R. *Angew. Chem., Int. Ed.* **2000**, *39*, 792. (c) Jung, T. A.; Schlitter, R. R.; Gimzewski, J. K. *Nature* **1997**, *386*, 696.
- (190) (a) Lorenzo, M. O.; Baddeley, C. J.; Muryn, C.; Raval, R. *Nature* **2000**, *404*, 376. (b) Barth, J. V.; Wekesser, J.; Trimarchi, G.; Vladimirova, M.; De Vita, A.; Cai, C. Z.; Brune, H.; Günter, P.; Kern, K. *J. Am. Chem. Soc.* **2002**, *124*, 7991. (c) Barth, J. V.; Wekesser, J.; Lin, N.; Dmitriev, A.; Kern, K. *Appl. Phys. A: Mater. Sci. Process.* **2003**, *76*, 645.
- (191) (a) De Feyter, S.; De Schryver, F. C. *Chem. Soc. Rev.* **2003**, *32*, 139. (b) Yokoyama, T.; Yokoyama, S.; Kamikado, T.; Okuno, Y.; Mashiko, S. *Nature* **2001**, *413*, 619.
- (192) Barlow, S. M.; Louafi, S.; Le Roux, D.; Williams, J.; Muryn, C.; Haq, S.; Raval, R. *Langmuir* **2004**, *20*, 7171.
- (193) Zhao, X. Y.; Zhao, R. G.; Yang, W. S. *Langmuir* **2000**, *16*, 812.
- (194) Woodruff, D. P. *J. Phys.: Condens. Matter* **1994**, *6*, 6067.
- (195) Fasel, R.; Parschau, M.; Ernst, K.-H. *Angew. Chem., Int. Ed.* **2003**, *42*, 5178.
- (196) Ernst, K.-H.; Kuster, Y.; Fasel, R.; Müller, M. *Chirality* **2001**, *13*, 675.
- (197) Ward, M. D. *Nature* **2003**, *426*, 615.
- (198) Xu, Q.-M.; Wang, D.; Wan, L.-J.; Wang, C.; Bai, C.-L.; Feng, G.-Q.; Wang, M.-X. *Angew. Chem., Int. Ed.* **2002**, *41*, 3408.
- (199) Schönherr, H.; Crego-Calama, M.; Vancso, G. J.; Reinhoudt, D. N. *Adv. Mater.* **2004**, *16*, 1416.
- (200) Brunsveld, L.; Folmer, B. J. B.; Meijer, E. W.; Sijbesma, R. P.; Reinhoudt, D. N. *Chem. Rev.* **2001**, *101*, 4071.
- (201) Prins, L. J.; Reinhoudt, D. N.; Timmerman, P. *Angew. Chem., Int. Ed.* **2001**, *40*, 2383.
- (202) Frommer, J. *Angew. Chem., Int. Ed. Engl.* **1992**, *31*, 1298.
- (203) (a) George, S. J.; Ajayaghosh, A.; Jonkheijm, P.; Schenning, A. P. H. J.; Meijer, E. W. *Angew. Chem., Int. Ed.* **2004**, *43*, 3422. (b) Engelkamp, H.; Middelbeek, S.; Nolte, R. J. M. *Science* **1999**, *284*, 785.
- (204) (a) Kawasaki, T.; Tokuhito, M.; Kimizuka, N.; Kunitake, T. *J. Am. Chem. Soc.* **2001**, *123*, 6792. (b) Fenniri, H.; Mathivanan, P.; Vidale, K. L.; Sherman, D. M.; Hallenga, K.; Wood, K. V.; Stowell, J. G. *J. Am. Chem. Soc.* **2001**, *123*, 3854. (c) Lee, H. S.; Syud, F. A.; Wang, X.; Gellman, S. H. *J. Am. Chem. Soc.* **2001**, *123*, 7721. (d) Seebach, D.; Jacobi, A.; Rueping, M.; Gademann, K.; Ernst, M.; Jaun, B. *Helv. Chim. Acta* **2001**, *83*, 2115.
- (205) Brunsveld, L.; Vekemans, J. A. J. M.; Hirschberg, J. H. K. K.; Sijbesma, R. P.; Meijer, E. W. *PNAS* **2002**, *99*, 4977.
- (206) Green, M. M.; Reidy, M. P.; Johnson, R. D.; Darling, G.; O'Leary, D. J.; Willson, G. *J. Am. Chem. Soc.* **1989**, *111*, 6452.
- (207) Palmans, A. R. A.; Vekemans, J. A. J. M.; Havinga, E. E.; Meijer, E. W. *Angew. Chem., Int. Ed. Engl.* **1997**, *36*, 2648.
- (208) Brunsveld, L.; Schenning, A. P. H. J.; Broeren, M. A. C.; Janssen, H. M.; Vekemans, J. A. J. M.; Meijer, E. W. *Chem. Lett.* **2000**, 292.
- (209) Langeveld-Voss, B. M. W.; Waterval, R. J. M.; Janssen, H. M.; Meijer, E. W. *Macromolecules* **1999**, *32*, 227.
- (210) Brunsveld, L.; Lohmeijer, B. G. G.; Vekemans, J. A. J. M.; Meijer, E. W. *Chem. Commun.* **2000**, 2305.
- (211) Brunsveld, L.; Meijer, E. W.; Prince, R. B.; Moore, J. S. *J. Am. Chem. Soc.* **2001**, *123*, 7978.
- (212) Wilson, A. J.; Masuda, M.; Sijbesma, R. P.; Meijer, E. W. *Angew. Chem., Int. Ed.* **2005**, *44*, 2275.
- (213) (a) Green, M. M.; Peterson, N. C.; Sato, T.; Teramoto, A.; Cook, R.; Lifson, S. *Science* **1995**, *268*, 1860. (b) Jha, S. K.; Cheon, K. S.; Green, M. M.; Selinger, J. V. *J. Am. Chem. Soc.* **1999**, *121*, 1655.
- (214) van Gestel, J.; Palmans, A. R. A.; Titulaer, B.; Vekemans, J. A. J. M.; Meijer, E. W. *J. Am. Chem. Soc.* **2005**, *127*, 5490.
- (215) van Gestel, J. *Macromolecules* **2004**, *37*, 3894.
- (216) Ishida, Y.; Aida, T. *J. Am. Chem. Soc.* **2002**, *124*, 14017.
- (217) Flory, P. J. *J. Am. Chem. Soc.* **1936**, *58*, 1877.
- (218) (a) Maeda, K.; Morino, K.; Okamoto, Y.; Sato, T.; Yashima, E. *J. Am. Chem. Soc.* **2004**, *126*, 4329. (b) Morino, K.; Watase, N.; Maeda, K.; Yashima, E. *Chem.—Eur. J.* **2004**, *10*, 4703.
- (219) (a) Yashima, E.; Maeda, K.; Okamoto, Y. *Chem. Lett.* **1996**, 955. (b) Yashima, E.; Nimura, T.; Matsushima, T.; Okamoto, Y. *J. Am. Chem. Soc.* **1996**, *118*, 9800. (c) Onouchi, H.; Maeda, K.; Yashima, E. *J. Am. Chem. Soc.* **2001**, *123*, 7441.
- (220) Brunsveld, L.; Prince, R. B.; Meijer, E. W.; Moore, J. S. *Org. Lett.* **2000**, *2*, 1525.
- (221) (a) Koe, J. R.; Fujiki, M.; Motonaga, M.; Nakashima, H. *Macromolecules* **2001**, *34*, 1082. (b) Nakashima, H.; Fujiki, M.; Koe, J. R.; Motonaga, M. *J. Am. Chem. Soc.* **2001**, *123*, 1963. (c) Fujiki, M. *J. Organomet. Chem.* **2003**, *685*, 15.
- (222) (a) Lifson, S.; Andreola, C.; Peterson, N. C.; Green, M. M. *J. Am. Chem. Soc.* **1989**, *111*, 8850. (b) Selinger, J. V.; Selinger, R. L. B. *Phys. Rev. E* **1997**, *55*, 1728.
- (223) Sato, T.; Terao, K.; Teramoto, A.; Fujiki, M. *Macromolecules* **2002**, *35*, 5355.
- (224) Nakashima, H.; Koe, J. R.; Torimitsu, K.; Fujiki, M. *J. Am. Chem. Soc.* **2001**, *123*, 4847.

CR050005K